University of Wollongong

Research Online

University of Wollongong Thesis Collection 1954-2016

University of Wollongong Thesis Collections

2016

An investigation into the biological activity of gold anti-arthritic compounds and gold nanoparticles

Lloyd Robert Andrew James
University of Wollongong

Follow this and additional works at: https://ro.uow.edu.au/theses

University of Wollongong

Copyright Warning

You may print or download ONE copy of this document for the purpose of your own research or study. The University does not authorise you to copy, communicate or otherwise make available electronically to any other person any copyright material contained on this site.

You are reminded of the following: This work is copyright. Apart from any use permitted under the Copyright Act 1968, no part of this work may be reproduced by any process, nor may any other exclusive right be exercised, without the permission of the author. Copyright owners are entitled to take legal action against persons who infringe their copyright. A reproduction of material that is protected by copyright may be a copyright infringement. A court may impose penalties and award damages in relation to offences and infringements relating to copyright material. Higher penalties may apply, and higher damages may be awarded, for offences and infringements involving the conversion of material into digital or electronic form.

Unless otherwise indicated, the views expressed in this thesis are those of the author and do not necessarily represent the views of the University of Wollongong.

Recommended Citation

James, Lloyd Robert Andrew, An investigation into the biological activity of gold anti-arthritic compounds and gold nanoparticles, Doctor of Philosophy thesis, School of Chemistry, University of Wollongong, 2016. https://ro.uow.edu.au/theses/4673

Research Online is the open access institutional repository for the University of Wollongong. For further information contact the UOW Library: research-pubs@uow.edu.au

UNIVERSITY OF WOLLONGONG

School of Chemistry

An Investigation into the Biological Activity of Gold Anti-arthritic Compounds and Gold Nanoparticles

Lloyd Robert Andrew James

This thesis is presented as part of the requirement for the Award of the Degree of Doctor of Philosophy of the University of Wollongong

March 2016

Primary Supervisor: Stephen Ralph

Co-supervisors: Carolyn Dillon, Ronald Sluyter and Jennifer Beck

Certification

I, Lloyd Robert Andrew James, declare that this thesis, submitted in partial fulfilment of the requirements for the award of Doctor of Philosophy, in the School of Chemistry, University of Wollongong, is wholly my own work unless otherwise referenced or acknowledged. The document has not been submitted for qualifications at any other academic institution.

Lloyd James

21 March 2016

Publications

James, L. R. A.; Xu, Z.-Q.; Sluyter, R.; Hawksworth, E. L.; Kelso, C.; Lai, B.; Paterson, D. J.; de Jonge, M. D.; Dixon, N. E.; Beck, J. L.; Ralph, S. F.; Dillon, C. T. An investigation into the interactions of gold nanoparticles and anti-arthritic drugs with macrophages, and their reactivity towards thioredoxin reductase, *Journal of Inorganic Biochemistry*, **2015**, *142*, 28-38.

Abstract

The overall aim of this project was to compare the interactions of anti-arthritic gold(I) compounds and gold nanoparticles, with RAW264.7 macrophage cells and the redox protein thioredoxin reductase. Cytotoxicity studies showed that auranofin exhibited the greatest toxicity towards the macrophages, with an IC_{50} of 4 μM after 24 h treatment. Aurothiosulfate and aurothiomalate proved to be far less toxic than auranofin, whilst citrate-stabilised gold nanoparticles were non-toxic when administered at a concentration of 60 μM. Cellular gold uptake experiments were performed using graphite furnace atomic absorption spectroscopy. The results of these experiments showed that treatment of the macrophages with gold nanoparticles led to greater levels of gold incorporation than treatment with aurothiomalate, aurothiosulfate or auranofin.

The sub-cellular distribution of gold in macrophages treated with auranofin, aurothiomalate or gold nanoparticles was investigated using synchrotron radiation X-ray fluorescence microscopy. These experiments were performed using small numbers of macrophages at the Advanced Photon Source (Argonne National Laboratory, USA) and showed that gold was distributed throughout the cells that had been treated with auranofin. In contrast, treatment with aurothiomalate or gold nanoparticles led to discrete hotspots within cells, which was attributed to formation of lysosomal bodies dense with gold. Similar cellular gold distribution experiments were performed at the Australian Synchrotron using larger populations of macrophages. The results of these experiments showed that treatment with auranofin or aurothiomalate led to a non-uniform uptake pattern across the cell populations, whilst treatment with gold nanoparticles resulted in a more uniform pattern of uptake. Scanning electron microscopy experiments provided supporting evidence that the gold associated with the

macrophages was internalised to varying depths within the cells, and not simply bound to their surfaces.

A series of investigations were performed that examined the effects on macrophage production of various cytokines associated with the inflammation response, resulting from treatment with gold compounds or nanoparticles before activation using lipopolysaccharide. Treatment with aurothiomalate was shown to have a minimal effect on the production of nitric oxide, reactive oxygen species and tumor necrosis factor. In contrast, treatment of the cells with auranofin resulted in much stronger inhibitory effects, with nitric oxide production reduced by 99%, reactive oxygen species production reduced by 94% and tumor necrosis factor production reduced by 52%. Somewhat surprisingly, treatment of the macrophages with gold nanoparticles did not affect inflammation mediator production, despite evidence from other experiments of extensive uptake and internalisation. A second series of investigations into inflammation mediator production was conducted using a number of commercially available gold nanoparticles, which varied in size and/or the composition of their protective outer shell. These experiments showed that none of the different types of gold nanoparticles were able to markedly affect the production of nitric oxide or reactive oxygen species.

Mass spectrometric investigations were conducted into the ability of different gold(I) compounds to bind to thioredoxin reductase, an enzyme that may be an intracellular target of anti-arthritic gold complexes or gold nanoparticles. The results of these experiments showed that aurothiosulfate exhibited the most extensive binding to the enzyme, followed by auranofin, then aurothioglucose and aurothiomalate, and finally sodium dicyanoaurate. With the exception of sodium dicyanoaurate, multiple gold ions were observed to readily bind to the enzyme. In the case of auranofin, a

number of different adducts were observed in which one or more gold-triethylphosphine moieties were bound to thioredoxin reductase, indicating that the gold binding event involved displacement of the acetylthioglucose ligand in the initial coordination sphere of the metal complex. The differences in the extent of binding were attributed to each compound's susceptibility to ligand displacement reactions. Experiments conducted with gold nanoparticles provided no evidence of binding of gold to thioredoxin reductase. This was attributed to either an inability of the nanoparticles to approach the active site of the enzyme owing to steric hindrance, or the interactions being too weak to survive the ionisation conditions present in the mass spectrometer.

Acknowledgements

Firstly, I acknowledge my primary supervisor Assoc. Prof. Stephen Ralph. You have provided much more than what was simply required to get this document together. I appreciate all of the support and inspiration throughout the project, even when some of the challenges seemed insurmountable. I am also particularly thankful for the opportunities and experiences you have included me in, from conferences to bushwalks to concerts, and beyond. I cherished these extracurricular high culture experiences.

I acknowledge the rest of my supervisory team, Dr. Carolyn Dillon, Assoc. Prof Ron Sluyter and Prof. Jenny Beck. This project has been a huge, multidisciplinary undertaking that, with full sincerity, simply would not have been possible without your specific advice and expertise. Thank you Carolyn, for putting in the hard yards, keeping me company at the synchrotrons and the electron microscopy labs; your efforts were noted and deeply appreciated. Thank you Jenny, for guiding me through the challenges of protein mass spectrometry, and for all the other advice along the way. Thank you Ron, for your patience as I bumbled my way into cell biology. Much of your more general advice has been very useful in shaping my goals for the project as a whole.

I acknowledge the help of Dr. Celine Kelso for training me and helping me crack some of the deeper problems in the thioredoxin reductase experiments (they wouldn't have been possible without your help!). I acknowledge and thank Dr. Zhi-Qiang Xu for guiding me through the expression of thioredoxin reductase. I acknowledge Prof. Nicholas Dixon for his advice in the thioredoxin reductase expression and mass spectrometry experiments, as well as in revising our Journal of Inorganic Biochemistry paper. I acknowledge Dr. Tony Romeo for helping run the electron microscopy experiments. I acknowledge Dr. David Paterson and Dr. Martin de

Jonge, and Dr. Barry Lai for helping run the experiments at the Australian Synchrotron and Advanced Photon Source, respectively. I acknowledge Prof. David Steel for his advice on the statistical analyses. I acknowledge and thank Dr. Matt Padula for doing the proteomics analysis on our thioredoxin reductase samples.

I thank Assoc. Prof. Glennys O'Brien, Dr. Simon Bedford, Dr. Christopher Richardson, Assoc. Prof Stephen Wilson, Cathy Lancaster and Sue Butler for giving me the opportunity to teach undergraduate chemistry. I have learnt much from your advice and from teaching those classes that I will carry onwards with me.

I acknowledge my lab mates in the Dillon and Sluyter labs, in particular Emma Hawksworth, Judith Carrall and Nicholas Geraghty. The discussions we had, bouncing scientific ideas and problems (or providing escapism from them) was deeply appreciated. I am proud to call you my friends.

I would like to thank my friends Aaron Fraietta, Sean Sweeney-Knapp, Anita Quinn, Luke Sweetman, Cassandra Smith, Holly Warren, Consulato Cara, Reece Gately, Jayne Emms, Kimberley Davis, Thomas Griffiths, Monica Birrento and Leighton Alcock for helping me keep it together over the years. I hold our memories together dearly and look forward to making many more in the years to come.

To my parents and grandmother, thank you. I thank you for helping me hold it together, for supporting me financially and emotionally and believing in my ability to get this thing done even when I thought I couldn't.

And finally, to Elisa: I can't imagine how I could have done this without you by my side. Your patience can probably only be appreciated by someone who has done a PhD or supported someone through a PhD. These years in limbo have been tough, but now they are over and we can begin to shape our lives together.

Table of Contents

List of Figures:

List of Tables:

List of Equations:

Abbreviations:

10×D-PBS	concentrated Dulbecco's phosphate-buffered saline
7AAD	7-aminoactinomycin D
Ag NPs	silver nanoparticles
AIDS	acquired immune deficiency syndrome
ANOVA	analysis of variance
APS	Advanced Photon Source
AS	Australian Synchrotron
ATO	arsenic trioxide
Au NPs	gold nanoparticles
bipy	bipyridine
CQ	chloroquine
D-PBS	Dulbecco's phosphate-buffered saline
d2pypp	1,3-bis(di-2-pyridylphosphino)propane
damp	dimethylaminomethylphenyl
DCF	2',7'-dichlorofluorescein
$DCFH_2$-DA	2',7'-dichlorodihydrofluorescein diacetate
DMSO	dimethylsulfoxide
DNA	deoxyribonucleic acid
DTT	dithiothreitol
DMARD	disease modifying anti-rheumatic drug
dppe	1,2-bis(diphenylphosphino)ethane
DTNB	5,5'-dithiobis-(2-nitrobenzoic acid)
EDTA	ethylenediaminetetraacetic acid
EDX	energy dispersive X-ray spectroscopy
ELISA	enzyme-linked immunosorbent assay
ESI-MS	electrospray ionisation mass spectrometry
FAD	flavin adenine dinucleotide
FBS	fetal bovine serum
FESEM	field emission scanning electron microscopy
GFAAS	graphite furnace atomic absorption spectroscopy
GSR	glutathione reductase
HEPES	4-(2-hydroxyethyl)-1-piperazineethanesulfonic acid
HIV	human immunodeficiency virus
HSA	human serum albumin
hTrxR	human thioredoxin reductase
IC_{50}	half maximal inhibitory concentration
Ig	immunoglobulin
IL	interleukin
IPTG	isopropyl-β-D-thiogalactoside
LC/MS	liquid chromatography/mass spectrometry
LDH	lactate dehydrogenase
LPS	lipopolysaccharide

MALDI-MS	matrix-assisted laser desorption ionisation mass spectrometry
MFI	median fluorescence intensity
MTT	3-(4,5-dimethylthiazol-2-yl)-2,5-diphenyltetrazolium bromide
NADPH	nicotinamide adenine dinucleotide phosphate
NED	*N*-(1-napthyl)ethylenediamine dihydrochloride
NF-κβ	nuclear factor-κβ
NMR	nuclear magnetic resonance
NO	nitric oxide
NSAID	nonsteroidal anti-inflammatory drug
PBMCs	peripheral blood mononuclear cells
PBS	phosphate-buffered saline
PEG	polyethylene glycol
PEt_3	triethylphosphine
PLN	popliteal lymph node
RA	rheumatoid arthritis
ROS	reactive oxygen species
RPMI-1640	Roswell Park Memorial Institute-1640
rTrxR	rat thioredoxin reductase
SDS-PAGE	sodium dodecyl sulfate polyacrylamide gel electrophoresis
Sec	selenocysteine
SR-XRF	synchrotron radiation X-ray fluorescence
TEM	transmission electron microscopy
terpy	terpyridyl
TLR	toll-like receptor
TNF	tumour necrosis factor
Trx	thioredoxin
TrxR	thioredoxin reductase
TWEEN	polysorbate-20

Chapter 1:
Introduction

The usage of gold(I) compounds for the treatment of rheumatoid arthritis has a history that spans the 1930s until the present day. However, in modern times, these compounds have become less popular due to the rise of newer, more efficacious therapeutics with reduced side-effects. Intriguingly, recent studies have also shown that gold nanoparticles might have potential for the treatment of rheumatoid arthritis that exceeds that of the traditional gold(I) compounds. Consequently, this chapter provides a brief review of rheumatoid arthritis, with emphasis on the role of macrophages in disease progression, and the development of modern therapeutics. The discovery of clinical gold anti-arthritic drugs is presented, including descriptions of what is known about their mechanisms of action. A survey of research into the potential of new gold compounds as treatments for other diseases is also presented. The biological role of thioredoxin reductase, an enzyme thought to be an important biological target of gold(I) compounds, is discussed, along with the conflicting results of investigations into the biological interactions of gold nanoparticles.

1.1 Rheumatoid Arthritis

Rheumatoid arthritis (RA) is a chronic autoimmune disease that typically arises as inflammation around the synovial joints of the body, causing discomfort and difficulty in movement. While joint swelling is often considered the defining characteristic of the disease, inflammation in the membranes around the heart or lungs, or in subcutaneous tissue is also observed in a large number of patients.[1] The prevalence rate of RA in the developed world is estimated to be approximately 0.5 – 1%,[2] with the disease usually presenting between ages 45 and 65,[3] and occurring more frequently in women.[4] **Table 1.1** shows the prevalence rates of RA in selected countries, which were compiled from several studies performed between 1997 and 2003.[5] In Australia, approximately 445,000 people reported having RA in 2014 giving a prevalence rate of 1.85 per 100 inhabitants.[6] Patients with RA have a lower life expectancy compared to the general populous, with men and women expected to live 4 and 10 years shorter, respectively.[7] This increased mortality has not been linked directly to joint damage that occurs due to the disease, but is instead likely to be due to other complications such as heart attack.[8,9]

Table 1.1: Prevalence rates of rheumatoid arthritis in selected countries.[5]

Country	Prevalence rate (per 100 inhabitants)	Country	Prevalence rate (per 100 inhabitants)
Brazil	0.5	Japan	0.3
China	0.2 – 0.3	Norway	0.4 – 0.5
England	0.8 – 1.1	Netherlands	0.9
France	0.6	Turkey	0.5
Indonesia	0.2 – 0.3	United States	0.9 – 1.1

While direct causes of the disease have still not been definitively identified, both genetic and environmental factors are thought to play a role.[2,10] The most important genetic factor centres on inheritance of a specific major histocompatibility complex antigen, known as HLA-DRB1.[11] A number of environmental risk factors have been identified, with smoking being the primary one.[2,12,13] There have also been a number of weaker links proposed between the incidence of RA and alcohol consumption, vitamin D intake, oral contraceptive usage and birthweight.[14] It has been postulated that certain viral infections may also lead to development of the disease. For example, in one study, three types of herpes viruses were detected in higher levels in the serum and peripheral blood mononuclear cells (PBMCs) of patients with RA.[15] However, a causal link has yet to be established, as the presence of the virus may also be due to the fact that the immune system of patients with RA is significantly compromised. Expression of auto-antibodies, which are antibodies that target a person's own proteins, are also thought to play a part in the disease. Between 50 – 80% of patients with RA have detectable levels of rheumatoid factor or anti-citrullinated protein antibodies.[2] This enables the presence of either of these two classes of protein to be used as biomarkers for disease diagnosis.[2]

Disease progression is associated with increased severity of synovitis (inflammation of the synovial lining), and eventual loss of joint function. Synovitis is largely caused by proliferation of synovial fibroblasts and infiltration by macrophages, T and B lymphocytes, plasma cells, and dendritic cells.[16] These cells all contribute to disease progression by producing pro-inflammatory cytokines and destructive proteases, which cause thinning of cartilage and degradation of bone. Progressive damage to the joints eventually leads to loss of function and personal disability in addition to decreased quality of life.[17] The specific role macrophages play in the disease through cytokine emission is discussed in the following section.

1.1.1 The Role of Macrophages and Immune Mediators

Macrophages are one of the major cell types involved in the progression of RA. The primary role of macrophages is to phagocytose cellular debris and pathogens; however, they also serve to produce inflammation and stimulate other immune cells. Macrophages can be differentiated into two different types, M1 and M2, which promote and reduce inflammation, respectively.[18] They perform these roles by emitting a number of immune mediators. These include the pro-inflammatory cytokines tumour necrosis factor (TNF), interleukin (IL)-1, IL-6, IL-12, the anti-inflammatory cytokine IL-10, as well as reactive oxygen species (ROS) and nitric oxide (NO).[16,19] A diagram depicting the relationship of macrophages with cytokine expression and joint destruction in RA is shown in **Figure 1.1**.[20]

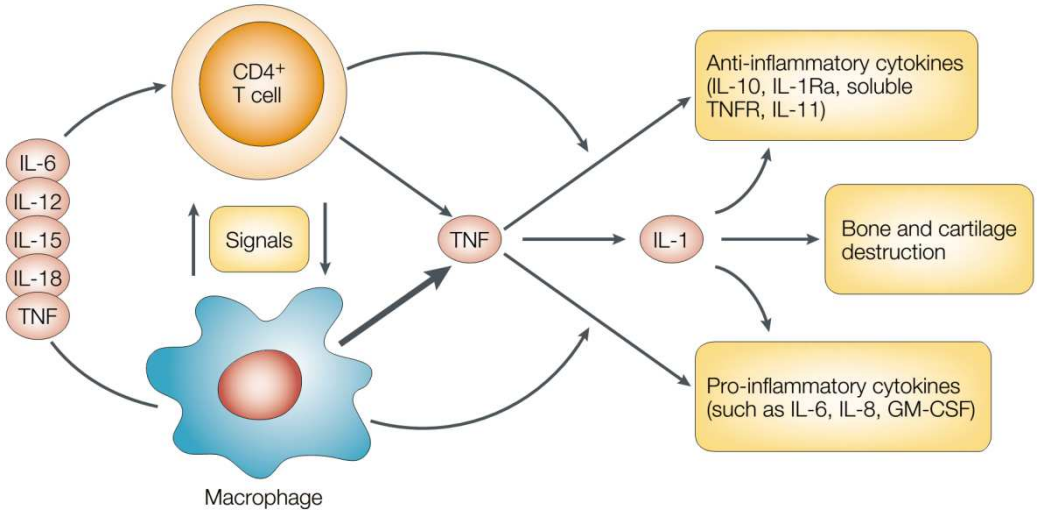

Figure 1.1: Key cytokine and cellular interactions in rheumatoid arthritis. Reprinted with permission from Macmillan Publishers Ltd: Nature Reviews Immunology, vol. 2, p. 364-371, copyright May 2002.[20]

High levels of TNF expression in the synovial fluid is a characteristic feature of RA and strongly linked to progression of the disease. This is believed to be due to the ability of TNF to stimulate the release of a large number of other inflammatory cytokines.[21] In addition to cytokine release, TNF can signal oxidative burst,[22] stimulate

production of prostaglandins,[23] and induce synthesis of matrix metalloproteinases.[24,25] Prostaglandins are a group of lipids that signal inflammation,[26] while matrix metalloproteinases are enzymes that cause cartilage destruction and bone resorption.[16]

IL-1 refers to a subset of cytokines involved in immune and inflammatory responses. Two of the more prominent molecules in this group are IL-1α, which is primarily located intracellularly, and IL-1β, which is secreted from cells. A third, important member of this group of cytokines is IL-1Ra, which acts as an antagonist for IL-1α and IL-1β by competing for the same receptors.[27] Like TNF, IL-1β has also been linked to the progression of RA, as it is expressed in greater quantities in the synovial fluid[28] and plasma of patients with this disease.[29] Further evidence of the importance of IL-1β is provided by observations of a correlation between plasma levels of this cytokine, with stiffness and pain scores in people suffering from RA. The functions of TNF and IL-1 seem to overlap. For example, IL-1 induces matrix metalloproteinase synthesis in a similar fashion to TNF.[30,31] Some animal models seem to suggest that IL-1 plays a larger role in joint destruction, while TNF is more important in production of inflammation.[32] However, it is highly likely that both cytokines play important roles in both processes. This is highlighted by a study which showed that each cytokine can upregulate production of the other.[27]

The term ROS refers to a number of compounds containing oxygen that are involved in cell signalling and homeostasis, and includes O_2, O_2^-, H_2O_2 and •OH.[33] Oxidative stress occurs when these molecules are produced in increased quantities, and can lead to significant damage to deoxyribonucleic acid (DNA), proteins and lipids.[34] In addition, ROS can degrade extracellular matrix materials such as collagens and proteoglycans,[35] which directly leads to joint degradation and inflammation. In patients with RA, oxidative stress is observed in the synovial fluid along with a decrease in the

activity of anti-oxidant enzymes.[36] This provides support for the conclusion that production of ROS is one of the main mechanisms of pathogenesis of the disease.[37]

NO is a free radical produced by a class of enzymes known as nitric oxide synthases. NO has a variety of biological roles as a signalling molecule in processes including vasodilation, neurotransmission and immune system regulation. Owing to its reactivity, NO is a very short-lived species ($t_{1/2}$ = 6 s) and exhibits low bioavailability. This results in the actions of NO being restricted to near its site of synthesis.[38] NO can form a number of related chemical species such as NO_2, NO_2^-, NO_3^-, N_2O_3 and $ONOO^-$. In addition, it may also react directly with biomolecules such as haem groups as part of its normal functions.[39] Under general physiological conditions NO is considered to have an anti-inflammatory effect.[38] In contrast, in certain inflammatory disorders such as RA, it is both a marker and pro-inflammatory mediator, particularly in macrophages.[40] This is illustrated by studies that showed that NO production is linked to generation of inflammatory cytokines, enhanced bone resorption,[38] diminished bone proliferation,[38] and chondrocyte apoptosis.[33] It is important to note that some studies have also shown that increased levels of cytokines result in enhanced production of NO.[40]

1.1.2 Approaches to Treatment of Rheumatoid Arthritis

Treatment of RA is usually in the form of a combination therapy involving administration of drugs belonging to two broad categories: nonsteroidal anti-inflammatory drugs (NSAIDs) and disease modifying anti-rheumatic drugs (DMARDs). Corticosteroids are occasionally also used for providing relief from the inflammation associated with RA. However, their long term use is not recommended due to the severe side-effects associated with such treatment.[41] NSAIDs are regularly used to treat

patients with RA owing to their analgesic and anti-pyretic effects, which result from inhibition of the cyclooxygenase class of enzymes.[42,43] These enzymes catalyse the first two steps in the synthesis of prostaglandins.[26] Although NSAIDs are very effective at providing relief from the pain associated with inflammation, there are concerns over their continued use for RA therapy as they can lower prostaglandin levels in the stomach, causing ulceration and bleeding. Lower prostaglandin levels may also result in kidney damage, leading to renal failure.[26]

In comparison to NSAIDs, the DMARDs are used to treat RA with the intention of slowing or halting the disease. The structures of some clinically used DMARDs are shown in **Figure 1.2**. Two examples of DMARDs are the anti-malarial compounds chloroquine and hydroxychloroquine (**Figure 1.2 a and b**), which have been used since the 1950s, and act by inhibiting the release of IL-1 by monocytes.[44] *D*-Penicillamine (**Figure 1.2 c**) is another example of a DMARD and has been used since the 1970s. It is thought to act as a immunosuppressant, by decreasing proliferation of T lymphocytes and inhibiting macrophage function.[41] The purine analogue sulfasalazine (**Figure 1.2 d**), also acts as a DMARD by reducing lymphocyte numbers,[45,46] while cyclosporine (**Figure 1.2 e**), which was developed in the 1970s to prevent rejection of transplanted organs, is thought to work by inhibiting IL-1 release by monocytes and IL-2 release by T-helper cells.[47] More recently, the biologics infliximab and etanercept were licensed for medical use in 1998, and reduce inflammation by specifically inhibiting TNF.[48] Of all the DMARDs used by rheumatologists for the treatment of RA, methotrexate (**Figure 1.2 f**) is perhaps now the most popular.[49–52] Methotrexate was originally developed as an anti-cancer compound in the 1950s, but is thought to also work as a DMARD by inhibiting purine metabolism.[41,53]

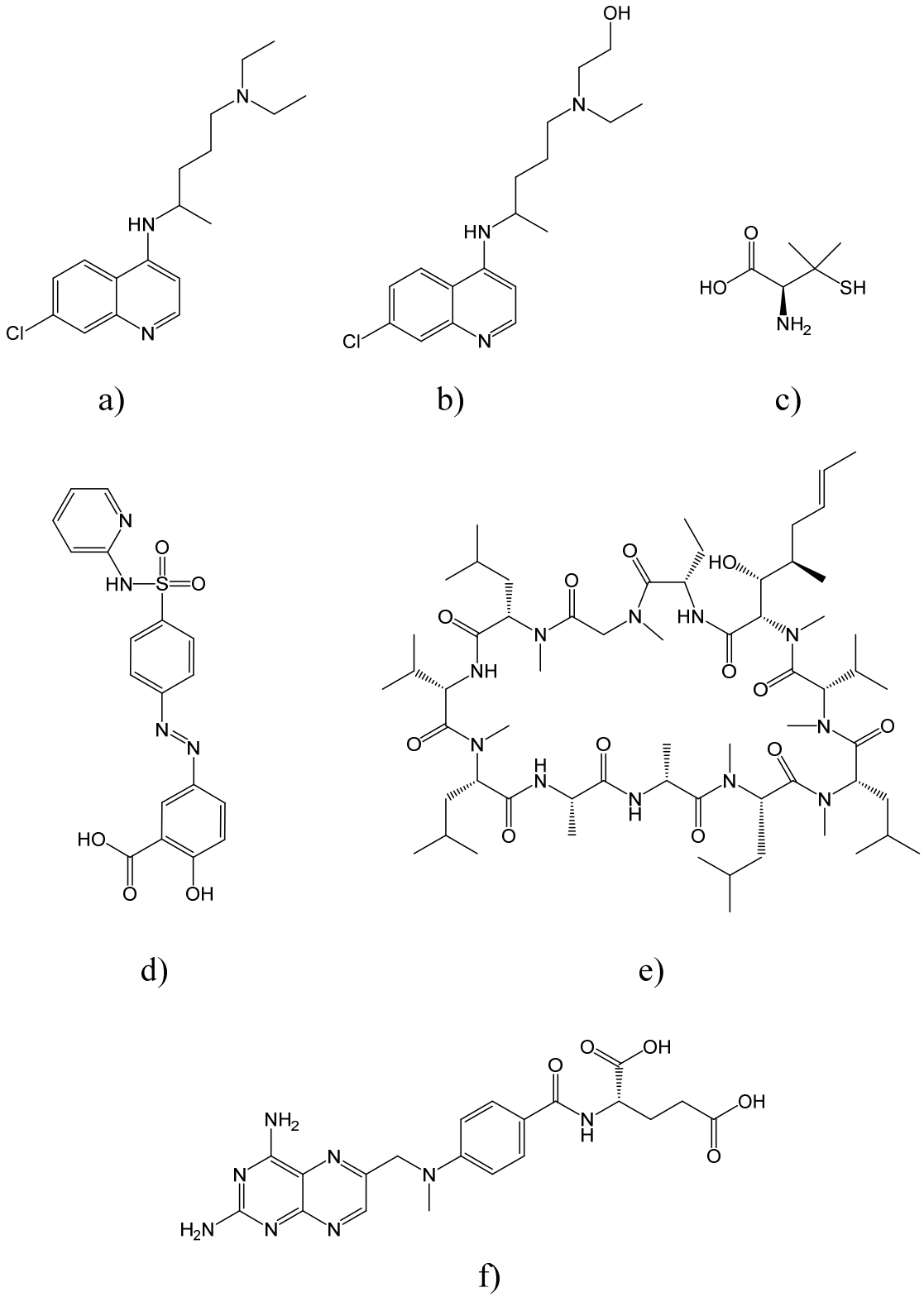

Figure 1.2: Structures of some typical disease modifying anti-rheumatic drugs used clinically for the treatment of rheumatoid arthritis: **a)** chloroquine; **b)** hydroxychloroquine; **c)** *D*-penicillamine; **d)** sulfasalazine; **e)** cyclosporine; and **f)** methotrexate.

1.1.3 Therapeutic Usage of Gold in Rheumatoid Arthritis

Another major class of DMARDs, that has been used successfully for treating RA are various gold(I) salts. **Figure 1.3** shows the structures of some of these compounds. Their clinical usage is sometimes called chrysotherapy in recognition of the Greek word 'chrysos' for gold. The history of medicinal usage of gold metal dates back thousands of years.[54] However, the usage of gold compounds for RA therapy can be traced to the discovery by Robert Koch in the late 1800s, that the gold complex $K[Au(CN)_2]$ powerfully inhibits the growth of the bacterium *Mycobacterium tuberculosis*,[55–57] the causative agent of tuberculosis. Although the ability of this gold complex to treat tuberculosis subsequently proved to be limited in part due to its toxicity, in the 1920s and 1930s, Jacques Forestier performed a number of clinical studies into the ability of various simple gold compounds to treat RA.[58–61] The impetus for these investigations was based upon the then erroneous understanding that RA was an infectious disease similar to tuberculosis.[7,62,63]

In order to investigate the potential of gold compounds for treating RA, Forestier conducted an initial trial where 15 patients were given intramuscular injections of sodium aurothiopropanol sulfonate (Allochrysine, **Figure 1.3 a**) on a weekly basis for 10-12 weeks.[58] After completion of the trial, five patients had shown an excellent response, while a further five patients showed significant improvement in their symptoms, and the remaining five showed minimal to no response. Despite the overall positive results from this trial, Forestier warned of some toxic side effects from treatment with gold, including fever, diarrhoea and vomiting. A second trial into the effects of gold therapy on patients with RA was published by Forestier in 1930.[59] This study involved optimised administration of Allochrysine to a total of 33 patients. Forestier noted that beneficial effects of gold treatment were not seen until 3-6 months

after treatment had commenced. In 1934, Forestier published the results of a much larger trial, involving 500 patients with RA who were treated with a variety of gold salts.[61] On this occasion a 70 – 80% success rate was reported for patients receiving gold salts via injection, with sodium aurothiomalate (brand name Myocrisin, **Figure 1.3 b**) and aurothioglucose (brand name Solganol, **Figure 1.3 d**) being the most effective gold compounds. The successful treatment of patients with RA using gold compounds was confirmed in a number of subsequent papers,[63–66] and led to the widespread clinical usage of gold for this purpose for several decades and, to a lesser extent, the present.

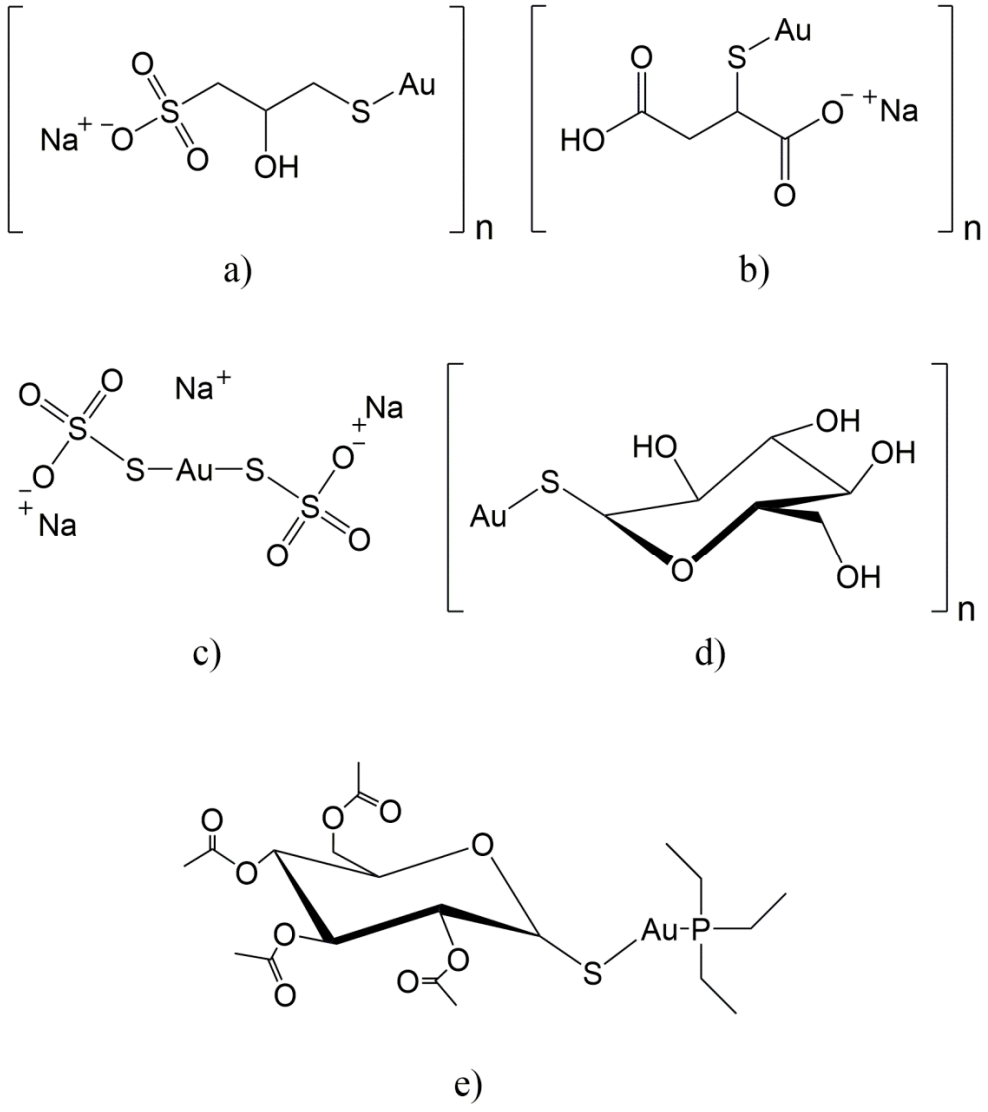

Figure 1.3: Structures of some typical gold(I) compounds used clinically for treatment of rheumatoid arthritis: **a)** sodium aurothiopropanol sulfonate; **b)** sodium aurothiomalate; **c)** sodium aurothiosulfate; **d)** aurothioglucose; and **e)** auranofin.

The clinical effectiveness of gold compounds for treating RA, not surprisingly, is often limited by the extent to which side effects occur. In approximately 40% of patients undergoing chrysotherapy a variety of side effects are observed, including mouth ulcers, skin rashes and dermatitis, anaemia, low platelet counts, elevated urine protein levels, kidney and liver damage, vomiting, diarrhoea and sometimes in the case of prolonged treatment, permanent grey/blue skin discolouration.[57] In the 1980's, a new orally administered Au(I) drug, auranofin (**Figure 1.3 e**, brand name Ridaura) was developed that was found to have fewer or less severe side-effects than the intramuscularly injected gold compounds.[67] Another contrast between auranofin and many of the other widely used chrysotherapeutic agents is that it is a discrete mononuclear compound, which is bound to thioacetylglucose and triethylphosphine ligands. Although less toxic than many other clinically used gold compounds, auranofin also proved to be less efficacious, which has limited its popularity among rheumatologists.[50,67] Today, the clinical use of gold(I) drugs for treatment of RA has largely been superseded by some of the aforementioned DMARDs, such as methotrexate, TNF inhibitors, and biologics. This is due to the increased efficacy observed at lower doses when patients are administered with these classes of therapeutic agents, as well as reduced side effects. Despite this, chrysotherapy continues to be used for treating refractory forms of RA. For example, a 2002 survey of Canadian rheumatologists reported that 40% use injectable gold(I) salts frequently, and 56% use them occasionally.[50] Similarly, a 2004 survey of British rheumatologists reported that 20 – 40% use injectable gold(I) compounds as the third or fourth choice in therapy.[51]

1.1.4 Potential Uses of Gold Compounds for Treatment of Other Diseases

While gold compounds have only found clinical use for the treatment of RA, their potential for treatment of other diseases has been noted, and is being widely investigated. This section will briefly discuss some other areas of interest for medicinal gold complexes, commencing with the search for new anti-cancer agents.

The potential of Au(I) compounds for the treatment of cancer was highlighted by studies which demonstrated the cytotoxicity of auranofin towards the HeLa cervical cancer cell line *in vitro*[68] and leukaemia cells *in vivo*.[69] This was followed by the development and screening of a number of auranofin analogues, which exhibited strong *in vitro* activity against a melanoma cell line, having half maximal inhibitory concentration (IC_{50}) values less than 5 μM.[70] However, the *in vivo* anti-cancer activity of these complexes in mice with leukaemia proved limited.[70] A series of gold(I) dppe (dppe = 1,2-bis(diphenylphosphino)ethane) complexes has also been prepared and was found to show promising *in vitro* anti-cancer activity, with $[Au(dppe)_2]Cl$ having an IC_{50} of 2 μM against melanoma cells.[71] However, these complexes also exhibited cardiovascular toxicity that precluded further development.[72] A number of gold(III) complexes featuring the dimethylaminomethylphenyl (damp) ligand have shown promising anti-cancer activity,[73] as well as other complexes containing *N*-methylimidazole, 2-methylbenzoxazole, or 2,5-dimethylbenzoxazole as ligands.[74] The structures of some of these complexes are shown in **Figure 1.4**. More recent efforts in this area have focussed on gold(I) phospholes or complexes containing *N*-heterocyclic carbene ligands, as well as a variety of Au(III) compounds designed to act as inhibitors of the enzyme thioredoxin reductase. This enzyme will be discussed in more detail in **Section 1.3**.

The potential of using gold complexes for the treatment of human immunodeficiency virus/acquired immunodeficiency syndrome (HIV/AIDS) was first sparked by a report regarding an AIDS patient that was receiving auranofin for treatment of psoriatic arthritis. The patient was refusing treatment for their HIV, yet showed a significant increase in the number of $CD4^+$ T lymphocyte cells, when a decrease would have been expected with progression of the illness.[75] Subsequently, it has been shown that dicyanoaurate inhibits proliferation of HIV in a strain of $CD4^+$ T lymphocytes,[76] and that aurothioglucose can inhibit HIV reverse transcriptase.[77] Unfortunately aurothioglucose proved ineffective in cell culture tests of HIV-inoculated lymphoid and leukaemia cells owing to lower levels of uptake.[74,77]

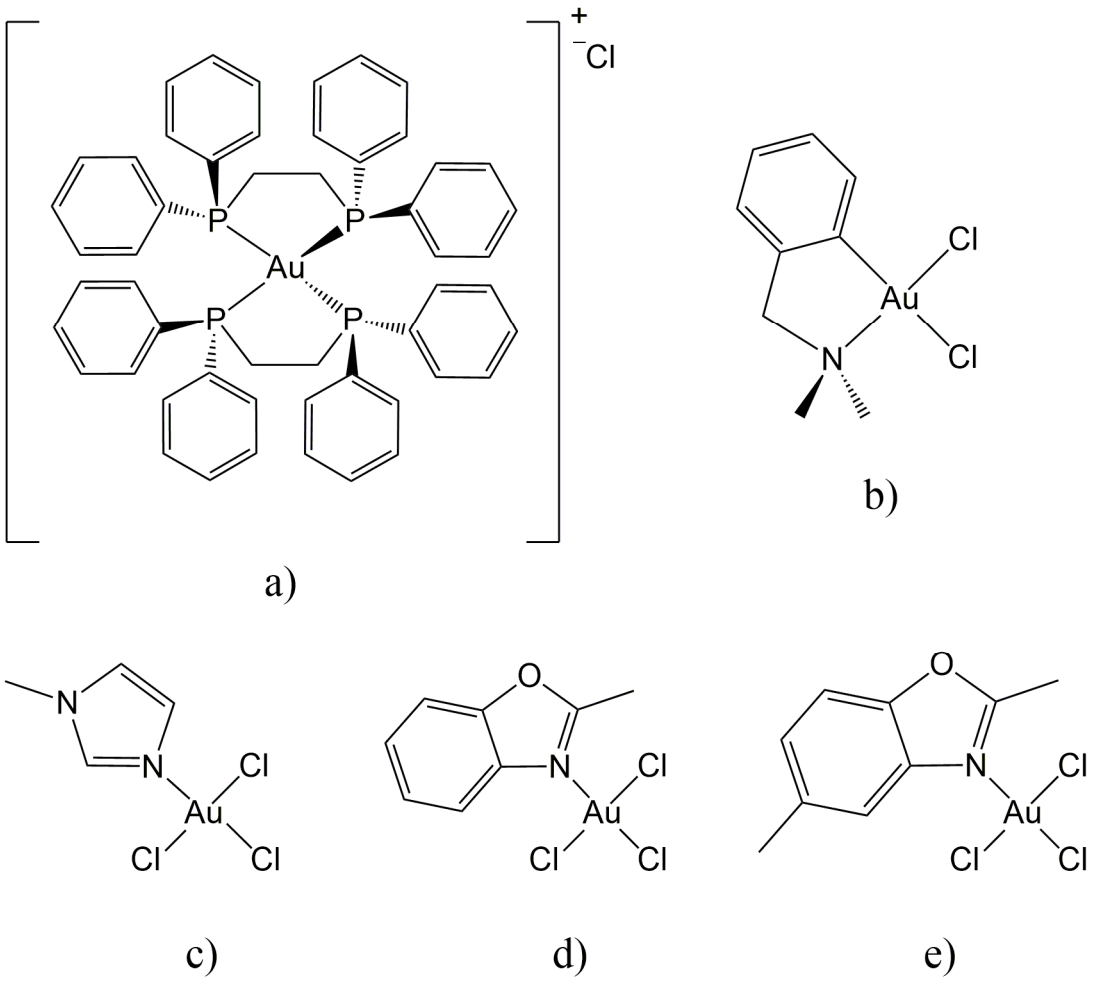

Figure 1.4: Structures of some gold(I) and gold(III) complexes investigated for anti-cancer activity: **a)** $[Au(dppe)_2]Cl$; **b)** $[Au(damp)Cl_2]$; **c)** [Au(N-methylimidazole)Cl_3]; **d)** [Au(2-methylbenzoxazole)Cl_3]; and **e)** [Au(2,5-dimethylbenzoxazole)Cl_3]

Chloroquine (CQ, **Figure 1.2 a**) has been one of the most widely used compounds for the treatment of malaria.[78] However, in recent years its effectiveness has diminished, owing to the development of resistance to the drug in the protozoan *Plasmodium falciparum*, one of the most important agents of the disease.[79] As a result, researchers have been searching for derivatives of chloroquine that are still effective against malaria. This has led to the discovery that [Au(triphenylphosphine)(CQ)]PF_6 (**Figure 1.5**), containing gold(I), showed promising *in vitro* activity against three species of *Plasmodium*.[80] When compared to the phosphate salt of chloroquine, the gold complex was found to have an IC_{50} twenty times lower towards *Plasmodium berghei*, as well as five times and ten times lower towards two strains of chloroquine-resistant *Plasmodium falciparum*. The complex also showed *in vivo* activity against rats infected with *Plasmodium berghei*, with rats treated with the Au-CQ complex exhibiting 3.5× lower numbers of parasites than rats treated with chloroquine iteself.[80]

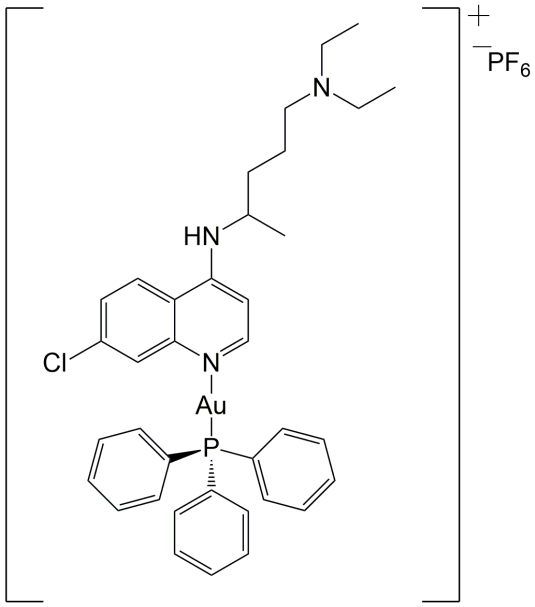

Figure 1.5: Structure of [Au(triphenylphosphine)(CQ)]PF_6, investigated for anti-malarial activity.

1.2 Mechanisms of Action of Gold Anti-Arthritic Agents

The mechanism of action of gold(I) salts used to treat RA remains an area of debate, but is generally thought to involve a number of effects. All of the clinically used gold drugs are considered prodrugs, and undergo changes in structure through either ligand loss or a change in oxidation state to form biologically active metabolites.[57,74] The latter include $[Au(CN)_2]^-$, Au(III) complexes, Au(0), and a range of Au(I)-protein complexes that result from ligand displacement reactions. In considering the many reactions that are likely to occur *in vivo*, it is important to note that although Au(I) exhibits a high degree of thermodynamic affinity for S- and Se-containing ligands, it remains a kinetically labile metal ion. This lability allows frequent ligand exchange reactions to occur with biomolecules, especially considering the high concentrations of thiol-containing species present in plasma and cells. Some of the key features of gold drug metabolites are discussed in the following sections, followed by some of their key interactions with cells and biomolecules.

1.2.1 Gold Metabolites

The majority (80 – 95%) of the gold(I) administered to patients with RA rapidly loses a ligand and binds to human serum albumin (HSA), the most abundant protein in plasma.[81] The HSA then functions as a *de facto* transport agent and carries the bound gold(I) fragments to a large variety of other binding sites in the body.[74] In the case of auranofin, it is only the tetraacetylthioglucose ligand which is initially lost during the binding process with HSA,[82] whereas the polymeric gold(I) compounds typically break apart to release a single gold ion which binds to the protein, and the original coordinated ligand.[83] HSA contains 35 cysteine residues, all but one of which normally form intramolecular disulfide bonds. The one exception is Cys34; its thiol group is free to react with endogenous species,[84] and has been shown by a variety of techniques,

including electrospray ionisation mass spectrometry (ESI-MS) to be the main residue to which gold(I) drugs bind.[85–88]

One important set of reactions that occurs after gold(I) complexes are administered to patients are those leading to formation of $[Au(CN)_2]^-$. Thiocyanate (SCN^-) is a normal component of plasma owing to direct dietary intake, and may be converted directly to cyanide by the enzyme, myeloperoxidase, which is found in plasma or polymorphic leukocytes.[89] Owing to the higher affinity of gold(I) for cyanide compared to thiol ligands,[90,91] it is highly likely that Au-HSA complexes *in vivo* might undergo one or more ligand displacement reactions to form a cyanoaurate-thiol complex, or the dicyanoaurate ion.[57,92] The dicyanoaurate ion is thought to facilitate gold uptake into cells, as it has been shown to be rapidly taken up by both red blood cells[76,93] and T lympocytes.[76] Its importance as a metabolite of compounds used for chrysotherapy is highlighted by studies that showed patients who are also cigarette smokers have higher incidences of side effects resulting from an increased formation of $[Au(CN)_2]^-$ and associated higher levels of gold uptake in cells.[93,94]

It is also likely that $[Au(CN)_2]^-$ participates in redox chemistry *in vivo*. For example, it has been shown that $[Au(CN)_2]^-$ undergoes oxidation in the presence of the biological oxidant, hypochlorite, to form *trans*-$[Au(CN)_2Cl_2]^-$.[95] The same study also showed that in the presence of excess cyanide ions, this species rapidly forms $[Au(CN)_4]^-$. Further evidence of redox reactions involving various gold metabolites is discussed below.

There is a large amount of evidence to suggest that formation of Au(III) is an important outcome of administration of Au(I) compounds to patients as part of a chrysotherapy treatment regime.[89,95–99] For example, it has been demonstrated *in vitro*

that Au(I) may be oxidised to Au(III) by hypochlorous acid,[100] which is generated *in vivo* by myeloperoxidase in phagolysosomes of activated macrophages and granulocytes.[101] In another study that searched for evidence that gold(III) is formed *in vivo*, the proliferation of T-lymphocytes, which are adaptive immune cells, was measured using a popliteal lymph node (PLN) assay.[96] This assay scores proliferation by comparing the weight of a treated PLN and an untreated PLN within the same animal. Proliferation of T-lymphocytes in response to exposure to a molecule is strong evidence of sensitisation, or prior exposure, to that chemical compound. For this experiment, mice were treated with aurothiomalate, and 5-7 weeks later were exposed to gold(I) or gold(III) compounds. Six days later the PLN assay was performed to assess if proliferation had occurred. Neither aurothiomalate nor AuCl caused sensitisation, but exposure to either $AuCl_3$ or $HAuCl_4$ did cause T-lymphocyte proliferation. This suggests that there had been prior *in vivo* formation of Au(III) from the aurothiomalate initially given to the mice.

Another investigation set out to test the hypothesis that mononuclear phagocytes are a significant source of oxidation of Au(I) compounds to Au(III) species.[98] It was demonstrated that Au(III)-primed T-lymphocytes exhibited no sensitisation towards aurothiomalate, but did show sensitisation after exposure to $HAuCl_4$, or to peritoneal cells containing mononuclear phagocytes that were isolated from aurothiomalate-treated rats. In the same study, mononuclear phagocytes were separated from peritoneal cells, then treated with aurothiomalate, prior to being exposed to Au(III)-primed T-lymphocytes. Evidence of significant sensitisation was obtained, indicating that it was likely that the aurothiomalate had been oxidised to Au(III) compounds within the phagocytes, probably by hypochlorous acid produced by myeloperoxidase.[98]

To confirm these observations in humans, patients with RA who had been treated using chrysotherapy compounds and suffered adverse side effects, then had their T-lymphocytes collected, cultured *in vitro*, and exposed to either aurothiomalate or $HAuCl_4$, or one of several copper, platinum or nickel salts.[97] Only treatment with $HAuCl_4$ resulted in sensitisation, but only in patients who also suffered from dermatitis as a side effect. These findings reinforce the view that Au(III) species are metabolites of chrysotherapeutic agents, and also suggest that Au(III) formation may be associated with some of the adverse effects of treatment.

The possibility of Au(III) metabolites causing some of the side effects associated with chrysotherapy is plausible in view of their highly reactive nature in biological environments.[57] Au(III) compounds are strong oxidants and react readily with a host of biological reductants. For example, it has been shown that Au(III) compounds can oxidise thiols to sulfides,[74] and thioethers such as methionine to sulfoxides.[102] Furthermore, they can even oxidise disulfides.[103] Each of the above reactions can result in significant changes to the tertiary structure, and therefore, the function of various biomolecules. These events could be beneficial for the treatment of RA if they involve biomolecules that enhance inflammation or produce reactive oxidative species. Alternatively the reactions may result in harm if the altered biomolecules then interact with non-specific targets in other regions of the body, as is likely to be the case.

Another notable metabolite that may be formed during chrysotherapy is elemental gold. Zou *et al*. used nuclear magnetic resonance (NMR) spectroscopy to study the reactions of $[AuCl_4]^-$ with glycine under various conditions.[104] They indicated that Au(III) could oxidise the glycine, resulting in loss of NH_4^+ and formation of glyoxylic acid. It was also suggested that another molecule of $[AuCl_4]^-$ could further oxidise the glyoxylic acid to produce formic acid, CO_2 and Au(0). These results follow

on from earlier work indicating that Au(0) is formed as a major product from the oxidation of disulfides by Au(III) complexes.[103] While there has been a limited number of investigations into the likelihood and clinical importance of *in vivo* formation of Au(0) during chrysotherapy, a large amount of work has been performed examining the biological interactions of Au(0) in the form of gold nanoparticles. These will be discussed further in **Section 1.4**.

There is a body of evidence which suggests that the majority of intracellular gold resulting from chrysotherapy is localised in lysosomal bodies that have a characteristic morphology.[105,106] These special lysosomes have been termed aurosomes, and have been the subject of investigations using synchrotron radiation X-ray absorption spectroscopy.[107,108] In these experiments, X-ray absorption near-edge structure spectroscopy and X-ray absorption fine structure measurements were performed. The results of these studies demonstrated that aurosomes isolated from the kidneys of rats treated with aurothiomalate contained Au(I), which was likely bound to two sulfur atoms.[107] In addition, it was found that even when gold was administered as Au(III) (as $Na[AuCl_4]$), the gold in the aurosomes existed as Au(I) and was probably bound to two sulfur atoms.[107] Similar experiments performed with auranofin also showed that the gold in the aurosomes was bound to two sulfur atoms,[108] indicating that the triethylphosphine group had been displaced, as expected.

What is notable about the results discussed above is that despite many reports suggesting that formation of Au(III) occurs *in vivo*, and that production of Au(0) is also likely, there is no spectroscopic evidence available that shows the formation of either. This may be reflective of the short-lived nature of any Au(III) metabolites formed *in vivo*, as well as the overall complexity of the Au(III)/Au(I)/Au(0) redox system. Further

studies are therefore required to fully elucidate the redox reactions that take place after administration of gold compounds to living organisms.

1.2.2 The Sulfhydryl Shuttle Mechanism

The sulfhydryl or thiol shuttle mechanism has been proposed as the most likely method of cellular uptake for gold metabolites. This mechanism is depicted in **Figure 1.6** and stems from studies of auranofin uptake.[109] In biological media the first reaction that auranofin most likely undergoes is loss of the acetylthioglucose ligand, resulting in a gold-triethylphosphine moiety, which may become bound to any number of membrane transport proteins containing sulfhydryl groups. These subsequently carry the $AuPEt_3$ (PEt_3 = triethylphosphine) moiety across cell membranes and release it into the cytoplasm, where it may cause a number of effects. Gold transport out of the cell also involves sulfhydryl-containing membrane transport proteins, and is notably an energy-independent process.[109] In other words, the transport of gold into or out of a cell by the sulfhydryl shuttle mechanism is controlled by an equilibrium between intracellular and extracellular gold sources. The existence of this equilibrium was confirmed by an experiment in which additional serum was added to a culture medium containing macrophages.[109] Extracellular gold became serum bound, resulting in a net movement of gold out of the macrophages and into the culture medium. This is consistent with expectations if an equilibrium exists between the intra- and extracellular regions.[109] Similarly, red blood cells that had accumulated gold as a result of being treated with auranofin, showed a marked efflux of gold when resuspended in fresh serum.[110]

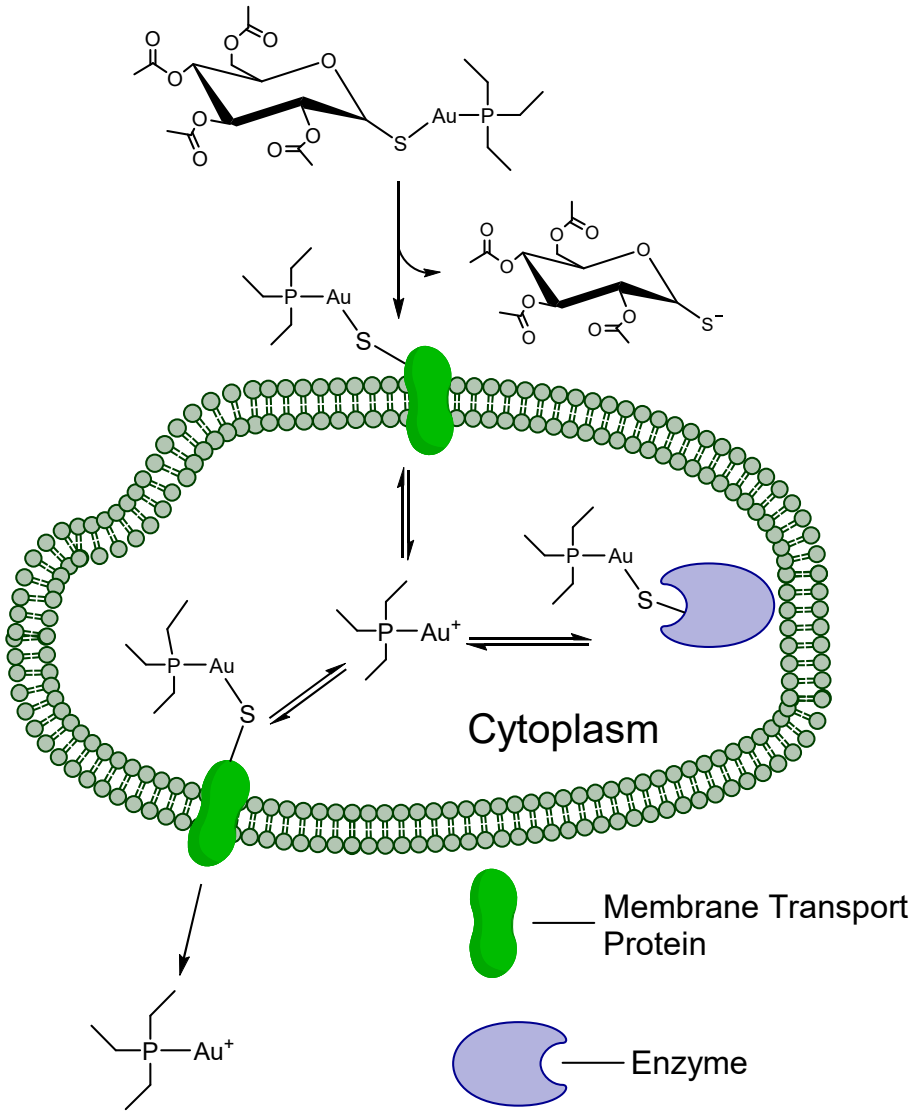

Figure 1.6: The sulfhydryl shuttle mechanism for auranofin uptake and efflux by cells. Adapted with permission from Chemical Reviews, 1999, vol. 99 (9), p. 2589-2600.[74] Copyright 1999 American Chemical Society.

The sulfhydryl shuttle mechanism is also believed to be the principal means by which other metabolites of chrysotherapy drugs, such as Au-HSA, and gold-cyanide complexes, enter cells.[74] This is because the uptake mechanism is only contingent upon a ligand displacement reaction with a membrane transport protein, which can occur due to the kinetic lability of the Au(I) ion. In the case of gold-cyanide complexes, evidence for the importance of the sulfhydryl shuttle mechanism was provided by experiments where an anion channel did not alter gold uptake by red blood cells in culture.[76] In contrast, addition of free CN^- inhibited gold uptake, indicating that ligand dissociation

is required for gold transport to occur.[76] This is consistent with what would be predicted if gold transport occurred via the sulfhydryl shuttle mechanism.[76]

1.2.3 Intracellular Gold Targets

This section will discuss some of the effects various gold metabolites have upon a broad range of cells and biomolecules. These include diminished proliferation and function of specific cell types, inhibition of cytokine expression and transcription factors, modification of receptor function, and diminished activity of specific protein targets.

One major mode of action of gold metabolites is through alteration of cell to cell signalling. It has been shown that aurothiomalate can interfere with receptor-mediated T lymphocyte signalling by inhibiting the cysteine residues at the active-site of a number of protein-tyrosine phosphatases essential for this signalling process.[111] One proposed mechanism involves Au^{+} ions that form a Cys-Au-Cys bridge between cysteine residues either in the same protein, or between two separate protein molecules.[57]

Administration of injectable gold has been shown to lead to a decrease in immunoglobulin (Ig) levels in ~50% of patients with RA, whereby severe depletion can be a problematic side-effect in some cases.[112] In particular, two studies have been performed which examined the effect of aurothiomalate upon B lymphocytes. The relevance of B lymphocytes to RA stems from the fact that they produce large quantities of extracellular IgM and rheumatoid factor.[113,114] Treatment with aurothiomalate showed decreased production of both IgM and rheumatoid factor, consistent with decreased activation of B lymphocytes. *In vitro* assays have also shown that aurothiomalate is an inhibitor of the differentiation and development of monocytes

isolated from patients with RA.[115] These processes are strongly linked to RA pathogenesis.[115]

In recent years TNF has been recognised as a critical cytokine in the development of RA. Therefore it is not surprising that a number of studies of the effects of chrysotherapy compounds on TNF expression have been performed. In one investigation, mononuclear cells were isolated from the synovial membranes of patients with RA that were undergoing aurothiomalate treatment. The levels of expression of IL-1α, IL-1β, IL-6 and TNF were all reduced, as was the number of inflammatory monocytes.[116] In another investigation, PBMCs were isolated from patients with RA and healthy individuals, and the effects of aurothiomalate with and without co-administration of the 'toll-like' receptor (TLR) 4 ligand lipopolysaccharide (LPS), upon TNF production were determined.[117] It was found that when PBMCs were pre-incubated with LPS and subsequently treated with aurothiomalate, TNF production was inhibited regardless of whether the PBMCs were sourced from RA patients or healthy individuals. In contrast, treatment of PBMCs only with aurothiomalate caused a mild increase in TNF production. A subsequent investigation using PBMCs only from healthy individuals found significant heterogeneity in the samples, but still largely confirmed the results of the previous study.[118] In particular, the authors highlighted that aurothiomalate could stimulate or inhibit production of TNF, depending on whether LPS was also absent or present, respectively.[118] These results highlight the intricate balance present between inflammatory cytokine expression and inhibition.[118]

As discussed earlier, the majority of gold present in cells isolated from patients with RA undergoing chrysotherapy is found in lysosomal bodies termed aurosomes,[105,106] where it is bound to two sulfur atoms.[107] This localisation of gold inhibits release of lysosomal enzymes that are otherwise responsible for joint

degradation.[57] *In vitro* experiments have shown that auranofin, aurothiomalate and aurothioglucose all inhibit resorption of bone by rat osteoclasts, and exhibit cytotoxicity towards an osteoblast-like cell line.[119] Leukocyte infiltration of synovial joints is a key factor in RA pathogenesis, that is targeted and facilitated by the expression of adhesion molecules by endothelial cells. Aurothiomalate inhibits the cytokine-stimulated expression of some of these adhesion molecules.[120] Similarly, the ability of cytokines to induce polymorphonuclear neutrophils to adhere to endothelial cells is inhibited by auranofin and aurothiomalate. The alternative DMARD sulfasalazine did not elicit similar results, indicating that the two classes of DMARDs may exhibit different mechanisms of biological activity.[121]

Aurothiomalate also inhibits both the progesterone[122] and glucocorticoid[123] transcription receptors, as well as the activator protein 1 transcription factor.[124] In addition, auranofin, aurothiomalate, aurothioglucose and $AuCl_3$ inhibited IκB kinase in RAW264.7 mouse macrophages that had been stimulated by LPS.[125] This was a significant result because IκB kinase activates nuclear factor-κβ (NF-κβ), a transcription factor implicated in the expression of many inflammatory genes. The authors were also able to demonstrate that inhibition of IκB kinase by auranofin led to reduced NF-κβ activity, and suggested that inhibition was likely to be a result of blocking of the thiol group at the active site.

While gold may interact with a large number of intracellular enzymes, two in particular have attracted attention in discussions of the modes of action of anti-arthritic gold drugs. These are thioredoxin reductase (TrxR), which will be discussed in more detail in **Section 1.3;** and the enzyme family, protein kinase C. The latter enzymes phosphorylate other proteins, as part of signalling pathways involved in a large number of processes.[126] In a series of experiments investigating the effects of aurothiomalate,

aurothioglucose and auranofin on Jurkat cells, which are a line of T-lymphocytes, it was found that all three compounds inhibited proliferation of the cells and reduced production of the pro-inflammatory cytokine, IL-2.[127] The authors also showed that treatment of Jurkat cells with aurothiomalate led to a decrease in overall protein kinase C activity that was most likely due to inhibition of thiol groups at the active site, indicating one potential pathway towards anti-inflammatory effects.[127]

1.3 Thioredoxin Reductase

One enzyme which has been implicated in a number of human diseases, including cancer and RA, is TrxR. As a result, this enzyme has been highlighted by a number of researchers in recent years as a target for metallodrugs, and in particular, gold compounds. The following sections will discuss the structure and functions of TrxR, and summarise evidence that shows that the binding of metallodrugs to the enzyme can affect its activity, and potentially lead to a therapeutic effect.

1.3.1 Structure and Mechanism of Action

TrxR is a homodimeric flavoprotein, with a similar structure to glutathione reductase (GSR). In humans, each monomer is approximately 55 kDa in size and contains a flavin adenine dinucleotide (FAD) and a nicotinamide adenine dinucleotide phosphate (NADPH) binding site.[128] Both TrxR and GSR feature an identical active site disulfide sequence near the N-terminus, which is composed of Cys-Val-Asn-Val-Gly-Cys.[129] However, a key difference in the amino acid sequence of TrxR is the 16-residue extension at the C-terminus, which contains a penultimate selenocysteine (Sec) residue.[130] The monomers in TrxR are arranged spatially such that the C-terminal selenocysteine of one monomer is oriented towards the active site disulfide of the other monomer. The structure of dimeric human TrxR, determined crystallographically by

Fritz-Wolf *et al.*,[131] is shown in **Figure 1.7**. The Sec residue is found in all mammalian forms of TrxR, and is essential for the function of the protein. This has been confirmed by experiments that examined the effects of removing or modifying the Sec residue by carboxypeptidase digestion, or through alkylation. In both cases these changes led to inactivation of the protein.[132] Two isoforms of TrxR have been identified in mammals: cytosolic TrxR (TrxR1) and mitochondrial TrxR (TrxR2). The two isoforms are very similar in sequence, with the mitochondrial form featuring a 33-residue N-terminal extension that functions as a mitochondrial import sequence.[128]

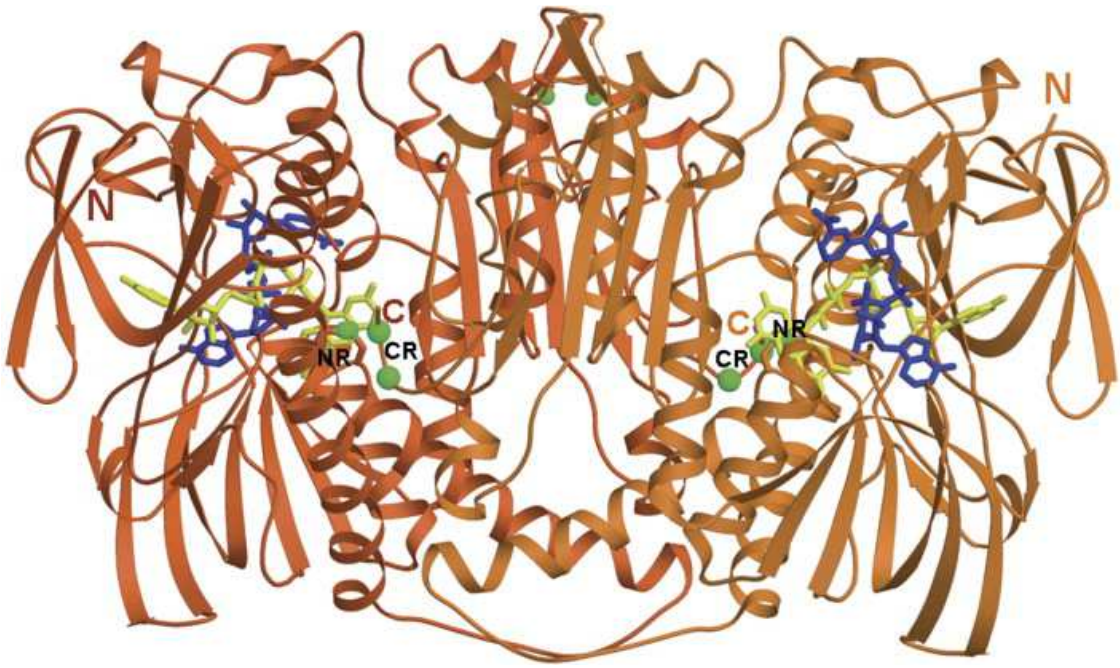

Figure 1.7: Structure of the human thioredoxin reductase dimer, determined crystallographically by Fritz-Wolf *et al.*[131] The two monomers are coloured dark orange (left) and orange (right). Bound FAD is coloured yellow and $NADP^+$ is coloured blue. Active site sulfur atoms are indicated in green. Reprinted from Journal of Molecular Biology, vol. 370, p. 116-127, with permission from Elsevier.

TrxR is named for its ability to catalyse the reduction of the oxidised form of the 12 kDa redox enzyme, thioredoxin (Trx), by NADPH. It is the only protein known that performs this function, and achieves this role by transferring electrons from a bound NADPH to the Trx bound at the active site via the FAD cofactor.[128] The overall set of reactions that constitute what is known as the thioredoxin cycle is depicted in **Figure**

1.8. The redox active centre of Trx is composed of a four amino acid sequence: Cys-Gly-Pro-Cys.[133,134] In its reduced form, the Cys residues exist as a pair of thiols (Trx-$(SH)_2$); however, in the oxidised form of the protein (Trx-S_2) they form a disulfide bridge.

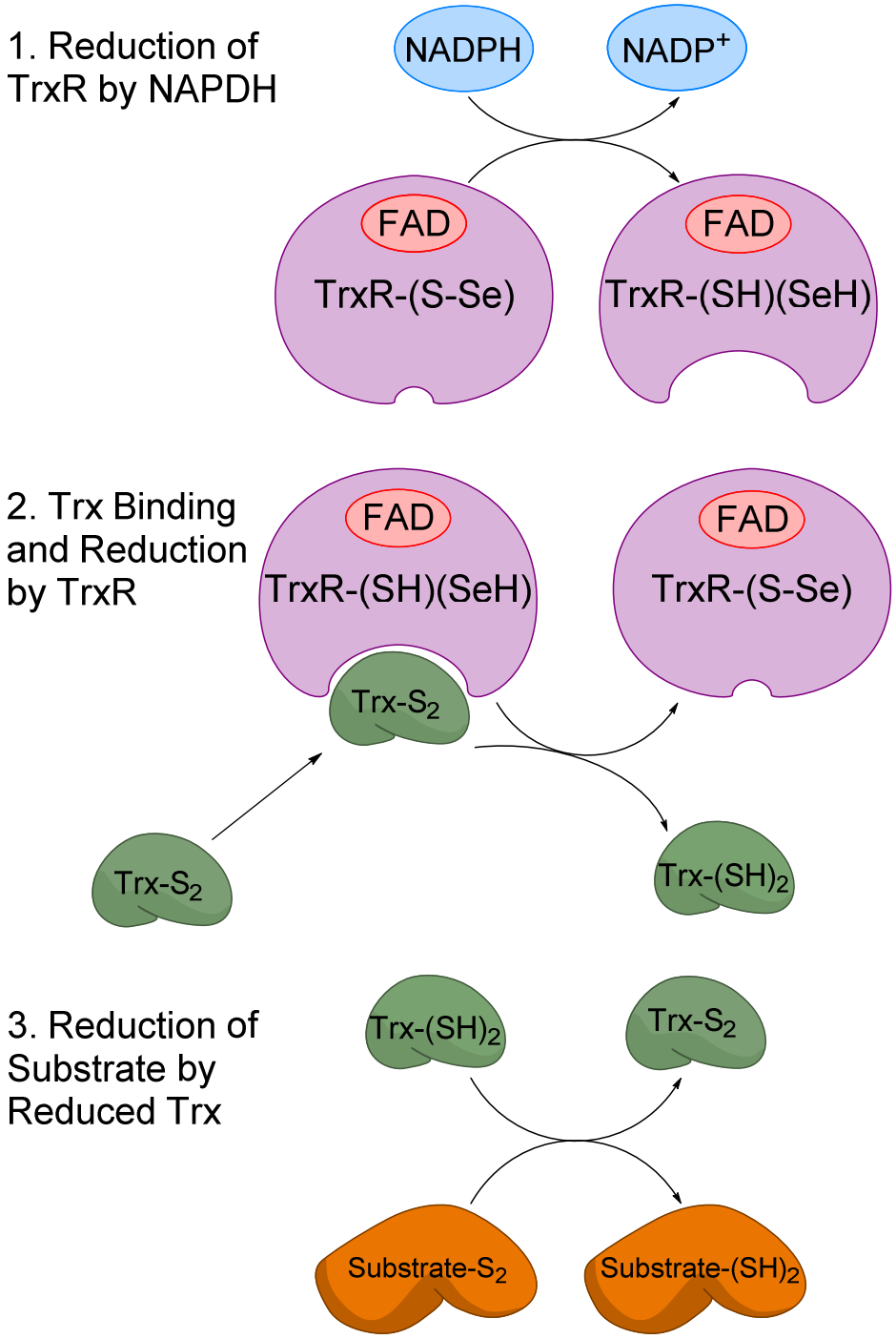

Figure 1.8: Schematic illustration of the reactions of the thioredoxin cycle.

Insight into how TrxR catalyses the reduction of Trx has been gained through a number of studies, some utilising a mutant form of human TrxR1 (hTrxR1), where the selenocysteine residue was altered to a cysteine, and an N-terminal hexahistidyl tag was added to facilitate expression in *E. coli*.[131,135] In other cases experiments have been performed with the native Sec-containing form of rat TrxR (rTrxR1).[136] All of the above studies have helped to establish a probable mechanism of action for reduction of oxidised Trx (Trx-S_2) by TrxR. In the first step, upon NADPH binding, the oxidised N-terminal disulfide of the first hTrxR1 monomer, which is hidden from the surface of the protein, is reduced. The electrons released by this process are transferred to the FAD prosthetic group, reducing it to $FADH_2$. A charge-transfer complex is then formed between the $FADH_2$ and the second Cys residue in the N-terminal active site of the first hTrxR1 monomer, reducing each residue to a thiol. At this stage, the oxidised C-terminal active site of the second hTrxR1 monomer (hTrxR1′) containing the selenylsulfide bond, is oriented towards the N-terminal active site, allowing reduction to selenol and thiol residues. This reduction causes the C-terminal active site to move away from the N-terminal disulfide, a process which is facilitated by a series of residues, Trp407′, Asn418′ and Asn419′, which form a flexible 'guiding bar' for the hTrxR1′ C-terminal chain. After Trx binds to hTrxR1, the C-terminal active site becomes exposed to surrounding solvent molecules, and the selenol residue forms an intermolecular bond with the first Cys residue of Trx, which subsequently promotes protonation and electron transfer from the remaining C-terminal hTrxR1′ Cys residue to form reduced Trx (Trx-$(SH)_2$). This reduced protein then departs the active site of hTrxR1, leaving the oxidised form of the latter protein ready to restart the catalytic cycle.

1.3.2 Functions of Thioredoxin

As TrxR is the only known enzyme capable of reducing Trx, the functions of Trx can be considered indirect functions of TrxR. This section will discuss some of the key functions that Trx plays both intra- and extracellularly.

Thioredoxin is involved in a number of cellular processes in its reduced form, through regulating and regenerating other enzymes. As a consequence, Trx is considered critical for normal cellular function, and it has been referred to as a 'moonlighting' protein due to its capacity to perform a variety of roles in cells.[137] Thioredoxin most commonly functions by reducing substrates through disulfide exchange reactions, or acting as a hydrogen atom donor to maintain the activity of other enzymes. One important substrate for Trx is ribonucleotide reductase, which is an enzyme essential for DNA synthesis owing to its role in catalysing the formation of all four deoxyribonucleotides from ribonucleotides.[134,138] Here, Trx reduces the enzyme ribonucleotide reductase by acting as a hydrogen atom donor.

Trx has been linked to a large number of other biochemical processes,[139,140] including reducing a number of peroxiredoxins[141] and thioredoxin peroxidase.[142,143] These are proteins that protect cells from oxidative stress and apoptosis by reducing H_2O_2. Trx also plays a role in regulating the activity of methionine sulfoxide reductases, which are enzymes that repair proteins by reducing methionine sulfoxide residues to methionine.[144] Other roles of Trx include inhibition and activation of the transcription factors NF-κB and activator protein-1, respectively,[145] and regulation of the glucocorticoid receptor,[140,146] which can either upregulate anti-inflammatory proteins in the nucleus or down-regulate pro-inflammatory proteins in the cytosol.[147] It also binds to the enzyme apoptosis signal-regulating kinase 1, which leads to the formation of a

complex which inhibits the enzyme from performing its function of initiating apoptosis.[148] When secreted extracellularly Trx acts as a growth factor, stimulating cellular growth, proliferation and differentiation.[140] It is secreted by lymphocytes, hepatocytes, fibroblasts, and a number of cancer cells.[149–151] Trx has also been shown to increase the expression of cytokines such as IL-1, IL-2, IL-6, IL-8 and TNF,[152] and to increase TNF induced expression of the pro-inflammatory IL-6 and IL-8 by RA synovial fibroblasts.[153]

1.3.3 Thioredoxin Reductase as a Drug Target

In recent years, there has been interest in TrxR as a target for medicinal chemistry due its overall role in regulating the important regulatory redox enzyme Trx. In particular, the involvement of the Trx system in DNA synthesis and inhibition of apoptosis make it a compelling target for anti-cancer therapies, especially since Trx has been shown to be over-expressed in a number of cancer cell types, when compared to relevant control cells.[154–158] Furthermore, TrxR expression levels have also been shown to be higher than normal in a number of classes of cancer cells, such as breast, skin, thyroid and colorectal cancer cells.[158,159] Given the critical role of Trx for maintaining the redox state of cells, its involvement in signalling the expression of IL-6 and IL-8, and the upregulation of TrxR in synovial cells[160] and synovial fluid,[161] the Trx system also poses a potential target for the treatment of RA. Many of the investigations into the potential of TrxR as a drug target have examined the ability of various classes of metallodrugs to inhibit the enzyme. These studies were focussed upon the presence of the penultimate selenocysteine residue as the primary target for the metal complexes. A number of key chemical features of Sec differentiate it from Cys, and make it ideal as a target for some types of metal complexes. Firstly, free Sec has a lower pKa than Cys (5.2 vs 8.5), resulting in the former being negatively charged at physiological pH and

hence more nucleophilic. Secondly, Sec is a softer base than Cys, making it more attractive to softer metals with which it reacts more quickly and forms stronger bonds.[162]

An example of a clinically-used metallodrug that may inhibit TrxR is arsenic trioxide (ATO), which is effective in the treatment of promyelocytic leukemia.[163] A 2007 study used a number of methods to investigate whether TrxR inhibition was a contributor to the anti-cancer activity of ATO,[164] as it had been previously noted that arsenic(III) exhibits strong binding interactions with selenols.[165] In one investigation the *in vitro* effects of ATO on the activity of rTrxR was studied spectrophotometrically by monitoring the reduction of 5,5'-dithiobis-(2-nitrobenzoic acid) (DTNB).[164] It was shown that ATO binding to rTrxR was irreversible, with an IC_{50} value of 0.25 μM. Matrix-assisted laser desorption ionisation mass spectrometry (MALDI-MS) of a trypsinised sample of TrxR that had been previously reacted with ATO, indicated that the arsenic was bound to both the Cys and Sec residues at the C-terminus.[164] In another experiment, human breast cancer cells were treated with ATO, then lysed, and the activity of the Trx/TrxR system in the lysates subsequently measured by following the reduction of insulin.[164] The results of these experiments showed that a decrease in the activity of the Trx/TrxR system occurred as the ATO concentration was increased. All of the above results highlight the potential for anti-cancer activity exerted via interactions with TrxR.

It has also been shown that the thioredoxin system is a potential therapeutic target for platinum complexes. For example, cisplatin and transplatin were both shown to inhibit the activity of calf TrxR in experiments where the ability of the enzyme to catalyse the reduction of insulin by NADPH was measured. The second order rate constants for reduction of insulin in the presence of cisplatin and transplatin were 21 ±

3 $M^{-1}.s^{-1}$, and 84 ± 22 $M^{-1}.s^{-1}$, respectively.[166] A primary metabolite of cisplatin inside cells, bis-(glutathionato)platinum(II), was also studied and shown to inhibit the mammalian Trx system but not a bacterial Trx system. Bacterial TrxR does not contain the penultimate Sec residue, indicating the potential importance of the selenol residue in the mechanism of inhibition of these platinum complexes.[166] This is further demonstrated by another study, which showed that cisplatin could effectively inhibit calf TrxR, but not the structurally related GSR, which does not contain a selenocysteine residue.[167]

Platinum(II) compounds containing the terpyridyl (terpy) ligand have also been investigated as potential anti-cancer drugs that exert their biological effects as a result of binding to TrxR. One study measured the activity of hTrxR after incubation with different platinum terpy compounds, in the presence of DTNB. It was found that six of the compounds had IC_{50} values below 10 nM.[168] In contrast, the level of activity towards GSR was found to be 3-4 orders of magnitude lower, again highlighting the specificity of platinum complexes for the selenol active site.[168] In another study, a mutant form of TrxR1 was studied, where the Sec had been replaced by a Cys.[169] The effect of $Pt(terpy)^{2+}$ complexes on the ability of hTrxR1 to reduce DTNB was similarly assessed, and the IC_{50} values obtained were found to range from 55 – 80 nM. This is a lower level of inhibition than in the previous study, which is most likely attributable to replacement of the Sec residue with Cys, resulting in lower affinity towards the platinum complexes. The specific interactions between [Pt(terpy)(*N*-acetyl-4-aminothiophenolato)]$^{+}$, shown in **Figure 1.9**, and hTrxR1, were revealed in a crystal structure of the metal/protein complex. Further information about these interactions were derived by performing a tryptic digest on the adducts formed between the enzyme and the platinum complex, and analysing the resultant fragments by MALDI-MS. Both

techniques provided evidence of terpyridineplatinum(II) moieties binding at the C-terminal active site of the enzyme.

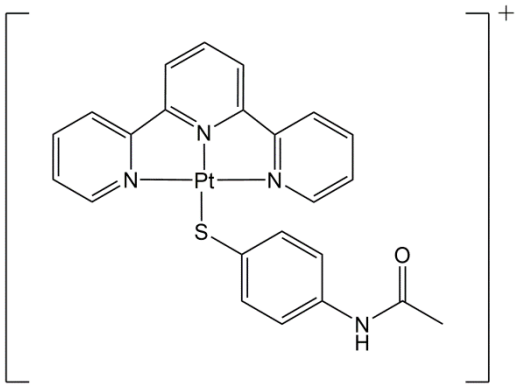

Figure 1.9: Structure of [Pt(terpy)(*N*-acetyl-4-aminothiophenolato)]$^{+}$.[169]

1.3.4 Interactions of Gold Drugs with TrxR

While impressive results have been obtained from studies of the binding interactions between TrxR and other metals, it was thought that gold(I) compounds might be even more potent TrxR inhibitors due to the metal ion being a typical soft acid, and as such being expected to bind strongly to thiol or selenol residues. Consistent with this, a study was published in 1998 that showed that the anti-rheumatic drugs, aurothioglucose and auranofin, strongly inhibited hTrxR, with IC_{50} values of 65 and 20 nM, respectively.[170] A high degree of specificity towards the enzyme was also demonstrated in this study, as the two gold(I) compounds had to be present at 1000 times higher concentrations for comparable levels of inhibition of GSR to be observed. Another study used spectrophotometry to directly compare the ability of gold(I) and gold(III) compounds to inhibit reduction of DTNB by rTrxR2, with that of other metal compounds.[171] The structures of some of these compounds are shown in **Figure 1.10**, while the IC_{50} values of these compounds towards rTrxR2 are displayed in **Table 1.2**.

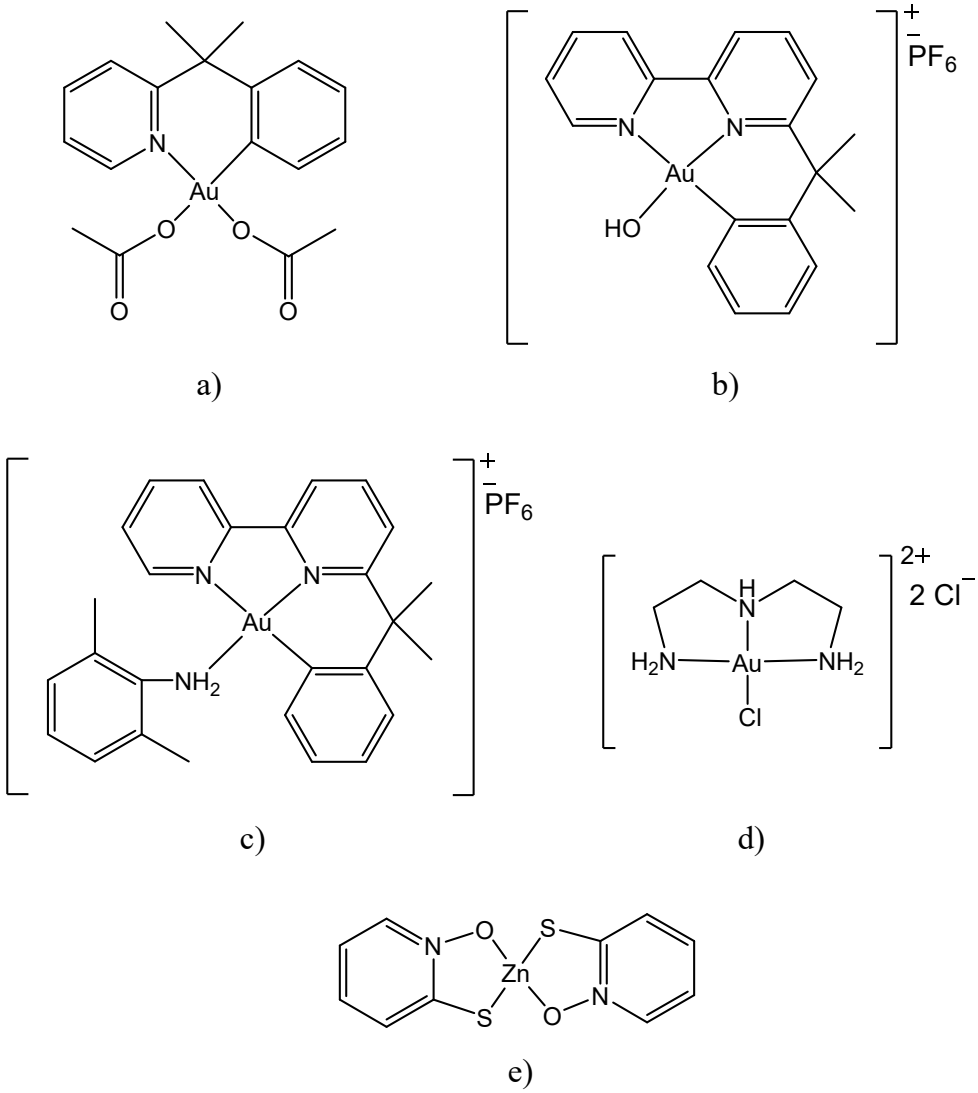

Figure 1.10: Structures of some metal complexes investigated as TrxR inhibitors:
a) Au(py^{dmb}) = [Au(2-(1,1-dimethylbenzyl)-pyridine)($CH_3COO)_2$];
b) Au(bipy^{dmb}) = [Au(6-(1,1-dimethylbenzyl)-2,2'-bipyridine))(OH)](PF_6);
c) Au(bipy^{dmb})(xyl) = [Au(6-(1,1-dimethylbenzyl)-2,2'-bipyridine))(2,6-xylidine)](PF_6);
d) Au(dien) = [Au(2,2'-diethylenediamine)Cl]Cl_2; and
e) zinc pyrithione = [Zn(2-mercaptopyridine-*N*-oxide)$_2$].

All of the gold complexes produced the same high degree of inhibition of rTrxR2, but at much lower concentrations than the other metal compounds. **Table 1.2** also shows that gold(I) complexes containing a triethylphosphine ligand were particularly powerful inhibitors. The investigators also examined the ability of gold(I) and gold(III) compounds to inhibit the activity of GSR, and found that negligible inhibition occurred when the concentration of gold was ≤ 10 μM. This further demonstrates the significant extent of enzymatic specificity exhibited by these compounds. It was also shown that the gold compounds could alter mitochondrial

membrane permeability and induce mitochondrial swelling, but they did not affect the mitochondrial respiratory chain as strongly as complexes of other metal ions. This may indicate that while TrxR is an extremely important enzyme, its inhibition does not necessarily affect the overall redox state of the organelle.

Table 1.2: Comparison of IC_{50} values derived from a spectrophotometric examination of the ability of metal complexes to inhibit reduction of DTNB by rTrxR2.[171]

Metal Compound	Metal Ion	IC_{50} (μM)
Aurothiomalate	Au(I)	0.280
Triethylphosphine gold	Au(I)	0.065
Auranofin	Au(I)	0.020
$Au(py^{dmb})$	Au(III)	1.42
$Au(bipy^{dmb})$	Au(III)	0.28
$Au(bipy^{dmb})(xyl)$	Au(III)	0.21
Au(dien) chloride	Au(III)	0.42
Tributyltin chloride	Sn(IV)	76.1
Cisplatin	Pt(II)	36.9
Cadmium acetate	Cd(II)	23.5
Zinc acetate	Zn(II)	19.5
Zinc pyrithione	Zn(II)	11.8

A number of more recent studies have also investigated the ability of gold(III) compounds to act as anti-cancer compounds as a result of their ability to bind to and inhibit TrxR.[172,173] The results of these studies, and those presented in **Figure 1.10**, all suggest that Au(I) compounds are more potent TrxR inhibitors than similar Au(III) compounds. This is most likely due to the softer nature of the Au(I) ion compared to Au(III), which would be expected to lead to more favourable binding interactions with the penultimate selenocysteine residue of TrxR.[174] In view of these studies some researchers have investigated the *in vitro* effects of a range of Au(I) complexes in selected cell lines. The structures of some of these compounds are shown in **Figure 1.11**. For example, a pair of Au(I)-phosphole complexes (**Figure 1.11 a** and **b**) that

were shown to be very potent inhibitors (IC_{50} < 10 nM) of both hTrxR and hGSR, were also found to exhibit significant toxicity (IC_{50} ~5-15 μM) against three glioblastoma cell lines, and strong binding interactions with single-stranded plasmid DNA.[175]

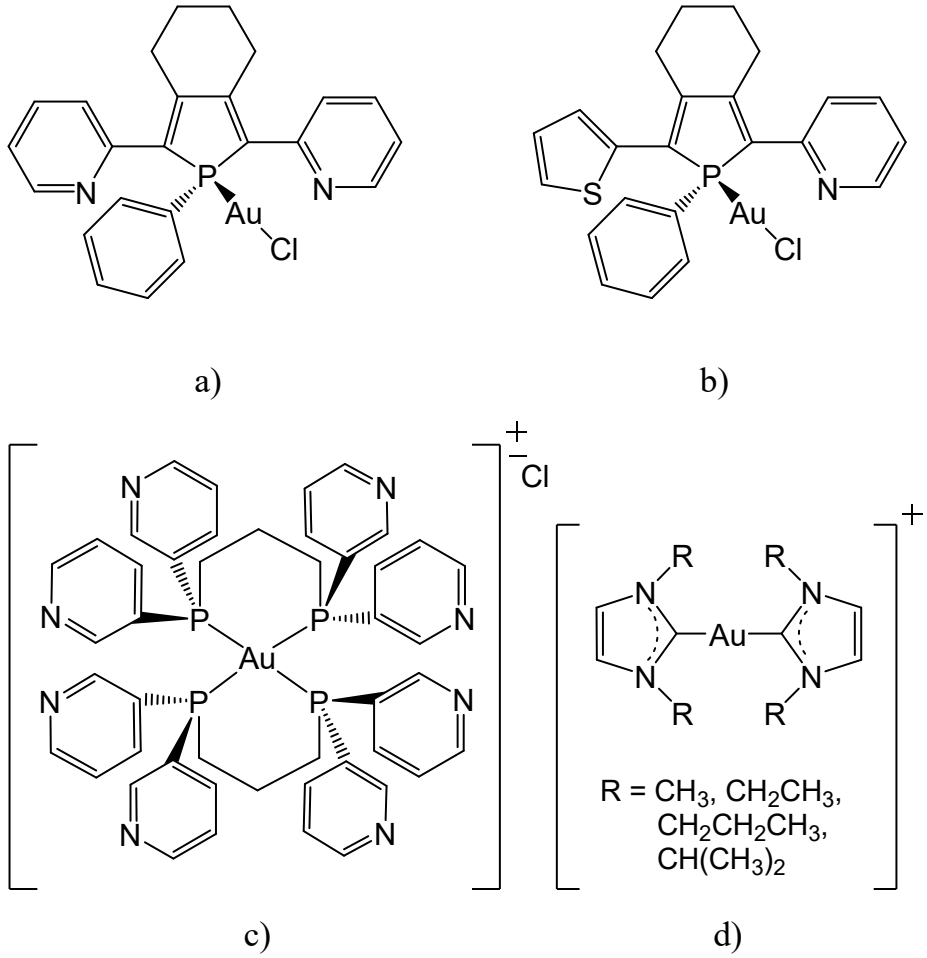

Figure 1.11: Structures of some gold(I) complexes investigated as potential anti-cancer drugs that act by inhibiting TrxR: **a)** [Au(1-phenyl-2,5-di(2-pyridyl)phosphole)Cl]; **b)** [Au(1-phenyl-2,5-di(2-thienyl)phosphole)Cl]; **c)** [Au(1,3-bis(di-2-pyridylphosphino)propane$_2$]Cl; and **d)** [Au(1,3-di-R-imidazol-2-ylidene$_2$]$^+$

The four-coordinate Au(I) complex, [Au(d2pypp)$_2$]Cl (d2pypp = 1,3-bis(di-2-pyridylphosphino)propane, **Figure 1.11 c**), has also been shown to affect rTrxR activity towards insulin reduction, and is cytotoxic towards human breast cancer cells.[176] Although it was less active against rTrxR than some of the compounds discussed above (IC_{50} = 1 μM for insulin reduction), it did show strong and selective toxicity against human breast cancer cells when administered at only 5 μM concentration. The latter

cells showed an 80% drop in cellular Trx activity and a 40% drop in cellular rTrxR activity. These results highlight the importance of comparing *ex vivo* with *in vitro* results to fully investigate a compounds potential as an enzymatic inhibitor.

Gold(I) complexes of *N*-heterocyclic carbene ligands have become an area of considerable focus recently, with many studies demonstrating these compounds can significantly inhibit TrxR.[177–186] In many of these studies the toxicity of the compounds towards cancer cells was explored along with their ability to inhibit TrxR, or the overall Trx system. For example, one study showed gold compounds of this type (**Figure 1.11 d**) were more toxic towards human breast cancer cells than healthy breast cells, and also exhibited greater affinity towards TrxR compared to the structurally related GSR.[186] This study also further highlighted the importance of the selenol residue in TrxR for the overall affinity of the enzyme towards metal complexes. This was demonstrated by kinetics experiments which showed that the reactions of the metal complexes with selenocysteine were 20-80 times higher than for the corresponding reactions with cysteine at physiological pH.

1.3.5 Mass Spectrometric Investigations

Various types of mass spectrometers have been used for studying the interactions between drug molecules and enzymes, with MALDI-MS and ESI-MS proving to be particularly useful. For example, MALDI-MS has been used to monitor the binding of auranofin and sodium aurothiomalate, as well as some gold(III) drugs, to intact rTrxR1.[187] **Figure 1.12** shows the MALDI mass spectra of reaction mixtures containing different ratios of the complex $[Au(bipy)(OH)_2][PF_6]$ (bipy = bipyridine) and rTrxR1. Each spectrum shows a very broad peak, attributable to the presence of protein molecules containing many different numbers of bound solvent molecules and other low

molecular weight species. Broad peaks are commonly observed in MALDI mass spectra, and limit the accuracy with which the molecular mass of a protein or protein complex can be determined. Addition of 3 and 10 equivalents of the gold complex resulted in increases in the mass of the species in solution of ~1200 and ~3000 Da, respectively (**Figure 1.12 a** and **b**). While this is strong evidence of binding of the gold complex to the protein, the number of bound molecules and the structure of the bound fragments could not be accurately determined due to the broad peaks observed. Much more information about the nature of the gold/TrxR binding interaction could be derived if narrower signals could be obtained for free protein molecules and protein/drug adducts in the same spectrum.

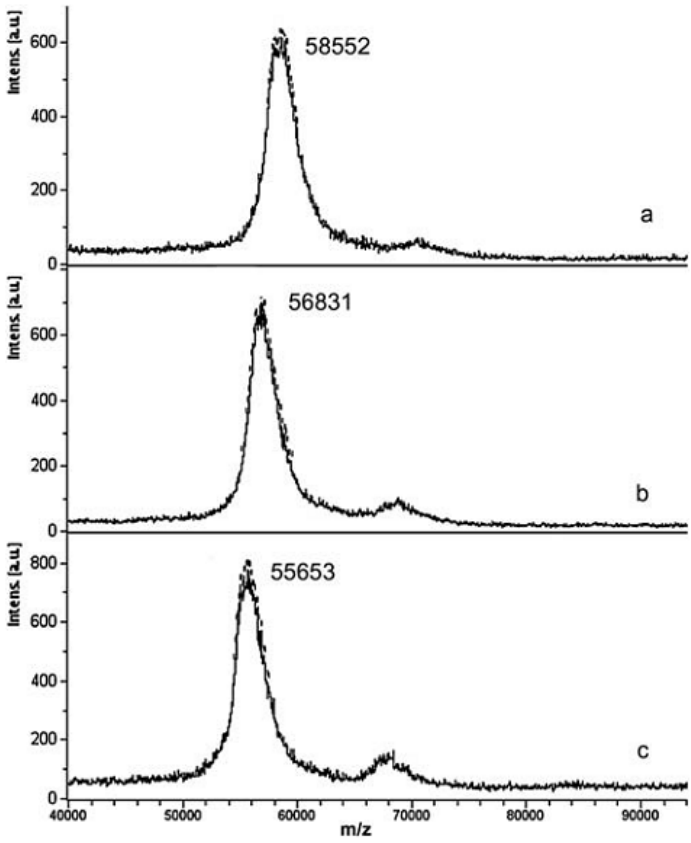

Figure 1.12: MALDI mass spectra of solutions containing different ratios of rTrxR1 and $[Au(bipy)(OH)_2][PF_6]$: **a)** Au : rTrxR1 = 10 : 1; **b)** Au : rTrxR1 = 3 : 1; **c)** free rTrxR1. Reproduced from Medicinal Chemistry Communications, 2011, vol. 2(1), p. 50-54 with permission of The Royal Society of Chemistry.[187]

ESI-MS offers a number of potential advantages for researchers wishing to examine the binding of small molecules to proteins. This is because the technique examines protein samples present in solution, as opposed to a matrix as is the case for MALDI-MS. In addition, ESI-MS provides raw spectra consisting of an envelope of ions corresponding to protein molecules in different states of protonation. This is exemplified by the spectrum of HSA shown in **Figure 1.13 a)**.[88] The presence of so many ions, each differing by a single charge, enables more accurate determination of the molecular mass of the species in solution. This is also true for the transformed spectrum shown in **Figure 1.13 b)**.

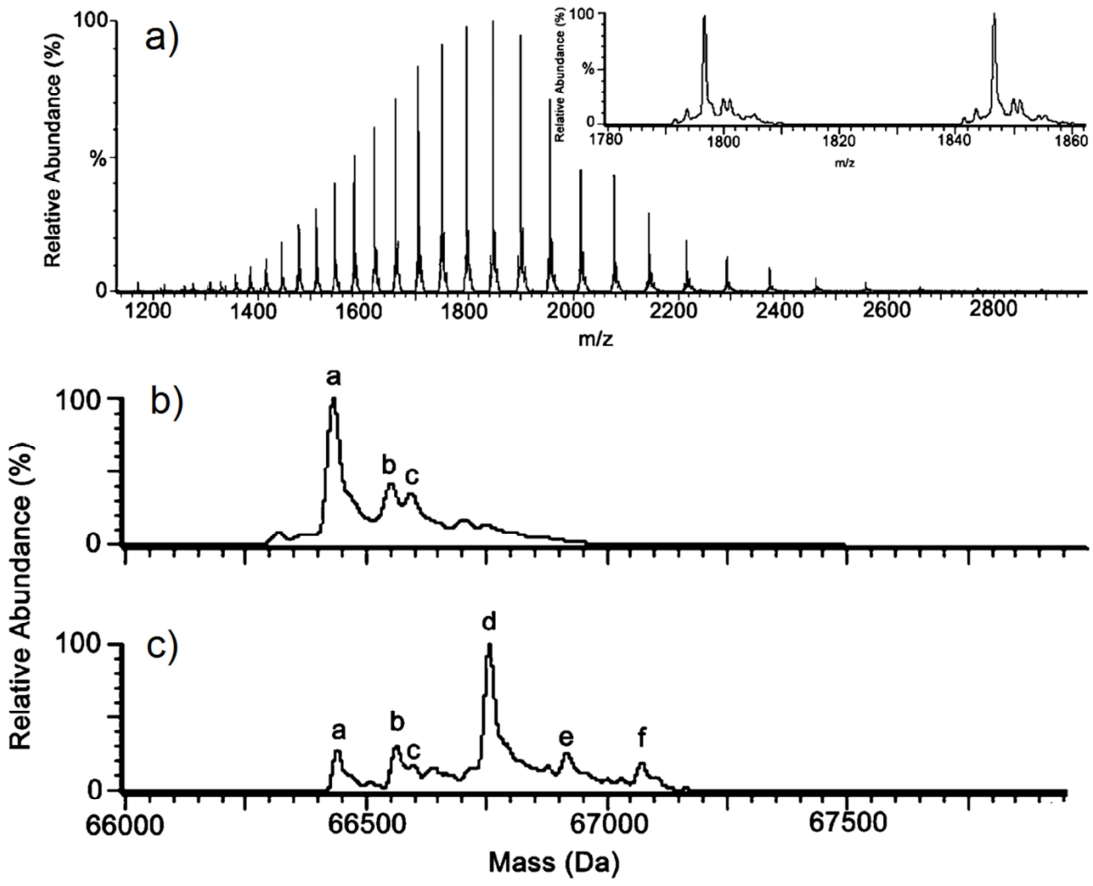

Figure 1.13: ESI mass spectra of HSA in 3% acetic acid: **a)** raw spectrum of free HSA, with an inset showing a magnified view between *m/z* 1780 and 1860; **b)** spectrum of free HSA transformed to a mass scale; and **c)** spectrum of a solution containing $AuPEt_3Cl$: HSA = 1 : 1 obtained after 4 h, transformed to a mass scale. Components a-f are free HSA, HSA + Cys, HSA + glucose, HSA + $AuPEt_3$, HSA + glucose + $AuPEt_3$, HSA + $2AuPEt_3$, respectively. Reprinted from Journal of Biological Inorganic Chemistry, 2006, 11 (5), p. 559-570, with kind permission from Springer Science and Business Media.[88]

Another advantage of the narrow signals observed in ESI mass spectra is that it provides greater opportunities to observe separate ions from free protein, and protein molecules with one or more drug molecules or drug fragments bound. For example, in **Figure 1.13 b)** and **c)** additional ions are present, which were attributed to cysteine and glucose molecules bound to HSA. In addition, in **Figure 1.13 c)**, there are also ions from protein molecules with a $AuPEt_3$ moiety bound. Observation of these separate ions allowed the relative abundance of each species to be determined. Despite these impressive results, to date no one has used ESI-MS to explore the binding of gold complexes, or those of any other metal ions, to intact TrxR.

1.4 Gold Nanoparticles

Recent years have seen considerable research focussed upon the potential for gold nanoparticles (Au NPs) to be used for a wide range of purposes in biology and medicine, such as diagnostic agents, bio-sensors, drug-delivery platforms and pharmaceuticals.[188] Gold nanoparticles have been known to humans since the times of ancient Rome as a material for staining glass.[189] One hundred and fifty years ago colloidal suspensions of gold were prepared by Michael Faraday using a procedure involving reduction of Au(III) with phosphorus.[189] In 1951 a simpler method for preparing Au NPs was described by Turkevich *et al*.,[190] and developed further by Frens *et al*. in the 1970's.[191] In both cases, the synthetic method involved addition of sodium citrate to a hot solution of $H[AuCl_4]$, with the overall reaction scheme shown in **Figure 1.14**. The citrate molecules reduce the gold complex to the +1 oxidation state, after which a disproportionation reaction occurs, regenerating a Au(III) ion and producing elemental gold atoms that act as a nucleation point for further reactions forming Au(I). Excess citrate ions then act as a stabilizing agent for the resulting colloid, preventing gold atoms from aggregating and producing particles that are 10 – 100 nm in size.[191]

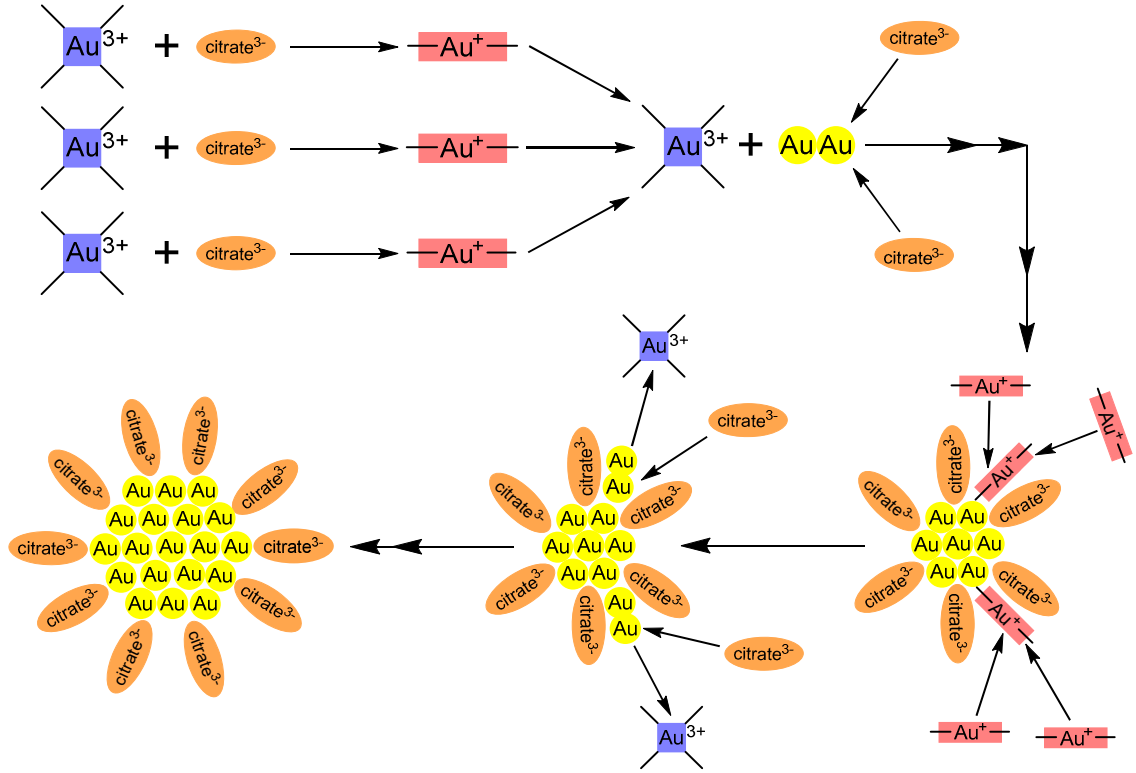

Figure 1.14: Reaction scheme for formation of Au NPs by citrate reduction.

A variety of methods now exist to produce Au NPs with different shells, sizes and stability in non-aqueous solvents.[192–194] The methods generally all start with reduction of a Au(III) complex in aqueous solution in the presence of a stabiliser to form the initial colloid, before either replacing the shell or utilising phase-transfer chemistry to change the shell. The capacity to functionalise the stabilising outer shell with groups such as thiols or amines is a major focus in this area, with small biomolecules also often employed.[188]

1.4.1 Treatment of Rheumatoid Arthritis Using Au NPs

A small number of studies have shown that Au NPs have potential for the treatment of RA. For example, in 1997 a case report was published in the United States involving a group of ten chronic sufferers of RA, who exhibited minimal response to several different therapies. These patients were then given an oral formulation of Au NPs, called Aurasol, which was synthesised by the citrate method with several

undisclosed 'proprietary modifications.'[195] Nine of the ten patients had previously been administered either aurothiomalate or auranofin, which proved to be either clinically ineffective or, in the case of five of the patients, resulted in adverse side effects. Prior to treatment (in week 0) the patients had their tenderness and swelling symptoms assessed by a semi-quantitative scoring system, in which a higher score corresponded to a greater severity of the symptoms. In addition, the levels of several Igs (IgG, IgM and IgA), rheumatoid factor, and the cytokines TNF and IL-6 were all determined. The average values obtained for each of these clinical markers at various time points throughout the study are shown in **Table 1.3**. Within one week of commencing treatment there was a pronounced reduction in tenderness and swelling symptoms, which continued with further treatment. A statistically significant drop in the levels of IgG, IgM, TNF, IL-6 and rheumatoid factor was also observed by the end of the study. The authors also commented that the patients showed no evidence of toxicity in either clinical or laboratory tests.

Table 1.3: Effects of an oral Au NPs treatment regime on some inflammation markers of ten patients with chronic RA.[195]

Marker	Week 0	Week 1	Week 4	Week 16	Week 24	Week 52
Tenderness	54.8 ± 16.2	19.2 ± 6.3	8.4 ± 4.5	9.5 ± 2.6	5.4 ± 2.0	5.9 ± 2.5
Swelling	42.5 ± 10.5	15.9 ± 5.9	13.2 ± 5.8	4.5 ± 1.3	3.3 ± 1.2	3.6 ± 2.2
IgG	34.6 ± 7.3	-	-	21.4 ± 4.4	18.8 ± 3.0	19.9 ± 3.4
IgM	24.0 ± 4.9	-	-	15.6 ±3.1	16.0 ± 3.5	19.4 ± 2.9
IgA	5.9 ± 0.81	-	-	4.5 ± 0.79	5.6 ± 1	4.7 ± 0.91
TNF	207 ± 33	-	-	105 ± 30	74 ± 25	-
IL-6	241 ± 66	-	-	107 ±20	104 ± 25	-
RF	143.6 ± 23.7	-	-	-	145.9 ± 22.1	117.9 ± 18.9

Note: Reported numbers are the means for all 10 patients. Tenderness and swelling are mean scores and unitless. All other markers were reported without units. Week 0 is before treatment began. Errors are standard error of the mean. - indicates data for that parameter not reported.

A subsequent investigation in 2008 examined the effects of citrate-stabilised Au NPs on two strains of rats in which polyarthritis had been induced by injections of either *Mycobacterium tuberculosis*, collagen or pristane, a saturated alkane.[196] The effectiveness of treatment using Au NPs was compared to that involving injection with aurothiomalate, with the rats given a mean arthritis score based upon the extent of paw and tail swelling, paw inflammation, and general well-being. With this approach a higher mean arthritis score indicated greater severity of symptoms. Both rats treated with aurothiomalate, and those administered Au NPs exhibited significantly lower mean arthritis scores than the group of control rats, in which arthritis had been induced using *Mycobacterium tuberculosis*. However, only rats treated with Au NPs had statistically lower mean arthritis scores than control rats where arthritis was induced by collagen or pristane. There were no signs of adverse side effects resulting from treatment with Au NPs. This study and the case report involving human patients both highlight the potential for Au NPs to be used for the treatment of RA or other inflammatory diseases. However, many questions remain concerning how the Au NPs exerted their anti-arthritic effects, and how their effectiveness compares to the traditional gold(I) drugs.

1.4.2 *In Vitro* Investigations Involving Au NPs

Chithrani *et al*. published a number of studies examining the cellular uptake characteristics of different types of Au NPs.[197–199] For example, in 2006 they published the results of an investigation on the effect of particle size on the extent of uptake of Au NPs by HeLa cells. This study involved citrate-stabilised Au NPs that were 14, 30, 50, 74 and 100 nm in diameter.[197] The number of particles incorporated into cells increased as the size of the particles increased from 14 to 30 and finally 50 nm. However, increasing the size of the nanoparticles further resulted in the extent of cellular uptake decreasing. In the same publication, it was also noted that a similar trend was apparent

for Au NPs coated with transferrin, a serum protein that is involved in regulating iron levels. Notably, the overall number of particles incorporated into cells was always approximately three times smaller for transferrin-coated Au NPs than those coated with citrate.[197] It was also demonstrated that Au NPs were most likely incorporated by receptor-mediated endocytosis, a process where the particle binds to a receptor on the surface of a cell, and is subsequently internalised upon membrane invagination and release of the particle from the receptor.[197] The authors also reported that spherical Au NPs were taken up by cells in larger quantities than those with a rod shape.[197]

A subsequent investigation focussed solely on the uptake of Au NPs coated with transferrin by HeLa, STO (fibroblast) and SNB19 (brain tumour) cell lines.[198] It was again shown that the nanoparticles entered the cells by receptor-mediated endocytosis. In addition, the membrane-bound protein clathrin was demonstrated to play a large role in this process, while the rate of exocytosis of the nanoparticles was shown to decrease with increases in particle size.[198] Subsequently it was shown in another study that Au NPs are initially packaged into endosomes, then fused with lysosomes, before being exocytosed.[199] A scheme depicting the mechanism of uptake of Au NPs revealed by these studies is illustrated in **Figure 1.15**.

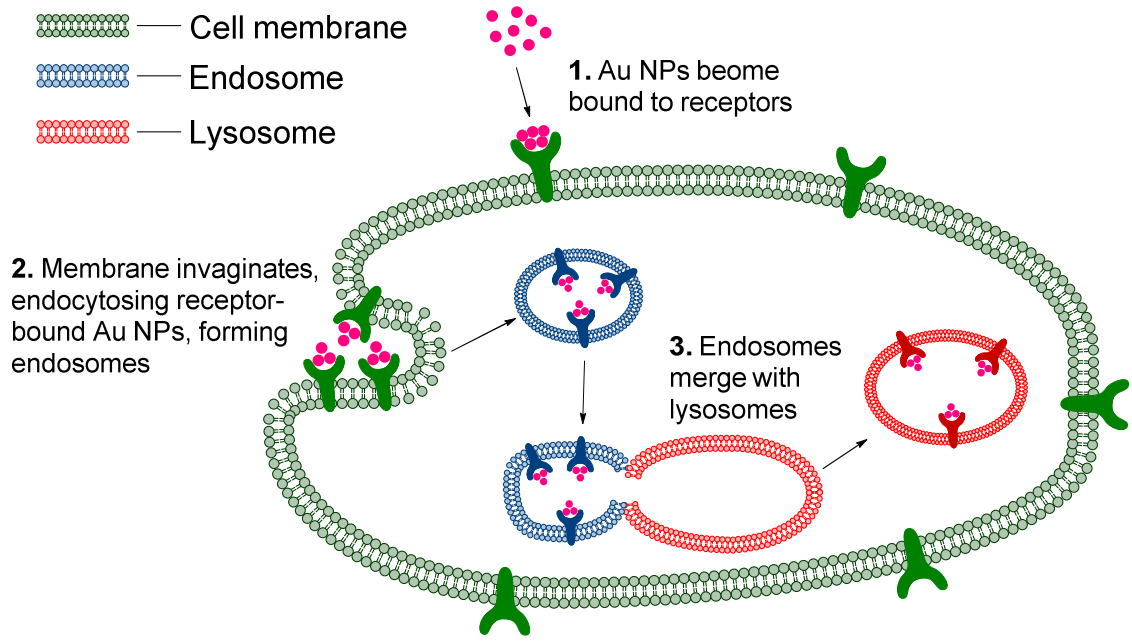

Figure 1.15: Cellular uptake of Au NPs by receptor-mediated endocytosis. Adapted from Nanomedicine: Nanotechnology, Biology, and Medicine, 2009, vol. 5 (2), p. 118-127 with permission from Elsevier.[199]

The cytotoxicity of, and extent of uptake of citrate-stabilised Au NPs by MC3T3-E1 cells, a mouse osteoblast cell line, has been recently investigated by Mustafa *et al.*[200] No change in mitochondrial activity was found after treatment of the cells with Au NPs; however, there was an increase in expression of lactate dehydrogenase (LDH), an enzyme which is released upon cell damage or lysis. Using transmission electron microscopy (TEM), Au NPs were observed becoming encapsulated by the plasma membrane, with nanoparticle clusters also observed in the cytoplasm. These images demonstrate that Au NPs are transported into cells by endocytosis,[200] as had been initially observed by Chithrani *et al.*[197,198] Mustafa *et al.* also suggested that the observed release of LDH could be a result of the disturbance of membrane integrity caused by endocytosis, as opposed to being an indicator of the cytotoxicity of the Au NPs.[200]

To evaluate the biocompatibility of Au NPs, murine RAW264.7 macrophages were used to investigate whether Au NPs coated with lysine and poly-L-lysine elicit inflammatory and cytotoxic effects.[201] Macrophages were chosen for this study due to

their role in the inflammatory response. Evidence of significant amounts of cellular uptake of Au NPs was obtained, along with indications that this occurred via receptor-mediated endocytosis. Despite this, there was no indication that mitochondrial activity had been affected, and the levels of reactive nitrogen and oxygen species did not change significantly. This was also true for the pro-inflammatory cytokines TNF and IL-1β, and the level of general cellular protein expression.[201] Contrasting results were reported by Yen *et al*. in a 2009 study using Au NPs obtained from Global Nanotech Industries in Taiwan.[202] These Au NPs were synthesised by what was described as physical manufacturing and did not contain surface modifying or stabilizing agents. The cytotoxicity towards and extent of secretion of the pro-inflammatory cytokines TNF, IL-1, and IL-6 by murine J774.A1 macrophages was investigated after treatment with Au NPs. The results obtained with this different macrophage line showed significant cytotoxicity and increased levels of production of these cytokines, which became even more severe as the particle size decreased.[202] These two studies highlight some of the conflicting evidence available in the literature concerning the biological interactions of nanomaterials, and the need for further investigations into the effects of changes in the physical characteristics of Au NPs, such as the presence and identity of stabilising 'shell' molecules, on their cytotoxicity and other biological effects.

One area that remains controversial is whether or not Au NPs can prevent or reduce emission of inflammatory molecules in cells. A 2010 investigation by Ma *et al*. published in *Nitric Oxide* described 10 - 15 nm diameter Au NPs as having the capacity to attenuate production of NO by RAW264.7 macrophages.[203] In this study the macrophage cells were pre-treated with Au NPs, after which the inflammation-stimulating molecule, LPS, was added. The concentration of NO_2^-, a decay product of NO, produced by the cells was subsequently determined and shown to decrease as the

concentration of Au NPs increased. This was attributed to decreased expression of inducible nitric oxide synthase.[203] The authors of the study also showed that this could be due to suppression of the transcription factor NF-κB. In contrast, the Au NPs did not affect expression levels of the pro-inflammatory cytokines, TNF, IL-1β and IL-6.[203]

In evaluating the significance of the above results it is important to note that the abstract of the article indicated that the Au NPs used were coated with polyethylene glycol (PEG).[203] In contrast, in the methods section it was stated that the nanoparticles were purchased from the company Natural F & P (Seoul, Korea), and synthesised using the citrate approach. A reference is provided for the synthetic procedure used; however, the methods section of that article did not indicate that PEG had been used.[204] As discussed above, the synthetic method employed to prepare Au NPs, and the identity of any molecules in the surrounding 'shell' may play an important role in determining how the nanoparticles interact with biological systems. In the discussion section of their article, Ma *et al*. state that a prior investigation into the effects of Au NPs on J774.A1 cells, conducted by Yen *et al*.,[202] obtained evidence which indicated that exposure to gold resulted in attenuation of cytokine production. Inspection of the original data, however, shows that the Au NPs had the opposite effect. Furthermore, a letter to the editor by Leroy *et al*. in 2011, also published in *Nitric Oxide*,[205] questioned the significance of the results reported by Ma *et al*.,[203] and highlighted the fact that the composition of the nanoparticles in the study was unclear. Furthermore, in their letter to the editor, Leroy *et al*. presented results that showed that Au NPs stabilised with either citrate or dihydrolipoic acid did not attenuate LPS-induced formation of NO in NR8383 cells, a rat macrophage cell line.[205]

It is clear that there are conflicting results in the literature concerning the effects of Au NPs on production of reactive nitrogen-containing species. Further confusion in

this area stems from the results of an investigation into the effects of 28 nm diameter Au NPs coated with PEG, on LPS-activated RAW264.7 macrophages.[206] The Au NPs did not induce significant formation of NO or IL-6 in the cells when the latter were exposed only to the nanoparticles. However, treatment of the macrophages with both Au NPs and LPS led to a small but significant increase (10 – 20%) in NO and IL-6 levels, as well as increased expression of inducible nitric oxide synthase.[206] These results contrast those from the 2010 study by Ma *et al.*, and further highlight the importance that the nanoparticle size and shell composition may have in determining biological effects such as inflammation. Therefore it is essential that researchers in this field unambiguously report the synthetic procedure they employ to prepare Au NPs, and fully characterise the resulting materials.

1.4.3 Interactions of Gold Nanoparticles with Proteins, Including Thioredoxin Reductase

There have also been a number of recent investigations into the biological interactions of Au NPs with proteins. For example, the binding of Au NPs to bovine serum albumin has been studied using zeta potential measurements and quartz crystal microbalance techniques.[207] It was tentatively concluded that electrostatic forces, possibly involving the carboxylate groups of citrate anions on the surfaces of the Au NPs, and protonated amines of surface lysine residues of the protein, were responsible for the observed interactions. In another study circular dichroism spectroscopy and dynamic light scattering were used to perform measurements on systems containing citrate-stabilized Au NPs of various sizes, and a range of proteins found in human blood.[208] It was concluded that in these systems protein molecules formed an outer layer, or 'corona,' on the surface of the Au NPs, and the overall strength of interactions between the two components increased along with nanoparticle size.

To date there appears to be very little work reported in the literature describing interactions between Au NPs and TrxR. The lack of studies in this area is surprising considering the body of evidence demonstrating the potency of Au(I) and Au(III) compounds as TrxR inhibitors. In one recent study, evidence of interactions between TrxR and small nanoclusters composed of 25 gold atoms stabilized by a tridecapeptide was reported.[209] The clusters inhibited the activity of TrxR directly, and in HeLa cells, leading to higher levels of ROS and apoptosis. Apart from this investigation, there appears to have been only one other study which has examined the interactions between Au NPs and the Trx system.[210] The aim of this study was to determine whether Au NPs can induce oxidative stress *in vivo* in a marine organism, the mussel *Mytilus edulis*. The mussels were exposed to Au NPs over a 24 hour period. Subsequently, gold was detected primarily in the digestive glands of the mussels. The effect of exposure to gold on the level of activity of TrxR was also examined; however, no significant changes were detected.

The above results contrast those obtained in a study where A549 lung cancer cells were exposed to silver nanoparticles (Ag NPs), and the effects of these nanoparticles on the synthesis of selenoproteins and activity of TrxR were monitored.[211] Treatment with the Ag NPs inhibited incorporation of selenium into selenoproteins, and inhibited TrxR activity in a dose-dependent manner. This was attributed to the effects of Ag^+ ions leaching from the nanoparticles, as opposed to the direct effects of the nanoparticles themselves. Consistent with this hypothesis, the extent of inhibition of TrxR activity in A549 cells was ten times greater after exposure to Ag^+ ions than Ag NPs.[211] The researchers were also able to show in a cell-free system that TrxR1 is inhibited by Ag^+ ions; however, they did not indicate if Ag NPs were also able to directly inhibit the enzyme. The results of this study may, therefore, imply that Ag NPs

are unable to interact with TrxR or the Trx system. As yet it has not been conclusively shown if this is also true for Au NPs.

In summary, whilst a limited number of *in vivo* studies have suggested that Au NPs may have promising anti-inflammatory effects, this has not been supported by the results of laboratory experiments. It is also likely from a number of studies that have been performed, that the physical characteristics of Au NPs greatly contribute to their overall biological effects and interactions. Despite this, and the clear demonstration that gold compounds can significantly affect the activity of TrxR, there is still a gap in our understanding of how, if at all, Au NPs interact with the thioredoxin system.

1.5 Project Aims

The overall aim of this project was to compare the biological activity and effects of gold nanoparticles, to that of gold(I) drugs used for the treatment of rheumatoid arthritis. The specific aims of the project were to:

- compare the cytotoxicity of gold nanoparticles towards macrophages with that of gold(I) anti-arthritic drugs;
- compare the extent of uptake of gold compounds and nanoparticles by macrophages;
- investigate the intracellular fate of gold(I) drugs and gold nanoparticles in macrophages using microprobe synchrotron radiation X-ray fluorescence imaging;
- compare the relative abilities of gold(I) drugs and gold nanoparticles to affect the production of pro- and anti-inflammatory cytokines, reactive oxygen species, and nitric oxide in macrophages; and

- investigate the binding of gold(I) drugs and gold nanoparticles to thioredoxin reductase using electrospray ionisation mass spectrometry.

Chapter 2:

Materials and Methods

This chapter provides a detailed description of how the experiments described in this thesis were performed, along with details of where the many commercial reagents were obtained.

2.1 Materials

All aqueous solutions were prepared using Milli Q™ water (18.2 MΩ, Millipore, Billerica, USA) unless otherwise specified. Sodium aurothiomalate, sodium aurothioglucose, auranofin, gold(III) chloride (99.9%), dithiothreitol (99.0%, DTT), ethylenediaminetetraacetic acid (99%, EDTA) sodium citrate, caesium iodide (Fluka brand, 99.999%), trypan blue solution (0.5% w/v in phosphate-buffered saline, PBS), 3-(4,5-dimethylthiazol-2-yl)-2,5-diphenyltetrazolium bromide (MTT), sulfanilamide, *N*-(1-naphthyl)ethylenediamine dihydrochloride (NED), sodium nitrite, trace metals pure NaCl (99.999%), conc. hydrochloric acid (HCl, 98%), rat thioredoxin reductase (batch #033M4083V) and lipopolysaccharide (*Escherichia coli* serotype 055:B5) were obtained from Sigma-Aldrich (St. Louis, USA). Sodium aurothiosulfate was obtained from Alfa Aesar (Ward Hill, USA). Sodium hydroxide pellets (98%), sodium chloride, potassium chloride, potassium dihydrogen phosphate, sodium hydrogen phosphate, polysorbate 20 (TWEEN) and 4-(2-hydroxyethyl)-1-piperazineethanesulfonic acid (HEPES) (all ACS grade) were obtained from Amresco (Solon, USA). Ammonium acetate (98%), glacial acetic acid (99.5%), isopropanol (99.0%), methanol (99.8%) and ethanol (99.5%) were obtained from Ajax Finechem (Seven Hills, Australia), while dimethylsulfoxide (DMSO, 99.98%) was obtained from Fisher Scientific (Waltham, USA). Ultrapur nitric acid (HNO_3, 60% v/v) was obtained from Merck Millipore (Darmstadt, Germany), whilst a certified Au standard solution (997 mg/L Au, 10% HCl (v/v)) was obtained from PerkinElmer (Waltham, USA). Au NPs were purchased from BBI (product codes EM.GC2, EM.GC20 and EM.GC100; diameters 2, 20 and 100 nm, respectively) and Sigma-Aldrich (product codes 741965 and 753610; both have diameters of 20 nm, stabilised in citrate buffer and PBS, respectively).[*] Mouse

[*] Sigma-Aldrich state that both contain a "proprietary surfactant as stabilizer."

interleukin-10 and mouse tumour necrosis factor enzyme-linked immunosorbent assay (ELISA) kits (ELISA MAX™ Deluxe) were obtained from BioLegend (San Diego, USA). Invitrogen (Grand Island, USA) was used to obtain 2',7'-dichlorodihydrofluorescein diacetate ($DCFH_2$-DA), pre-cast NuPAGE 4-12% Bis-Tris gels, and Novex Sharp protein standards. Enzo Life Sciences (Plymouth Meeting, USA) was used to obtain 7-aminoactinomycin D (7AAD). PBS tablets (Oxoid brand) were obtained from Thermo Fisher Scientific (Waltham, USA). Fetal bovine serum (FBS, heat-inactivated) was obtained from Bovogen Biologicals (East Keilor, Australia). GlutaMAX™ and Roswell Park Memorial Institute-1640 (RPMI-1640) cell culture medium powder were obtained from Life Technologies (Carlsbad, USA). Disposable pipettes, 6-mL round bottom polystyrene tubes and 96 well plates for MTT assays were obtained from BD (Franklin Lakes, USA). Cell culture flasks (75 cm^2 surface area, T75 flasks), cell culture dishes (60 mm), 24-well plates, 96-well plates for Griess assays and cell scrapers were obtained from Greiner Bio-One GmbH (Frickenhausen, Germany). 15 mm diameter Nunc™ Thermanox™ coverslips were purchased from Emgrid Australia (The Patch, Australia). Silicon nitride (Si_3N_4) membranes (frame size = 5 mm × 5 mm; sample surface area = 1.5 mm × 1.5 mm; membrane thickness = 500 nm; and frame thickness = 200 nm) were obtained from Silson (Northampton, UK).

2.2 Synthesis of Gold Nanoparticles

A stock solution of gold nanoparticles was synthesised according to the classical method described by Turkevich et. al.,[190] but with some modifications. Milli-Q water (30 mL) was heated to near boiling and a solution of $HAuCl_4.3H_2O$ (10.00 mM in water, 2.000 mL) was added. This was followed by a solution of tri-sodium citrate (20.00 mM, 4.000 mL) and the resulting solution turned red (from colourless). The solution was subsequently heated for one hour, cooled to room temperature, and then

transferred to a volumetric flask (50.00 mL) to which Milli-Q water was added to produce a solution with a final concentration of 400 µM Au(0), assuming complete conversion of Au(III). More concentrated solutions of Au NPs required for nitric oxide formation experiments were prepared by centrifuging the above preparation of Au NPs (11000×g, 10 min), removing the top aqueous layer, and re-suspending the pellet containing the nanoparticles in a smaller volume of water.

Absorption spectra of Au NPs were obtained using a Varian (Santa Clara, USA) Cary 500 UV-VIS-NIR spectrophotometer and quartz cuvettes. Particle size analysis was performed on Au NPs using a Malvern (Malvern, UK) Zetasizer Nano S, while field emission scanning electron microscopy (FESEM) images were obtained using a JEOL (Akishima, Japan) JSM-7500FA FESEM instrument. The FESEM samples were prepared by allowing small volumes of Au NP solutions to evaporate on carbon-copper films.

2.3 Cell Culture

The adherent RAW264.7 macrophage cell line was obtained from the American Type Culture Collection (Manassas, USA) as frozen permanents. The cells were maintained in Roswell Park Memorial Institute-1640 (RPMI-1640) medium containing 10% (v/v) fetal bovine serum (FBS) and 2 mM GlutaMAX™ (complete medium) at 37 °C and 5% CO_2/95% air in a Revco (Twinsburg, USA) Ultima incubator. Cells were subcultured at 90% confluence, and used between 3 and 30 passages. Cells were lifted from the surface of flasks by gentle scraping. Treatment solutions containing sodium aurothiomalate or sodium aurothiosulfate were prepared in RPMI-1640 medium containing 2 mM GlutaMAX™ (incomplete medium). Control cells were also treated with incomplete medium. Treatment solutions containing auranofin were prepared by

first dissolving the metal complex in DMSO, and then diluting to the desired auranofin concentration using incomplete medium. The final concentration of DMSO in auranofin treatment solutions was 1% (v/v). Treatment solutions containing gold nanoparticles were prepared using a solvent consisting of 15% (v/v) water and 85% (v/v) incomplete medium. For inflammation assays (**Section 2.9**), gold nanoparticle treatment solutions were spiked with a small volume of concentrated Dulbecco's phosphate-buffered saline (10×D-PBS, preparation described in **Section 2.9.1)** to counteract disturbance of isotonicity due to dilution of the incomplete medium. The gold nanoparticle treatment solutions for these experiments were prepared using a solvent consisting of 1.5% (v/v) 10×D-PBS, 15% (v/v) water, 83.5% (v/v) incomplete medium.

2.4 Trypan Blue Assays

Trypan blue assays were performed to assess the number of viable cells in a sample, and were performed by adding cell suspension (50 µL) to trypan blue solution (50 µL). The resulting solution was loaded onto a Neubauer-improved bright-line haemocytometer (Marienfield-Superior, Lauda-Königshofen, Germany) and the number of viable (colourless) and non-viable (blue) cells were counted according to the manufacturer's instructions using a Motic (Causeway Bay, Hong Kong) AE20 light microscope at 10× magnification.

2.5 MTT Assays

The cytotoxicity of the gold compounds and Au NPs was assessed using the MTT assay.[212] This technique provides a measure of the cellular toxicity exhibited by a compound by spectrophotometrically quantifying the extent of mitochondrial enzymatic reduction of the yellow compound 3-(4,5-dimethylthiazol-2-yl)-2,5-diphenyltetrazolium bromide (MTT) to form the purple formazan, (*E*,*Z*)-5-(4,5-dimethylthiazol-2-yl)-2,5-

diphenylformazan.[212] This reaction (**Figure 2.1**) occurs in living cells with functioning mitochondria.[213] As such, the amount of purple formazan formed is directly proportional to the number of viable cells.

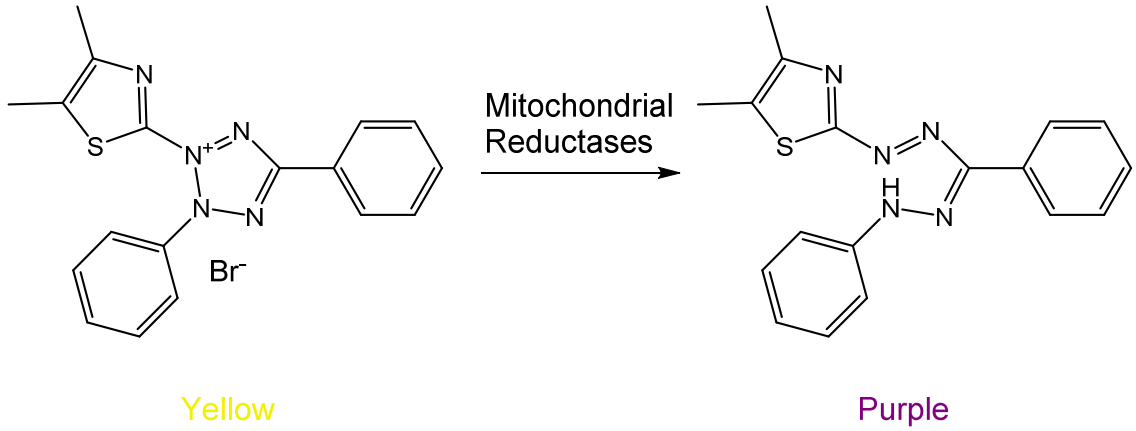

Figure 2.1: Reduction of yellow MTT to form a purple formazan compound.

RAW264.7 cells in complete medium were seeded into a 96-well plate (5×10^4 cells/100 µL/well) and incubated overnight (37 °C, 5% CO_2). The cell medium was then removed by aspiration and the cells were washed twice with incomplete medium (300 µL) to remove any FBS. Freshly prepared treatment solutions containing gold compounds or Au NPs at the required concentrations were added to the wells (100 µL/well) and incubated for either 4 h or 24 h. At the end of the treatment period, the treatment solutions were removed by aspiration, and the adherent cells were washed twice with incomplete medium (300 µL). For the 4 h treatments, the cells were incubated for an additional 20 h in incomplete medium (100 µL) before the addition of MTT solution (50 µL, 2 mg/mL in PBS) and subsequent incubation for 4 h. For the 24 h treatments, cells were incubated for 4 h with incomplete medium (100 µL) and MTT solution (50 µL, 2 mg/mL in PBS) immediately after washing the cells. At this time, the solutions were aspirated from the cells, and the resulting purple crystals dissolved in DMSO (200 µL/well). The absorbance of these solutions was then measured at 570 nm and 630 nm using a BMG Labtech (Offenburg, Germany) POLARstar Omega

microplate reader. The absorbance at 630 nm was used as a background subtraction, whilst the absorbance at 570 nm measured the amount of the formazan. In each assay six wells were allocated for each concentration of the gold compound or Au NPs being assessed, and eighteen wells were used for the control cells. The change in absorbance of each group of six or eighteen wells was averaged for calculations of the cell viabilities (**Equation 2.1**).

$$\text{Cell Viability (\%)} = \frac{A_{570} - A_{630}(\text{treated cells})}{A_{570} - A_{630}\ (\text{control cells})} \times 100 \qquad \textbf{2.1}$$

Each experiment was performed three times, and the errors reported here are the standard deviations between calculated cell viabilities for a given concentration on each plate.

2.6 Graphite Furnace Atomic Absorption Spectroscopy (GFAAS)

The quantity of gold associated with macrophages after treatment with gold compounds or Au NPs was determined by GFAAS.[43,214] RAW264.7 cells in complete medium (5×10^6/5.00 mL/dish) were seeded into sterile 60-mm cell culture dishes and incubated for 24 h. The cell medium was then removed, and the cells were washed once with PBS and once with incomplete medium to remove any FBS. Treatment solutions containing the Au compounds or Au NPs were then added to cells, which were then incubated for 24 h. At this point the treatment solutions containing any dying/lifted cells were collected in centrifuge tubes. Incomplete medium (5 mL) was added to the dishes and the adherent cells were harvested by gentle scraping and added to the cells contained in the treatment solutions. The combined cells were centrifuged (300×g, 5 min) and washed twice with incomplete medium (5 mL) followed by further centrifuging (300×g, 5 min). The resultant cells were resuspended in incomplete

medium (1.000 mL), and an aliquot (50.0 µL) then removed and the cell number and viability were assessed by the trypan blue method described in **Section 2.4**. The remaining cells were then centrifuged and washed twice with saline solution (preparation described in **Appendix A:**). The pellets were freeze-dried for 2 h and digested in nitric acid (10 - 100 µL Ultrapur, 60% v/v) overnight, whereby the volume of acid was dependant on the final dilution volume. The resulting solutions were subsequently diluted in 5.00 mL or 50.00 mL volumetric flasks with a final nitric acid concentration of 0.6% v/v. Triplicate cell samples were prepared for each concentration of gold compound or Au NPs examined.

GFAAS measurements were performed on the final solutions using a PerkinElmer AAnalyst 600 atomic absorption spectrometer equipped with the Winlab 32 AA Furnace program, incorporating Zeeman-effect background correction, an AS-800 autosampler, and an AA Accessory cooling system. A gold hollow cathode lamp (PerkinElmer) was employed that emitted radiation at a wavelength of 242.8 nm. A slit width of 0.7 nm was used to give an instrument energy reading of approximately 50 W. A certified Au standard solution (997 mg/L Au, 10% HCl (v/v)) was used to prepare the stock Au standard solution (50 µg/L, 0.6% HNO_3 v/v) for generation of a calibration curve (correlation coefficients: 0.992 - 0.994). The analyte (20 µL) was mixed with matrix modifier solution (5 µL), and atomised from the surface of a pyrolytic graphite-coated tube using the furnace operating conditions described in **Appendix A:**. Argon gas was used throughout the analysis, with absorption measurements conducted during the atomisation stage (1800 °C).

Triplicate measurements were performed for each sample and averaged to give the gold content per unit of volume for that sample. This was then converted into the mass of gold per cell using the results of the trypan blue assay determined prior to

sample digestion. Errors are reported as the standard deviation of the mean, n = 3. Statistical significance was tested by one-way analysis of variance (ANOVA) with a Tukey post-test set at 95% confidence intervals, performed using GraphPad Prism version 5.03. These tests were performed on two subgroups of samples based upon treatment concentration (2.5 μM and 60 μM).

2.7 Microprobe Synchrotron Radiation X-Ray Fluorescence (SR-XRF) Imaging

The spatial distribution of gold and other elements within macrophages that had been treated with either Au(I) compounds or Au NPs was determined by microprobe SR-XRF imaging.[215–219] In this experiment, the sample is bombarded with focussed X-rays from a synchrotron source. If the X-ray beam possesses high enough energy to excite core electrons of an atom of interest, these electrons are ejected into the continuum producing an unstable ion with a vacancy in the core shell. This vacancy is subsequently filled by an electron from an outer energy level, releasing an X-ray fluorescent photon. This principle, illustrated in **Figure 2.2**, results in emission of fluorescent photons that are characteristic of the elements analysed, due to the unique energy transitions between orbitals of different elements. As such it is possible to detect a range of elements present in a sample simultaneously without the need for additional treatment steps.

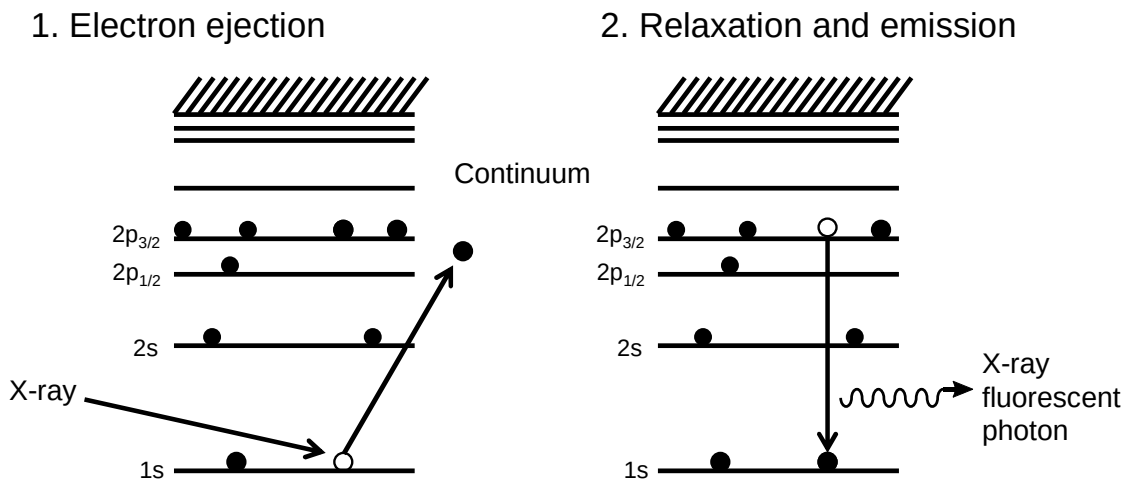

Figure 2.2: Illustration of X-ray fluorescence utilised in SR-XRF.

2.7.1 Preparation of Samples

Samples for both high and low resolution mapping were prepared on Si_3N_4 membranes, which were initially washed once with ethanol (70% v/v), twice with sterile PBS, and finally once in cell growth medium, before being placed in a 60 mm cell culture dish. RAW264.7 cells in complete medium (5×10^6/5 mL) were seeded into the dishes and incubated overnight. After confirming that the cells had grown to a sufficient confluence on the Si_3N_4 membranes, the medium was removed and the cells were washed twice with incomplete medium to remove any FBS. Treatment solutions (5.00 mL), containing the appropriate concentrations of Au(I) compounds or Au NPs, were then added to the dishes prior to incubation for 24 h. Following this period the membranes were removed from the dishes, and washed by sequentially dipping in two solutions of PBS and then three solutions of ammonium acetate (200 μM) to remove any excess phosphate or chloride ions.[220,221] The cells were then fixed by dipping once in methanol.[222,223] The membranes were freeze-dried overnight and stored in a desiccator until analysed.

2.7.2 High Resolution Mapping

Microprobe SR-XRF analysis of individual cells was performed on the 2-ID-D beamline at the Advanced Photon Source (APS), Argonne National Laboratory (Chicago, United States) using a monochromatic 13.45 keV X-ray beam focused to 0.3 μm^2 using two stacked zone plates. The silicon nitride (Si_3N_4) membranes were mounted on a high precision XYZ motorised stage (PM20076), and the fluorescent X-rays were detected using a Vortex EM (Radiant Detector Technologies, LLC, Northridge, USA, 165-VTX-EM) silicon drift detector operating in fluorescence mode. High resolution elemental maps were acquired over pre-determined scan areas using a 0.5 µm step size and 0.5 s/point dwell time. The elements were quantified with the aid of corresponding measurements from the thin film standards NBS-1832 and NBS-1833, obtained from the National Bureau of Standards (Gaithersburg, USA).

2.7.3 Low Resolution Mapping

Elemental mapping of large cell areas (120 µm × 120 µm) with lower resolution was performed at the XFM beamline at the Australian Synchrotron (AS, Clayton, Australia) to compare gold uptake across a large population of cells. These experiments were performed using a monochromatic 12.055 keV X-ray beam focused to 2 µm in the horizontal and vertical dimensions using a Kirk-Patrick Baez mirror and a silicon drift diode detector operating in fluorescence mode.[216] Elemental maps were acquired using a 2 µm step size and 1 s/point dwell time.

2.7.4 Data Analysis

The full fluorescence spectra obtained at either the APS or AS were fitted to modified Gaussians and the data was processed using the MAPS software package, version 1.7.1.03, provided by Dr Stefan Vogt at APS.

2.8 Scanning Electron Microscopy of Cells

Samples were prepared on 15 mm diameter Nunc™ coverslips, which were initially washed with ethanol (70% v/v) and then complete medium, before being placed in a 60-mm cell culture dish. RAW264.7 cells in complete medium (3×10^6/5.00 mL/dish) were seeded into the dishes and incubated overnight. After confirming that the cells had grown to a sufficient confluence on the coverslips, the medium was removed and the cells were washed twice with incomplete medium to remove FBS. Treatment solutions (5.00 mL) containing the appropriate concentrations of Au NPs were then added to the dishes prior to incubation for 24 h. Following this period the coverslips were removed from the dishes, washed in PBS twice and then placed into glutaraldehyde solution (2% v/v in PBS) for 2 h at room temperature. At the end of this period, the coverslips were washed twice in PBS, then dehydrated by incremental increases of ethanol solution (30% × 2, 50% × 2, 70% × 2; v/v; 10 min/solution) and refrigerated overnight in 70% ethanol. The coverslips were cut to size, then further dehydrated by incremental increases of ethanol solution (70% × 1, 80% × 1, 90% × 1, 100% × 3; v/v; 10 min/solution).

At this point, the samples were dried by critical point drying (CPD) using an EM CPD030 instrument (Leica, Wetzlar, Germany). Briefly, the samples were submerged in ethanol at 8 °C in the chamber of the instrument, and liquid CO_2 added until the chamber was full. After 15 min, the chamber was partially drained and refilled with liquid CO_2, which was repeated three times. The chamber was then heated to 40 °C and CO_2 gas slowly drained to dry the samples. At this point, the samples were mounted in a sample holder, coated with 10 nm of platinum and analysed using a JEOL JSM-6490LV FESEM instrument for general images and a JEOL JSM-7500FA FESEM instrument for variable accelerating voltage and electron dispersive X-ray (EDX) images.

2.9 Inflammation Assays

2.9.1 Solutions

Investigations into the formation of inflammation markers required a number of different solutions and cell media, prepared as described in **Appendix A:**. Their names and components are briefly described here. Dulbecco's phosphate-buffered saline (D-PBS) consisted of KCl (2.67 mM), KH_2PO_4 (1.47 mM), NaCl (138 mM) and Na_2HPO_4 (8.10 mM). 10×D-PBS contained KCl (26.7 mM), KH_2PO_4 (14.7 mM), NaCl (1.38 M) and Na_2HPO_4 (81.0 mM). Enzyme-linked immunosorbent assay (ELISA) wash buffer contained 0.5% v/v TWEEN/D-PBS. Incomplete NaCl medium contained KCl (5 mM), HEPES (10 mM) and NaCl (145 mM), while complete NaCl medium was prepared by adding glucose (5 mM) to incomplete NaCl medium.

Solutions containing commercial Au NPs, required for NO and ROS formation experiments were administered to cells using the Au NPs vehicle, which consisted of 1.5% (v/v) 10×D-PBS, 15% (v/v) water, 83.5% (v/v) incomplete medium. The concentration of Au NPs in treatment solutions prepared from commercial nanoparticle solutions was generally 40 µM. The only exception to this was stock solutions containing 2 nm Au NPs which were originally obtained from BBI. In this case, the final concentration of the stock solution was 9 µM.

2.9.2 Assays

The initial preparation of samples for determining the extent of inflammation marker formation was performed using the following, similar steps. RAW264.7 cells were seeded into a 24-well plate (5×10^5/1.000 mL/well) and incubated overnight. The medium was removed by aspiration and the cells were washed three times with incomplete medium (1 mL). The relevant vehicle (500 µL/well) containing LPS (a

positive control treatment), gold compounds or Au NPs was added and incubated with the cells for 24 h. In other experiments, cells in incomplete medium (500 µL/well) were pre-incubated with gold compounds or Au NPs for 4 h, after which LPS (100 ng/mL) was added and the cells were incubated for a further 20 h.

Sections 2.9.3 - 2.9.5 describe the procedures used to determine the extent of inflammation marker formation after the treatment described above.

2.9.3 Nitric Oxide Formation

The production of reactive nitrogen species including nitric oxide (NO) was assessed by measuring total nitrite concentration using the Griess assay.[203,224] Nitrite (NO_2^-) is a major cellular decay product of NO, an inflammation mediator that has a short biological half-life. As a consequence, the amount of NO_2^- released from cells is commonly used to infer relative amounts of NO production.[224] In the presence of nitrite and acid, sulfanilamide and *N*-(1-naphthyl)ethylenediamine (NED) combine to form the Griess reagent, an azo compound that is pink in colour (**Figure 2.3**).

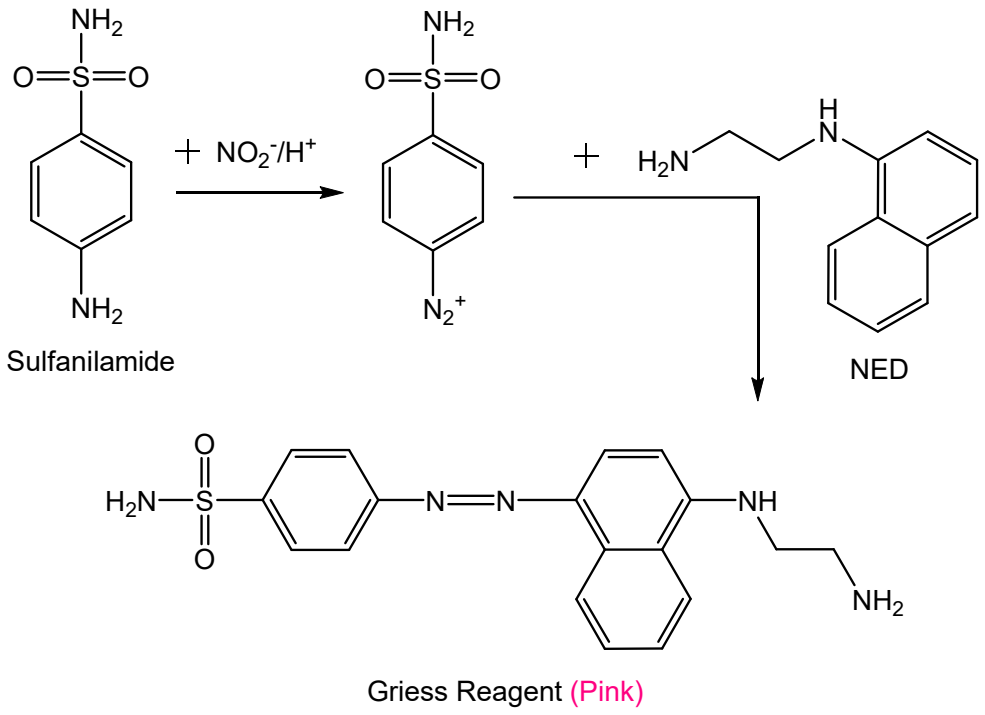

Figure 2.3: Reaction scheme for formation of the Griess reagent in assays used to detect nitrite.

Prior to commencement of an assay, a stock solution of sulfanilamide was prepared by dissolving 1.0 g in 100 mL of 5% (v/v) HCl. In addition, a stock solution of NED was prepared by dissolving the dihydrochloride salt (0.1 g) in Milli-Q H_2O (100 mL). Macrophages were first treated with gold compounds or Au NPs as described in **Section 2.9**, after which the resulting solutions were removed by aspiration and centrifuged (300×*g*, 5 min) to obtain cell-free supernatants. Triplicate aliquots (50 µL) of each supernatant or freshly prepared $NaNO_2$ standards (0 – 100 µM, in 10 µM increments) were added to the wells of a 96-well plate. The sulfanilamide stock solution (25 µL) was added to each well using an 8-channel micropipette, followed by NED stock solution (25 µL). The plate was then incubated at room temperature for 10 min. Wells containing nitrite changed to a pink colour. The absorbance at 540 nm (A_{540}) was measured using a Molecular Devices (Sunnyvale, USA) SpectraMAX Plus 384 microplate reader. The mean absorbance of the triplicates for each sample or standard were calculated and the concentration of nitrite in each sample was interpolated from a linear standard curve (0 – 100 µM, 11 points, 10 µM increments) using GraphPad Prism version 5.03 (GraphPad Software, Inc., La Jolla, USA). The experiment was performed three times, with the errors reported being the standard error of the mean for each replicate experiment.

2.9.4 Reactive Oxygen Species Formation

The production of reactive oxygen species (ROS) was assessed by measuring the extent of cellular conversion of 2',7'-dichlorodihydrofluorescein diacetate ($DCFH_2$-DA) to 2',7'-dichlorofluorescein (DCF).[225,226] $DCFH_2$-DA is readily taken up by cells and subsequently converted in two steps to a fluorescent dye. Intracellular esterase enzymes remove the two acetyl groups of $DCFH_2$-DA to form $DCFH_2$, which is subsequently oxidised to the conjugated fluorescent molecule DCF by cellular ROS (**Figure 2.4**). By

targeting cells with a laser, it is possible to excite and then detect any DCF present within cells and thus infer the amount of ROS that has been formed.

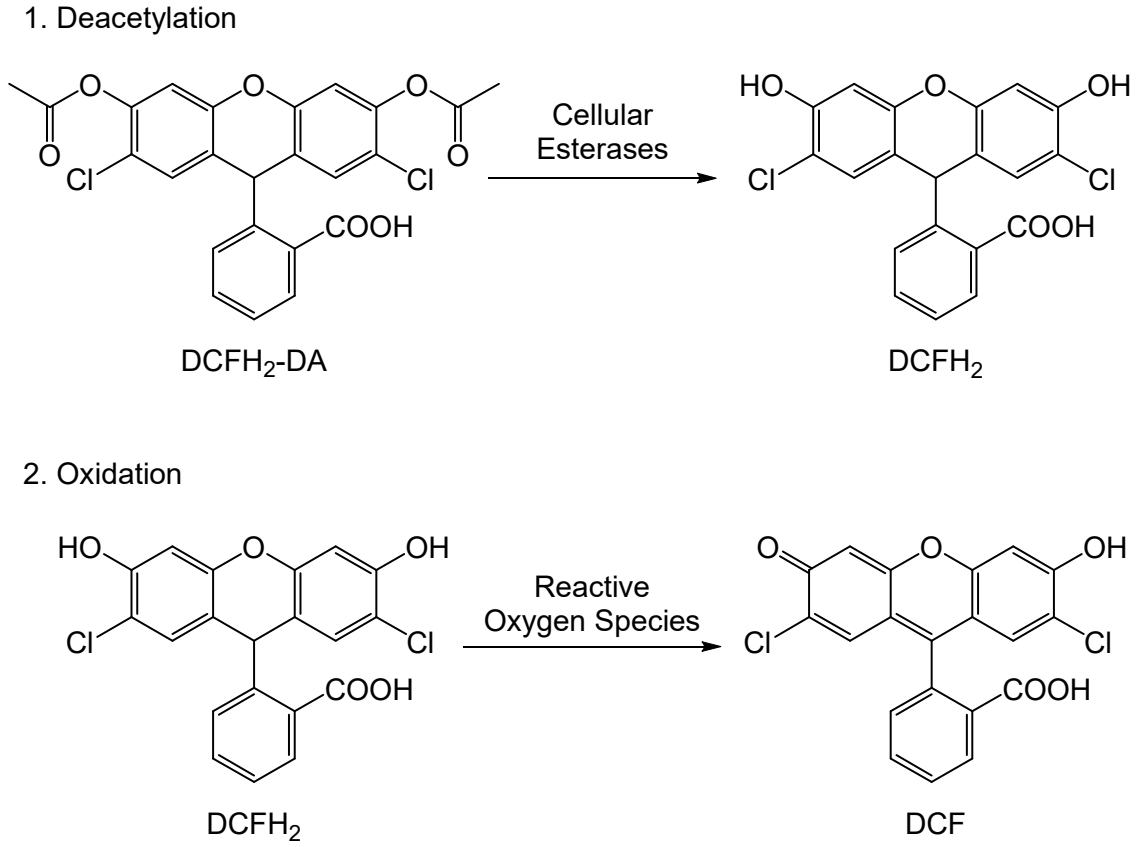

Figure 2.4: Reaction scheme for conversion of $DCFH_2$-DA to DCF employed for the detection of ROS.

The following describes a typical experiment assessing the extent of ROS production using DCF. Stock solutions containing $DCFH_2$-DA were dissolved in DMSO to obtain a concentration of 5 mM and were stored frozen at -20 °C in 30 µL aliquots. Experiments were performed in minimal light to prevent photodecay of the fluorescent dyes. After macrophages were treated with gold compounds or Au NPs as described in **Section 2.9**, the treatment solution was removed by aspiration and the cells were washed three times with incomplete NaCl medium (1 mL). $DCFH_2$-DA (500 µL, 10 µM in complete NaCl medium) or DMSO for autofluorescence control samples (500 µL, 0.2% in complete NaCl medium) was added to the wells and the plate was incubated for 30 min. The cells were then washed three times with incomplete NaCl

medium (1 mL) before being harvested by gentle scraping in complete NaCl medium (500 µL). The cell suspensions were then transferred to 6 mL round bottom polystyrene tubes and centrifuged (300×*g*, 5 min) to produce a pellet. The supernatant was decanted and the resuspended cells (<50 µL) were incubated with 7-aminoactinomycin D (7AAD, 1 µL, 1 mg/mL) at room temperature for 5 min. Complete NaCl medium (300 µL) was added and the suspension analysed using a Becton Dickinson (San Jose, USA) LSR II flow cytometer. The samples were excited using a blue laser (488 nm) with emissions measured at 515 nm and 695 nm corresponding to DCF and 7AAD fluorescence, respectively. 10000 events were counted for each sample. Instrumental fluorescence compensation was applied in some experiments to account for 'bleeding' of one high intensity fluorescent marker into the other.

The data was analysed using FlowJo (Tree Star, Ashland, USA), with ROS production reported as the median fluorescence intensity at 515 nm for viable cells. Viable cells were gated initially on the basis of forward scatter and side scatter, and secondly on the basis of fluorescence at 695 nm, to exclude 7AAD high (non-viable) cells. The median fluorescence intensity (MFI) at 515 nm for DMSO-treated autofluorescence control samples was subtracted from that of the relevant sample treated with $DCFH_2$-DA to determine the amount of ROS production following each treatment. The experiment was performed five times with the errors reported as the standard error of the mean. For the LPS-induced ROS production experiment, final median fluorescence intensity values were normalised to the control sample (incomplete medium only) and reported as percentages.

2.9.5 IL-10 and TNF Release

The extent of production of the cytokines IL-10 and TNF was assessed by ELISAs performed using pre-packaged kits obtained from BioLegend. These kits contained all the buffers, standards, antibodies and high-binding 96-well plates required to perform the assays, with the exception of the wash buffer, which was prepared as described in **Appendix A.5.** The protocol for performing the ELISAs was provided by the manufacturer and is described in the following sections. All wash steps were performed by inverting the plate, blotting the plate dry on paper towel and adding approximately 300 µL of wash buffer. Prior to use, cell treatment supernatants were removed and centrifuged (300×*g*, 5 min) to pellet any floating cells.

Wells of a high-binding 96-well ELISA plate were incubated overnight at 4 °C with the specific capture antibody required for the ELISA to be performed, which was present in coating buffer (100 µL). Wells were then washed three times with wash buffer and blocked with the assay diluent (200 µL) for 1 h at room temperature. The ELISA plate was then washed once with wash buffer, and duplicate aliquots (100 µL) of each sample or respective cytokine standard were added to each well and incubated at room temperature for 2 h. The wells were then washed five times with wash buffer, the respective detection antibody was added (100 µL), and the wells incubated at room temperature for 1 h. The wells were then washed with wash buffer five times and Avidin-HRP (100 µL) added prior to incubation at room temperature for a further 30 min. At this point, the wells were washed (seven times for TNF and twelve times for IL-10) with wash buffer, substrate solution (100 µL) then added to each well and the resulting mixtures incubated at room temperature for a further 15 min. Finally, H_2SO_4 (1 M, 50 µL) was added to each well and the absorbance of each well was measured at

450 nm and 570 nm using a Molecular Devices SpectraMAX Plus 384 microplate reader.

The absorbance at 570 nm was used as a background subtraction, whilst the absorbance at 450 nm corresponded to the blue colour arising from the presence of either cytokine. The absorbance of duplicate wells for each sample or standard was averaged and used for calculations. The concentration of cytokine in each sample was interpolated from a standard curve (0 – 2000 pg/mL for IL-10, 0 – 500 pg/mL for TNF; 8 points per curve, 2 fold increments), which was transformed to the log scale on both axes using GraphPad Prism version 5.03. Each experiment was performed three times, with the errors reported as the standard error of the mean for each replicate experiment.

2.9.6 Statistical Analyses

Statistical significance was tested by using either a one-way ANOVA with a Tukey post-test set at 95% confidence intervals, or a two-tailed unpaired *t*-test with a 95% confidence interval. The tests were applied on subgroups of samples based on what vehicle was used. Specifically, both concentrations of aurothiomalate-treated samples were sub-grouped with their vehicle (incomplete medium) and tested by one-way ANOVA, whilst both concentrations of Au NP-treated samples were sub-grouped with the Au NPs vehicle and also tested by one-way ANOVA. Samples treated with 2.5 µM auranofin were grouped with the auranofin vehicle treatment and tested by *t*-test. The auranofin and Au NPs vehicles were both grouped with incomplete medium and tested by one-way ANOVA. As such, significance reported for a sample refers to when it is compared to its relevant vehicle. All statistical analyses were performed using GraphPad Prism version 5.03.

2.10 Expression and Purification of Human TrxR

A plasmid containing human thioredoxin reductase (hTrxR), pET46-$(His)_6$-hTrxR1, was obtained from A. Wang.[169] The expressed protein had the codon for selenocysteine-498 mutated to a cysteine to facilitate bacterial expression and contained an N-terminal His_6 tag to assist purification. *E. coli* BL21(λDE3)/pLysS containing the $TRXR^+$ plasmid was grown in lysogeny broth (tryptone (7.5 g), yeast extract (3.75 g), NaCl (7.5 g) in Milli-Q H_2O (750 mL)) at 37 °C to A_{600} = 0.6. The culture was cooled to 23 °C, and TrxR production was induced with isopropyl-β-D-thiogalactoside (IPTG, 1 mM) overnight. Cells were collected by centrifugation (10000×*g*, 15 min) and resuspended in buffer A (50 mM Tris-HCl, pH 8.0, 500 mM NaCl, 10 mM imidazole), before being lysed using a French press. The lysate was then clarified (28000×*g*, 30 min) and the supernatant loaded onto a Ni^{2+}-affinity column (HisTrap HP, GE Healthcare).

The column was eluted with imidazole (12 mL, 25 mM), followed by a linear gradient (30 mL) of imidazole (25 – 350 mM) in buffer A. Fractions containing the purest preparation of TrxR, as assessed by sodium dodecyl sulfate polyacrylamide gel electrophoresis (SDS-PAGE, described below) were combined, dialyzed into buffer B (30 mM Tris-HCl, pH 8.0, 2 mM DTT, 1 mM EDTA), and loaded onto an anion-exchange column (8-mL MonoQ GL, GE Healthcare). Purified hTrxR was eluted with NaCl (12 mL, 120 mM) followed by a linear gradient (160 mL) of NaCl (120 – 300 mM) in buffer B. Fractions containing ≥ 90% purified hTrxR were pooled, frozen in liquid nitrogen and stored at –80 °C.

Assessment of protein purity was performed using denaturing SDS-PAGE. Protein samples were mixed with SDS loading buffer (300 mM Tris base, 50 mM DTT,

2% (w/v) SDS, 10% (v/v) glycerol and 0.03% (w/v) bromophenol blue) and heated to 90 °C for 5 min before loading into a pre-cast NuPAGE 4-12% Bis-Tris gel. Loaded gels were electrophoresed at 200 V for 1 h using an Xcell4 Midi-Cell (Invitrogen, Grand Island, USA) apparatus. Following electrophoresis, the gels were stained with hot Coomassie staining solution (40% (v/v) methanol, 10% (v/v) acetic acid, 0.3% (w/v) Coomassie brilliant blue) for 20 min, then destained with hot destaining solution (25% (v/v) methanol 10% (v/v) acetic acid). De-stained SDS-PAGE gels were imaged using a Molecular Imager Gel Doc XR+ system (Bio-Rad, Hercules, USA). Protein band positions were compared to a Novex Sharp protein standard.

2.11 Electrospray Ionisation Mass Spectrometry

The following section describes how a typical investigation into the reactivity of gold compounds towards either human or rat TrxR was undertaken using ESI-MS.[88,227] Frozen TrxR (200 µL) was thawed on ice, and dialysed for 3 h against ammonium acetate (100 mM or 500 mM, pH 7.2) containing DTT (1 mM) using tubing with a molecular weight cut off of 12 000 mass units. The dialysis was performed twice more (3 h each) using the same solutions but without DTT present. The absorbance of the solution at 280 nm was determined using a Thermo Scientific (Waltham, USA) NanoDrop 2000 spectrophotometer and the final protein concentration was determined using the Beer-Lambert law and extinction coefficients calculated using the ExPASY ProtParam tool[228,229] (ε = 65165 $L.mol^{-1}.cm^{-1}$ for hTrxR and ε = 58330 $L.mol^{-1}.cm^{-1}$ for rTrxR).

Stock solutions of each gold complex or Au NPs were freshly prepared on the day that they were used. The required volumes were added to the protein sample to give reaction mixtures containing the desired molar ratios of gold drug : TrxR, with the

protein concentration diluted with H_2O to approximately 1 µM. The reaction mixtures were left on ice to react for the pre-determined periods of time, after which glacial acetic acid was added (final concentration of 5% (v/v) for hTrxR, 1% (v/v) for rTrxR). For rTrxR, methanol was also added (final concentration 10% (v/v)) to assist ionisation. The reaction mixtures were then immediately analysed using the mass spectrometer. Experiments investigating gold binding at different time points were performed similarly. The reaction mixtures were prepared and at the required time point an aliquot was removed and acetic acid or acetic acid/methanol added to it. The solution was then immediately analysed using the mass spectrometer.

Spectra were acquired using a Waters (Manchester, UK) Q-ToF Ultima ESI mass spectrometer operating in positive ion mode using a nanospray source, over the *m/z* range 1000–6500, with at least 50 acquisitions combined to give the final spectrum. The instrument was calibrated using a caesium iodide solution (10 mg/mL in 70% isopropanol/water). Raw spectra were background subtracted and smoothed using a Savitsky-Golay algorithm, and the charge series ions were transformed to a mass scale using MassLynx software (Waters, Manchester, UK). Stated masses and their errors were also calculated using MassLynx software.

2.12 Protein Identification by Proteomics

Experiments to definitively identify either human or rat thioredoxin reductase were performed by a collaborator, Dr. Matt Padula (University of Technology, Sydney). The procedure used is broadly described here. Purified TrxR samples were analysed by gel electrophoresis and bands of interest excised. The protein band was then buffered and digested using trypsin, and the resultant peptides chemically extracted from the gel. The peptides were then separated and analysed by liquid chromatography/mass

spectrometry (LC/MS). The detected peptides were compared to a protein database using the search engine Mascot (Matrix Software, Boston, USA)[230] and the proteins present in the sample subsequently identified.

Chapter 3:
Cellular Toxicity, Uptake and Localisation of Gold Complexes and Nanoparticles

---

This chapter compares the uptake and final distribution of a selection of anti-arthritic gold(I) compounds and gold nanoparticles within RAW264.7 macrophages. The toxicity of the gold compounds and nanoparticles was also investigated using the MTT assay, whilst quantification of the amount of gold incorporated into the cells was determined by graphite furnace AAS. The distribution of gold within individual macrophages and across a population of macrophages was investigated by performing microprobe SR-XRF imaging at the Advanced Photon Source, Argonne National Laboratory, and the Australian Synchrotron. Scanning electron microscopy was also used in an attempt to provide evidence that gold nanoparticles were internalised by the macrophages, and that they were not simply associated with the exterior cell surfaces. Parts of the work presented within this chapter were published in: James, L. R. A; et al., *J. Inorg. Biochem.*, **2015**, *142*, 28-38.

3.1 Introduction

One of the core aims of this research project was to compare the cellular toxicity, uptake and localisation of gold compounds and Au NPs. The cell line chosen for this and all other cellular experiments in this project was the murine macrophage line, RAW264.7. Macrophages phagocytose cellular debris and pathogens, and are heavily involved in RA progression as they promote inflammation and stimulate other immune cells through emission of various mediators.[18] Due to the controversies noted in **Section 1.4.2** regarding the biological interactions of Au NPs, those used in this project were characterised prior to use. In addition to allowing comparisons of cytotoxicity, the results of the MTT assays also provided the concentrations of the gold compounds and Au NPs to be used in all subsequent experiments. All statistical analyses presented in this chapter were performed using a one-way analysis of variance, with a Tukey-Kramer post-test set at 95% confidence intervals.

3.2 Characterisation of Gold Nanoparticles

The physical and electronic properties of Au NPs, prepared as described in **Section 2.2**, were characterised by absorption spectrophotometry, FESEM and particle size analysis. This facilitated comparisons with similar materials for which the biological properties had been previously reported, as it was noted earlier (**Section 1.4.2**) that differences in the physical or chemical characteristics of Au NPs can impact dramatically upon their biological interactions. **Figure 3.1** shows the absorption spectrum of a sample of the Au NPs. The spectrum featured one broad surface plasmon resonance band centred at 522 nm as well as significant absorbance at higher energies. The overall spectrum is consistent with that of other samples of gold nanoparticles.[231–233]

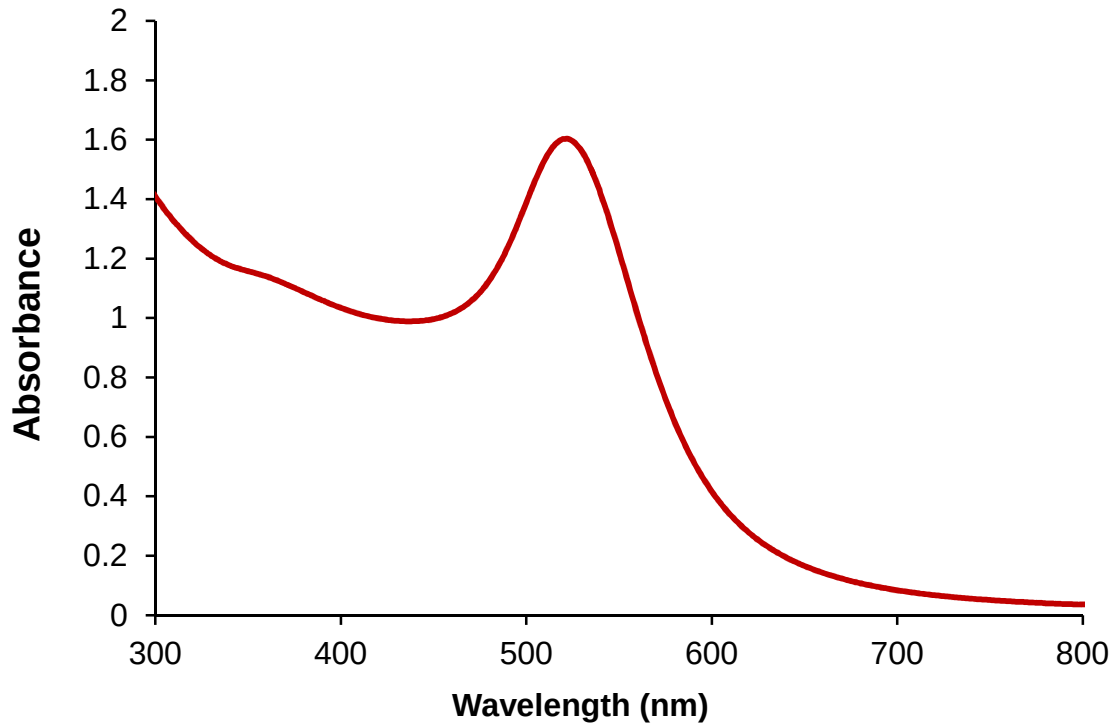

Figure 3.1: UV-visible absorption spectrum of a solution containing 400 µM Au NPs.

A FESEM image of a solution of Au NPs is shown in **Figure 3.2**. These were prepared by evaporation on a copper grid to produce particles that were generally spherical in shape and relatively uniform in size, with diameters ranging from 10 – 20 nm. These results were then compared with those obtained from particle size analysis performed using a zetasizer. This instrument assesses the distribution of particle sizes in a suspension by periodically shining a laser into the sample and measuring scattered light, a process known as dynamic light scattering.[234] Measurements performed using the zetasizer were analysed to reveal an average diameter of 23 ± 7 nm for the Au NPs, which is in good agreement with the results obtained from FESEM (**Figure 3.2**).

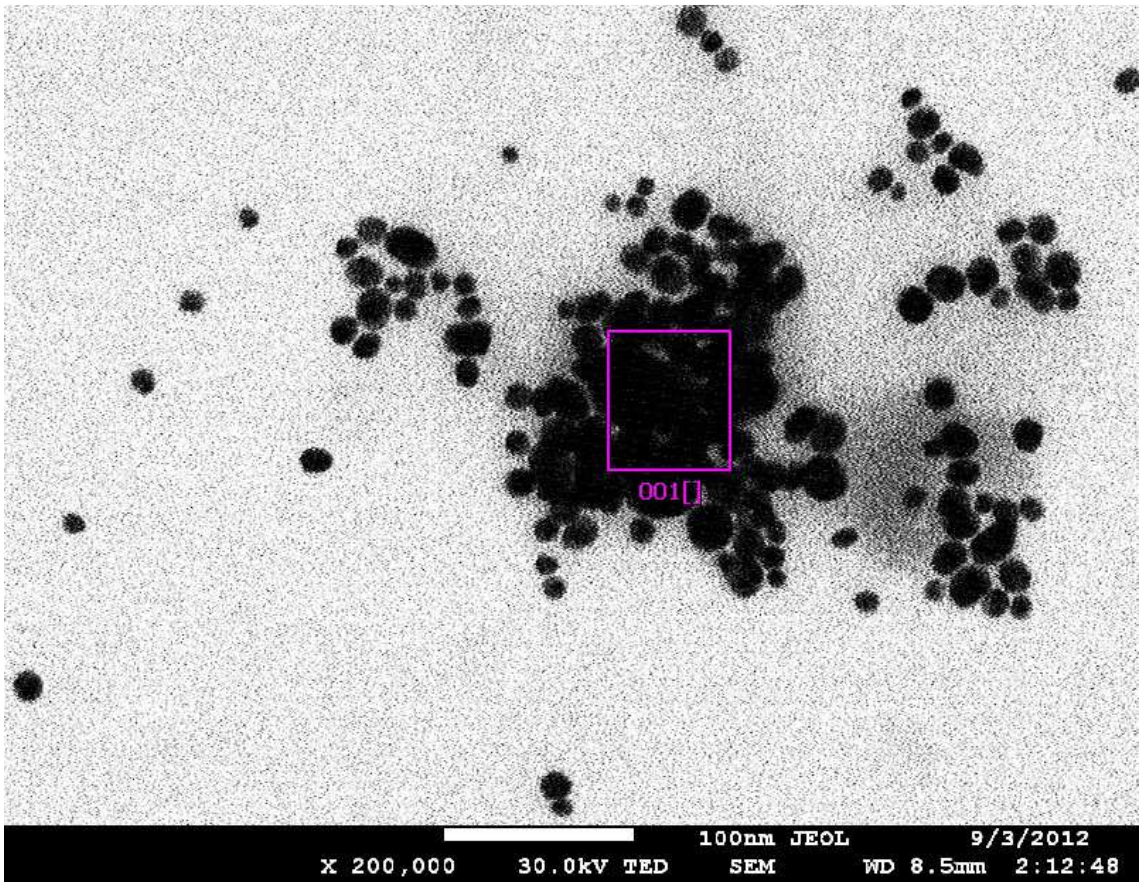

Figure 3.2: Field emission scanning electron micrograph of Au NPs evaporated on a copper membrane. A 100-nm scale bar is shown at the bottom of the image. The pink box indicates the area that was used to obtain an EDX spectrum.

EDX spectroscopy was performed simultaneously with FESEM, and afforded the spectrum shown in **Figure 3.3**. This technique operates on a similar principle to SR-XRF to allow simultaneous detection of a number of different elements present in a sample. The chief difference between the two methods is that EDX uses electrons to excite the sample, whilst SR-XRF uses X-rays. EDX spectroscopy detects the presence of any impurities, such as other metals in the nanoparticles. In addition to signals arising from gold, the spectrum in **Figure 3.3** contained intense peaks consistent with the presence of large quantities of carbon and copper, which are the main components of the carbon-copper support grid. Importantly, the spectrum did not reveal the presence of other metals, such as iron and manganese, which were viewed as potential contaminants.

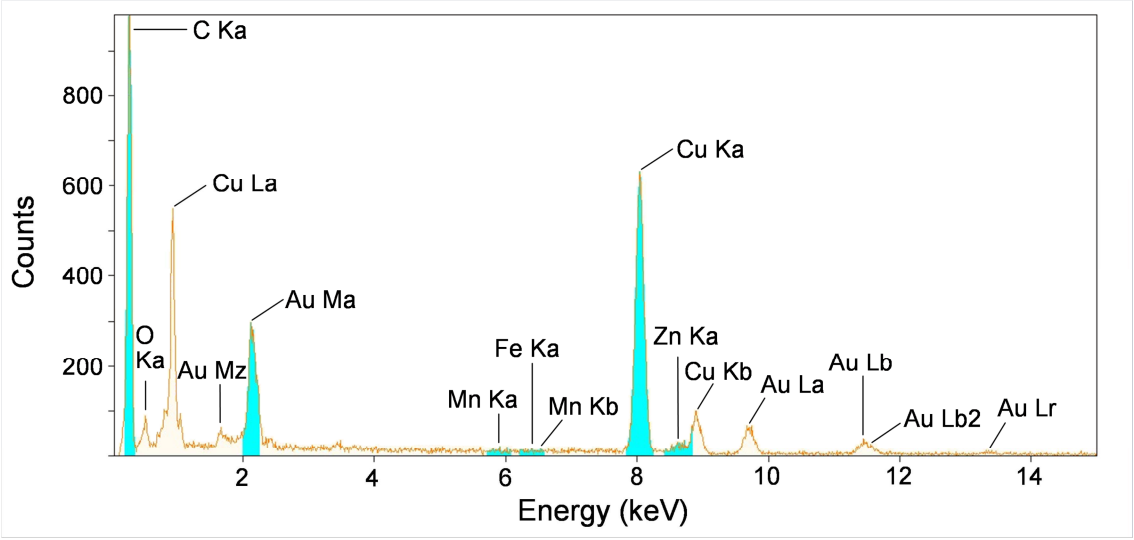

Figure 3.3: Energy-dispersive X-ray spectrum of Au NPs deposited on a carbon-copper membrane. Peaks highlighted in blue are the major signals arising from that element.

3.3 Cytotoxicity

The toxicity of a selection of gold(I) compounds with anti-arthritic activity, and Au NPs towards macrophages was compared for two reasons. First of all, while similar studies have been conducted previously using either gold compounds or Au NPs, none had previously directly compared the cytotoxicity of the two classes of gold species. Secondly, the results of these studies were needed to determine the concentrations of gold compounds and Au NPs to be used for subsequent cellular uptake and localisation experiments, as well as studies examining their effects on the expression of inflammation markers.

Since the gold compounds used in these experiments have different solubilities, a number of control cytotoxicity experiments were also performed to determine if any of the solvents or other reagents used had any significant toxicity. For example, while most of the gold compounds examined were soluble in water, this was not true for auranofin, which was instead very soluble in both ethanol and DMSO. Ethanol is a known cytotoxic substance,[235] whilst DMSO is better tolerated by cells and accordingly features in many tissue culture protocols.[236] As such, solutions of DMSO and

incomplete medium were selected for preparing solutions of auranofin to enable its administration. Therefore, it was necessary to assess the cytotoxicity of solutions containing varying amounts of DMSO and incomplete medium towards the macrophages. **Figure 3.4** presents the results obtained from this investigation.

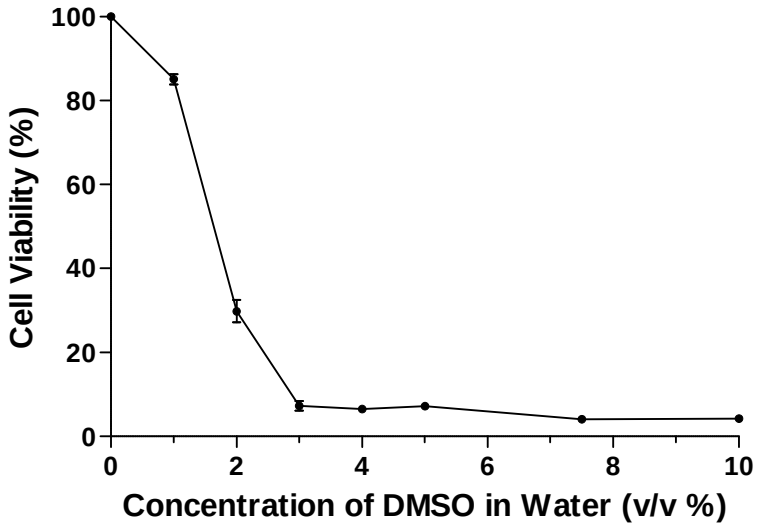

Figure 3.4: Cytotoxicity of solutions containing increasing amounts of DMSO dissolved in incomplete medium, towards RAW264.7 cells, as assessed by the MTT assay. The macrophages were incubated with the solutions at 37 °C under an atmosphere of 5% CO_2 for 24 h. The error bars represent one standard deviation calculated from triplicate plates.

Inspection of the graph shows that introduction of 1% (v/v) DMSO into complete medium resulted in cell viability falling to 85%, while increasing the amount of DMSO to 2% (v/v) resulted in cell viability falling much further to 30%. Further increases in the amount of DMSO present resulted in cell viability falling to ≤ 7%. Therefore cytotoxicity studies involving auranofin were performed with solutions prepared using a solvent consisting of 1% (v/v) DMSO in incomplete medium. Solutions of all other gold complexes were prepared using incomplete medium alone.

The results of initial cytotoxicity experiments performed by exposing the macrophages to gold compounds for 4 h are shown in **Figure 3.5**. It is clear from examining the figure that auranofin was the most toxic gold compound, with an IC_{50} of

5 µM. The next most toxic compound was dicyanoaurate, a notable chrysotherapy metabolite, with an IC_{50} of 35 µM. The other two compounds investigated, aurothiosulfate and aurothiomalate, did not show any signs of toxicity even in solutions containing the maximum concentrations of these two complexes, 100 and 10000 µM, respectively.

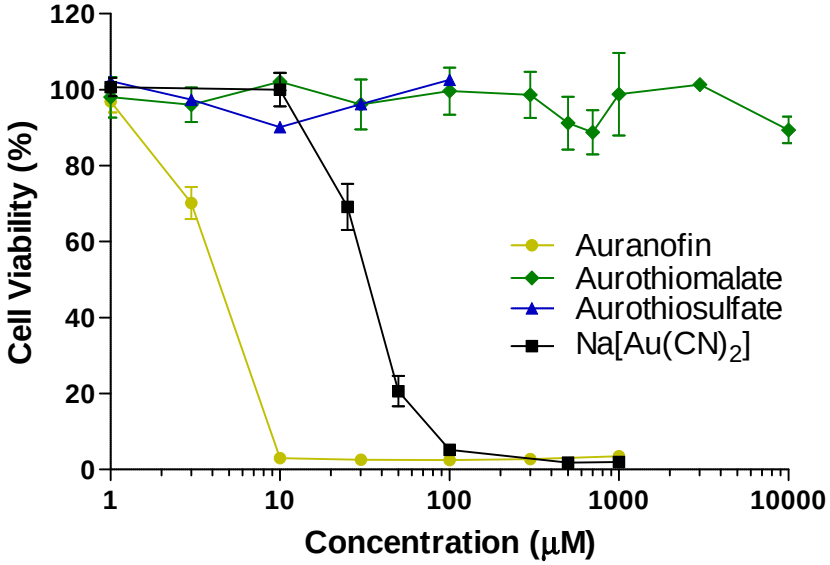

Figure 3.5: Cytotoxicity of some anti-arthritic gold compounds towards RAW264.7 cells, as assessed by the MTT assay. The macrophages were incubated with the gold compounds at 37 °C under an atmosphere of 5% CO_2 for 4 h. The error bars represent one standard deviation calculated from triplicate plates.

Investigations into the toxicity of the gold compounds towards macrophages after a 24-h treatment period were also performed, with the results obtained shown in **Figure 3.6**. Once again, auranofin proved to be the most toxic compound, with a slightly lower IC_{50} of 4 µM, compared to that obtained from the 4-h treatment. Dicyanoaurate exhibited significantly greater cytotoxicity as a result of the longer exposure period to the cells, as its IC_{50} value decreased to ~9 µM, compared to the value of 35 µM obtained after a 4-h treatment period. **Figure 3.6** shows that aurothiosulfate exhibited very low levels of cytotoxicity, with an IC_{50} of 650 µM. In

contrast, aurothiomalate remained non-toxic towards the macrophages, even when present at a concentration of 1000 µM.

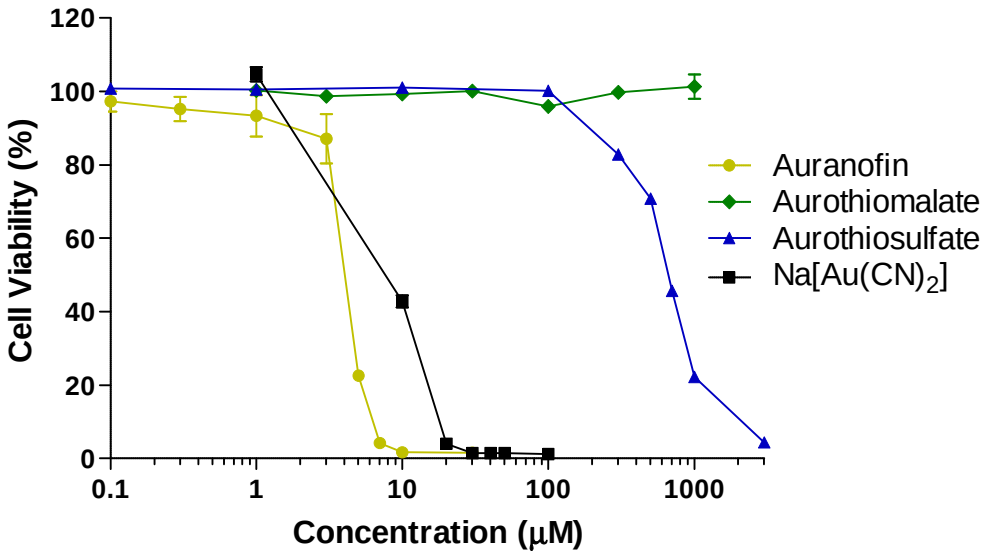

Figure 3.6: Cytotoxicity of some anti-arthritic gold compounds towards RAW264.7 cells, as assessed by the MTT assay. The macrophages were incubated with the gold compounds at 37 °C under an atmosphere of 5% CO_2 for 24 h. The error bars represent one standard deviation calculated from triplicate plates.

The low IC_{50} values determined for auranofin with the RAW264.7 macrophages at both treatment periods are consistent with the results of previous investigations into the toxicity of this drug. For example, auranofin was found to have an IC_{50} of 1.5 µM towards a B16 mouse melanoma cell line, using a clonogenic assay,[70] and an IC_{50} of 1.06 µM against a human ovarian cancer cell line using a 24-h MTT assay.[237] The small difference between the IC_{50} values obtained using 4- and 24-h treatment times suggests that there was little additional cellular uptake of this compound as a result of the increase in exposure time, or that the compound acts quickly. Support for the latter conclusion is provided by a study that showed that maximum uptake of auranofin by RAW264.7 cells exposed to a 5 µM solution of the drug occurred after 20 min.[109,238] The lack of difference in cytotoxicity indicates damage caused by a rapid mechanism of action, but may also in part be a result of the cells treated for 24 h having no recovery time prior to addition of the MTT.

The toxic nature of sodium dicyanoaurate has been noted previously in the literature,[57,239] including the nephrotoxic effect that acute doses produce *in vivo*.[240] In addition, a recent study reported the anti-proliferative effects of $K[Au(CN)_2]$ on four cancer cell lines, with IC_{50} values ranging from 0.10 – 0.13 µg/mL (0.34 – 0.45 µM).[241] Despite the large differences between these values and those obtained in the present study, it is important to note that the aim of the literature study was to assess the anti-proliferative activity of dicyanoaurate, not its cytotoxicity. Similarly, there do not appear to have been many investigations into the *in vitro* toxicity of aurothiosulfate. This most likely stems from the lack of clinical interest the compound received following initial human trials that investigated its effectiveness for the treatment of tuberculosis in the 1920's.[242] However, one study that was published in 2006 used the MTT assay to measure the effect of aurothiosulfate on human THP1 monocytes. It was reported that the cells showed no observable signs of cytotoxicity when exposed to aurothiosulfate at the relatively low concentration of 5 µM.[243]

The results presented in **Figure 3.5** and **Figure 3.6** show that aurothiomalate exhibited no toxicity towards the macrophages at all concentrations examined (from 1 to 1000 µM), for both exposure times. This is in direct contrast with the outcomes of a previous study conducted by Mirabelli et al.[70] The latter study reported that aurothiomalate showed significant toxicity towards the B16 mouse melanoma cell line, with an IC_{50} of 60 µM. The difference between these results could be due to variations in the experimental methodology employed. In the literature report, a clonogenic assay was used to assess toxicity towards the melanoma cell line, whereas in the present work the MTT assay was used to perform experiments with a macrophage cell line. An additional difference is that the previous study used the free acid form of aurothiomalate as opposed to the sodium salt used in the current study. It is important to note that the

results of the present investigation are generally consistent with those of a number of other studies.[120,243] For example, aurothiomalate showed no significant toxicity towards a human umbilical vein endothelial cell line in studies performed using both a ^{51}Cr release assay and an MTT assay, even at concentrations of up to 1000 μM.[120] In yet another study, aurothiomalate exhibited no toxicity towards THP1 monocytes when administered at a concentration of 500 nM, although this is significantly lower than the maximum value of 1000 μM used in the current study.[243]

The Au NPs used in cytotoxicity experiments were synthesised as a colloidal suspension in water, and were diluted using incomplete medium prior to administration to the macrophages. As a consequence, control experiments were first performed to determine the cytotoxicity of solutions containing increasing ratios of water in the cell medium. The results of these experiments are presented in **Figure 3.7**, and show that cell viability was not significantly affected until the amount of water present in the solvent mixture reached 30% H_2O (v/v). Therefore it was decided to use solutions consisting of 15% H_2O/85% incomplete medium (v/v) for all *in vitro* experiments involving Au NPs.

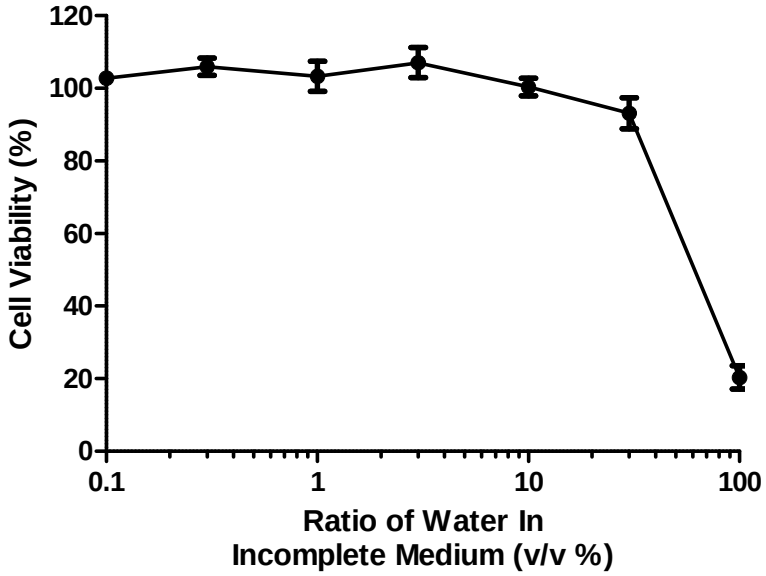

Figure 3.7: Cytotoxicity of solutions containing increasing amounts of water relative to incomplete medium towards RAW264.7 cells, as assessed by the MTT assay. Macrophages were incubated with the solutions at 37 °C under an atmosphere of 5% CO_2 for 24 h. The error bars represent one standard deviation calculated from triplicate plates.

Figure 3.8 compares the toxicity towards the macrophages of different concentrations of Au NPs, to that of the reagents used to synthesise the nanoparticles, including $H[AuCl_4]$ and trisodium citrate. Neither the Au NPs or trisodium citrate showed toxicity at the highest concentrations studied (60 µM and 1000 µM, respectively), whereas $H[AuCl_4]$ proved to be mildly cytotoxic, exhibiting an IC_{50} of 200 µM. The effect of higher concentrations of Au NPs could not be explored, as this would have necessitated using solutions that are hypotonic. Furthermore, stock solutions of Au NPs containing higher concentrations of nanoparticles than 400 µM could not be prepared, owing to aggregation of the particles.

There have been only a few studies that have examined the cytotoxicity of $H[AuCl_4]$. However, one investigation showed the corresponding sodium salt, $Na[AuCl_4]$, is cytotoxic towards a number of cancer cell lines.[244] These studies assessed cytotoxicity using the sulforhodamine B assay, and also explored the biological activity

of some gold(III) compounds with anti-cancer activity. The IC_{50} values for $Na[AuCl_4]$ ranged from 11.0 – 42.0 µM for 7 different cell lines (11.0, 12.6 17.7, 22.5, 26.5, 35.5 and 36.3 µM), which indicates that the sodium salt was appreciably more toxic towards those cells than the macrophages examined as part of the current work.

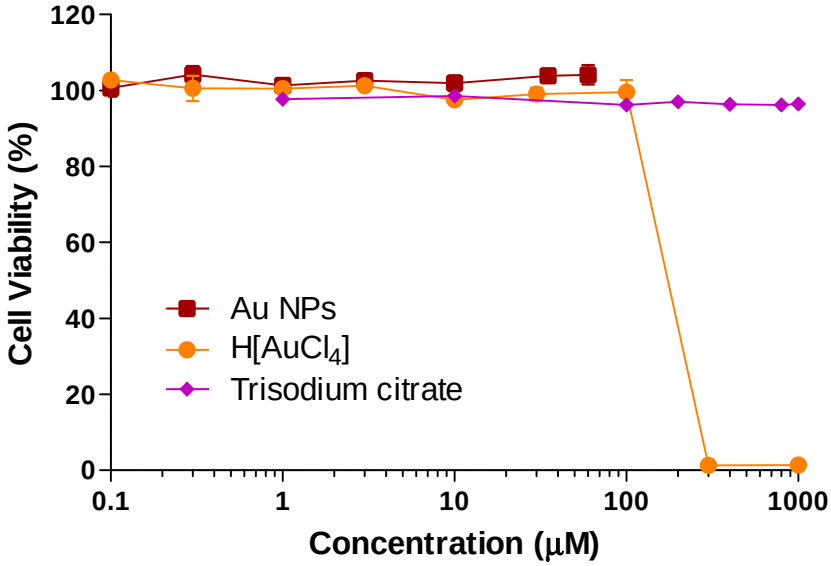

Figure 3.8: Cytotoxicity of Au NPs, and the reagents used in their preparation, towards RAW264.7 cells, as assessed by the MTT assay. The macrophages were incubated with the nanoparticles and compounds at 37 °C under an atmosphere of 5% CO_2 for 24 h. The error bars represent one standard deviation calculated from triplicate plates.

It was noted in **Section 1.4.2** that the toxicity and biocompatibility of Au NPs has been a relatively controversial area of the literature, possibly as a result of their biological activity being strongly dependent upon nanoparticle composition and size. Despite this, the results shown in **Figure 3.8** are consistent with those presented in some key literature studies. For example, in one investigation the toxicity of Au NPs prepared by the citrate reduction method towards PC-3 and MCF-7 cells was measured by both an MTT assay and an LDH release assay.[245] Significant decreases in cell viability were only observed when the concentration of Au NPs reached 558 µM. The same type of Au NPs were also shown to have little effect on the metabolic activity of MC3T3-E1 cells, even when the latter were exposed to solutions containing nanoparticle concentrations

of up to 1020 µM.[200] However, increases in LDH release were detected when the cells were exposed to solutions with Au NP concentrations of 508 µM or higher.[200] The lack of cytotoxicity observed in the current study is also consistent with a report by Shukla et al.,[201] who observed only minor decreases in cell viability, as determined by an MTT assay, when RAW264.7 cells were treated for 24 h with solutions containing 10–100 µM Au NPs coated with a poly-L-lysine shell.

Table 3.1 summarises the IC_{50} values obtained from experiments where the macrophages were exposed to gold compounds and Au NPs for 24 h. Using these results, the following order of increasing cytotoxicity is obtained:

aurothiomalate < aurothiosulfate < $H[AuCl_4]$ < $Na[Au(CN)_2]$ < auranofin

It was not possible to determine the absolute position of Au NPs within this series owing to the inability to prepare solutions with higher concentrations of nanoparticles to facilitate comparisons.

Table 3.1: Summary of IC_{50} values of gold compounds and Au NPs towards RAW264.7 cells.

Compound	**IC_{50} (µM)**
Auranofin	4 ± 0.3
Aurothiomalate	> 1000
Aurothiosulfate	650 ± 46
$Na[Au(CN)_2]$	9 ± 0.3
$H[AuCl_4]$	200 ± 40
Au NPs	> 60

Note: Cells were treated at 37 °C and under an atmosphere of 5% CO_2 for 24 h. Cytotoxicity was assessed by the MTT assay.

By using the cytotoxicity information obtained from these experiments, it was possible to determine the optimum concentrations of some of the gold compounds for use in other biological experiments performed using a treatment period of 24 h. For example, experiments with auranofin were performed using solutions containing 2.5 µM gold complex, which is slightly less than the total concentration of gold found in the serum of chrysotherapy patients, which typically ranges from 8 – 20 µM.[246–248] It was not possible to carry out experiments using higher concentrations of auranofin, however, owing to the extensive levels of cell death observed (**Figure 3.6**). In contrast, experiments were able to be performed using solutions containing 60 µM Au NPs, without affecting cell survival. Although this concentration is significantly higher than that of gold in the serum of chrysotherapy patients, it ensured that sufficient gold was incorporated into the macrophages to enable the gold uptake and distribution experiments to provide useful data. Similarly, experiments were successfully performed by incubating macrophages with solutions containing 1000 µM aurothiomalate, owing to the lack of toxicity of this gold compound at that concentration.

The trypan blue assay was also used to assess the impact of exposure of RAW264.7 macrophages to gold compounds or Au NPs. The benefit of this study was that it measured membrane integrity as an endpoint, and therefore provided information essential for interpreting the results of the gold uptake experiments presented later in this chapter. After exposure of the macrophages to various gold compounds or Au NPs for 24 h, cell viability was assessed by exposing the cells to trypan blue, an organic dye that can only enter cells that have compromised membranes. The results of these trypan blue studies are shown in **Figure 3.9**, and confirm that the vast majority of the macrophages exposed to Au NPs, aurothiosulfate or aurothiomalate remained viable as they retained intact cellular membranes. This is demonstrated by low proportions of

non-viable cells (< 9%) in each case where the macrophages were exposed to a gold complex or Au NPs. In contrast, for macrophages exposed to auranofin (2.5 µM), the number of viable and non-viable cells was significantly different ($P < 0.001$) to that of cells treated with the auranofin control solution (vehicle used for treatment). Importantly, the results of the trypan blue assay are consistent with those derived from the MTT assay (**Figure 3.6**), as both indicate that auranofin is significantly more toxic than any of the other gold compounds examined. In addition, the results of the experiments performed here are similar to those from another study where MCF-7 cells were exposed to auranofin at cytotoxic concentrations, and showed significant levels of compromised membrane integrity when examined using the trypan blue assay.[249]

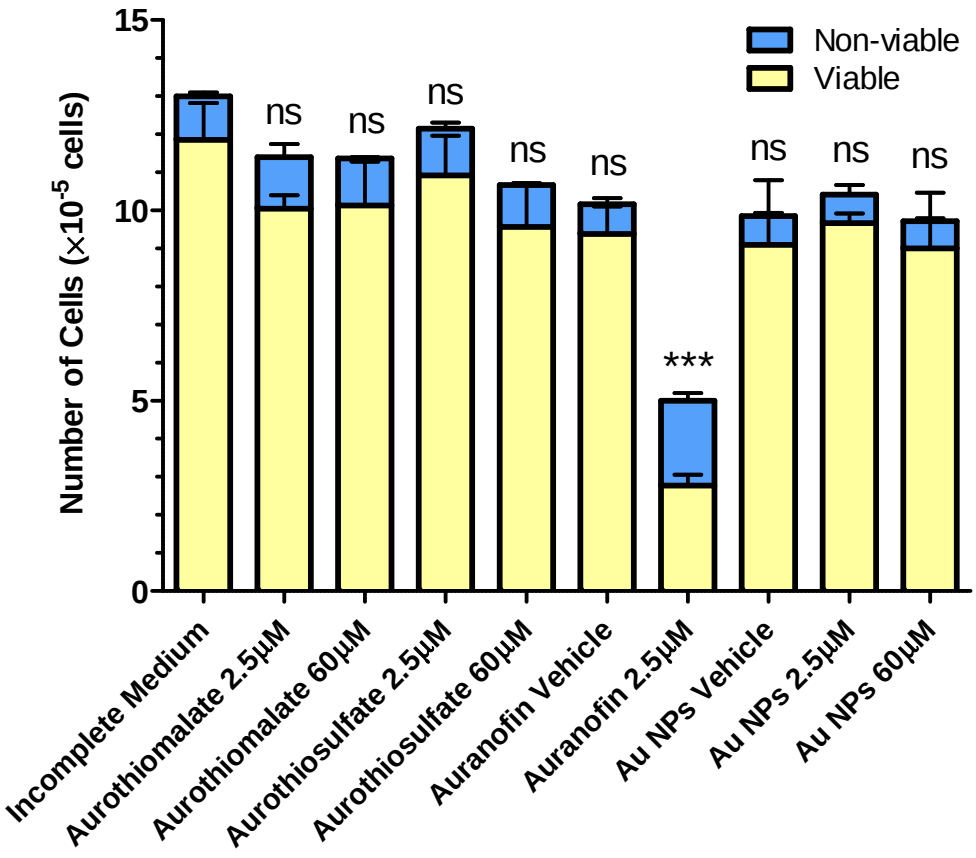

Figure 3.9: Membrane integrity of RAW264.7 cells after exposure to gold compounds or Au NPs, as assessed by the trypan blue assay. Macrophages were incubated with the gold compounds or Au NPs at 37 °C and under an atmosphere of 5% CO_2 for 24 h. The error bars represent one standard deviation calculated from triplicate samples. *** = Statistically significant ($P < 0.001$) compared to corresponding vehicle; ns = not significant compared to corresponding vehicle ($P > 0.05$).

3.4 Gold Uptake

A fundamental question that arises from the cytotoxicity results, is whether the observed variations between the drugs stems primarily from differences between the level of cellular uptake of the gold compounds or Au NPs. To address this question, GFAAS was used to determine the extent of uptake of gold by RAW264.7 cells exposed for 24 h to Au NPs, aurothiosulfate, auranofin or aurothiomalate at 2.5 and/or 60 µM concentrations. The results of these experiments are presented in **Figure 3.10**.

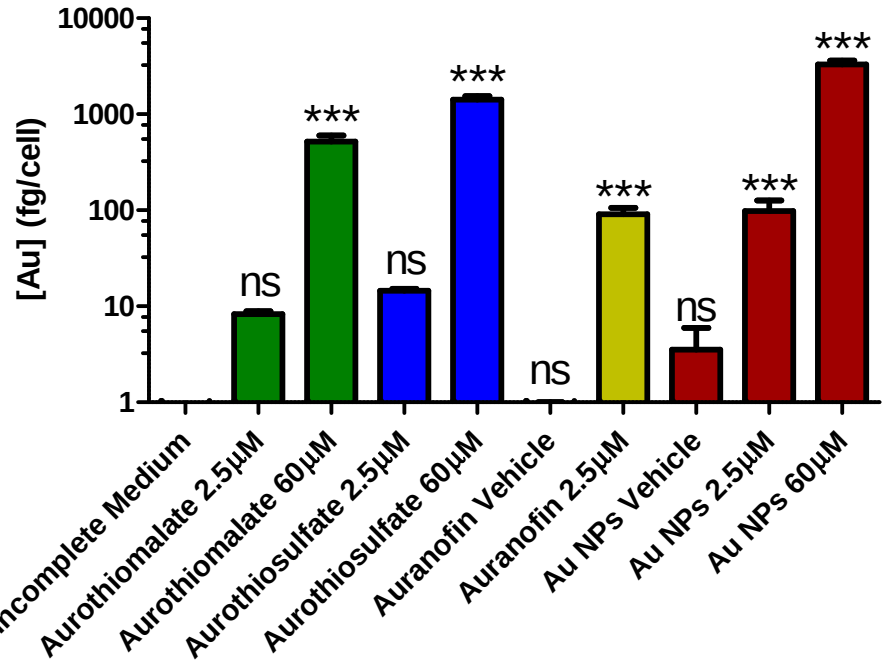

Figure 3.10: Cellular gold content (fg/cell) of RAW264.7 cells after exposure to gold compounds or nanoparticles as determined by GFAAS. Macrophages were incubated with the gold compounds or Au NPs at 37 °C under an atmosphere of 5% CO_2 for 24 h. The error bars represent one standard deviation as calculated from triplicate samples. *** = Statistically significant ($P < 0.001$) compared to corresponding vehicle; ns = not significant compared to corresponding vehicle ($P > 0.05$).

Data was also obtained for three different control samples consisting of the vehicles used for the treatment solutions. For instance, the vehicle used for aurothiomalate and aurothiosulfate (incomplete medium) was different to that for auranofin, and both of these solvents varied from that used for the Au NPs. As expected, the extent of incorporation of gold by macrophages exposed to each of the

vehicles was extremely low (< 4 fg/cell). Furthermore, there was no significant difference ($P > 0.05$) between the amounts of gold incorporated into cells exposed to the different vehicles. Inspection of **Figure 3.10** also reveals that there was very little incorporation of gold by macrophages exposed to 2.5 µM aurothiomalate or aurothiosulfate. In both cases, the level of cellular gold present was not statistically different ($P > 0.05$) from that of macrophages exposed to the corresponding vehicle. In contrast, macrophages exposed to 2.5 µM solutions of either auranofin or Au NPs did show levels of gold uptake that were statistically significantly higher ($P < 0.001$) than that of cells exposed to the corresponding vehicle.

The ability of macrophages to incorporate auranofin is not surprising, in view of the distinctly different structure of this complex compared to aurothiomalate and aurothiosulfate. Auranofin has a more lipophilic structure owing to the presence of the triethylphosphine moiety, that facilitates its transport across cell membranes,[250] and therefore contributes to its higher cytotoxicity. Conversely, the lower cytotoxicity of aurothiomalate and aurothiosulfate may be due to their poorer ability to enter cells, at least when present at low concentrations.

Increasing the concentration (to 60 µM) of aurothiomalate, aurothiosulfate or Au NPs in the treatment solutions resulted in enhanced levels of gold incorporation by the macrophages. For cells treated with aurothiomalate or aurothiosulfate, the amount of gold incorporated was statistically higher ($P < 0.001$) than that of vehicle-treated cells. In the case of aurothiomalate a ~70-fold increase in the amount of cellular gold (8.3 ± 0.3 to 520 ± 50 fg/cell) occurred as a result of increasing the concentration of the metal complex. An even more substantial increase in the level of gold uptake to 1420 ± 70 fg/cell was observed following treatment with 60 µM aurothiosulfate. This is 100 times

the value of 14.5 ± 0.4 fg/cell obtained when the cells were exposed to 2.5 µM aurothiosulfate.

Exposure to 60 µM Au NPs resulted in a greater level of cellular gold uptake compared to that observed when the macrophages were exposed to the same concentration of aurothiosulfate or aurothiomalate ($P < 0.001$). Furthermore, the amount of gold incorporated (3300 ± 200 fg/cell) was 33 times greater than that observed for cells treated with just 2.5 µM Au NPs (100 ± 20 fg/cell). As discussed in **Section 1.4.2,** it has been shown that Au NPs can enter a variety of cells (ovarian, brain, cervical and breast cancer cells; osteoblasts, and fibroblasts) via a receptor-mediated, clathrin-dependent endocytosis pathway,[197–200] and that the rate of uptake increases with decreasing nanoparticle size.[198] In contrast, auranofin enters cells by the sulfhydryl shuttle mechanism (**Section 1.2.2)**, in which the $Au(PEt)_3^+$ fragment binds to a membrane transport protein through a thiol group, and is subsequently transported through the membrane.[109] If the other gold drugs are incorporated into the macrophages by a similar mechanism to that used by auranofin, or one which is inhibited by their polymeric structures, then this might explain the differences between the amounts of gold incorporated by the gold(I) compounds compared to the Au NPs, that are shown in **Figure 3.10**.

It is instructive to compare the relative cytotoxicities of the various gold compounds and Au NPs as determined by the MTT assay, with the degree of cellular uptake. For example, if cytotoxicity was dependent on the amount of intracellular gold, then cytotoxicity would be expected to increase in the following order:

aurothiomalate < aurothiosulfate < auranofin < Au NPs.

Whilst the results of the MTT assays showed broad correlation with gold uptake for the gold compounds as listed in the above ordering, it was not possible to definitively determine whether or not Au NPs are more toxic than either aurothiosulfate or aurothiomalate due to the restricted concentration range of Au NP solutions that could be prepared. However, the cytotoxicity data obtained using treatment solutions containing 2.5 μM gold compounds or Au NPs strongly supports the hypothesis that Au NPs are far less toxic than auranofin. Furthermore, the data shown in **Figure 3.10** demonstrates that Au NPs were taken up in comparable or even larger quantities than auranofin by the macrophages without a noted cytotoxic effect. Since the results of the trypan blue assay indicate that Au NPs do not affect membrane viability, this further supports the conclusion that the quantity of gold incorporated into cells is not the sole determinant of cytotoxicity. Furthermore, since Au NPs were readily incorporated into macrophages without affecting their membrane integrity, it would appear that their incorporation occurs predominantly via a specific cellular mechanism, rather than as a consequence of membrane compromise. In contrast, macrophages treated with auranofin showed significant levels of membrane compromise. Further work will be required to determine if this is a direct consequence of the sulfhydryl shuttle mechanism of uptake proposed for this compound, or if membrane disruption occurs as a later necrotic event.

3.5 Intracellular Distribution of Gold

Insight into the molecular mechanisms of the cytotoxicity of drugs can often be obtained through identifying which parts of a cell the drug accumulates to the greatest extent. Therefore microprobe SR-XRF was used to determine the location of gold in single cells and small clusters of cells, after exposure to different concentrations of a variety of gold compounds or Au NPs for 24 h. Microprobe SR-XRF is particularly

well-suited for analysis of metal compounds in cells, as it does not require modification of the drug or addition of an imaging agent, and allows simultaneous detection of many other biologically relevant elements.[215,219] The results from these experiments are presented as elemental distribution maps. In the following sub-sections, selected examples of elemental maps derived from data obtained at the Advanced Photon Source and the Australian Synchrotron are presented and discussed. Experiments were performed at two synchrotrons to provide complementary information. Data obtained at the Australian Synchrotron was used to obtain images of large numbers of cells to determine the degree of homogeneity of gold uptake across a large number of macrophages. Experiments performed at the Advanced Photon Source provided higher resolution images of single macrophages or small groups of macrophages, which enabled the subcellular distribution of gold in the macrophages to be determined. The full set of results obtained from experiments performed at both synchrotrons is presented in **Appendix B:**. This includes the integrated XRF spectra used to derive the elemental distribution maps.

3.5.1 High Resolution Maps of Single or Small Numbers of Cells

Elemental distribution maps for a macrophage exposed only to incomplete medium are shown in **Figure 3.11**. The elemental distribution maps for chlorine, potassium and calcium can often be used to infer the overall size and shape of a cell, whilst only low concentrations of iron and copper are expected as a result of their essential roles in many metalloenzymes. The distribution maps for phosphorus and zinc can sometimes be used to identify the location of the cell nucleus, owing to the presence of these elements in the phosphate backbone of DNA, and zinc-fingers motifs of DNA-binding proteins, respectively. However, this approach is sometimes problematic for experiments performed with whole cells, as compression of the data obtained using a

three-dimensional sample into a two-dimensional image can result in an inability to resolve sub-cellular features. This problem can generally be overcome by obtaining images of thin-sectioned cell samples. However, this option was not explored as part of this project since locating Au NPs in the various thin sections can be time-consuming and there was very limited APS beamtime available for these experiments. Sulfur maps may be used to infer the location of proteins due to the predominance of thiol residues in protein molecules. A scatter map is also often included to show the degree of X-ray scattering occurring at a specific location, which is an indication of the overall amount of matter present at that site.

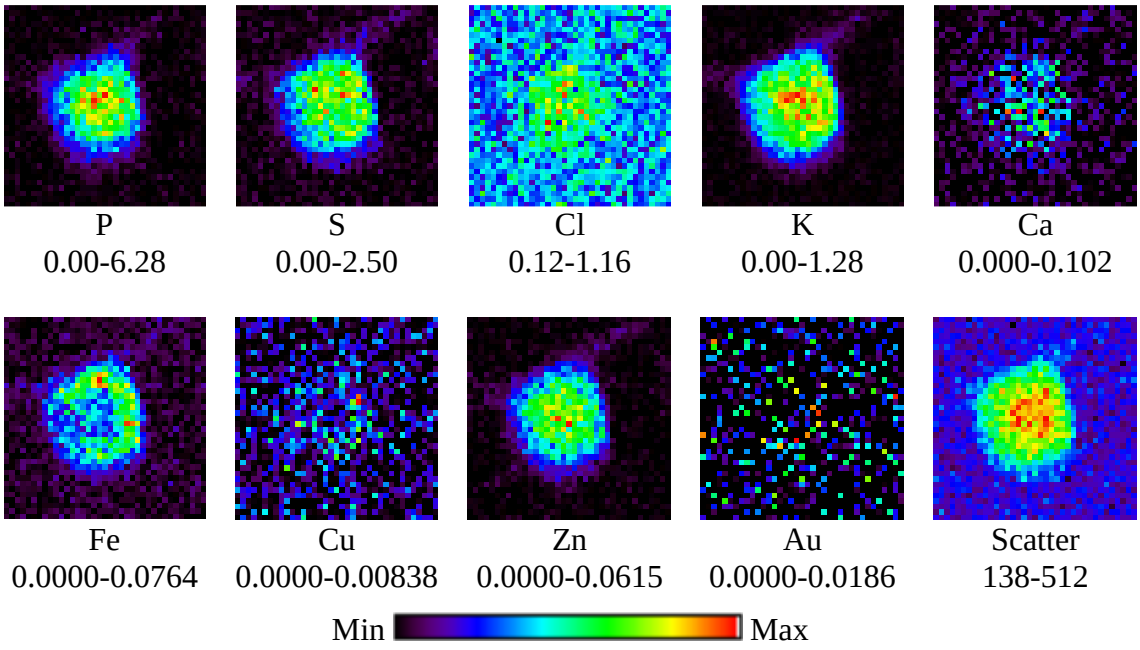

Figure 3.11: Microprobe SR-XRF elemental maps for RAW264.7 cells incubated with incomplete medium at 37 °C under an atmosphere of 5% CO_2 for 24 h. Scan dimensions (H x V) were 18.5 µm × 18.5 µm. All elemental concentrations are µg/cm^2.

Inspection of the P, S, K and Zn elemental maps shown in **Figure 3.11** reveals the presence of a cell with a rounded morphology. The Ca, Cl and Cu maps are relatively uninformative, as they reveal only slightly higher concentrations of these elements within the cell. In addition, the Cl map shows significant amounts of this element outside the cell, owing to the presence of this element in the cell medium used.

The Fe map reflects the approximate shape of the cell, but also exhibits localisation in a crescent shaped region around the inside edge of the right side of the cell. The Au map is consistent with the gold signal being essentially due to background noise, as there is effectively no gold present in the mapped area. This was an important result, as any gold identified as being present in greater quantities in macrophages treated with gold compounds or Au NPs could then be concluded to arise solely from the treatment. In view of the above discussion, only the S, K, Zn and Au maps have been shown in subsequent sections of this chapter as they are the most informative.

Elemental maps of RAW264.7 cells treated with 2.5 μM auranofin are shown in **Figure 3.12**. Each of the S, K and Zn maps clearly show four separate macrophages within the mapped area. This includes one in both the top-left and bottom-right corners that have a round morphology, as well as a third prominent cell in the middle of the image that instead shows a fibroblastic morphology. There is a fourth cell present in the image near the top-centre, which also has the same fibroblastic appearance, but which is fainter than the first three cells. The fibroblastic morphology is normal for RAW264.7 cells, while the rounded morphology is commonly associated with non-viable cells, such as those that have previously been exposed to acute cytotoxins.[251] It is therefore notable that examination of the Au map reveals that the gold is not evenly distributed between the cells. In contrast, both of the rounded cells have gold distributed throughout, while this element is completely absent from the fibroblastic cells. These observations are consistent with the cytotoxic nature of auranofin discussed previously, and the low treatment concentration used.

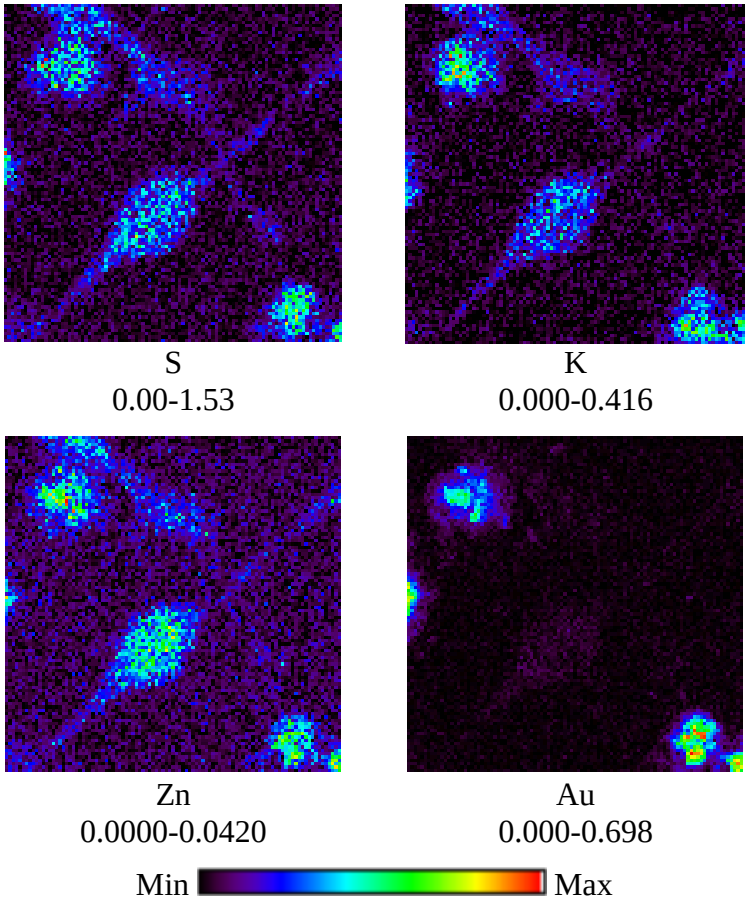

Figure 3.12: Microprobe SR-XRF elemental maps for RAW264.7 cells treated with 2.5 µM auranofin at 37 °C under an atmosphere of 5% CO_2 for 24 h. Scan dimensions (H x V) were 50.5 µm × 50.5 µm. All elemental concentrations are µg/cm^2.

This distribution of gold and, in particular, its co-localisation with sulfur, is highlighted in the co-localisation map shown in **Figure 3.13**. In this map, the round cells are pink/purple in colour as a result of the combination of red from the sulfur map and blue from the gold map. Gold was not uniformly incorporated into all macrophages due to the relatively low concentration of gold that the cells were exposed to. Those that did incorporate the gold compound were compromised owing to its cytotoxicity, and hence lost membrane integrity and subsequently their shape as they died.

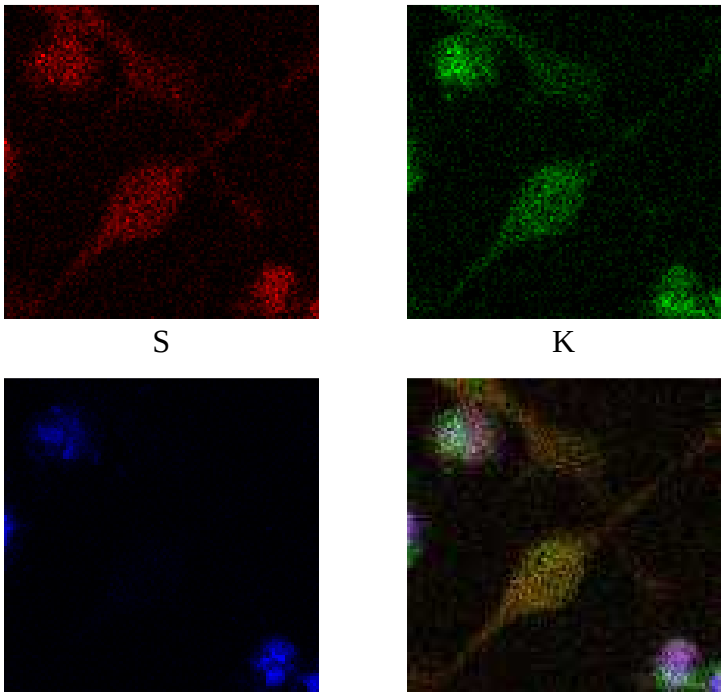

Figure 3.13: Individual elemental microprobe SR-XRF maps, and co-localisation map for RAW264.7 cells treated with 2.5 µM auranofin at 37 °C under an atmosphere of 5% CO_2 for 24 h. Scan dimensions (H x V) were 50.5 µm × 50.5 µm.

Figure 3.14 shows elemental maps for cells treated for 24 h with 1000 µM aurothiomalate. Examining the maps reveals the presence of two fibroblastic cells in close proximity to each other. The Au map shows the metal is primarily located in discrete areas within the cell at the bottom of the figure. In contrast, there are only two gold 'hotspots' in the upper cell, indicating that there has been less extensive incorporation of this metal. The region where gold is present in the highest amounts also happens to be the area where sulfur is most abundant, suggesting some co-localisation of these two elements.

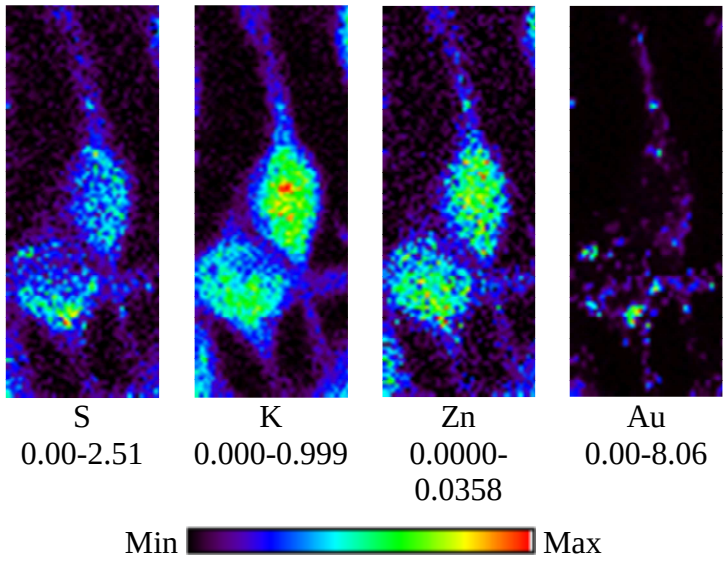

Figure 3.14: Microprobe SR-XRF elemental maps for RAW264.7 cells treated with 1000 µM aurothiomalate at 37 °C under an atmosphere of 5% CO_2 for 24 h. Scan dimensions (H x V) were 20.5 µm × 52.5 µm. All elemental concentrations are µg/cm^2.

The elemental maps for cells treated with 100 µM H[$AuCl_4$] for 24 h are shown in **Figure 3.15**. The S and Zn maps reveal the presence of a single cell with a round shape, whilst the Au map suggests that gold is present in relatively low concentrations throughout the cell. Comparison of the Au and S maps also provides evidence that there may be some co-localisation of these two elements within the cell.

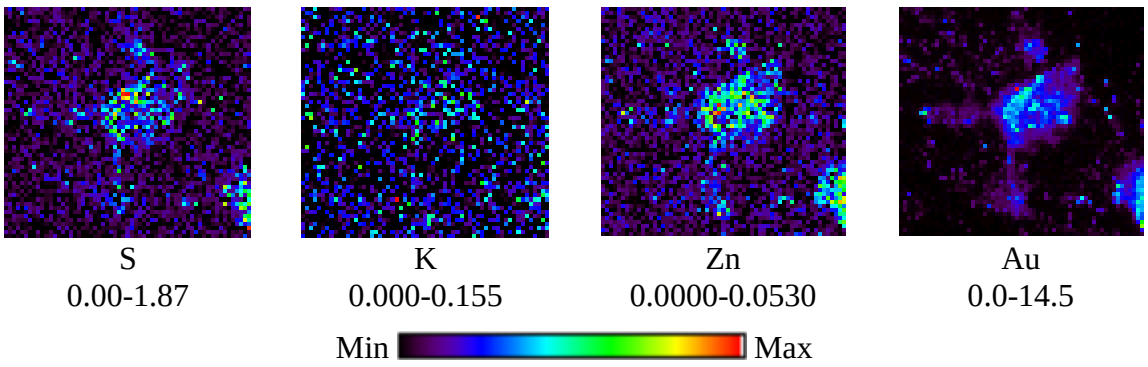

Figure 3.15: Microprobe SR-XRF elemental maps for RAW264.7 cells treated with 100 µM H$AuCl_4$ at 37 °C under an atmosphere of 5% CO_2 for 24 h. Scan dimensions (H x V) were 30.5 µm × 28.5 µm. All elemental concentrations are µg/cm^2.

Elemental maps for cells treated with 60 µM Au NPs for 24 h are shown in **Figure 3.16**. Examination of the K map reveals a single fibroblastic cell, whilst the Au map shows a number of very discrete hotspots for this metal, primarily in the bottom part of the cell. Comparison with the S and Zn maps suggests that there is a high degree of co-localisation of the latter two elements with each other, as well as with gold.

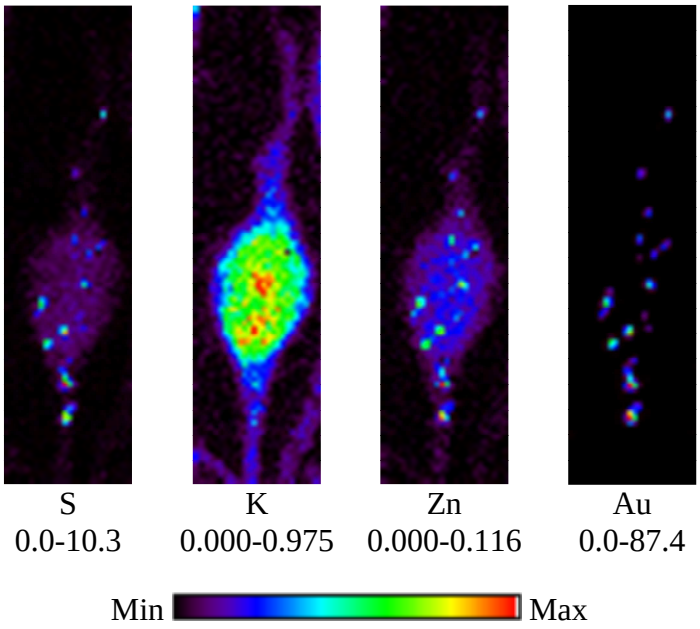

Figure 3.16: Microprobe SR-XRF elemental maps for RAW264.7 cells treated with 60 µM Au NPs at 37 °C under an atmosphere of 5% CO_2 for 24 h. Scan dimensions (H x V) were 13.5 µm × 50.5 µm. All elemental concentrations are µg/cm^2.

The images presented in **Figure 3.12 – Figure 3.16** all provide evidence that suggests there is some degree of cellular co-localisation of gold with sulfur. This is particularly striking in the case of cells treated with Au NPs. In the case of cells treated with sodium aurothiomalate, auranofin, or H[$AuCl_4$] a probable explanation for this observation is that the gold has become associated with sulfur that is endogenous to the cell, such as glutathione or sulfur-containing proteins. In addition, co-localisation might be accounted for by proposing that the sulfur-containing ligands present in sodium aurothiomalate and auranofin were not displaced upon uptake into the cell. However,

this explanation is unlikely, since it has been reported that the original sulfur-donor ligands associated with the gold complexes rapidly undergo ligand exchange reactions when the complexes are introduced into biological systems.[250] In addition, the results of the TrxR binding experiments described in **Chapter 5** also reveal rapid loss of the S-containing ligands initially present in the coordination sphere of the gold complexes under study.

Figure 3.16 suggests that the degree of co-localisation of Au and S within the cell treated with Au NPs is much greater than in the case of cells treated with the various gold compounds. Whilst it is very likely that the gold incorporated into the cell has become associated with endogenous sulfur, the co-localisation suggested by the results shown in **Figure 3.16** is largely the result of an issue arising from the method used to detect S and Au in the macrophages, which centres on the intense Au M line. **Figure 3.17** shows the integrated XRF spectrum of the elemental maps presented in **Figure 3.16**. Inspection of the spectrum reveals that the gold M line (2.1 keV) is in close proximity to the phosphorus (2.0 and 2.1 keV) and sulfur (2.3 and 2.4 keV) K lines. Owing to the intensity and breadth of the gold M line, overlap with the phosphorus and sulfur K lines is so extensive that it contributes significantly to the intensity of the latter signals.

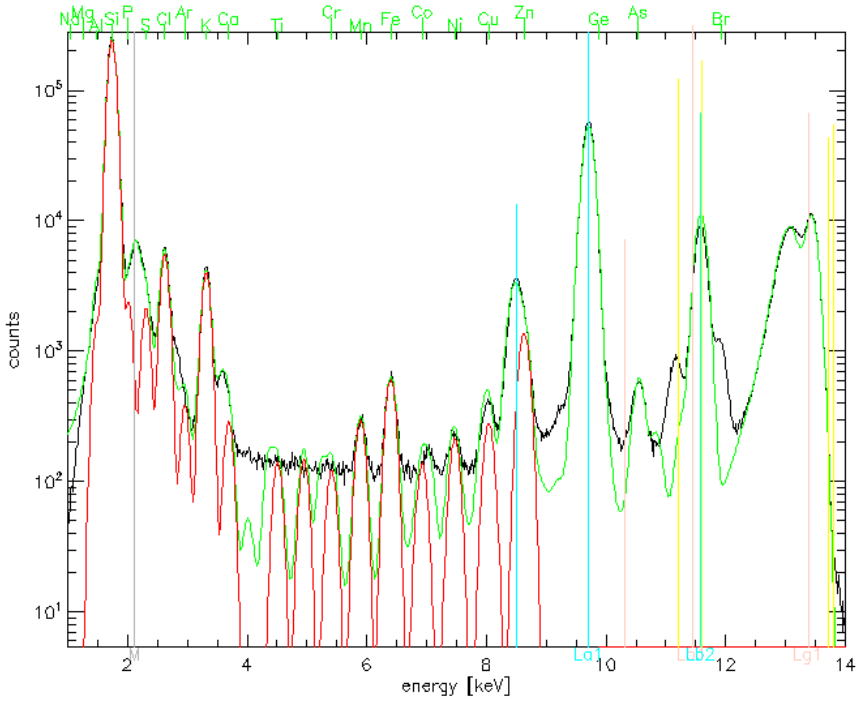

Figure 3.17: Integrated (black), fitted (green) and assigned Kα lines (red) of microprobe SR-XRF spectra of RAW264.7 cells treated with 60 µM Au NPs at 37 ℃ under an atmosphere of 5% CO_2 for 24 h. Vertical lines indicate the expected positions of gold L and M lines.

The overlap of the gold M line with the phosphorus and sulfur K lines is highlighted in **Figure 3.18**, which shows the integrated, fitted, background and assigned XRF spectra for the region from 1.5 keV to 3 keV. The integrated spectrum is essentially raw data, whilst the fitted spectrum is the integrated spectrum after modified Gaussians have been applied to it. The background spectrum is subtracted from the fitted to then produce the assigned spectrum, which is used to produce the elemental maps. Examining the spectra obtained for cells treated with incomplete medium (**Figure 3.18 a**), there is not much difference between the integrated/fitted spectra and the assigned spectrum. In the case of cells treated with auranofin (**Figure 3.18 b**), whilst there is a gap between the integrated/fitted spectra and the assigned spectrum at the position of the gold M line (2.12 keV), there is no major difference at the position of the sulfur K line (2.30 keV), indicating no effect upon assignment of that element. However, when examining the spectra for cells treated with aurothiomalate and Au NPs

(**Figure 3.18 c** and **d**) there is a clear peak present at the position of the gold M line that is large enough to overlap both the phosphorus and sulfur K lines. Although correction was attempted through subtraction of the background from the fitted spectrum (to produce the assigned spectrum), it is not possible to know how successful the subtraction was in removing the contribution of the gold M line to the spectral intensity of the surrounding elements.

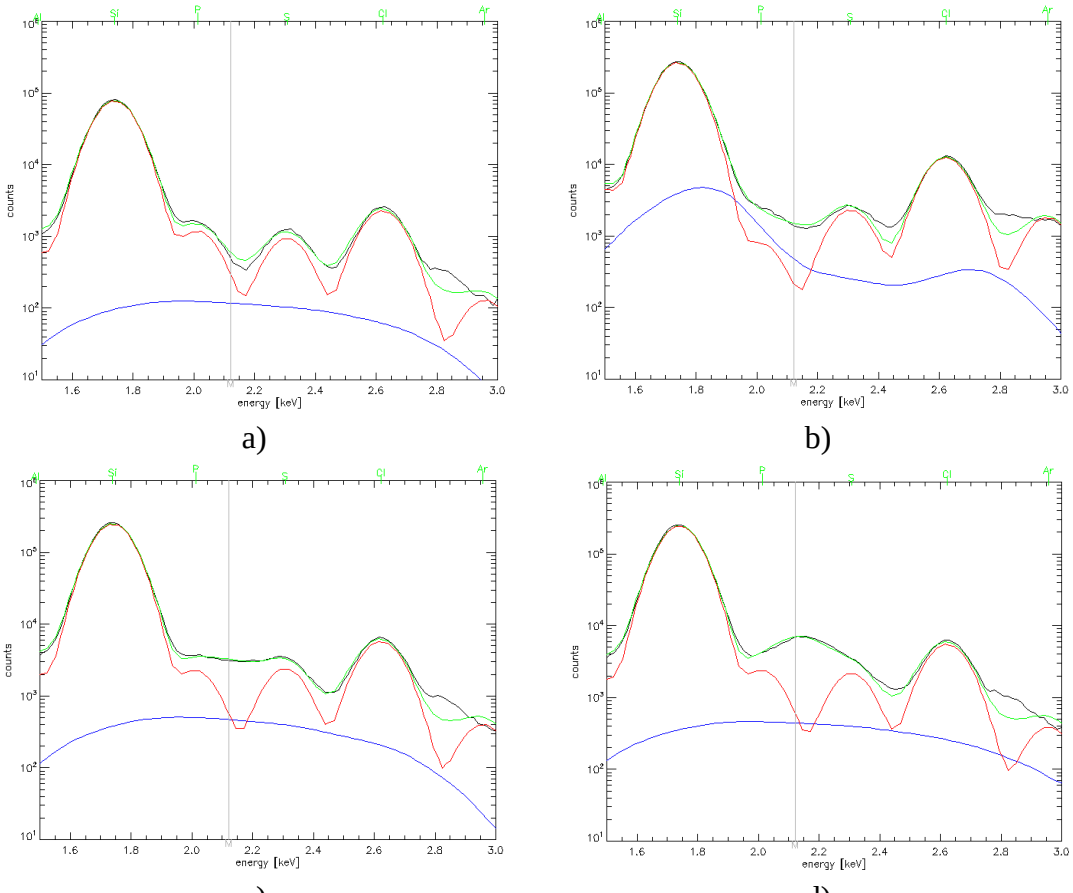

Figure 3.18: Integrated (black), fitted (green), background (blue) and assigned Kα lines (red) of microprobe SR-XRF spectra of RAW264.7 cells treated for 24 h at 37 °C under an atmosphere of 5% CO_2 with: **a)** incomplete medium; **b)** 2.5 µM auranofin; **c)** 1000 µM aurothiomalate; and **d)** 60 µM Au NPs. The vertical grey line indicates the expected position of the gold M line.

This analysis leads to the conclusion that some of the spectral intensity previously attributed to sulfur for the Au NPs-treated cells in **Figure 3.16** was due to the presence of gold. In contrast, the gold elemental maps shown in **Figure 3.16** and elsewhere were derived from the intensity of the gold L signal, which is present in a

different region of the spectrum (11.9 keV) where there are no overlapping spectral lines from other elements. Therefore it is possible to conclude that all the gold elemental maps presented in this thesis accurately reflect the cellular distribution of this element.

As such, it is not possible to conclude that the Au NPs had become associated with either exogenous or endogenous sulfur containing species on the basis of the XRF data. This issue is most striking in the case of cells treated with Au NPs, because the extent of incorporation of gold into the macrophages was significantly greater compared to when the cells were treated with the gold compounds (**Figure 3.10**). This is also evident from inspection of **Table 3.2**, which shows the maximum concentration of different elements observed in the individual elemental maps. **Table 3.2** also shows that the maximum concentration of gold in the maps of macrophages treated with Au NPs is much greater than that for the macrophages treated with discrete gold compounds. It is also evident that the maximum concentrations of phosphorus, sulfur and zinc in elemental maps of macrophages treated with Au NPs are approximately 1.7×, 4× and 1.8× higher than for the cells treated with incomplete medium only. This is also most likely due to the overlap of the Au XRF spectral lines with those from the P, S and Zn, and therefore contributing to the intensity of the latter. In contrast, the maximum concentrations of the latter three elements in cells treated with the gold complexes were very similar to that found in the case of macrophages treated with incomplete medium only (**Table 3.2**). In the case of these samples, the intensity of the gold M line was relatively low (**Appendix B:**) as a result of lower levels of gold uptake, and so did not overlap significantly with the spectral lines used to produce the maps for other elements. Therefore it may be concluded that co-localization of Au and S in the case of macrophages treated with the Au complexes was due to interactions between the gold complexes and sulfur-containing amino acids and proteins, most likely inside the cells.

It should also be noted that whilst it is possible to compare levels of gold uptake using the data presented in **Table 3.2**, it should be viewed with caution as this data was obtained from measurements performed on single cells only. In contrast, the gold uptake data presented in **Figure 3.10** was obtained from experiments performed on bulk cellular samples.

Table 3.2: Maximum concentrations of elements derived from microprobe SR-XRF maps of RAW264.7 cells.

	Maximum Elemental Concentration (μg/cm^2)			
Treatment	**P**	**S**	**Zn**	**Au**
Control	6.28	2.50	0.0615	0.0186
Auranofin (2.5 μM)	2.33	1.53	0.0420	0.698
Aurothiomalate (1000 μM)	3.70	2.51	0.0358	8.06
H[AuCl$_4$] (100 μM)	1.97	1.87	0.0530	14.5
Nanoparticles (60 μM)	10.9	10.3	0.116	87.4

Note: Macrophages were treated at 37 °C under an atmosphere of 5% CO_2 with various gold compounds and Au NPs for 24 h. The concentrations of auranofin and H[AuCl$_4$] used to treat the cells were chosen as they were close to their respective IC_{50} values. All other concentrations were chosen as they were expected to result in significant gold uptake by the cells.

The presence of discrete localised areas containing gold in the elemental maps of macrophages treated with Au NPs, is consistent with previous studies that used TEM to show that gold accumulated in structures known as endosomes, as well as lysosomes, following exposure of cells to Au NPs.[199,200] It has also previously been reported that macrophages treated with aurothiomalate show evidence of gold being packaged into lysosomes to form structures sometimes termed aurosomes, owing to their high gold content.[105,106] The size of the spots are approximately 0.5 – 1 μm in diameter, which is approximately 30 – 65 times the size of an administered nanoparticle. Therefore it is

likely that the gold hotspots observed in **Figure 3.16** are also attributable to aurosomes, formed as a result of endocytosis of Au NPs bound to the surface of the macrophage membrane. This is particularly consistent with macrophage behaviour, as one of their primary roles is to engulf foreign materials within their plasma membrane and invaginate them as vesicles.[252] These vesicles are combined into endosomes and eventually lysosomes.[252]

3.5.2 Low Resolution Maps of Large Numbers of Cells

In this section, elemental maps obtained at the Australian Synchrotron are presented to show the localisation of elements in samples consisting of large numbers of macrophages treated with the various gold compounds or Au NPs. The images are of much larger scan areas than those obtained at the APS, and allow comparisons to be made regarding the homogeneity of gold uptake across a larger percentage of the total cell population. Examples of characteristic X-ray spectra used to produce these maps are shown in **Appendix B:**. **Figure 3.19** shows the elemental maps for cells exposed to 'incomplete medium' only. The S, K and Zn maps provide a good overview of the overall appearance and location of cells in the mapped area, whilst the Au map shows that only a very small amount of this element was present, as expected, owing to its absence from the treatment solution. The maps show roughly 40–50 cells in total, which have grown together in dense clumps, and vary in morphology from fibroblastic to round.

Elemental maps showing cells treated with 2.5 μM auranofin are presented in **Figure 3.20**. The S, K and Zn maps show a lower population density of cells than was present in the control sample. This is most likely due to a significant percentage of the cells dying owing to the cytotoxicity of auranofin, and being washed off the silicon nitride membrane. Examination of the mapped area revealed the two distinct

morphologies for these cells noted earlier, namely fibroblastic and rounded cells. Examination of the Au map shows that this element was only present in significant amounts within the rounded cells, which is consistent with the results presented earlier in **Figure 3.12**, and the cytotoxic nature of this compound revealed in **Section 3.3**. This is further highlighted by the co-localisation map shown in **Figure 3.21**, in which only the rounded cells feature the pink/purple colour indicative of the presence of gold, potassium and sulfur in the same regions.

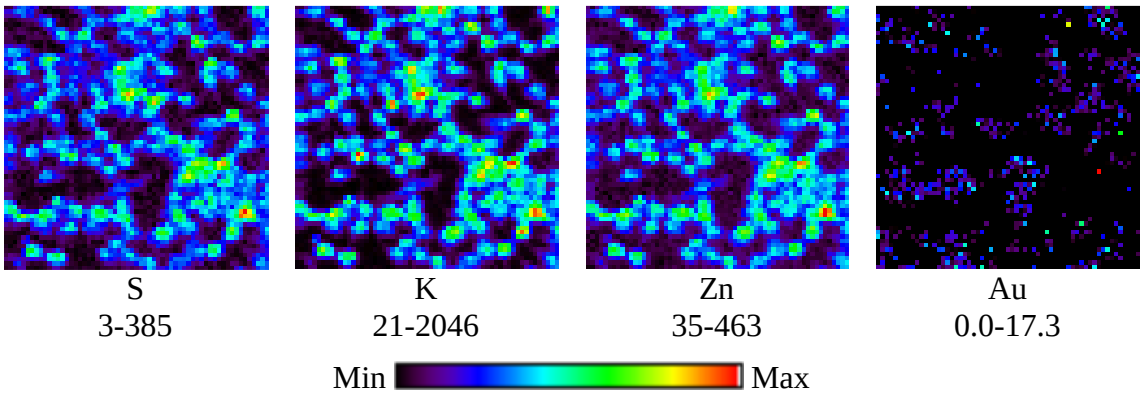

Figure 3.19: Microprobe SR-XRF elemental maps for RAW264.7 cells treated with incomplete medium at 37 °C under an atmosphere of 5% CO_2 for 24 h. Scan dimensions (H x V) were 120 µm × 120 µm. Values are relative quantifications and are unitless.

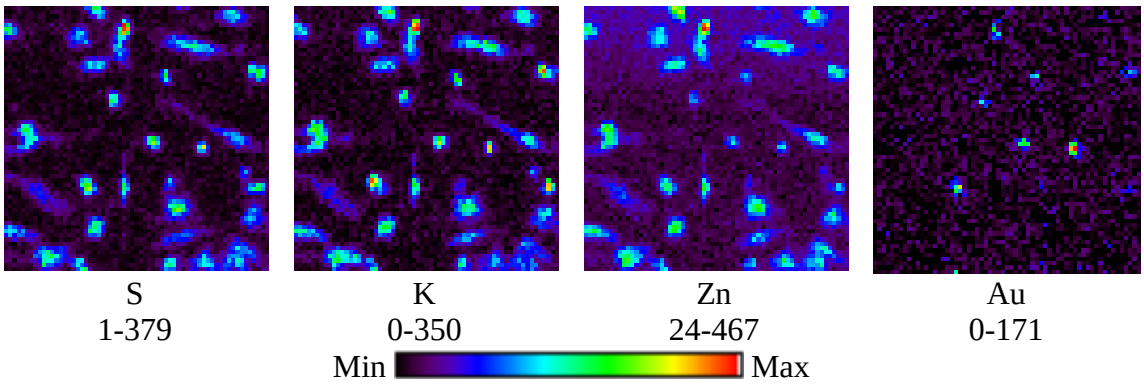

Figure 3.20: Microprobe SR-XRF elemental maps for RAW264.7 cells treated with 2.5 µM auranofin at 37 °C under an atmosphere of 5% CO_2 for 24 h. Scan dimensions (H x V) were 120 µm × 120 µm. Values are relative quantifications and are unitless.

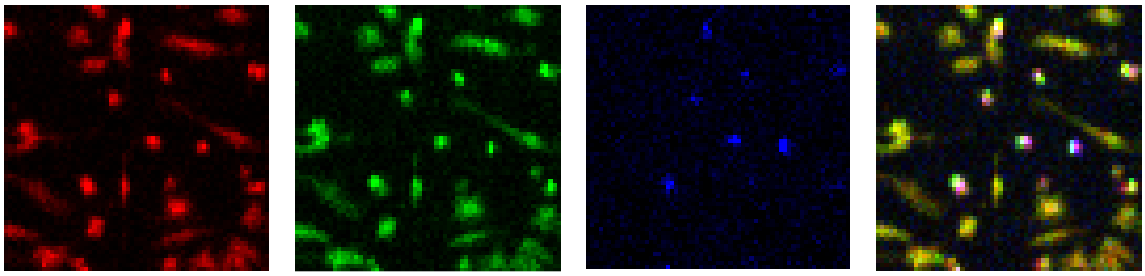

Figure 3.21: Individual elemental microprobe SR-XRF maps, and co-localisation map for RAW264.7 cells treated with 2.5 µM auranofin at 37 °C under an atmosphere of 5% CO_2 for 24 h. Scan dimensions (H x V) were 120 µm × 120 µm.

Elemental maps for cells treated for 24 h with 2.5 µM and 1000 µM aurothiomalate are shown in **Figure 3.22 a)** and **b)**, respectively. Examination of the S, K and Zn maps corresponding to cells treated with 2.5 µM aurothiomalate shows a significant number of macrophages. Inspection of the Au map reveals that the metal is randomly distributed throughout the entire mapped area at low concentrations, in a similar manner to that observed for the control sample. These observations indicate that little gold uptake occurred at this low treatment concentration. When the concentration of aurothiomalate in the treatment solution was increased to 1000 µM (**Figure 3.22 b**), the S, K and Zn maps showed a more dense population of macrophage cells. The Au elemental map now showed that the majority of cells contained regions of low gold concentration comparable to that seen with the control sample. However, some regions of the gold map feature 'hot spots' of gold corresponding to much higher concentrations of the metal that were associated with cellular material.

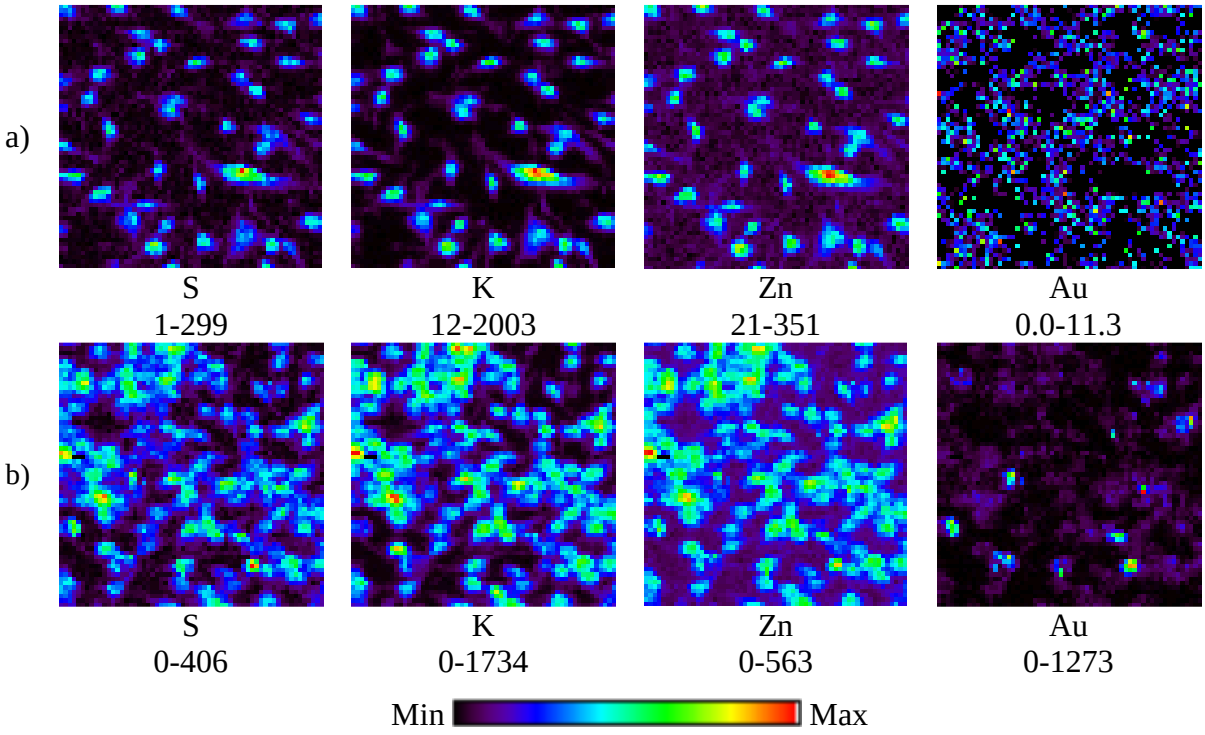

Figure 3.22: Microprobe SR-XRF elemental maps for RAW264.7 cells treated at 37 °C and under an atmosphere of 5% CO_2 for 24 h with: **a)** 2.5 µM aurothiomalate and **b)** 1000 µM aurothiomalate. Scan dimensions (H x V) were 120 µm × 120 µm. Values are relative quantifications and are unitless.

This non-uniform pattern of gold uptake is similar to what was observed for auranofin, and was also observed for cells treated with 2.5 µM aurothiosulfate (**Figure 3.23 a**). When the concentration of aurothiosulfate was increased to 500 µM, the elemental maps (**Figure 3.23 b**) provided evidence of cellular rupture, as there was a large amount of cellular debris distributed throughout the image area. This is possibly due to the treatment concentration of 500 µM resulting in significant cytotoxicity for the macrophages, leading eventually to membrane rupture and lysis.

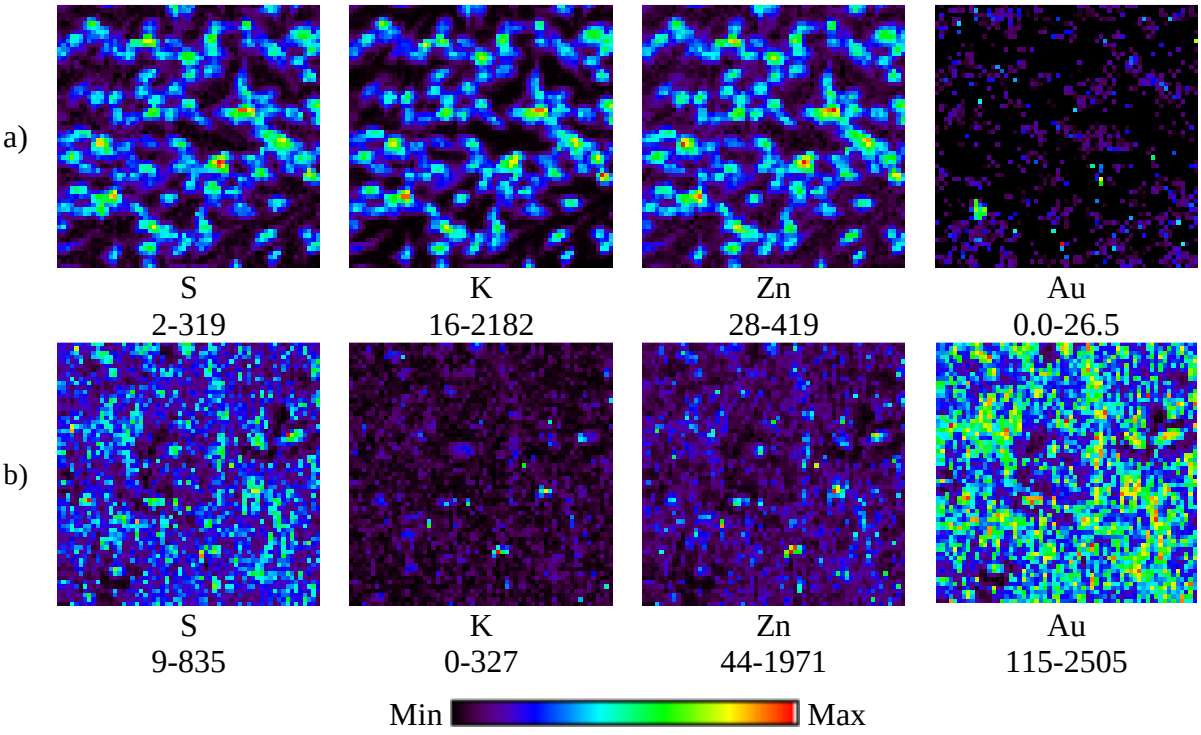

Figure 3.23: Microprobe SR-XRF elemental maps for RAW264.7 cells treated at 37 °C under an atmosphere of 5% CO_2 for 24 h with: **a)** 2.5 µM aurothiosulfate **b)** 500 µM aurothiosulfate. Scan dimensions (H x V) were 120 µm × 120 µm. Values are relative quantifications and are unitless.

Maps of macrophages exposed to Au NPs at concentrations of 2.5 µM and 60 µM are shown in **Figure 3.24 a)** and **b)**, respectively. In contrast to the gold(I) compounds discussed previously, exposure of the macrophages to either concentration of Au NPs resulted in gold elemental maps that showed a homogenous distribution of the metal across the cell population. This is consistent with the results of GFAAS studies presented earlier (**Figure 3.10**), which showed higher levels of gold incorporation into Au NP-treated cells. Comparison of the S and Au images suggests a high degree of co-localisation of these elements along with Zn within the cells. However, this is once again due to issues discussed earlier, which arise due to overlap of the gold M line with the sulfur K line and the gold L line with the zinc K line. Further evidence of this is provided by the integrated SR-XRF spectrum shown in **Appendix B:, Figure B.30.**

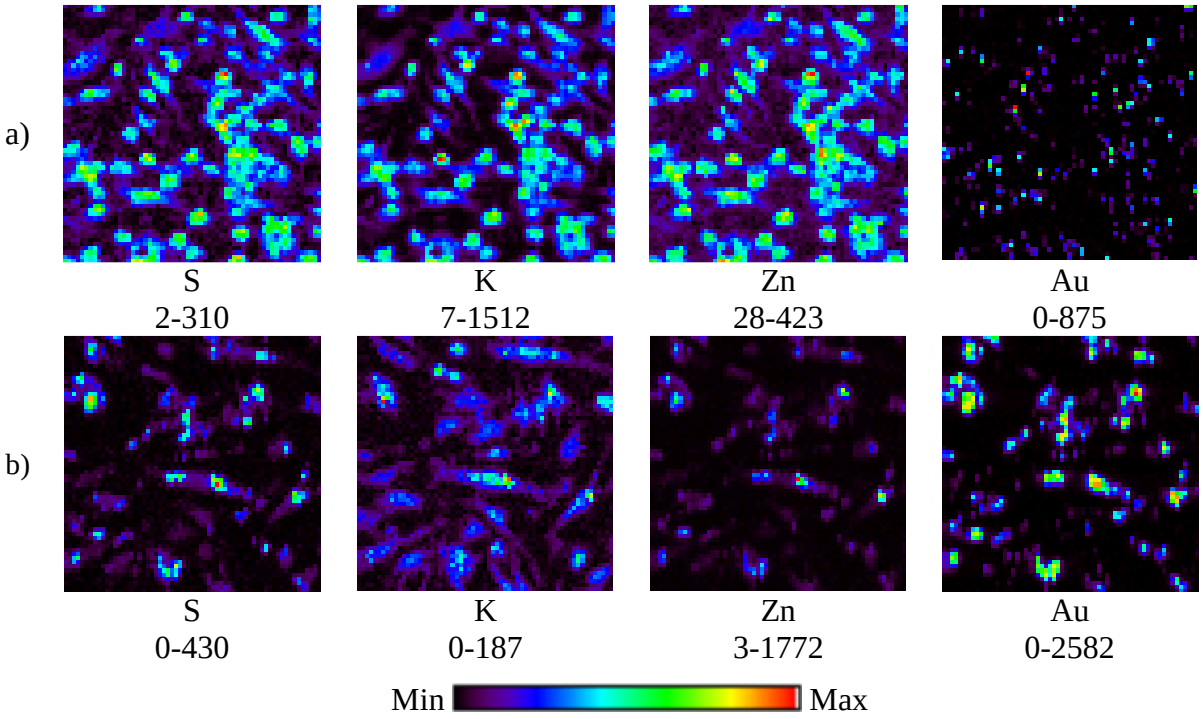

Figure 3.24: Microprobe SR-XRF elemental maps for RAW264.7 cells treated at 37 °C under an atmosphere of 5% CO_2 for 24 h with: **a)** 2.5 µM Au NPs, and **b)** 60 µM Au NPs. Scan dimensions (H x V) were 120 µm × 120 µm. Values are relative quantifications and are unitless.

3.6 Scanning Electron Microscopy Studies

Whilst the GFAAS gold uptake experiments described in **Section 3.4** provided evidence of extensive cellular uptake of Au NPs by macrophages, they did not afford any clues to the distribution of the gold throughout these cells. In contrast, whilst images obtained by microprobe SR-XRF in **Section 3.5** clearly showed association of gold with whole cells, these experiments were unable to discern whether the gold had been internalised, or was simply extracellularly bound. In order to definitively show that Au NPs had been incorporated into the cells, FESEM was employed. **Figure 3.25** shows the FESEM images for cells treated with incomplete medium or Au NPs. Examination of **Figure 3.25 a)**, the image of cells treated with incomplete medium, reveals a number of cells grown in close proximity to each other. Most have a rounded morphology, with one cell towards the top right of the image featuring extensive blebbing, indicating that it is late apoptotic or necrotic.

a)

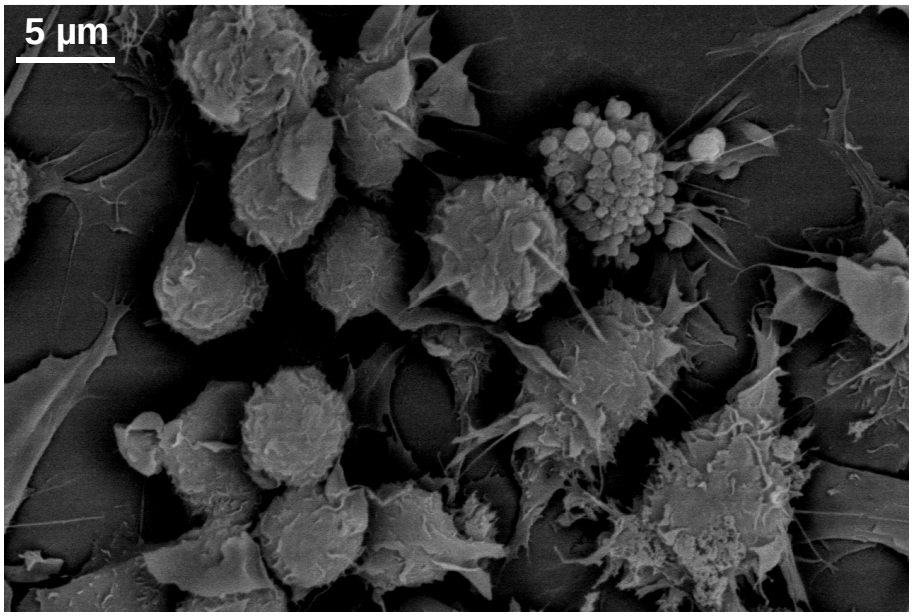

b)

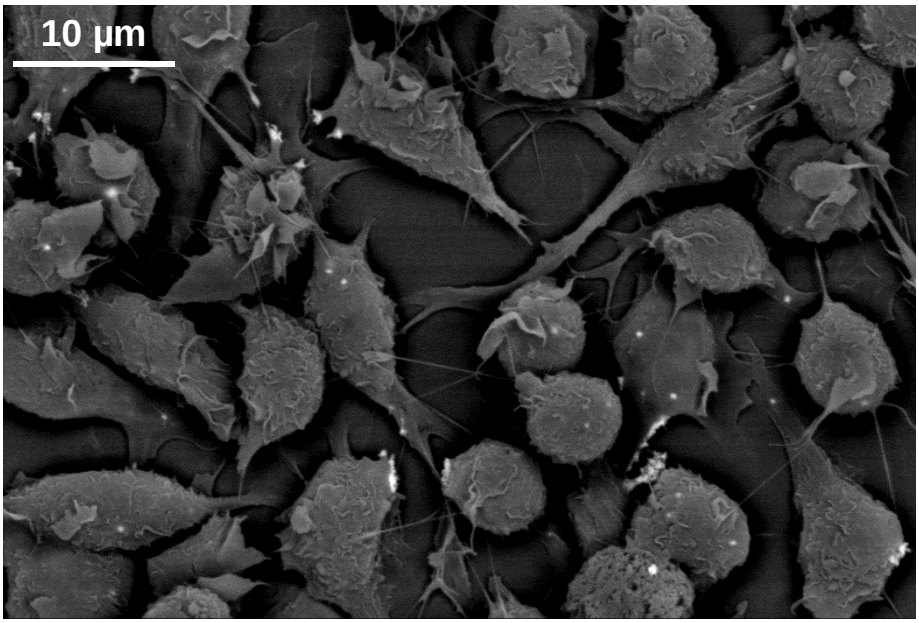

Figure 3.25: FESEM image of RAW264.7 macrophages treated at 37 °C under an atmosphere of 5% CO_2 for 24 h with: **a)** incomplete medium; and **b)** 60 µM Au NPs. Image **a)** was collected at ×2700 magnification, and **b)** at ×2200 magnification. Both were obtained using an accelerating voltage of 15 kV.

Figure 3.25 b) shows a scanning electron micrograph of macrophages treated with 60 µM Au NPs. Again, a number of cells are visible, featuring a mixture of rounded and fibroblastic morphologies. In contrast to **Figure 3.25 a)**, a number of bright white spots are now also visible, mostly located on the edges of the cells in the dendrites. Gold deposits are easily identified by FESEM owing to their pronounced electron scattering properties.[253] Scrutiny of **Figure 3.25 b)** also suggests that some

cells are extending their membranes to phagocytose the Au NPs, which is consistent with suggestions in the literature that Au NPs are taken up by cells through endocytosis.[199,200]

Confirmation that the white spots are gold was provided by comparing the FESEM image of a cluster of macrophages treated with Au NPs, to a gold elemental map of the same cells, obtained by EDX spectroscopy (**Figure 3.26**). Whilst there appears to be a fairly low signal-to-noise ratio in the gold EDX map, there are clearly hotspots corresponding to regions where there are higher concentrations of gold in the cell in the top-right quadrant. **Figure 3.26 c)** shows an overlay of the FESEM image and EDX gold map, and provides support for the conclusion that the hotspots in the EDX map correspond to the white spots of the FESEM image, identifying the latter as gold.

a)

b)

c)

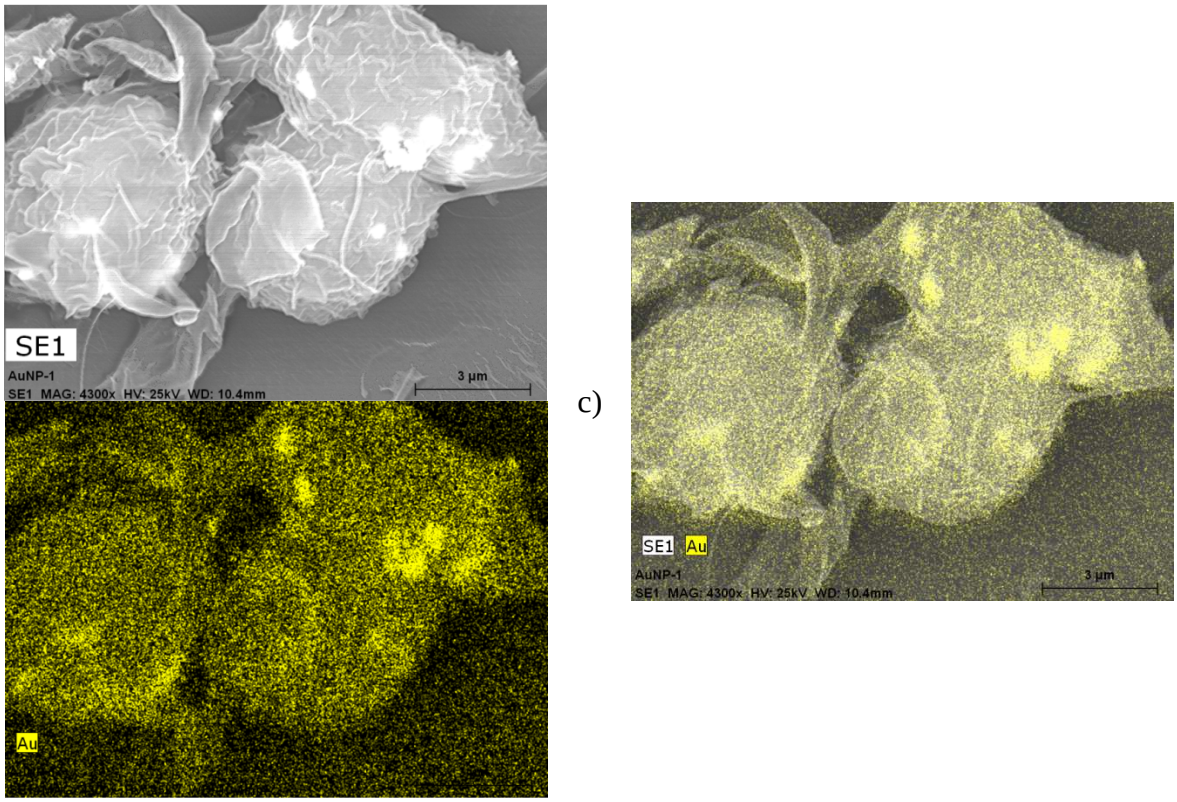

Figure 3.26: EDX and FESEM images of RAW264.7 cells treated with 60 µM Au NPs at 37 °C under an atmosphere of 5% CO_2 for 24 h. Images were collected at 4300× magnification with an accelerating voltage of 25 kV. EDX was collected for 90 min. **a)** FESEM image; **b)** EDX map for gold; **c)** overlay of a & b.

Figure 3.27 shows a series of FESEM images of an identical group of cells that had been treated with 60 µM Au NPs. Each image was collected using a different accelerating voltage. Higher voltages provide electrons with greater penetrating power through the sample thereby allowing detection of gold that is deeper below the surface of the cell. **Figure 3.27 a)** was collected at the highest accelerating voltage and shows three cells with many white spots most likely corresponding to Au NPs. The more diffuse spots are thought to be internalised gold below the membrane surface, whilst the more sharply defined spots, such as the one highlighted by a red arrow, are more likely to correspond to surface-bound gold. These surface-bound spots were visible at all accelerating voltages used. Inspection of all images in **Figure 3.27** reveals that as the accelerating voltage was decreased, the number of diffuse spots also decreased. This is consistent with the hypothesis that the diffuse spots correspond to gold particles located below the surface of the cell. Therefore, it can be concluded that a significant proportion of the cellular gold uptake measured by GFAAS, and gold observed in the microprobe SR-XRF images, is due to internalised Au NPs, and not simply due to particles located on the cell membrane. The results here are generally consistent with those of an earlier study, in which FESEM was used to show that 10 nm Au NPs were incorporated within macrophages to varying depths.[254]

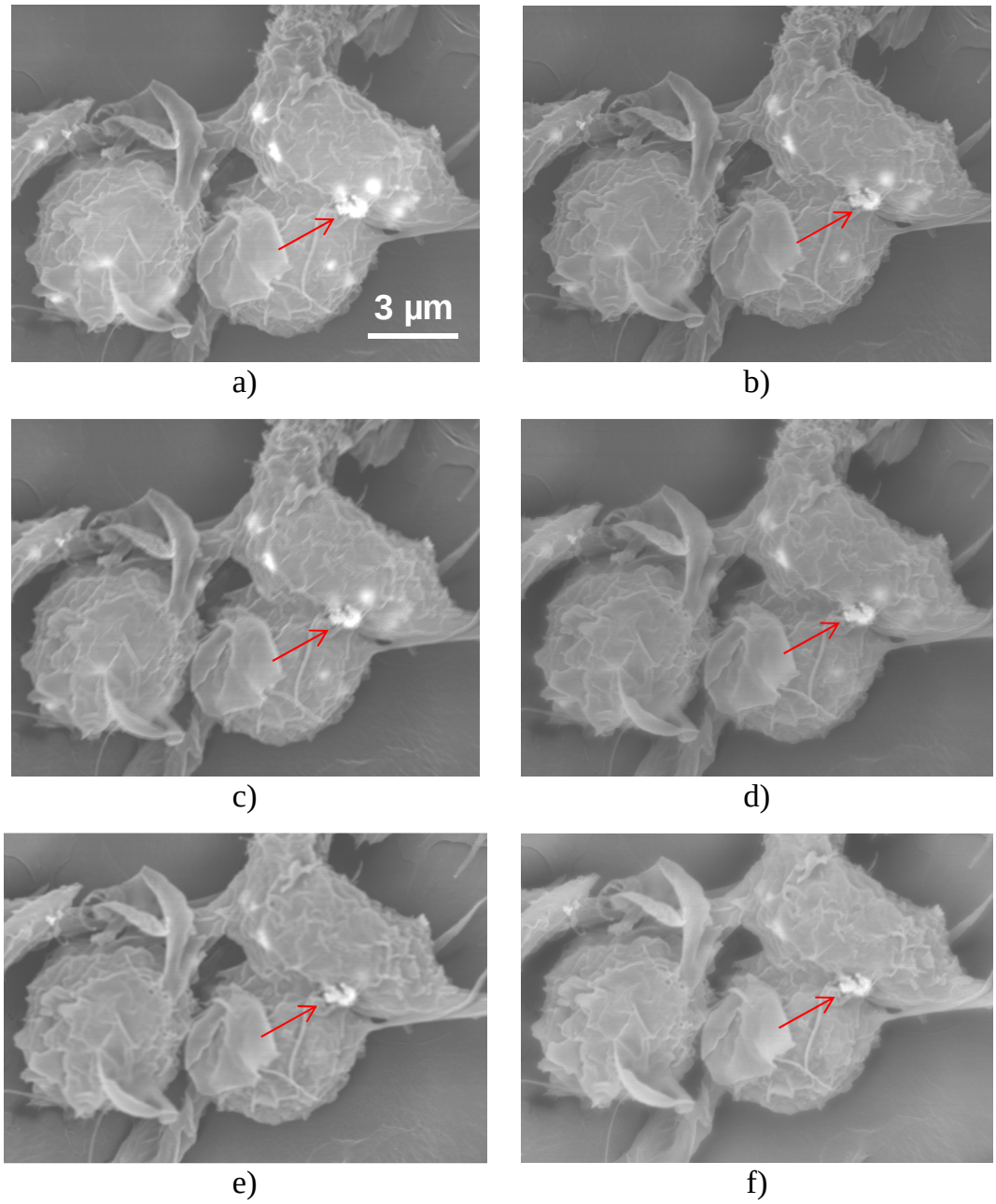

Figure 3.27: FESEM images of RAW264.7 macrophages treated with 60 µM Au NPs at 37 °C under an atmosphere of 5% CO_2 for 24 h. The images are of the same group of cells collected at ×4300 magnification and were obtained with accelerating voltages of: **a)** 25 kV **b)** 20 kV **c)** 18 kV **d)** 15 kV **e)**12 kV **f)** 10 kV.

Chapter 4:
Effects of Gold Compounds and Gold Nanoparticles on the Cellular Production of Inflammation Mediators

---

The investigations described in this chapter expand upon those of Chapter 3, by comparing the ability of anti-arthritic gold compounds and gold nanoparticles to exert anti-inflammatory effects, by altering the cellular expression of three pro-inflammatory mediators in macrophages. These were nitric oxide, reactive oxygen species and tumor necrosis factor. In addition, the ability of the gold compounds and nanoparticles to alter the production of the anti-inflammatory mediator interleukin-10 in macrophages was examined. The chapter concludes with an exploration of the effects of changing the size and composition of gold nanoparticles upon production of nitric oxide and reactive oxygen species in the same type of macrophages.

4.1 Introduction

The toxicity and cellular uptake of a number of gold complexes and Au NPs was compared in the previous chapter. The results of these studies showed that there was a higher level of incorporation of the Au NPs by macrophages, as well as a different pattern of cellular distribution compared to the gold compounds. To see how these differences might affect anti-inflammatory activity, the level of expression of a number of inflammation mediators after exposure of macrophages to gold compounds or Au NPs was compared. The mediators studied were NO, ROS, TNF and IL-10. Each was selected because of its known involvement in the inflammatory response associated with RA (**Section 1.1.1**). However, murine RAW264.7 macrophages do not constitutively produce appreciable quantities of these mediators, and as such the cells require 'activation.' The TLR4 ligand, LPS, was chosen to activate the macrophages, as it has also been used previously for similar studies.[201,203,206,255–260]

The results presented in this chapter follow a similar structure for each mediator studied, and were obtained from experiments performed as described in **Section 2.9**. First, experiments showing how mediator production by macrophages is affected by the addition of gold compounds or Au NPs are presented, with the effects of addition of LPS as a positive control also included. Following this, the results of experiments that investigated the ability of the gold compounds or Au NPs to attenuate LPS-induced mediator production are shown.

To focus the scope of the experiments, only the effects of addition of the anti-arthritic gold(I) compounds auranofin and aurothiomalate were compared to that of adding Au NPs. These two compounds were selected because they are the most broadly studied, and remain the most clinically relevant. In order to facilitate comparison with the toxicity

results presented in the previous chapter, the effects of adding 2.5 µM Au NPs, auranofin and aurothiomalate on the production of the inflammation mediators was explored. In addition, the effects of adding a higher concentration (60 µM) of aurothiomalate or Au NPs were also examined. As aurothiomalate was water soluble, its control solution (vehicle used for treatment) was incomplete medium. The auranofin control solution (vehicle) consisted of 1% DMSO/99% incomplete medium, while for Au NPs the control solution (vehicle) was 1.5% 10×D-PBS/15% H_2O/83.5% incomplete medium.

Statistical evaluations of the data were performed by using one-way ANOVA on sample subgroups to compare the gold compounds or Au NPs with their respective vehicle. One subgroup consisted of the auranofin vehicle, the Au NPs vehicle and incomplete medium. A second subgroup consisted of 2.5 µM and 60 µM aurothiomalate treatments as well as incomplete medium. Similarly, a third subgroup consisted of 2.5 µM and 60 µM Au NP treatments and the Au NPs vehicle. All one-way ANOVA tests were performed using a Tukey-Kramer post-test set at 95% confidence intervals. Results obtained from experiments performed using 2.5 µM auranofin were grouped only with the auranofin vehicle. Since this group consisted of only two samples, statistical analysis of the results was instead performed using a two-tailed unpaired *t*-test set with a 95% confidence interval. The tests were performed in these subgroups as the predominant interest in each experiment was whether a compound could cause inhibition or stimulation of inflammation mediator production, relative to its vehicle (solvent). This was a particularly important consideration for experiments involving auranofin or Au NPs, as both of their vehicles themselves had some significant effects on mediator production. The above statistical approach involving analysis of subgroups of samples was adapted instead of simply applying a one-way ANOVA on all samples at the same time, because the latter method

did not reveal significant effects caused by additional of specific gold agents due to a relatively large root mean squared (the measure of deviation across all tested data sets).

4.2 Effects on Production of Nitric Oxide

The free radical NO is an important signalling molecule that acts as a pro-inflammatory mediator in RA.[40] As it is a short-lived species, cellular production of NO must be inferred by determining the concentration of its major decay product, NO_2^-, using the Griess assay.[224] **Figure 4.1** compares the extent of production of NO_2^- by RAW264.7 cells after treatment with aurothiomalate, auranofin, Au NPs or LPS. None of the three different vehicles resulted in significant NO_2^- production by the macrophages. Furthermore, the addition of aurothiomalate, auranofin or Au NPs did not induce any formation of NO_2^- at any of the concentrations studied. However, the presence of LPS (0.1 µg/mL and 1 µg/mL) did induce formation of significant and similar quantities of nitrite. In view of the known cytotoxic effects caused by high concentrations of LPS,[261] and the minimal difference in NO_2^- produced at the two different concentrations used, it was decided to use 0.1 µg/mL LPS to induce NO production for the next experiment, as well as all other LPS-induced mediator formation experiments described in this chapter.

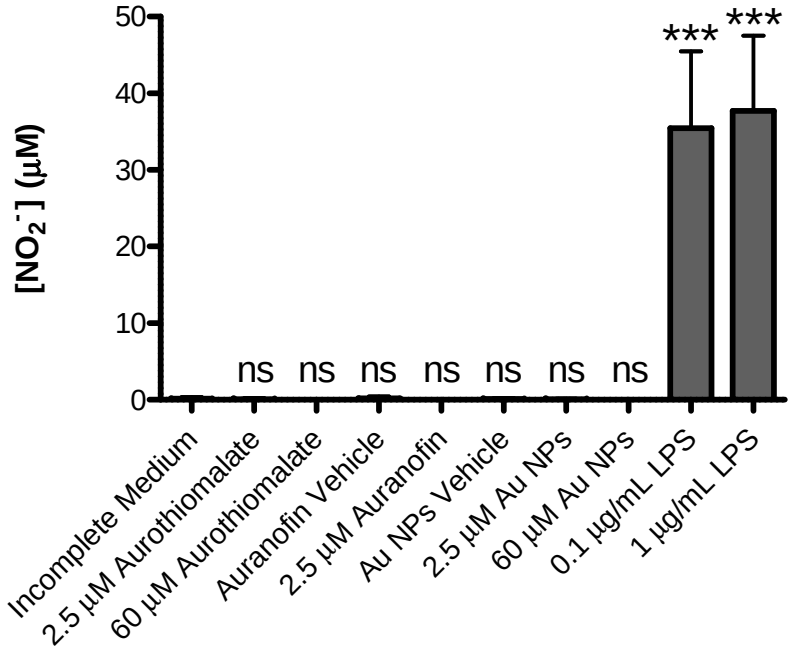

Figure 4.1: Effect of addition of aurothiomalate, auranofin, Au NPs or LPS on nitrite production by RAW264.7 macrophages. Cells were incubated with gold compounds, Au NPs or LPS at 37 °C under an atmosphere of 5% CO_2 for 24 h. Nitrite concentration was then measured by the Griess assay. The error bars represent one standard deviation calculated from triplicate plates. *** = statistically significant ($P < 0.001$) compared to incomplete medium; ns = not significant compared to corresponding vehicle ($P > 0.05$).

Figure 4.2 compares the extent of LPS-induced production of NO_2^- by RAW264.7 cells, after they had been previously incubated with aurothiomalate, auranofin, or Au NPs. Pre-incubation of the macrophages with either the auranofin or Au NP vehicles resulted in LPS-induced nitrite production levels that did not vary significantly from when the macrophages were pre-incubated with incomplete medium. Pre-incubation of the cells with 2.5 µM aurothiomalate also failed to produce a statistically significant reduction in formation of NO_2^- compared to incomplete medium. When the concentration of aurothiomalate in the pre-treatment solution was increased to 60 µM, a 40% drop in the amount of produced NO_2^- was recorded. In contrast, when the cells were pre-treated with 2.5 µM auranofin, almost complete inhibition of NO_2^- production was observed after addition of LPS. Pre-incubation of the macrophages with Au NPs at both concentrations

resulted in small, (~10%) statistically insignificant decreases in NO_2^- concentration compared to what was observed when the cells were first treated with the Au NPs vehicle.

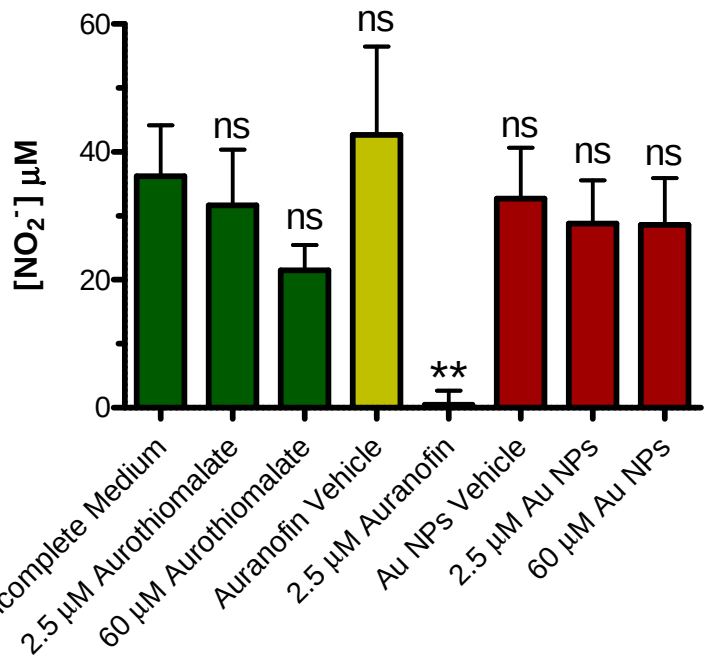

Figure 4.2: Effect of pre-incubation with gold compounds or Au NPs on LPS-induced nitrite production by RAW264.7 macrophages. Cells were pre-incubated with the gold compounds or Au NPs at 37 °C under an atmosphere of 5% CO_2 for 4 h, then 0.1 µg/mL LPS was added, and the cells incubated under the same conditions for a further 20 h. Nitrite concentration was then measured by the Griess assay. The error bars represent one standard deviation calculated from triplicate plates. ** = statistically significant ($P < 0.01$) compared to corresponding vehicle; ns = not significant compared to corresponding vehicle ($P > 0.05$).

The results obtained here with auranofin concur with those obtained in other studies using RAW264.7 cells, where similar reductions in the amount of LPS-induced nitrite were observed after first treating the cells using 3 and 20 µM solutions of auranofin.[257,259] Previous studies have also shown that pre-treatment with aurothiomalate resulted in moderate to large decreases in NO_2^- production for RAW264.7 cells activated by LPS,[262] as well as for murine H4 chondrocytes activated by IL-1β,[263] and non-activated peritoneal macrophages isolated from mice.[264] Whilst the results obtained using aurothiomalate in the current study (**Figure 4.2**) may not be statistically different from those obtained with the vehicle, incomplete medium, they suggest that pre-incubation with even higher

concentrations of this gold complex might leads to statistically relevant decreases in NO_2^- production.

The absence of a significant effect of pre-treatment with Au NPs on the production of NO_2^- contrasts results published by Ma *et. al* in the journal *Nitric Oxide*.[203] The latter authors used a very similar methodology to that followed in this thesis, which involved RAW264.7 cells being pre-incubated with Au NPs and subsequently activated using 0.1 µg/mL LPS. Ma *et. al* observed a dose-dependent reduction of NO_2^- production with increasing Au NPs concentration. Statistically significant reductions in the amount of NO_2^- produced of 28%, 52% and 76%, were reported in this literature study, when the macrophages were pre-treated using Au NP solutions containing 10, 20 and 40 µg Au/mL (equivalent to 51, 102 and 203 µM Au, respectively).

Since two of the three solutions containing Au NPs used in the Ma *et. al* study had much higher concentrations of gold compared to those in the current study, it was decided to repeat the experiment, using Au NP pre-treatment solutions with a greater range of concentrations. In order to prepare these solutions, newly synthesised Au NPs were concentrated by centrifugation. This enabled the preparation of Au NP solutions with concentrations up to 600 µM without particle aggregation. The results of this set of experiments are presented in **Figure 4.3**. A small drop in NO_2^- production was observed for macrophages that were pre-treated with solutions containing 400 or 600 µM Au NPs. However, the reduction in NO_2^- levels was still not statistically significant compared to the macrophage sample treated with the Au NPs vehicle. As noted in **Section 1.4.2**, there have been a number of conflicting studies in the literature concerning the effects of Au NPs on macrophages and other cells. In many cases, the physical characteristics of the nanoparticles were poorly described, making comparisons difficult. For example, Ma *et. al* indicated in the experimental section of their paper that the Au NPs used were synthesised

by the sodium citrate reduction method. However, in another part of the article it is mentioned that the Au NPs were coated in PEG, which may account for the difference between their results and those presented in this thesis.

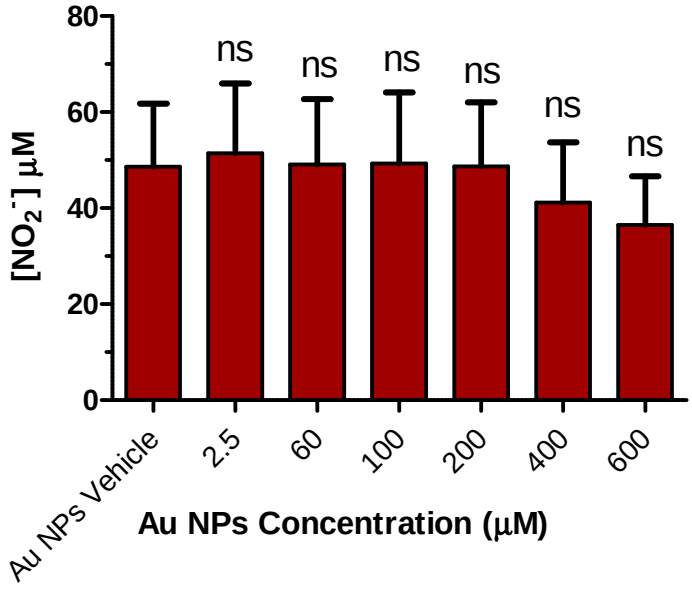

Figure 4.3: Effect of pre-incubation with Au NPs on LPS-induced nitrite production by RAW264.7 macrophages. Cells were pre-incubated with various concentrations of Au NPs at 37 °C under an atmosphere of 5% CO_2 for 4 h, then 0.1 µg/mL LPS added and the cells incubated under the same conditions for a further 20 h. Nitrite concentration was then measured by the Griess assay. The error bars represent one standard deviation calculated from triplicate plates. ns = not significant compared to Au NPs vehicle ($P > 0.05$).

Further confusion over the effects of Au NPs arises after reading the results of another study that showed pre-treatment of RAW264.7 macrophages with PEG-coated Au NPs caused a small increase in NO_2^- production, after subsequent treatment with 0.1 µg/mL LPS.[206] In addition, a letter published in the journal *Nitric Oxide* stated that in contrast to the results reported by Ma *et. al*, pre-treatment with Au NPs (stabilised with citrate or dihydrolipoic acid) caused no significant change in NO_2^- production by NR8383 cells, a rat macrophage cell line, after they were exposed to LPS.[205] The results of this last study mirror closely those presented in this thesis. This may be attributable to the Au NPs in both cases being stabilised only with low molecular mass compounds, whereas in some of the other studies discussed above the nanoparticles had a protective polymeric

coating.[203,206] This may have endowed the Au NPs with very different physical and chemical properties that could have affected their ability to inhibit LPS-induced formation of NO_2^-.

The results presented in this section showed that gold compounds and Au NPs can vary dramatically in their ability to inhibit LPS-induced formation of NO in RAW264.7 macrophages. In the next section, experiments are described that sought to determine if similar trends were observed when examining the ability of the gold compounds and Au NPs to inhibit production of ROS.

4.3 Effects on Production of Reactive Oxygen Species

The class of molecules known as ROS play an important biological role through their effects on cell signalling pathways, but when produced in large quantities contribute to oxidative stress associated with damage to DNA, lipids and proteins alike.[34] In patients with RA, increased oxidative stress is observed in the synovial fluid,[36] and is thought to be a major mechanism of disease progression.[37] It is possible to quantify ROS produced *in vitro* by measuring the extent of cellular conversion of the dye $DCFH_2$-DA to its fluorescent form, DCF, using flow cytometry.

Figure 4.4 shows exemplar flow cytometry data obtained from experiments performed with the three different vehicles and 0.1 µg/mL LPS. For each sample, three different sets of data are shown. The first of these (**Figure 4.4 a**) is a plot of forward scatter (cell size) against side scatter (cell granularity) for the cell population analysed, whilst the second (**Figure 4.4 b**) is a plot of forward scatter against fluorescence at 695 nm. Fluorescence at this wavelength corresponds to the relative amount of 7AAD present in each cell. This dye is similar to trypan blue, in that it is only able to enter cells with

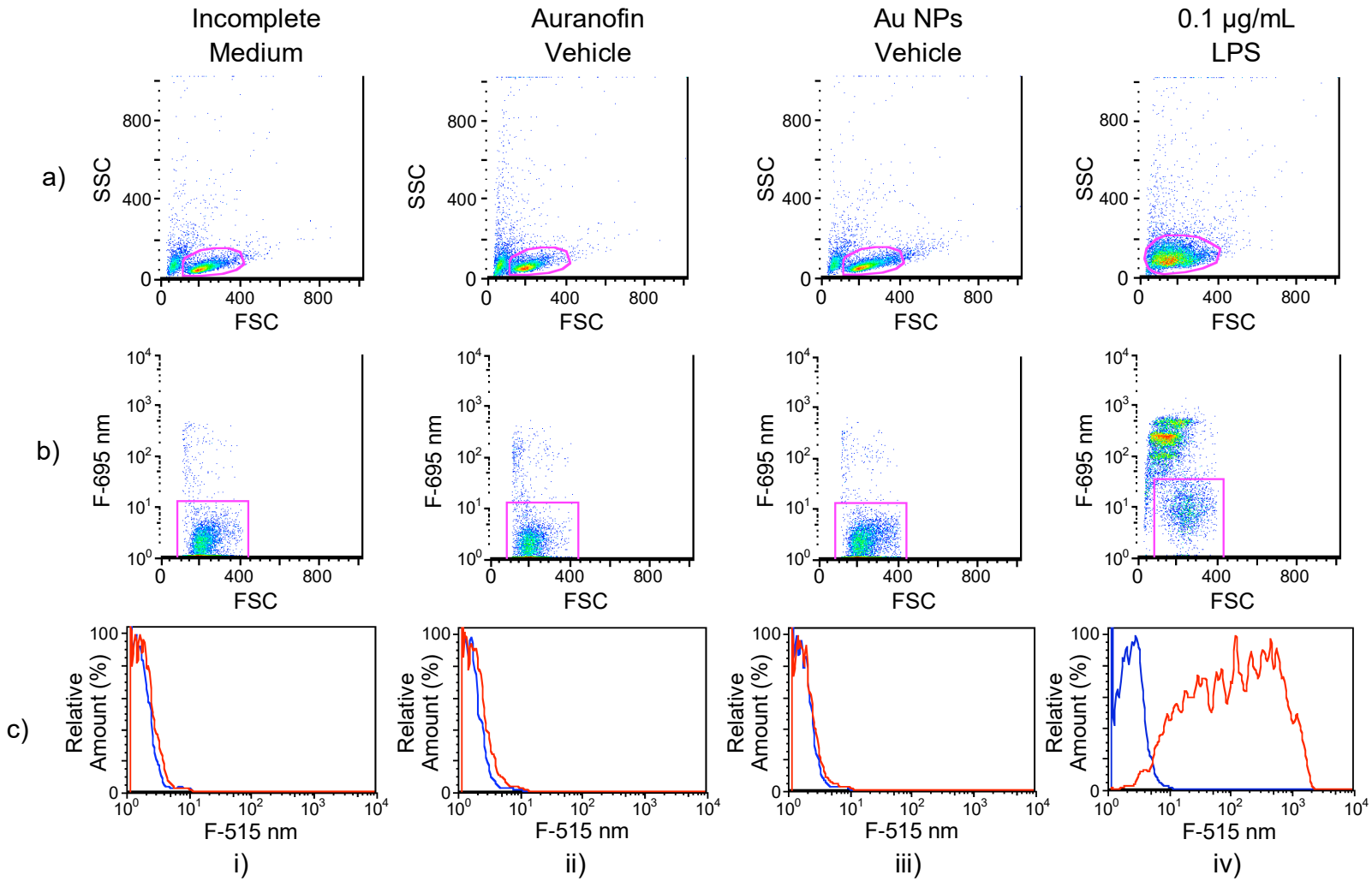

Figure 4.4: Exemplar flow cytometry data for macrophage samples treated with: **i)** incomplete medium; **ii)** auranofin vehicle; **iii)** Au NPs vehicle; or **iv)** 0.1 µg/mL LPS: **a)** dot plots for side scatter (y-axis) vs forward scatter (x axis); **b)** dot plots for fluorescence at 695 nm (y-axis) vs forward scatter (x-axis); and **c)** histograms of relative fluorescence at 515 nm for different gated cell populations. DMSO loaded samples are coloured blue and $DCFH_2$-DA loaded samples are coloured red.

compromised membranes, which can therefore be classified as 'non-viable.' The above parameters (forward scatter, side scatter, and fluorescence at 695 nm) allow the viable cell population to be selected within a 'gate' or region within the plots shown in **Figure 4.4** (shown as an oval or rectangle in the plots). The median fluorescence intensity (MFI) at 515 nm of the cell population within the gate is then measured. This corresponds to the amount of ROS formed by the cells. The histograms in **Figure 4.4 (c)** show the fluorescence at 515 nm for the gated populations shown in **Figure 4.4 (b).** These histograms compare cells loaded (treated) with $DCFH_2$-DA (coloured red in the histogram) with those loaded with DMSO (coloured blue in the histogram). The administered $DCFH_2$-DA is dissolved in DMSO, and as such, the DMSO loading acts as a control to measure whether the cells produce fluorescence at 515 nm that is not a result of production of DCF. This usage of DMSO is termed the autofluorescence control, because it measures the amount of native fluorescence (i.e. not from ROS) generated by the cells. The MFI of the DMSO loading is subtracted from the MFI of the $DCFH_2$-DA loading to give the amount of ROS formed.

Comparison of the data obtained for macrophages treated with the three different types of vehicles shows that these had little effect on cell morphology. In contrast, treatment with LPS resulted in significant changes to cell size and granularity, as well as an increase in fluorescence at 695 nm. The latter increase is typical for cells entering either the early or late stages of apoptosis,[265] and is consistent with the known cytotoxicity of LPS.[261] As a result, the LPS treated cell samples were gated differently to the other samples. Examination of the gated population of viable cells remaining after treatment with LPS also reveals an increase in relative fluorescence at 695 nm, compared to cells treated with the vehicles. This was likely caused by an increase in

autofluorescence of the macrophages as a result of being activated by LPS. This has been observed previously with monocyte-derived macrophages.[266]

Examination of **Figure 4.4 c)** shows there was little difference between the relative fluorescence at 515 nm for DMSO and $DCFH_2$-DA loaded cells for macrophages treated with the three different vehicles. This indicates that there was little ROS produced as a result of treatment with any of the vehicles, and that the detected fluorescence was from other molecules that fluoresce at 515 nm. In contrast, the cells treated with 0.1 µg/mL LPS showed a large difference between the relative fluorescence of the DMSO and $DCFH_2$-DA loaded samples, indicating that treatment with LPS induced formation of a large amount of ROS. The MFI for both the $DCFH_2$-DA and DMSO loaded cells was then derived from each of the histograms in **Figure 4.4 c)**. Subsequently, the MFI for the DMSO loaded cells was subtracted from that for the $DCFH_2$-DA loaded cells to give the amount of ROS produced for each sample.

Figure 4.5 shows the amount of ROS produced by RAW264.7 cells treated with aurothiomalate, auranofin, Au NPs or LPS. In each case, the amount of ROS produced is expressed as a MFI. Examination of **Figure 4.5** shows that none of the gold compounds or the Au NPs induced ROS production at any of the concentrations studied. In contrast, treatment of the macrophages with LPS resulted in production of a large amount of ROS at both concentrations studied, with the MFI for the 1 µg/mL treated sample being 1.7 times higher than that for the cells treated with just 0.1 µg/mL LPS. As treatment with 0.1 µg/mL LPS produced significant quantities of ROS, this concentration was used in all subsequent studies. This also facilitated comparisons with the results of investigation into the effects of gold compounds and Au NPs on NO formation, which were described in the previous section, and where macrophages were also treated with 0.1 µg/mL LPS.

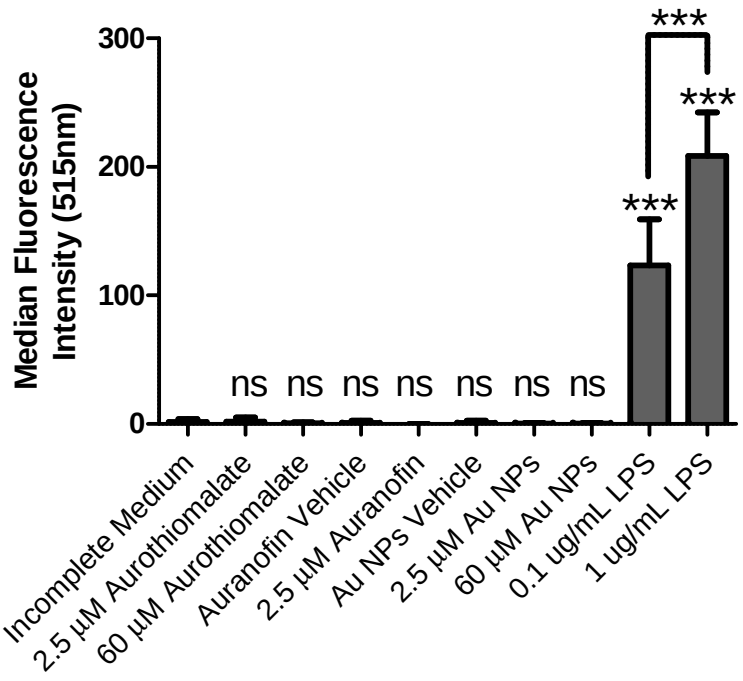

Figure 4.5: Effect of treatment with gold compounds, Au NPs or LPS on ROS production by RAW264.7 macrophages. Cells were incubated with gold compounds, Au NPs or LPS at 37 °C under an atmosphere of 5% CO_2 for 24 h. ROS was measured by the DCF assay and is presented as a MFI at 515 nm. The error bars represent one standard deviation calculated from triplicate samples. *** = statistically significant ($P < 0.001$) compared to incomplete medium; ns = not significant compared to the corresponding vehicle ($P > 0.05$).

Figure 4.6 shows the effects of pre-incubation with aurothiomalate, auranofin, or Au NPs on production of ROS by RAW264.7 cells subsequently treated with LPS. The data presented for each experiment has been normalised by expressing the MFI obtained as a percentage of the result obtained when the cells were treated with incomplete medium. This normalisation procedure was performed to reduce the impact of the variability inherent in the fluorescence intensities as a result of differences in $DCFH_2$-DA loadings from one experiment to another.

Examination of **Figure 4.6** shows that treatment with 2.5 µM aurothiomalate had little effect on the production of ROS by the macrophages. However, when the concentration of aurothiomalate was increased to 60 µM, a 44% drop in ROS production was observed. As a result of the large standard deviation associated with this

result, it was not statistically significant in the ANOVA analysis performed on this subset of samples. This is most likely due to the relatively large errors associated with the results for the aurothiomalate-treated (as well as other) samples, which are not uncommon for experiments of this type. The results, nonetheless, suggest that treatment with aurothiomalate can decrease the amount of ROS produced by LPS-induced macrophages.

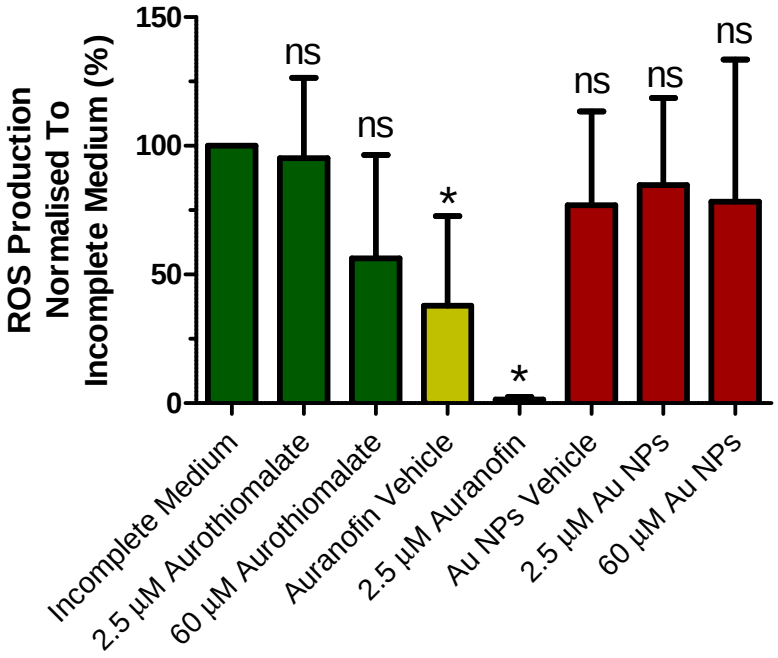

Figure 4.6: Effect of pre-treatment with gold compounds or Au NPs on LPS-induced ROS production by RAW264.7 macrophages. Cells were pre-incubated with the gold compounds or Au NPs at 37 °C under an atmosphere of 5% CO_2 for 4 h, then 0.1 µg/mL LPS was added and incubation continued under the same conditions for a further 20 h. ROS was measured by the DCF assay and presented as normalised MFI values at 515 nm, relative to incomplete medium. The error bars represent one standard deviation calculated from triplicate samples. * = statistically significant ($P < 0.05$) compared to the corresponding vehicle; ns = not significant compared to the corresponding vehicle ($P > 0.05$).

Treatment of the macrophages with the auranofin vehicle, consisting of 1% (v/v) DMSO/99% (v/v) incomplete medium caused a significant (62%, $P < 0.05$) drop in ROS production relative to that caused by the pre-treatment with incomplete medium. Pre-treatment with 2.5 µM auranofin led to almost complete loss of ROS formation ($P <$

0.05), suggesting that this compound may have a much stronger effect on production of ROS than aurothiomalate. When the macrophages were pre-treated with the Au NPs vehicle, or solutions containing 2.5 µM or 60 µM Au NPs, there was no impact on the amount of ROS produced compared to cells pre-treated with incomplete medium.

The data in **Figure 4.6** suggests that pre-treatment with the auranofin vehicle may have had a notable impact on the amount of ROS produced, compared to samples which were pre-treated with incomplete medium. This is most likely a result of the DMSO present in the auranofin vehicle. A similar conclusion was reached in a previous study performed using neuroblastoma cells and the DCF assay.[267] **Figure 4.6** also strongly points to a major effect on ROS production by the macrophages as a result of pre-treatment with auranofin. This observation is also consistent with results reported previously in the literature. While its effect on total ROS production does not appear to have been measured previously, auranofin has been shown to inhibit the formation of the superoxide ion (O_2^-) in a number of studies using phagocytes,[268] polymorphonuclear leucocytes,[269–271] and neutrophils.[272] In addition, auranofin has been shown to quench highly reactive singlet oxygen.[273] It is also worth noting that the results presented here using aurothiomalate are consistent with literature reports, which show this gold compound has a weaker inhibitory effect on the formation of superoxide than auranofin.[268–271] It has been suggested that one mechanism by which these two compounds produce their inhibitory effects is through activation of the heterodimeric transcription factor Nrf2/small maf, that upregulates anti-oxidant proteins.[274] In addition, it has been reported that both auranofin and aurothiomalate can suppress the pro-inflammatory transcription factor NF-κβ.[125]

The lack of a significant effect of Au NPs on production of ROS shown in **Figure 4.6**, appears to contradict the findings of a number of other researchers. For

example, one study showed that Au NPs bought from BBI (Cardiff, UK) could reduce ROS formation by human PBMCs.[275] A luminol-dependent chemiluminescence assay was used to measure ROS in this study, which also showed that Au NPs with smaller diameters were more effective at inhibiting ROS formation. One key difference between this study and that described in this thesis, is that ROS formation was induced using the glucan molecule zymosan,[275] and not LPS. This is potentially important as zymosan is a TLR2 ligand, whilst LPS is a TLR4 ligand, meaning that they may signal their inflammatory effects through separate pathways, which in turn, the Au NPs may interact differently with.

Au NPs synthesised by reaction of $[AuCl_4]^-$ with the soil bacterium *Bacillus licheniformis* have also been shown to inhibit ROS formation and lipid peroxidation in diabetic mice.[276] In this study, treatment of the mice with Au NPs caused upregulation of the anti-oxidant molecule glutathione and the anti-oxidant proteins superoxide dismutase and glutathione peroxidase. It was concluded that the greater abundance of these proteins may have been the cause of the lower ROS levels observed.[276] In another study ROS production was not changed when RAW264.7 cells were treated with poly-L-lysine-coated Au NPs for a 24 h period.[201] However, exposure to a 100 μM solution of the Au NPs for 48 h did result in a significant reduction.[201]

Despite the above literature studies suggesting that various types of Au NPs can inhibit ROS formation in cells, there are a number of other investigations, which did not involve the use of an inflammation-stimulating molecule, which showed they have the opposite effect. For example, the DCF assay was used to show that leukaemia and liver cell lines treated with 30, 50 and 90 nm Au NPs purchased from CymitQuímica (Barcelona, Spain) exhibited an increase in total ROS production, coupled with strongly decreased glutathione levels and superoxide dismutase activity.[277] In addition, Au NPs

(1.4 nm in diameter) stabilised by triphenylphosphine monosulfate caused significant ROS formation in leukaemia cells, with the effect becoming more pronounced with longer exposure periods.[278] Similarly, leukaemia cells exposed to various types of 2 nm Au NPs with organic stabilizers of different lengths, showed high levels of ROS production, according to measurements performed using the DCF assay.[279]

The variety of results in the literature once again highlights the likely importance of variations in the size and chemical composition of Au NPs on their biological activity. No literature studies appear to have looked at the effect of citrate stabilised Au NPs on ROS formation, making the results presented in this thesis distinct from those in the literature. The absence of a significant effect on ROS production, together with the minimal influence on NO production shown in **Section 4.2**, suggests that the Au NPs studied here either do not have significant anti-inflammatory properties, or that they exert their effects through a different mechanism or mechanisms. In order to test the latter hypothesis, the effects of the Au NPs (and gold compounds) on the production of the inflammation cytokines TNF and IL-10 was studied next.

4.4 Effects on Production of Tumor Necrosis Factor

TNF is a pro-inflammatory cytokine strongly linked to RA progression, as it is involved in signalling the release of ROS,[22] degradative enzymes,[24] and other inflammatory cytokines.[21] The clinical importance of TNF is highlighted by clinical usage of the biologics infliximab and etanercept, which treat RA through inhibition of TNF.[48] It was decided to investigate the ability of the gold compounds and Au NPs to inhibit production of TNF, as this might be a mechanism by which they exert their anti-arthritic effects. Production of TNF by RAW264.7 cells was assessed using a commercial ELISA kit.

Figure 4.7 displays the amount of TNF produced by RAW264.7 macrophages in response to treatment with aurothiomalate, auranofin, Au NPs or LPS. Treatment of the cells with either 0.1 or 1 µg/mL LPS caused release of much larger amounts (~80 times) of TNF than that elicited by any of the gold compounds or Au NPs. For example, treatment of the cells with 60 µM aurothiomalate only resulted in production of 1.04 ng/mL of TNF, which was not significantly different ($P > 0.05$) compared to the amount of this cytokine produced when the macrophages were treated with incomplete medium (0.177 ng/mL). Similarly, treatment of the macrophages with auranofin or Au NPs failed to result in statistically significant increases in TNF production.

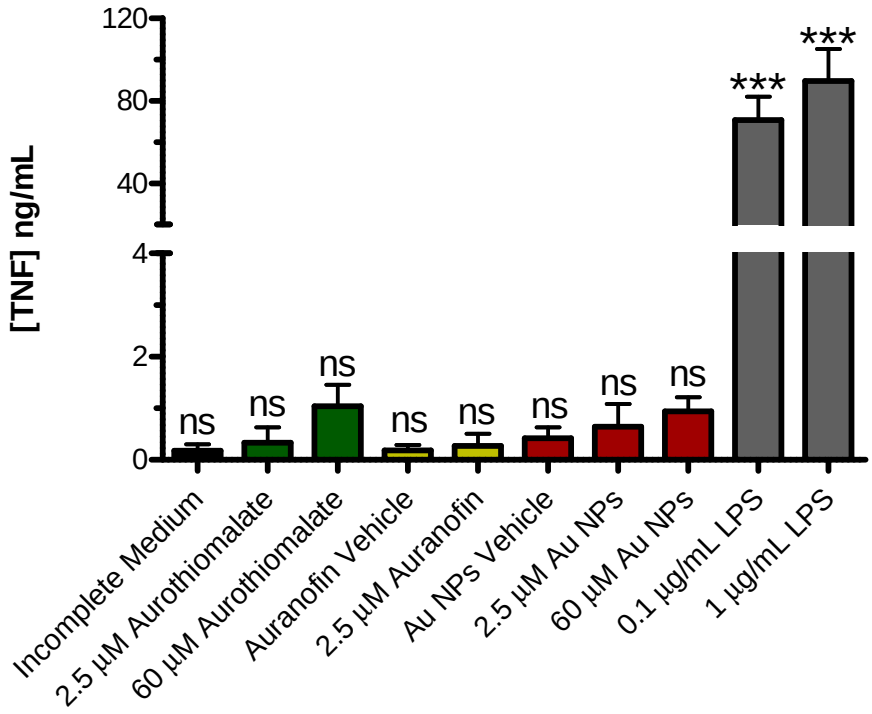

Figure 4.7: Effect of treatment with gold compounds, Au NPs or LPS on TNF production by RAW264.7 macrophages. Cells were treated with the gold compounds, Au NPs, or LPS and incubated at 37 °C under an atmosphere of 5% CO_2 for 24 h, and the amount of TNF produced then measured by ELISA. The error bars represent one standard deviation calculated from triplicate samples. *** = statistically significant ($P < 0.001$) compared to incomplete medium; ns = not significant compared to the corresponding vehicle ($P > 0.05$).

In view of these results, it appeared that the gold compounds and Au NPs do not induce production of significant amounts of TNF. In contrast, the amount of TNF produced after treating the cells with LPS was similar to that observed in other studies involving RAW264.7 macrophages, where the cells were treated with 0.01 µg/mL,[280] 0.1 µg/mL[281] or 0.5 µg/mL LPS.[282]

There are very few papers in the literature that discuss the basal effects of auranofin and aurothiomalate on TNF production. In contrast, the effects of Au NPs have been reported, with differing outcomes being observed depending on the size and composition of the nanoparticles. In one study, Au NPs with diameters less than 20 nm were used.[202] The authors of this study stated that the nanoparticles were produced by physical manufacturing and did not contain any surface modifiers or stabilisers. Treatment with these Au NPs resulted in an increase in the level of TNF in murine J774.A1 macrophages.[202] In contrast, another study showed that lysine and poly-L-lysine coated Au NPs do not affect TNF levels in RAW264.7 macrophages.[201] The importance of the coating surrounding the Au NPs is further highlighted by another study that compared the levels of cytokines produced by bone marrow-derived macrophages in response to treatment with either citrate-coated Au NPs or peptide-coated Au NPs.[283] Both TNF and other pro-inflammatory cytokines were produced by the macrophages after treatment with the peptide coated Au NPs, but not the citrate coated Au NPs.

Figure 4.8 shows the effects of pre-incubation of RAW264.7 macrophages with aurothiomalate, auranofin or Au NPs, on TNF production by the cells after treatment with 0.1 µg/mL LPS. Pre-incubation with 2.5 µM aurothiomalate resulted in no significant effects on the amounts of TNF produced. In contrast, when the concentration

of aurothiomalate was increased to 60 µM, a statistically insignificant (P > 0.05) stimulatory effect was observed.

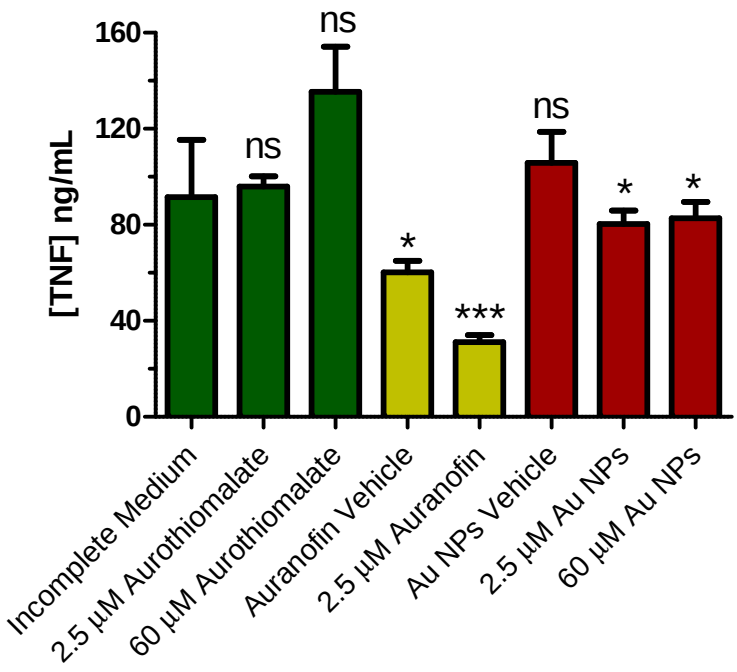

Figure 4.8: Effect of pre-incubation with gold compounds or Au NPs on LPS-induced TNF production by RAW264.7 macrophages. Cells were pre-incubated with the gold compounds or Au NPs at 37 °C under an atmosphere of 5% CO_2 for 4 h, and then 0.1 µg/mL LPS added and incubation continued under the same conditions for a further 20 h. TNF was measured by ELISA. The error bars represent one standard deviation calculated from triplicate samples. * = statistically significant (P < 0.05) compared to corresponding vehicle; *** = statistically significant (P < 0.001) compared to corresponding vehicle; ns = not significant compared to corresponding vehicle (P > 0.05).

This contradicts some reports in the literature that showed aurothiomalate has a small inhibitory effect on LPS-induced TNF production in human PBMCs.[118,284,285] A possible explanation for this difference could be that the experiments described in this thesis were performed using a murine macrophage cell line, as opposed to PBMCs isolated directly from humans[118,285] or mice.[284] It could also arise from differences in methodology, such as the exclusion[118,285] or dramatic shortening (< 5 min compared to 4 h in this thesis)[284] of a pre-incubation period for the studied compounds, use of a lower LPS concentration (maximum of 0.02 µg/mL compared to 0.1 µg/mL in this thesis),[118,284,285] or lower aurothiomalate concentrations (maximum of ~27µM compared

to 60 µM in this thesis).[118,284,285] It should also be noted even within the literature there are reports that suggest aurothiomalate has no effect on production of TNF. For examples, one study that also investigated human PBMCs (from RA patients) showed that aurothiomalate does not alter LPS-stimulated TNF production,[117] whilst another reported that the compound does not affect TNF mRNA levels in LPS-stimulated murine macrophages.[255]

Figure 4.8 also shows that pre-treatment of the macrophages with 2.5 µM auranofin resulted in a significant decrease (~50%, $P < 0.001$) in TNF production compared to the auranofin vehicle. This is consistent with the outcomes from a previous study that showed there was inhibition of LPS-induced TNF formation in PBMCs following treatment with auranofin.[255,284] It should also be noted that **Figure 4.8** indicates that pre-treatment using the 1% DMSO auranofin vehicle may also have a significant ($P < 0.05$) inhibitory effect on TNF formation. A similar effect of DMSO upon TNF formation has previously been demonstrated for murine alveolar and peritoneal macrophages.[286]

Pre-treatment using either 2.5 or 60 µM Au NPs resulted in small decreases in LPS-induced TNF production that were statistically significant ($P < 0.05$) when compared to the amount of cytokine produced when the pre-treatment was performed using the Au NPs vehicle. These results are generally consistent with those reported by Ma *et. al*,[203] who indicated that Au NPs had no effect on LPS-induced TNF production. In contrast, pre-treatment with Au NPs coated with poly-*N*-vinylpyrrolidone was shown to enhance TNF production by RAW264.7 cells subsequently incubated with LPS.[287] This once again highlights the importance that the composition of the nanoparticle shell may play in determining overall biological activity. The absence of a significant effect on LPS-induced TNF formation follows on from results presented earlier in this chapter,

which revealed an inability of Au NPs to affect the levels of the inflammatory mediators NO and ROS.

4.5 Effects on Production of Interleukin-10

The results presented earlier in this chapter showed that pre-treatment of RAW264.7 macrophages with Au NPs does not have a significant effect on the levels of the pro-inflammatory mediators NO, ROS and TNF. It was therefore decided to investigate whether Au NPs might produce anti-inflammatory activity by instead upregulating anti-inflammatory cytokines. The cytokine chosen for these experiments was IL-10, which has been shown to suppress production of the pro-inflammatory mediators IL-1α, IL-6 and IL-8,[288] as well as TNF and NO in macrophages.[289] Further interest in IL-10 stems from previous studies using RAW264.7 cells that showed these cells can be converted into one of two subtypes. These are the pro-inflammatory M1 and anti-inflammatory M2 subtypes of macrophages.[18] Therefore, if gold compounds or Au NPs were found to lead to increased anti-inflammatory activity, this might be a result of conversion of the macrophages to the M2 subtype.

Figure 4.9 shows the amounts of IL-10 produced by RAW264.7 cells exposed to aurothiomalate, auranofin, Au NPs or LPS. The figure shows that when the cells were treated with either of the gold compounds or Au NPs, IL-10 production was below the detection limit for the assay. This result implies that none of the above gold reagents promote an anti-inflammatory process involving IL-10 as a means of biological action. In the case of auranofin in particular, this result is not unexpected considering the results presented earlier in this chapter where the gold compound was shown to have a significant ability to suppress production of the pro-inflammatory mediators NO and ROS in LPS-stimulated cells; i.e. auranofin's mechanism of action involves suppression

of pro-inflammatory responses rather than inducing anti-inflammatory responses. Aurothiomalate is likely to behave similarly to auranofin due to similarities in their uptake mechanisms and metabolites noted in **Section 1.2**.

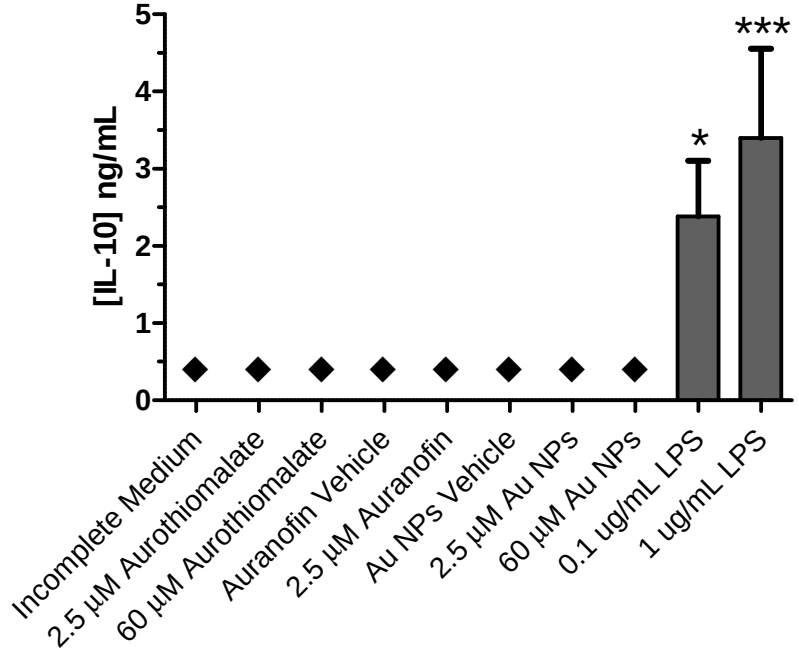

Figure 4.9: Effect of gold compounds, Au NPs, or LPS on IL-10 production by RAW264.7 macrophages. Cells were treated at 37 °C under an atmosphere of 5% CO_2 for 24 h, and IL-10 produced then measured by ELISA. The error bars represent one standard deviation calculated from triplicate samples. ◆ = below detection limit; * = statistically significant ($P < 0.05$) compared to incomplete medium; *** = statistically significant ($P < 0.001$) compared to incomplete medium.

To date there has only been one report in the literature that has discussed the effects of aurothiomalate on IL-10 expression. This study showed that treatment with this gold compound led to an increase in the total number of PBMCs that had expressed IL-10, but also found that this did not result in an increase in supernatant IL-10 concentration.[290] This is broadly consistent with the results presented in **Figure 4.9**, as no change in supernatant IL-10 was detected in the current study. Similarly, there is little literature available regarding the effect of Au NPs on IL-10 production. However, one study investigated how 8.8 nm diameter Au NPs prepared in citrate buffer, and Au NPs with a mixture of peptide and organic capping agents, affected cytokine production

by PBMCs.[291] Treatment of the cells with the citrate-stabilised Au NPs led to an increase in IL-10 production, whilst the second type of Au NPs had no noticeable effect.[291] It should be noted that the observed increase in IL-10 levels elicited by the citrate-stabilised Au NPs was accompanied by an increase in production of IL-2 and interferon-γ. Therefore the observed increase in IL-10 production by the cells may have been a regulatory response to the increase in production of these two pro-inflammatory cytokines.

The most significant result presented in **Figure 4.9** is that treatment of the macrophages with LPS, at both 0.1 and 1 μg/mL, resulted in expression of large amounts of IL-10. This is most likely a response to LPS inducing the production of pro-inflammatory mediators such as TNF. It has previously been shown that after 12 – 24 h treatment with LPS, bone marrow derived macrophages upregulate IL-10 to suppress formation of the pro-inflammatory cytokine IL-1β.[292] Since IL-10 is an anti-inflammatory cytokine, it might be expected that anti-RA drugs could further promote its production in cells. To test this hypothesis, a series of experiments were performed to see whether pre-treatment with any of the gold compounds or Au NPs led to changes in the amount of LPS-induced IL-10 produced by the macrophages. **Figure 4.10** shows the results of these studies.

Figure 4.10 shows that pre-treatment of the macrophages with the auranofin vehicle resulted in a significant decrease ($P < 0.01$) in IL-10 levels when compared to pre-treatment of the cells with incomplete medium. Additionally, pre-treatment with 2.5 μM auranofin also resulted in a large decrease in IL-10 levels. Whilst it may appear that the effect observed for this pre-treatment may be due largely to the effects of the DMSO, it should be noted that this decrease was significant ($P < 0.01$) when compared to the auranofin vehicle. This decrease may be explained by considering results

presented earlier in this chapter, which showed that pre-treatment with either auranofin or the auranofin vehicle led to a reduction in the amount of LPS-induced TNF produced by the macrophages. Therefore, the decrease in IL-10 levels may not be a direct result of inhibition by either DMSO or auranofin, but may instead be a consequence of reduced levels of production of TNF.

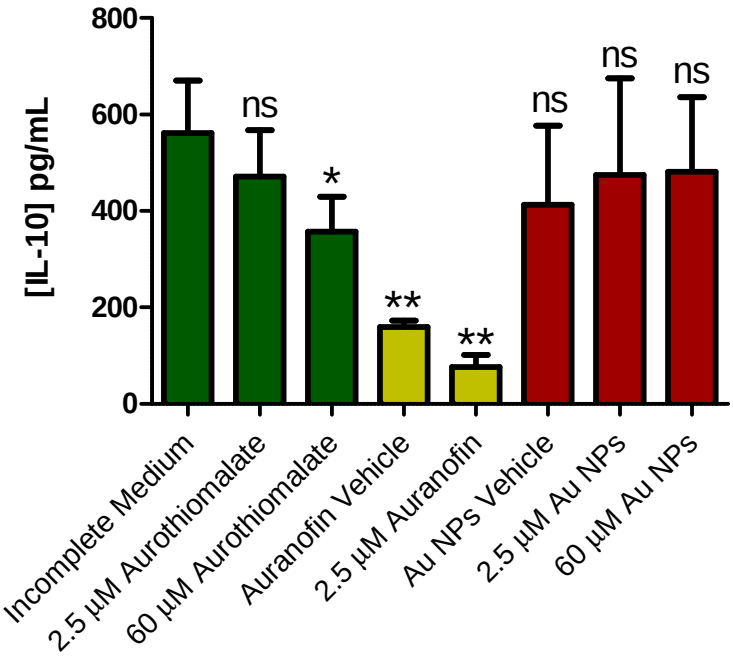

Figure 4.10: Effect of pre-incubation with gold compounds or Au NPs on LPS-induced IL-10 production by RAW264.7 macrophages. Cells were pre-incubated with the gold compounds or Au NPs under 37 °C under an atmosphere of 5% CO_2 for 4 h, and then 0.1 µg/mL LPS added and incubation continued at the same conditions for a further 20 h. IL-10 was measured by ELISA. The error bars represent one standard deviation calculated from triplicate samples. * = statistically significant ($P < 0.05$) compared to corresponding vehicle; ** = statistically significant ($P < 0.01$) compared to corresponding vehicle; ns = not significant compared to corresponding vehicle ($P > 0.05$).

To test this hypothesis, the data presented in **Figure 4.8** and **Figure 4.10** that were obtained using aurothiomalate can be considered. **Figure 4.10** shows that pre-treatment of the macrophages with 60 µM aurothiomalate resulted in a small, but statistically significant decrease in the amount of IL-10 produced. For the explanation proposed above to be true, a decrease in production of TNF would also be expected. However, **Figure 4.8** shows that the opposite result was in fact observed. This is instead

consistent with the notion that aurothiomalate inhibits the auto-regulatory production of IL-10, thereby causing the observed increase in amount of TNF produced relative to incomplete medium. **Figure 4.10** shows that treatment of the macrophages with Au NPs did not cause any significant change to the amount of IL-10 produced compared to the Au NPs vehicle, again indicating a lack of interaction between the Au NPs and the macrophages.

4.6 Studies Using Commercial Au NPs

The results described in the previous sections showed that the citrate-stabilised Au NPs prepared as part of this research project generally failed to have a significant effect on the production of various cytokines associated with inflammation, by LPS-stimulated macrophages. In some instances, these results are consistent with those presented in the literature, while in others there was significant disagreement. A possible explanation for these differences in behaviour is variation in the size or chemical composition of the Au NPs being used. To test this hypothesis, some of the assays were repeated using commercial Au NPs with different sizes (2 nm, 20 nm and 100 nm) or stabilised in different media (PBS or citrate buffer). The ability of these different commercial Au NPs to affect the formation of NO and ROS in LPS-stimulated macrophages was compared to that of the citrate-stabilised Au NPs synthesised as part of this project, as well as auranofin. The latter was also included in these experiments as a positive control, as it was shown earlier in this chapter to attenuate LPS-induced formation of both NO and ROS.

4.6.1 Effects on Production of Nitric Oxide

The effects of treating RAW264.7 cells directly with the various types of commercial Au NPs on nitrite production are shown in **Figure 4.11**. Addition of LPS

showed once again that the cells were functioning as expected by producing significant amounts of NO_2^-. None of the different types of commercial Au NPs had a significant ability to stimulate production of NO_2^-, with the exception of the citrate-buffered Au NPs obtained from Sigma, which resulted in formation of approximately one third the amount of NO_2^- as that elicited by LPS. This was a surprising result as **Figure 4.1** showed that the citrate-stabilised Au NPs prepared for this project did not show this ability. One key reason for the observed difference is that the citrate-buffered Au NPs purchased from Sigma are stated to contain a proprietary surfactant as a stabiliser, which may affect their biological activity.

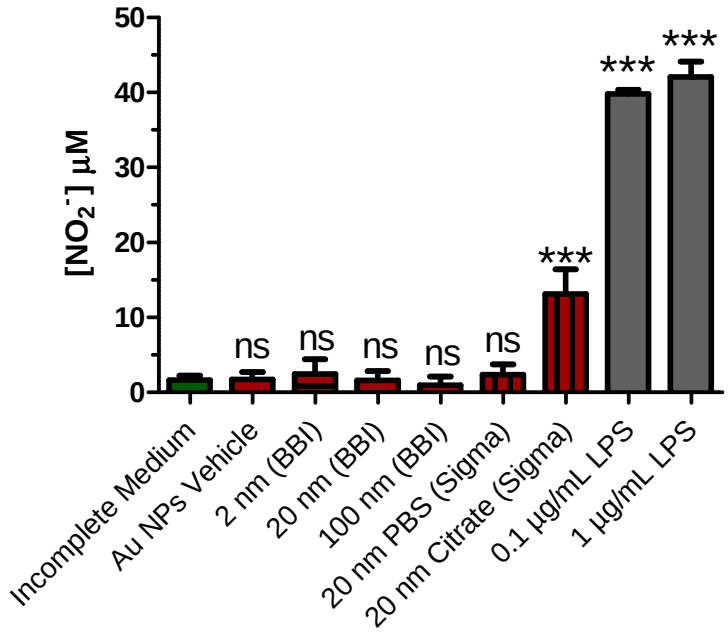

Figure 4.11: Effect of addition of commercial Au NPs on nitrite production by RAW264.7 macrophages. Cells were incubated with the Au NPs at 37 °C under an atmosphere of 5% CO_2 for 24 h, and nitrite concentration then measured by the Griess assay. All Au NP treatment solutions contained 40 µM gold, with the exception of the 2 nm (BBI) Au NPs, which contained 9 µM gold. The error bars represent one standard deviation calculated from triplicate plates. *** = statistically significant ($P < 0.001$) compared to corresponding vehicle; ns = not significant compared to corresponding vehicle ($P > 0.05$).

Figure 4.12 shows the effect on production of NO_2^- by LPS-stimulated RAW264.7 macrophages, of pre-incubation with various commercial Au NPs, as well as auranofin and the Au NPs prepared for this project. Treatment with 2.5 µM auranofin resulted in a significant decrease in NO_2^- production, as observed previously (**Figure**

4.2). However, none of the commercial Au NPs resulted in a statistically significant decrease in the amount of NO_2^- produced compared to that elicited by the Au NPs vehicle, although the 2 nm BBI Au NPs did produce a 20% reduction. This indicates that regardless of the size or the identity of the stabilising shell, all of the Au NPs were largely ineffectual in altering the amount of LPS-induced NO_2^- produced. This included, once again, the citrate-stabilised Au NPs prepared for this project. It should be noted that despite producing an increase in basal cellular NO_2^- production, the citrate-buffered Sigma Au NPs did not elicit a similar increase in NO_2^- with macrophages already stimulated with LPS. This suggests that the ability of LPS to increase nitrite production was more significant than that of these Au NPs.

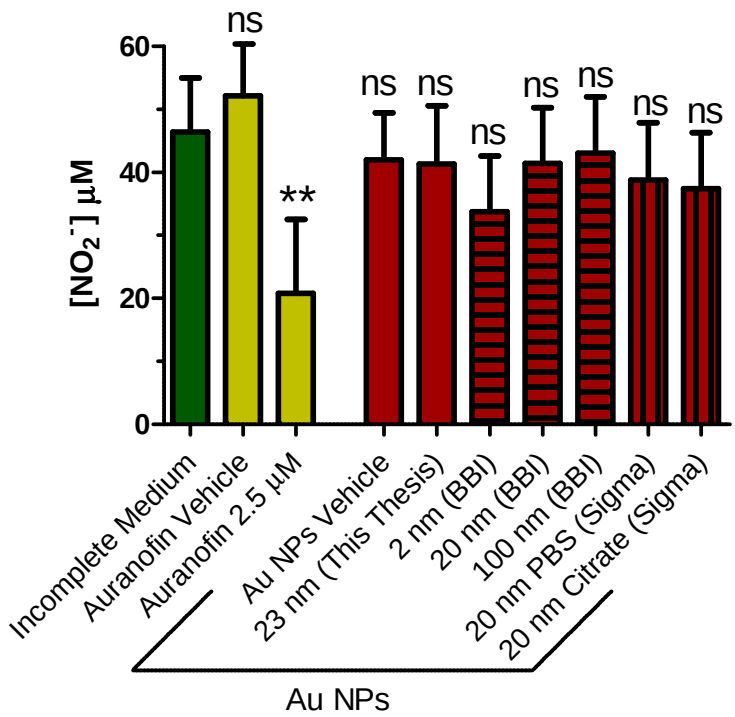

Figure 4.12: Effect of pre-incubation with commercial Au NPs on LPS-induced nitrite production by RAW264.7 macrophages. Cells were pre-incubated with auranofin or Au NPs at 37 °C and under an atmosphere of 5% CO_2 for 4 h, and then 0.1 µg/mL LPS added and incubation continued under the same conditions for a further 20 h. Nitrite concentration was measured by the Griess assay. All Au NP treatment solutions contained 40 µM gold, with the exception of 2 nm (BBI) Au NPs, which contained 9 µM gold, and the Au NP solutions produced as part of this thesis, which contained 60 µM gold. The error bars represent one standard deviation calculated from triplicate plates. ** = statistically significant (P < 0.01) compared to corresponding vehicle; ns = not significant compared to corresponding vehicle.

4.6.2 Effects on Production of Reactive Oxygen Species

After observing minimal effects of commercial Au NPs upon NO_2^- formation, it was of interest to see whether any of the nanoparticles would have an effect on ROS formation. **Figure 4.13** shows the effect of treating macrophages with commercial Au NPs upon ROS formation. Addition of LPS induced formation of large amounts of ROS, with no statistically significant difference between the amounts produced in response to the two treatment concentrations used. None of the commercial Au NP products induced formation of significant amount of ROS, including the citrate-buffered Au NPs obtained from Sigma, which were shown in the previous section to stimulate production of NO. This suggests that these Au NPs were stimulating formation of NO by a pathway specific to NO signalling.

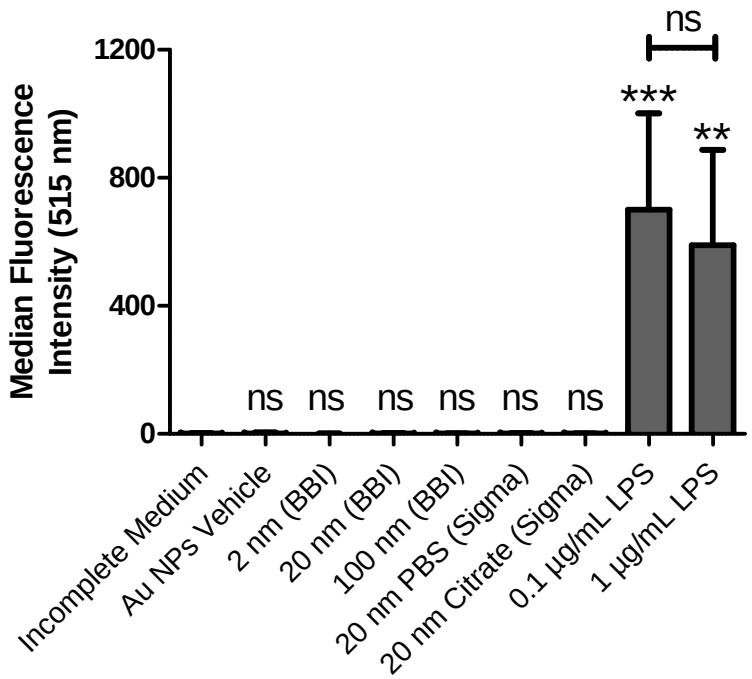

Figure 4.13: Effects of addition of commercial Au NPs on ROS production by RAW264.7 macrophages. Cells were incubated with the Au NPs at 37 °C under an atmosphere of 5% CO_2 for 24 h. ROS was measured by the DCF assay and presented as MFI at 515 nm. All Au NP treatment solutions contained 40 µM gold, with the exception of the 2 nm (BBI) Au NPs, which contained 9 µM gold. The error bars represent one standard deviation calculated from triplicate samples. ** = statistically significant (P < 0.01) compared to incomplete medium; *** = statistically significant (P < 0.001) compared to incomplete medium; ns = not significant compared to corresponding vehicle (P > 0.05).

The effects of the commercial Au NPs on ROS production in LPS-stimulated macrophages are shown in **Figure 4.14**. Treatment with 2.5 μM auranofin led to powerful inhibition of LPS-induced ROS formation, as observed previously (**Figure 4.6**). In contrast, none of the commercial Au NPs produced statistically significant changes in the amount of LPS-induced ROS formation, as was also the case for the Au NPs synthesised for this project. It is worth noting that addition of the citrate-buffered Au NPs obtained from Sigma, and the Au NPs synthesised for this project, had similar effects on the amount of ROS produced by the macrophages. In both cases the amount of ROS detected was higher than that observed when the Au NPs vehicle was used. However, in view of the variability inherent with experiments of this type, it was not possible to determine whether or not this was a real effect with certainty at this stage.

Overall, the results presented here, along with those in **Section 4.6.1** suggest that Au NPs do not have a significant effect on the production of either NO or ROS by macrophages. Addition of PBS-stabilised Au NPs caused no changes to either NO or ROS expression, both in macrophages that had been treated with LPS and those that had not. In contrast, treatment with the commercial citrate-stabilised Au NPs caused an increase in NO_2^- levels for macrophages that had not been treated with LPS. The 20 and 100 nm diameter BBI Au NPs also caused no changes to NO or ROS expression under any circumstances. However, the 2 nm BBI Au NPs resulted in a small decrease in LPS-induced NO production, suggesting that these smaller size nanoparticles may have been able to interact with the macrophages to a greater extent. This has been suggested by other studies, and is usually correlated with increases in other toxicity markers.[202,278]

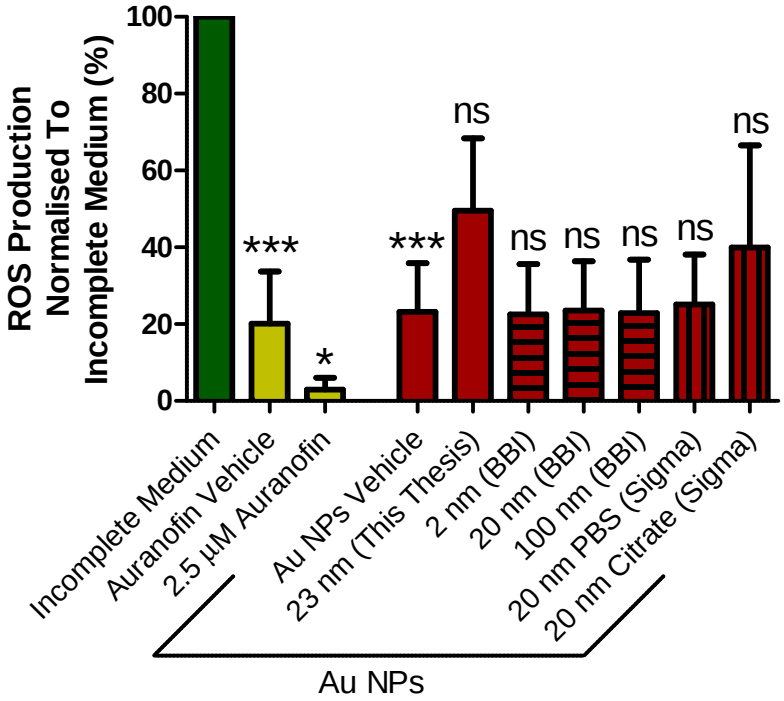

Figure 4.14: Effect of pre-incubation with auranofin or commercial Au NPs on LPS-induced ROS production by RAW264.7 macrophages. Cells were pre-incubated with auranofin or Au NPs at 37 °C under an atmosphere of 5% CO_2 for 4 h, and then 0.1 µg/mL LPS added and incubation continued under the same conditions for a further 20 h. ROS was measured by the DCF assay and presented as normalised MFI values at 515 nm, relative to incomplete medium. All Au NP treatment solutions contained 40 µM gold, with the exception of the 2 nm (BBI) Au NPs, which contained 9 µM gold and the Au NPs prepared for this thesis, which contained 60 µM gold. The error bars represent one standard deviation calculated from triplicate samples. * = statistically significant ($P < 0.05$) compared to corresponding vehicle; *** = statistically significant ($P < 0.001$) compared to corresponding vehicle; ns = not significant compared to corresponding vehicle ($P > 0.05$).

Chapter 5:

Mass Spectrometric Investigation of the Binding of Gold Complexes and Gold Nanoparticles to Thioredoxin Reductase

---

This chapter compares the results of binding studies involving either anti-arthritic gold(I) compounds or gold nanoparticles, and the redox enzyme thioredoxin reductase. These binding studies were initially performed using electrospray ionisation mass spectrometry and a mutant form of human thioredoxin reductase. The enzyme was obtained by transforming the corresponding mutant gene into the bacterium *Escherichia coli*, inducing overexpression of the protein, and subsequently purifying it using column chromatography. Additional experiments were performed using a commercial sample of wild type rat thioredoxin reductase. Selected results presented in this chapter were published in: James, L. R. A; et al., *J. Inorg. Biochem.*, **2015**, *142*, 28-38.

5.1 Introduction

Interest in studying the inhibition of the homodimeric redox enzyme thioredoxin reductase (TrxR) using gold compounds stems from research that demonstrated the potential of the thioredoxin system to serve as a drug target.[174,293] The thioredoxin system is essential for normal cellular function, however both Trx and TrxR are overexpressed in various types of cancer cells,[154–159] as well as synovial cells[160] and the synovial fluid[161] of patients with RA. The presence of an active site selenocysteine residue within the sequence of TrxR makes it an attractive target for compounds containing metals such as gold, which show higher levels of reactivity and binding selectivity for selenols compared to thiols.[162,186] Further interest in TrxR is due to its involvement in the redox activity of RAW264.7 macrophages.[294–296] Therefore, it was of interest to investigate the binding of gold(I) compounds used in the treatment of RA to this enzyme, as its inhibition might form part of their mechanism of action.

Whilst a number of studies have examined the inhibition of TrxR by various types of gold compounds, few have provided specific information about the gold/protein interaction, including how many of the original ligands bound to the metal complex are retained after binding. ESI mass spectra are well suited for providing this information, so solutions containing different ratios of gold compound or Au NPs, and TrxR were analysed in this work. As relatively large quantities of enzyme were required to perform these studies, it was decided to obtain the protein by over-expressing it in *E. coli*. Since expression of selenocysteine-containing proteins require species specific translation machinery, it is difficult to express mammalian selenoproteins in *E. coli*. Therefore, a plasmid containing a mutant form of human TrxR (hTrxR) was selected for transformation into *E. coli*. This mutant form of hTrxR had been previously used to investigate the binding of platinum compounds to TrxR,[169] and was kindly provided by

Yan-Chung Lo and Andrew Wang (Academia Sinica, Taiwan). The mutant plasmid had the selenocysteine codon replaced by that for cysteine, thereby enabling a form of the enzyme to be obtained whose active site largely retained its structure and function.[297]

5.2 Characterisation of Human Thioredoxin Reductase

After initial collection and chromatographic separation of hTrxR from the mixture of proteins produced by *E. coli*, the purity of the collected protein fractions was investigated using SDS-PAGE. **Figure 5.1** shows the image of an SDS-polyacrylamide gel containing purified hTrxR fractions, and a marker lane to indicate the approximate molecular mass of the contents of the collected fractions. The majority of fractions in the gel show one major component with a molecular mass between 50 and 60 kDa, along with a lower abundance component with a molecular mass of ~120 kDa. Calculation of the expected molecular mass of hTrxR from its protein sequence (**Appendix C.1.1**) gave a value of 56288.3 Da per monomer, after cleavage of the initiating methionine residue.[228] It was therefore concluded that the fractions in this gel most likely contain pure hTrxR, with the lower abundance band corresponding to dimeric hTrxR that did not separate under the denaturing conditions of SDS-PAGE. Lanes 22 and 23 in **Figure 5.1** also appear to contain a third band corresponding to protein molecules with a molecular mass between 60 and 80 kDa. Owing to their lower purity, these fractions and those collected after them were not used in any further experiments.

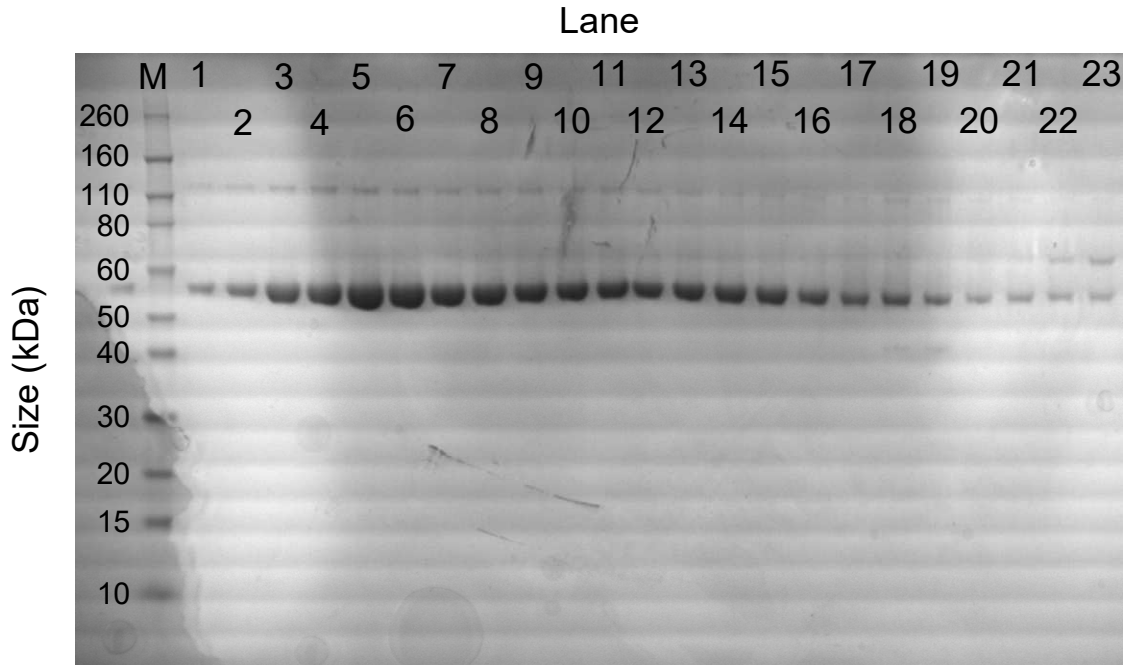

Figure 5.1: SDS-PAGE of human TrxR fractions after chromatographic purification. Each lane is numbered; M stands for the marker lane.

After confirming the purity of TrxR by SDS-PAGE, the protein was dialysed into solutions containing ammonium acetate for analysis by ESI-MS. **Figure 5.2** shows the spectra of hTrxR obtained under different conditions of pH and ammonium acetate concentration. The spectrum in **Figure 5.2 a)** was obtained using a solution of hTrxR in 100 mM ammonium acetate, 5% acetic acid, pH 3.7. It shows several distinct envelopes of peaks, with the most abundant being in the range *m/z* 2400 – 3800. Each peak corresponds to a different charge state of the protein, with some of the most prominent charge states labelled in the figure. Peaks with an $m/z \leq 3200$ are relatively narrow, and arise from the monomeric form of the protein. For example, the peak at *m/z* 2682 corresponds to $[TrxR + 23H]^{23+}$. The molecular mass of the protein determined from these peaks is 56305 Da, which is close to the calculated molecular mass of 56288.3 Da for one hTrxR monomer. This is good agreement given the errors associated with molecular mass determination under these conditions.[298]

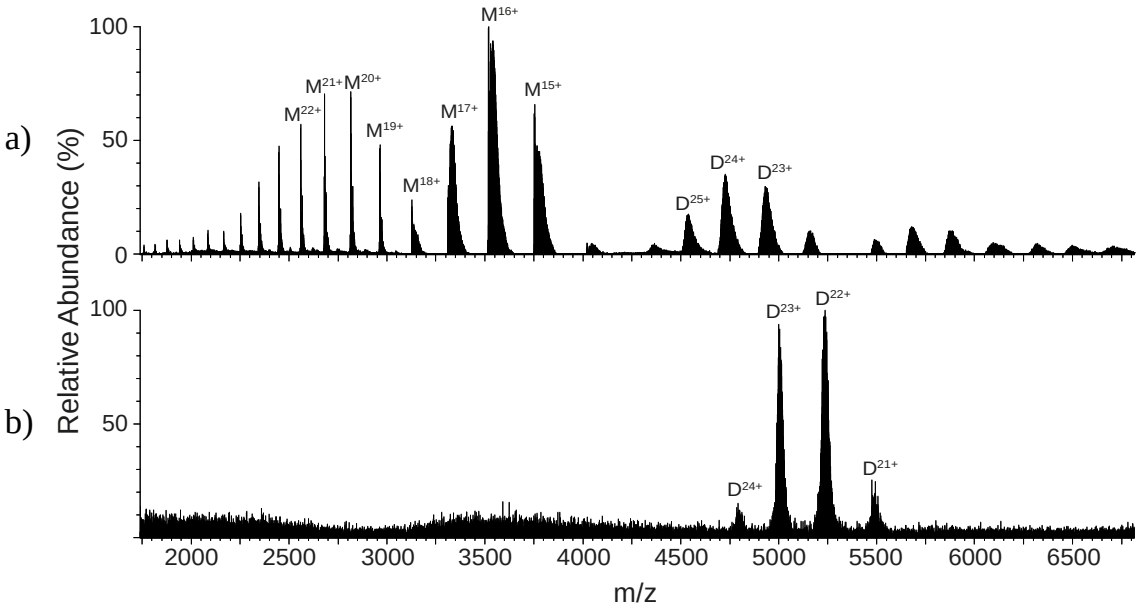

Figure 5.2: Positive ion electrospray ionisation mass spectra of 5 µM TrxR in: **a)** 100 mM ammonium acetate and 5% acetic acid, pH 3.7 and **b)** 500 mM ammonium acetate, pH 7.2. M corresponds to a charge state arising from monomeric protein, D corresponds to a charge state arising from dimeric protein.

The spectrum shown in **Figure 5.2 b)** was obtained using a solution of TrxR in 500 mM ammonium acetate, pH 7.2, and is very different to that presented in **Figure 5.2 a)**. It instead features a small number of relatively broad peaks in the range, *m/z* 4800 – 5600. These are attributable to the dimeric form of hTrxR, with a molecular mass of 114998 Da obtained from the spectrum. For example, the peak at ~*m/z* 4999 can be assigned to $[2\text{TrxR} + 23\text{H}]^{23+}$. The molecular mass of 114998 Da derived from the dimeric protein from **Figure 5.2 b)** is more than twice that of the monomer, but is still within experimental error of the expected value.

The above results show that solutions containing higher ammonium acetate concentrations favour formation of dimeric hTrxR, whilst those with lower ammonium acetate concentrations and acidic pH result in some dissociation to the monomer and unfolding of the protein. This is more than twice the mass for the monomer but is within the error expected. The broad peaks in **Figure 5.2 a)** and **b)** at *m/z* > 3000 are from protein (or dimer) molecules that are folded. Hence, water molecules and salts are

included in the protein. As the measured mass is determined from the centre of the peak, these included water or salt molecules result in a mass measurement that is greater than expected for the native protein.

Inspection of **Figure 5.2 a)** reveals the presence of separate envelopes of peaks arising from the monomeric and dimeric forms of TrxR. This suggests that separate populations of both types of protein molecules that were unfolded to varying extents were present in the solution.[298] The observation of relatively narrow peaks attributable to the monomeric form of the protein (width at half height ~2.5 Th) identified these conditions as being more suitable for binding studies involving metal complexes. This is because the difference in *m/z* for some charge states arising from free protein molecules and protein molecules with a single bound gold ion is ~10 Th. The broadness of peaks from the dimeric form of the enzyme made it difficult for separate peaks from free protein and metallated protein molecules to be resolved in preliminary experiments. Therefore, reactions of gold compounds and hTrxR were carried out in 100 mM ammonium acetate where the protein was folded and predominantly a dimer, but analysis by ESI-MS was carried out after acidification of the mixture. This dissociated the dimer and resulted in sharper peaks in the spectra that enabled greater peak resolution to be obtained.

Further attempts were made to optimise conditions towards a mass spectrum with sharper peaks. A range of conditions were tested, including dilution of the hTrxR to between 1 and 2 μM, as well as lowering the ammonium acetate concentration to between 10 and 30 mM. These conditions afforded the spectrum shown **Figure 5.3 a)**, which only contained ions attributable to the monomeric form of hTrxR. Transformation of the spectrum in **Figure 5.3 a)** from a *m/z* scale to one with a mass scale afforded the spectrum shown in **Figure 5.3 b)**. Three distinct peaks are present,

the most abundant of which is at 56304 Da, and is attributable to monomeric hTrxR. The second and third peaks at 56482 and 56562 Da correspond to hTrxR molecules with mass additions of ~178 and ~258 Da, respectively. The vertical red lines in the figure correspond to the calculated mass of hTrxR (56288 Da), as well as hTrxR + 178 (56466 Da) and hTrxR + 258 (56546 Da). The spectrum remained essentially unchanged when the protein was dialysed against 0.1% formic acid (**Appendix C.1.2, Figure C.1**), consistent with the two heavier hTrxR ions arising from covalently modified protein molecules, and not being attributable to contaminants bound electrostatically to the protein that survived the electrospray process.

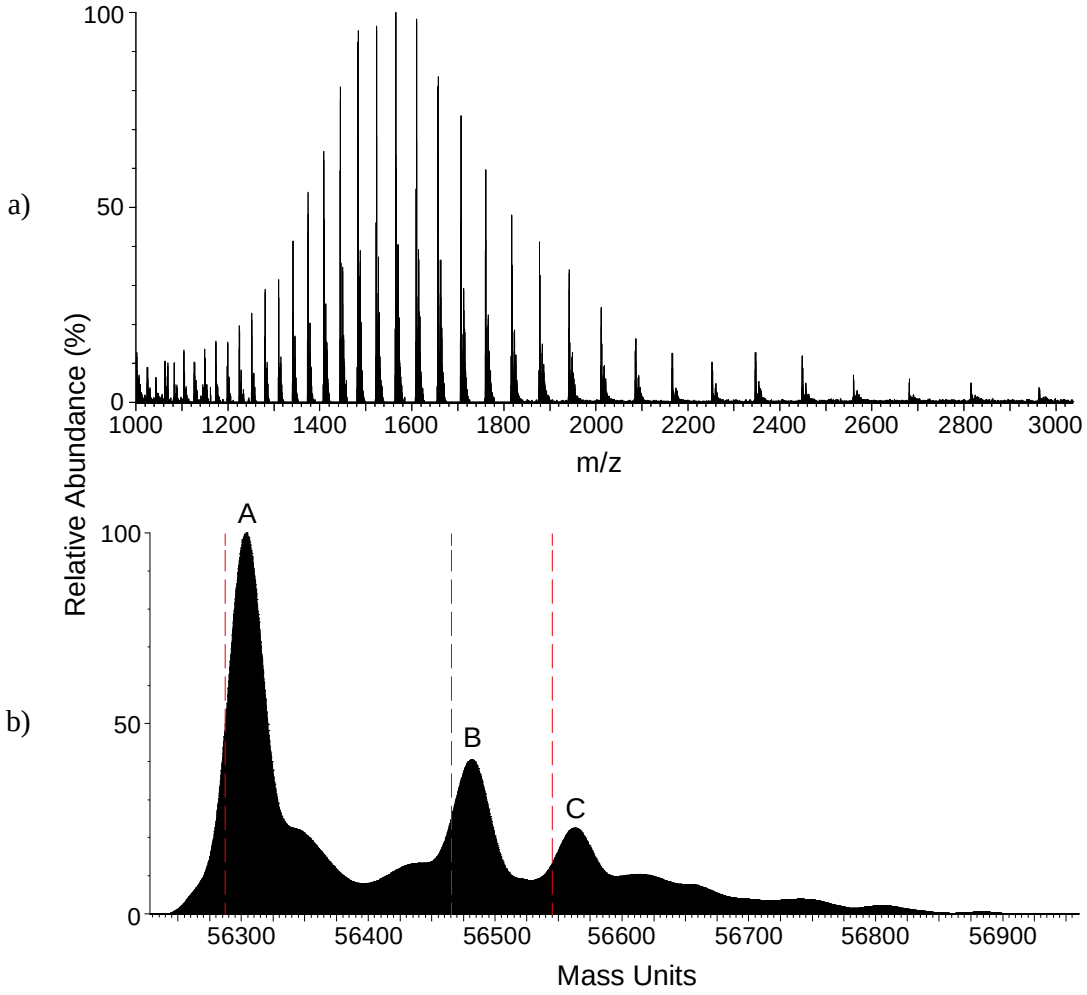

Figure 5.3: Positive ion electrospray ionisation mass spectra of 1.5 µM hTrxR in 23 mM ammonium acetate and 5% acetic acid. The data are represented in two different ways: **a)** raw spectrum and **b)** the spectrum after transformation to a mass scale. The red lines represent the expected masses of each peak, which are: A = 56288 mass units; B = 56466 mass units; C = 56546 mass units.

It was initially thought that the peak corresponding to hTrxR plus an additional 178 Da might be from protein molecules that had not been completely cleaved from the initiating N-formyl-methionine reside (residue mass 169 Da). However, the mass addition observed was slightly too large to be consistent with this explanation. Examination of the literature revealed that the two additional peaks were likely to be the result of a phosphogluconoylation reaction occurring at the amine group of the N-terminus.[299] Geoghegan *et al.* showed that addition of 6-phosphoglucono-1,5-lactone to the N-terminus of ~100 amino acid long fragments of human β-adrenergic receptor kinase, expressed in *E. coli*, resulted in formation of protein adducts that were heavier than the native protein by 258 Da. Furthermore, if the species were dephosphorylated by a cellular phosphatase then the masses of the adducted moieties decreased to 178 Da. The authors concluded that the presence of an engineered N-terminal hexa-histidyl tag activated the terminal amino group of the proteins to this particular transformation. This tag is commonly used when expressing recombinant proteins,[300] as it allows a very simple purification procedure to be employed in which the required protein is eluted through a column containing a divalent metal ion, typically nickel, cobalt or zinc.[300] The form of hTrxR expressed for this thesis contained an N-terminal hexa-histidyl tag, and as such it is likely the observed mass additions are due to the modifications described above.

To confirm that the two heavier ions were not a result of a contaminating protein or proteins with a similar size to hTrxR, a purified enzyme fraction was subjected to tryptic digestion to produce a range of peptide fragments, which were then analysed by gel electrophoresis followed by LC/MS to separate the various peptides.[*] The peptides detected by the mass spectrometer were compared to a protein database using the search

[*] Performed by Dr. Matt Padula (University of Technology, Sydney)

engine Mascot, and the proteins present subsequently identified. The results of this analysis (**Appendix C.1.3, Figure C.2**) showed that only peptides belonging to the cytoplasmic isoform of human thioredoxin reductase were present in the sample.

Having confirmed that the only protein present in the purified hTrxR fractions was hTrxR, it is highly likely that the higher mass species in **Figure 5.3** were the result of phosphogluconoylation. As such, hTrxR containing the gluconoyl group was termed G-hTrxR, and hTrxR containing the phosphogluconoyl group was termed PG-hTrxR. A mechanism for the addition of these groups is depicted in **Figure 5.4**. Owing to the difficulty associated with trying to separate three very similar forms of the same enzyme, or removing the gluconoyl group, the protein fractions were used without any further purification for gold binding studies.

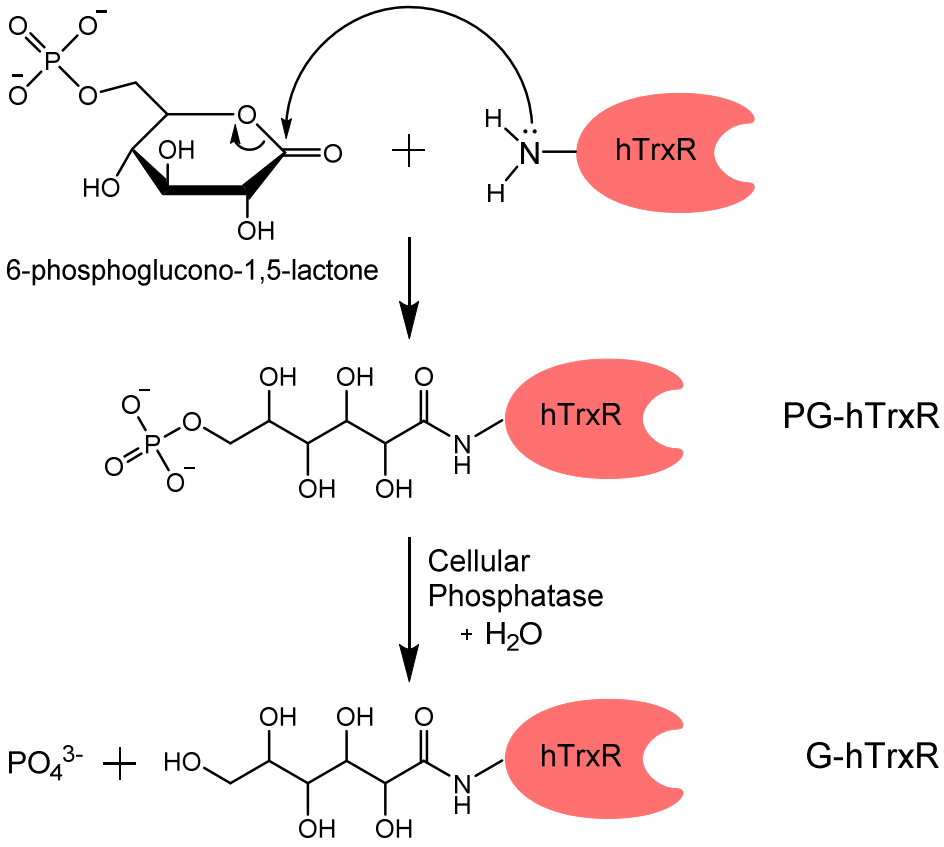

Figure 5.4: Schematic illustration of N-terminal addition of 6-phosphoglucono-1,5-lactone to hTrxR. Adapted from Analytical Biochemistry, 1999, vol. 267 (1), p. 169-184 with permission from Elsevier.[299]

5.3 Gold-Binding Experiments

The results of binding studies performed using ESI-MS, and solutions containing different gold compounds or gold nanoparticles and hTrxR are presented in this section. All spectra shown here were transformed to a mass scale to facilitate identification of protein adducts. The reactions were performed by mixing the required quantities of stock metal and protein solutions in ammonium acetate solution, and allowing the mixtures to stand on ice for approximately 4 h, thereby allowing sufficient time for reaction to occur. The reactions were performed under conditions where the protein was predominantly in its dimeric form. Acetic acid was then added to the solutions immediately prior to obtaining ESI mass spectra, to ensure the proteins were positively charged, and that peaks in the spectra were relatively sharp and well resolved. Initial experiments were performed using solutions containing different ratios of aurothiomalate and hTrxrR. The ESI mass spectra of these solutions are presented in **Figure 5.5**.

The spectrum in **Figure 5.5 a)** shows hTrxR only, with peak A assigned to monomeric hTrxR, peak B assigned to hTrxR containing a gluconoyl group (G-hTrxR), and peak C to hTrxR containing a phosphogluconoyl group (PG-hTrxR). **Figure 5.5 b)** shows the spectrum of a solution containing a 1:1 ratio of aurothiomalate : hTrxrR. Whilst some new peaks were observed, that arising from hTrxR remained the dominant feature. Peak B, which was assigned to G-hTrxR was now broader, most likely as a result of overlap of ions from G-hTrxR with those from hTrxR + Au, where a gold ion had become bound to the native protein. As these two species are close in molecular mass (hTrxR plus 178 or 197), and the resolution of the mass spectrometer under these conditions was insufficient to resolve these ions, a single broadened peak was observed.

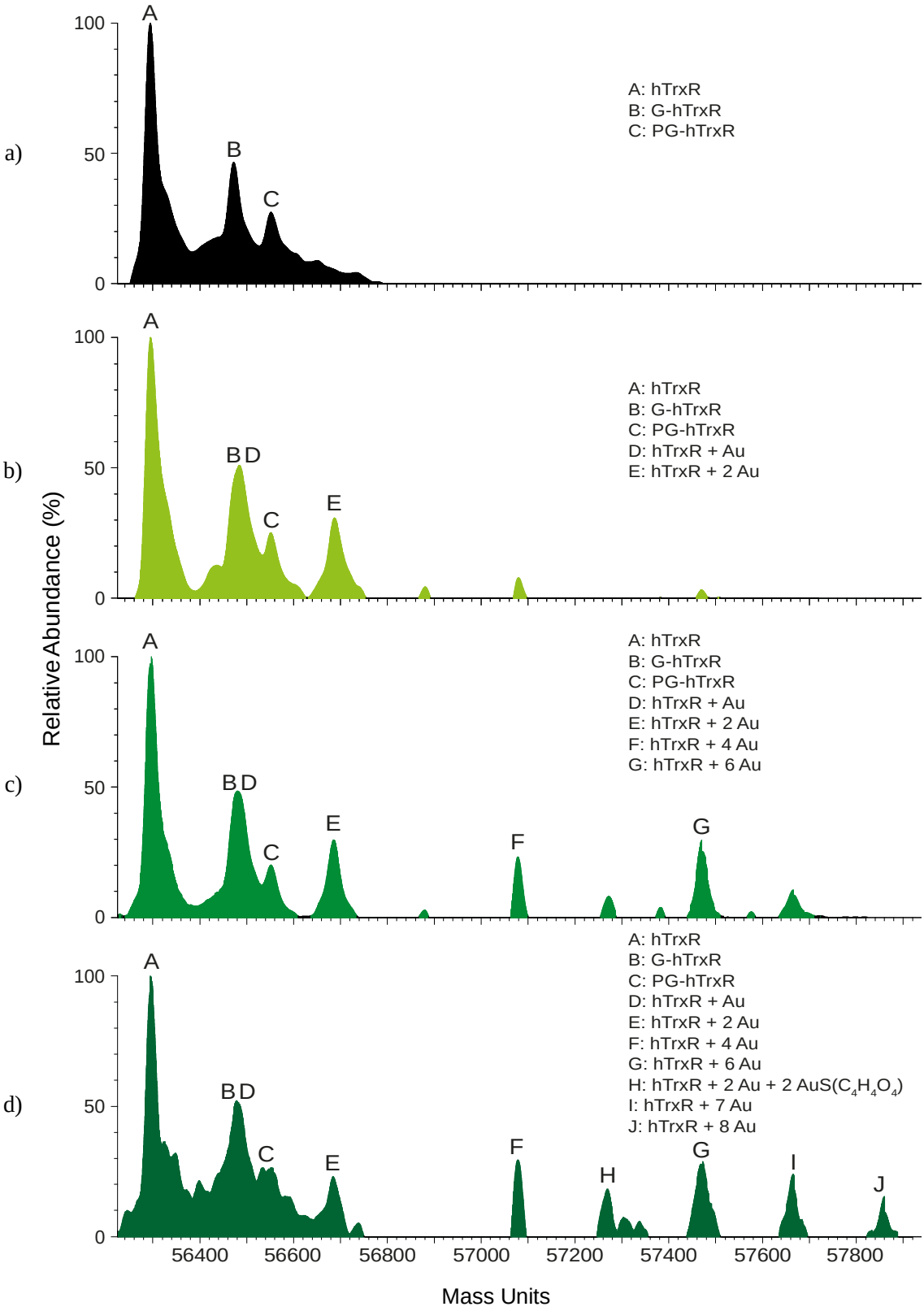

Figure 5.5: Positive ion ESI mass spectra of solutions containing different ratios of aurothiomalate and hTrxR, after transformation to a mass scale. **a)** gold : hTrxR = 0:1; **b)** gold : hTrxR = 1:1; **c)** gold : hTrxR = 3:1; and **d)** gold : hTrxR = 5:1. In each case, solutions containing aurothiomalate and hTrxR were allowed to react for 4 h on ice before the spectrum was obtained. For ESI-MS, each sample contained 1.1 µM hTrxR in 5% acetic acid and 26 mM ammonium acetate.

This peak has therefore also been labelled with D, to signify the presence of ions from hTrxR + Au. Another new peak in **Figure 5.5 b)** is that at 56686 Da (peak E), which has been assigned to hTrxR molecules with two bound Au^+ ions.

The ESI mass spectra of solutions containing 3:1 and 5:1 ratios of aurothiomalate : hTrxR (**Figure 5.5 c** and **d**, respectively) again showed peaks from all three forms of the protein, as well as hTrxR + Au, with similar relative abundances to those in **Figure 5.5 b)**. However, several new peaks were now present that corresponded to protein complexes containing up to eight bound Au^+ ions. Only in one instance did any of these peaks correspond to protein adducts containing thiomalate moieties along with gold ions (peak H in **Figure 5.5 d**). This suggests that the binding of gold to the protein is typically accompanied by the loss of the original ligands bound to the metal complex and/or the gold-aurothiomalate bond is readily broken under the mass spectrometry conditions used. The spectrum of the solution containing a 5:1 ratio of aurothiomalate : hTrxR was noisier than any of the other spectra, particularly in the region between 56300 and 56700 Da. This is most likely due to the formation of protein adducts containing variable numbers of sodium ions, owing to the presence of a large excess of sodium aurothiomalate in solution. The presence of sodium ions has been noted previously to result in poorer quality ESI mass spectra of protein samples.[301] **Figure 5.5 d)** shows that despite the large excess of gold complex present, peaks from free protein remained the most abundant. This observation, along with that of peaks of low to medium abundance from protein adducts containing up to eight bound gold ions, suggests that the protein contains numerous low affinity binding sites for this metal ion.

The above result is consistent with a previous MALDI-MS study that showed between five to ten moieties of gold(I) and gold(III) compounds can bind to mammalian TrxR.[187] Some of the most likely positions for gold binding are the two cysteine

residues present at each of the N-terminal and C-terminal active sites. There are also an additional ten cysteine residues within the protein sequence (**Appendix C.1.1**), although many of these are likely to be present as disulfide bonds maintaining the protein's tertiary structure, and as such, are inaccessible for gold binding. Some lower affinity binding sites may be histidine residues, as it has been previously shown by ESI-MS that gold may weakly interact with this amino acid.[88] hTrxR has a total of nine histidine residues, with the mutant form used in these investigations having an additional six added to facilitate purification. As such, a significant number of high and low affinity sites are available for gold binding.

It should be noted that none of the spectra in **Figure 5.5** provide evidence concerning the location of the gold binding sites on the protein. Additional experiments, involving the use of reagents that effectively block specific amino acids from binding to metallodrugs, or proteomics techniques, would be required to provide that information for the gold/protein adducts observed in **Figure 5.5**, as well as all other figures presenting mass spectral binding data shown later in this chapter. These experiments were not performed owing to time limitations.

ESI mass spectra of solutions containing different ratios of aurothioglucose and hTrxR are shown in **Figure 5.6**. The spectrum of a solution containing a 1:1 ratio of aurothioglucose : hTrxR (**Figure 5.6 b**) is very similar to that of a solution containing the protein only (**Figure 5.6 a**). However, some broadening and increase in abundance of peak B was observed, consistent with formation of protein complexes with one Au^+ ion bound. In addition, **Figure 5.6 b)** shows a peak with low abundance assigned to protein molecules with two Au^+ ions bound (peak E). Increasing the ratio of aurothioglucose : hTrxR to 3:1 (**Figure 5.6 c**) resulted in an increase in abundance of

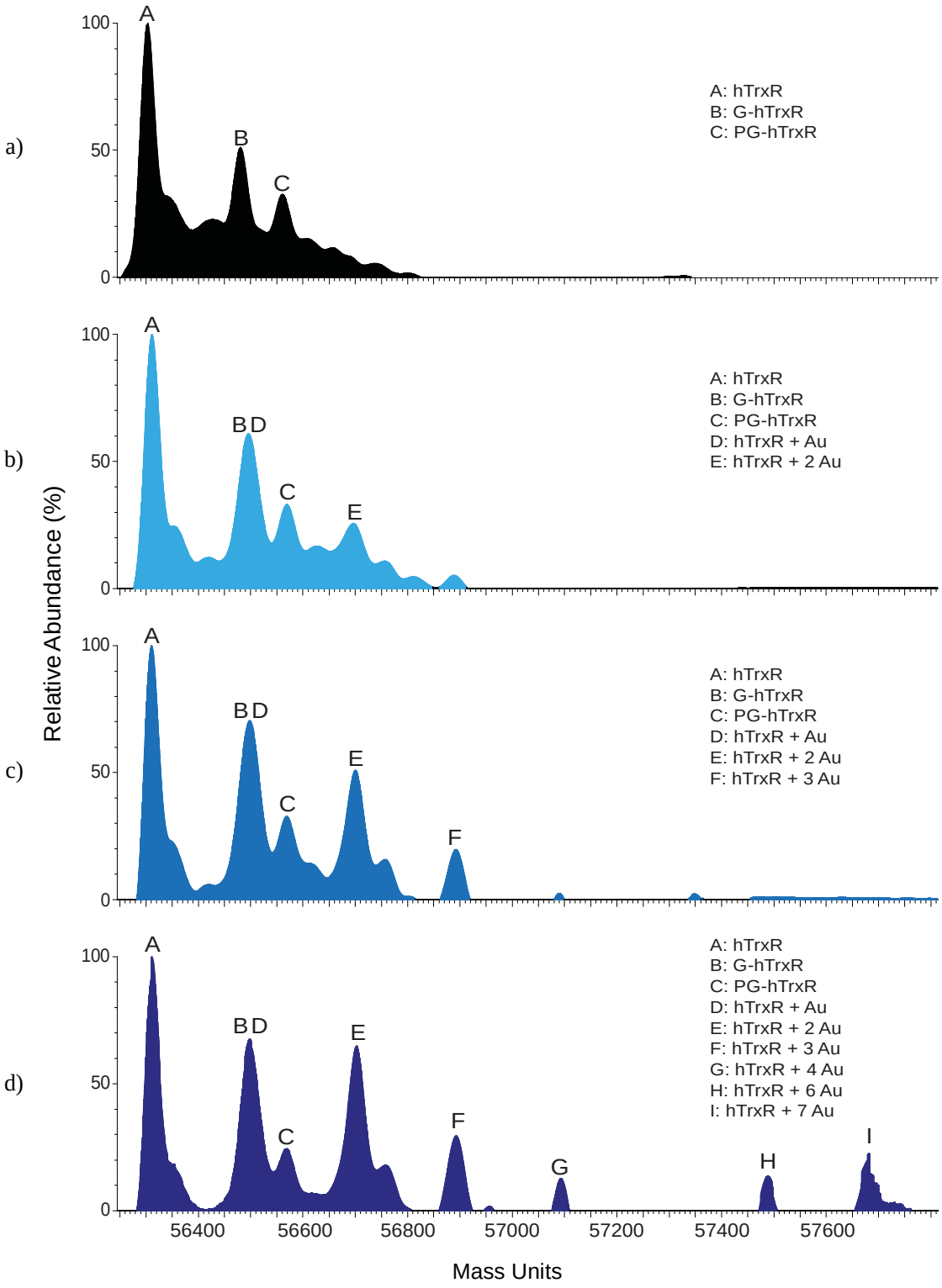

Figure 5.6: Positive ion ESI mass spectra of solutions containing different ratios of aurothioglucose and hTrxR, after transformation to a mass scale. **a)** gold : hTrxR = 0:1; **b)** gold : hTrxR = 1:1; **c)** gold : hTrxR = 3:1; and **d)** gold : hTrxR = 5:1. In each case, solutions containing aurothioglucose and hTrxR were allowed to react for 4 h on ice before the spectrum was obtained. For ESI-MS, each sample contained 1.1 µM hTrxR in 5% acetic acid and 20 mM ammonium acetate.

the latter peak, as well as a new peak from protein adducts in which hTrxR is bound to three Au^+ ions (peak F). When the ratio of gold complex : protein was increased to 5:1, the resulting spectrum (**Figure 5.6 d**) showed a number of additional peaks with low (< 20%) relative abundance, corresponding to hTrxR molecules with four, six and seven Au^+ ions bound. The peaks corresponding to protein molecules with one and two Au^+ ions bound increased in abundance again, but free hTrxR remained the most abundant component of the spectrum.

Making definitive assignments for some of the peaks in **Figure 5.6** was difficult, owing to the similar molecular weights of thioglucose (195) and a single gold atom (197). For example, peak E in **Figure 5.6 c)** (56700 Da) could be assigned to hTrxR molecules with two bare gold atoms bound, protein molecules containing a single aurothioglucose moiety, or a mixture of both types of adducts. In contrast, the spectra of solutions containing different ratios of aurothiomalate and hTrxR (**Figure 5.5**) contained many peaks that could be unambiguously assigned to protein adducts containing different numbers of bound gold atoms only. Since the bonds between gold and sulfur in aurothiomalate and aurothioglucose would be expected to be similar in strength, it is reasonable to expect that coordination of aurothioglucose to TrxR would also occur concomitantly with cleavage of Au–S bonds, and displacement of the original ligands bound to the metal ion.

The results of mass spectrometric experiments performed using solutions containing aurothiosulfate and hTrxR are shown in **Figure 5.7**. The spectrum of a solution containing a 1:1 ratio of aurothiosulfate : hTrxR (**Figure 5.7 b**) shows that the abundance of peak B had increased significantly, compared to what was observed in the spectrum of hTrxR alone (**Figure 5.7 a**). This was most likely due to a greater proportion of the protein binding to a single Au^+ ion, than what was observed in spectra

of the corresponding solutions containing a 1:1 ratio of either aurothioglucose or aurothiomalate, and hTrxR, presented earlier in this chapter. The observation of peaks in **Figure 5.7 b)** from protein molecules with two and three Au^{+} ions bound provides further support for the hypothesis that aurothiosulfate more effectively transfers gold ions to hTrxR than both aurothioglucose and aurothiomalate.

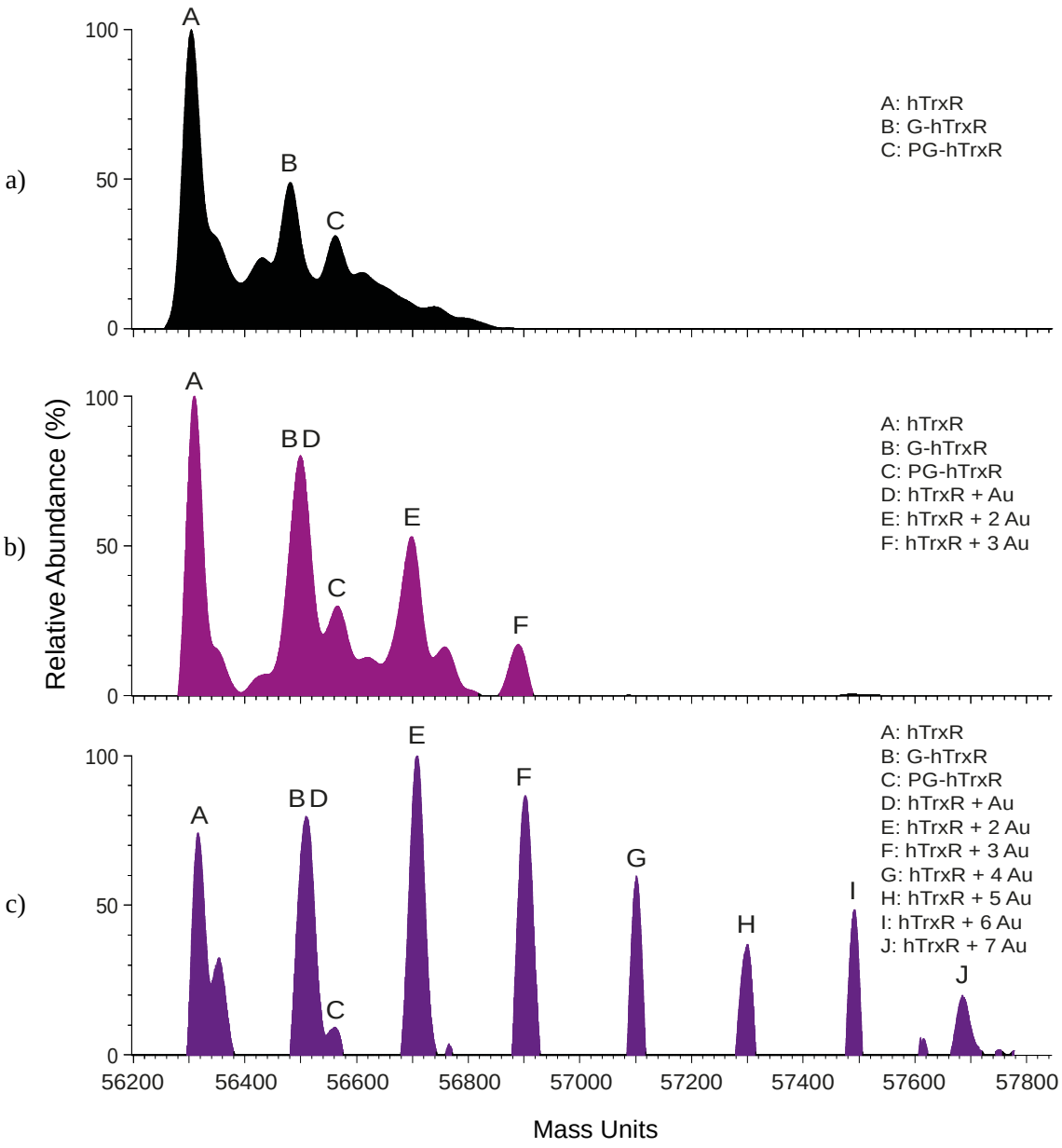

Figure 5.7: Positive ion ESI mass spectra of solutions containing different ratios of aurothiosulfate and hTrxR, after transformation to a mass scale. **a)** gold : hTrxR = 0:1; **b)** gold : hTrxR = 1:1; and **c)** gold : hTrxR = 3:1. In each case, solutions containing aurothiosulfate and hTrxR were allowed to react for 4 h on ice before the spectrum was obtained. For ESI-MS, each sample contained 1.1 µM hTrxR in 5% acetic acid and 20 mM ammonium acetate.

When the ratio of aurothiosulfate : hTrxR was increased to 3:1, the spectrum obtained (**Figure 5.7 c**) showed a number of substantial differences compared to that in **Figure 5.7 b)**. To begin with, the peak assigned to free hTrxR was no longer the most abundant in the spectrum, with peaks from both hTrxR + 2 Au and hTrxR + 3 Au of markedly greater abundance. In addition, peaks of low to medium abundance corresponding to complexes of hTrxR with four to seven Au^+ ions bound were also observed.

When aurothiosulfate was reacted with hTrxR in a 5:1 ratio, a dramatic shift in the position of the entire envelope of ions in the conventional mass spectrum (i.e. before transformation to a mass scale) was observed, as shown in **Figure 5.8**. For both the spectrum of the solution containing only the protein, and that of the solution containing a 3:1 ratio of aurothiosulfate : hTrxR (**Figure 5.8 a** and **b**, respectively), peaks of high abundance (i.e relative abundance > 70%) were found between *m/z* 1300 – 1500. In contrast, the most abundant peaks in the spectrum of a solution containing a 5:1 ratio of aurothiosulfate : hTrxR (**Figure 5.8 c**) were found between *m/z* 1700 and 1850. This shift to higher *m/z* was observed repeatedly for different solutions containing a 5:1 ratio of aurothiosulfate : hTrxR. In addition, these spectra featured a lower signal-to-noise ratio than spectra containing lower ratios of aurothiosulfate : hTrxR, most likely due to the higher concentration of Na^+ ions in solution from having dissolved greater quantities of sodium aurothiosulfate. Owing to these factors, it was not possible to accurately transform the spectrum to a mass scale.

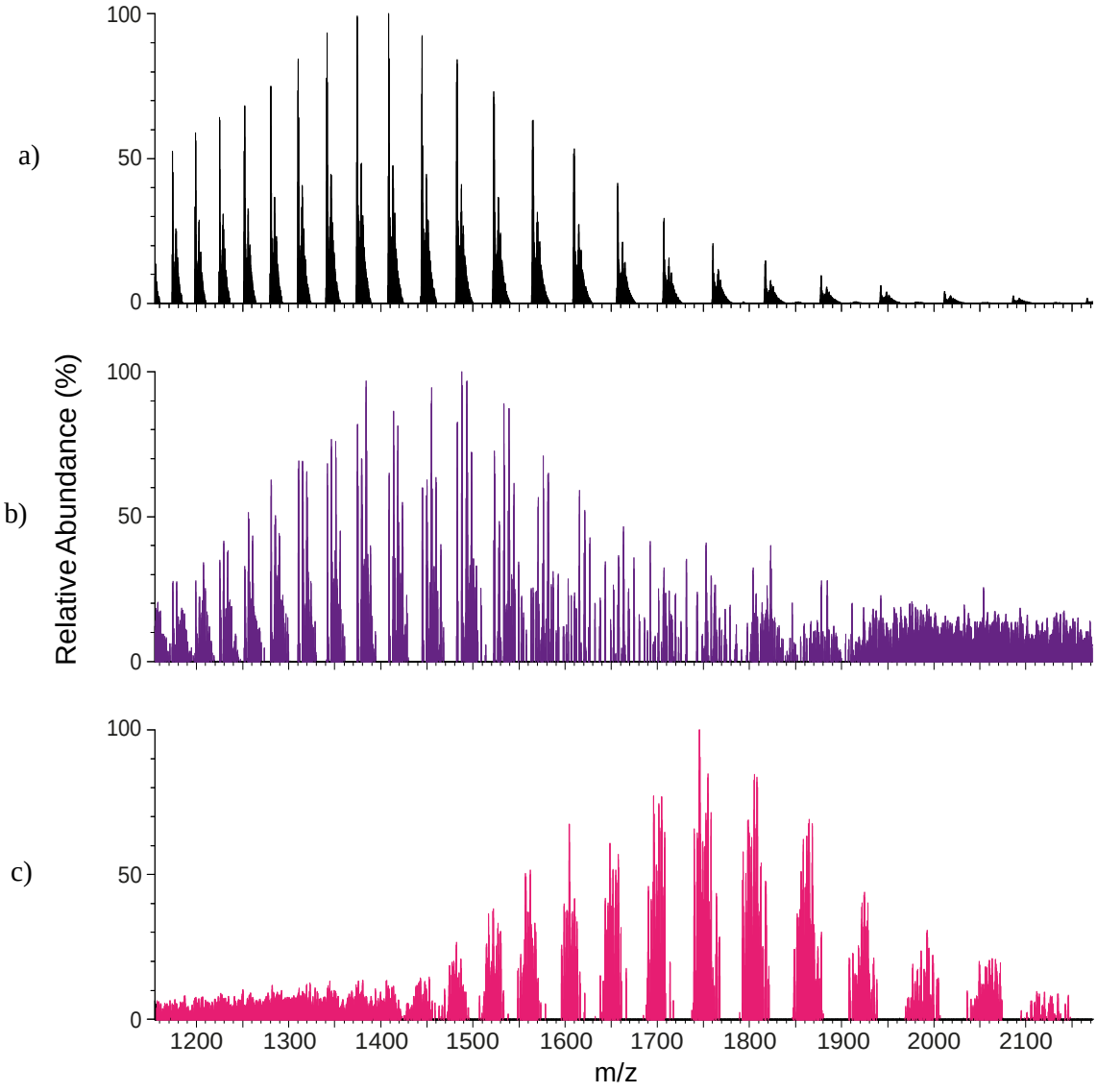

Figure 5.8: Raw positive ion ESI mass spectra of solutions containing different ratios of aurothiosulfate and hTrxR. **a)** gold : hTrxR = 0:1; **b)** gold : hTrxR = 3:1; and **c)** gold : hTrxR = 5:1. In each case, solutions containing aurothiosulfate and hTrxR were allowed to react for 4 h on ice before the spectrum was obtained. For ESI-MS, each sample contained 1.1 µM hTrxR in 5% acetic acid and 20 mM ammonium acetate.

It is worth noting that the majority of the ions in **Figure 5.7 b) and c)** correspond to protein molecules with one or more bound gold ions that did not retain any of their original thiosulfate ligands. This again suggests that binding of the gold complexes to hTrxR occurs concomitantly with ligand displacement. The observation of peaks corresponding to hTrxR with up to seven gold ions bound in the spectrum of a solution containing just a 3:1 ratio of aurothiosulfate : hTrxR, strongly suggests that it

contains many as yet unidentified amino acid side chains capable of binding to aurothiosulfate.

Figure 5.9 shows the ESI mass spectra of solutions containing the chrysotherapy metabolite $[Au(CN)_2]^-$, and hTrxR. Examination of the spectrum of the solution containing a 1:1 ratio of $[Au(CN)_2]^-$ to hTrxR (**Figure 5.9 b**), reveals that unlike the other gold(I) compounds discussed earlier in this chapter, addition of $[Au(CN)_2]^-$ resulted in very little change to the spectrum of the protein. Similarly, the only notable difference in the spectrum of the solution containing a 3:1 ratio of $[Au(CN)_2]^-$: hTrxR (**Figure 5.9 c**) was some broadening of peak B, which is again attributable to the presence of hTrxR molecules with one Au^+ ion bound. However, the spectrum of the solution containing a 5:1 ratio of $[Au(CN)_2]^-$: hTrxR (**Figure 5.9 d**), showed more substantial changes. Three new peaks were observed, with one (labelled E) corresponding to the protein with one Au(CN) moiety bound, appearing as a shoulder on the high mass side of peak D. The other two types of peaks were of low relative abundance (~20% relative abundance), and were assigned to G-hTrxR with either one Au^+ ion, or one Au(CN) moiety bound (peaks F and G, respectively). The reason for the lower amount of gold binding observed here is likely related to the very high affinity of the cyanide ligands in $[Au(CN)_2]^-$ for the metal ion.[57,90] Since the Au-CN bonds do not undergo ligand exchange reactions as readily as the Au-S bonds in the three gold complexes discussed previously in this chapter, it is far less likely for $[Au(CN)_2]^-$ to bond to the cysteine residues in hTrxR. It is also worth noting that **Figure 5.9 d**) suggests that a significant proportion of the gold bound to the protein has retained one of its two original cyanide ligands. This is also likely to be a consequence of the greater stability of Au-CN linkages compared to Au-S bonds, which also enables the former to survive the ionisation conditions present in the mass spectrometer source.

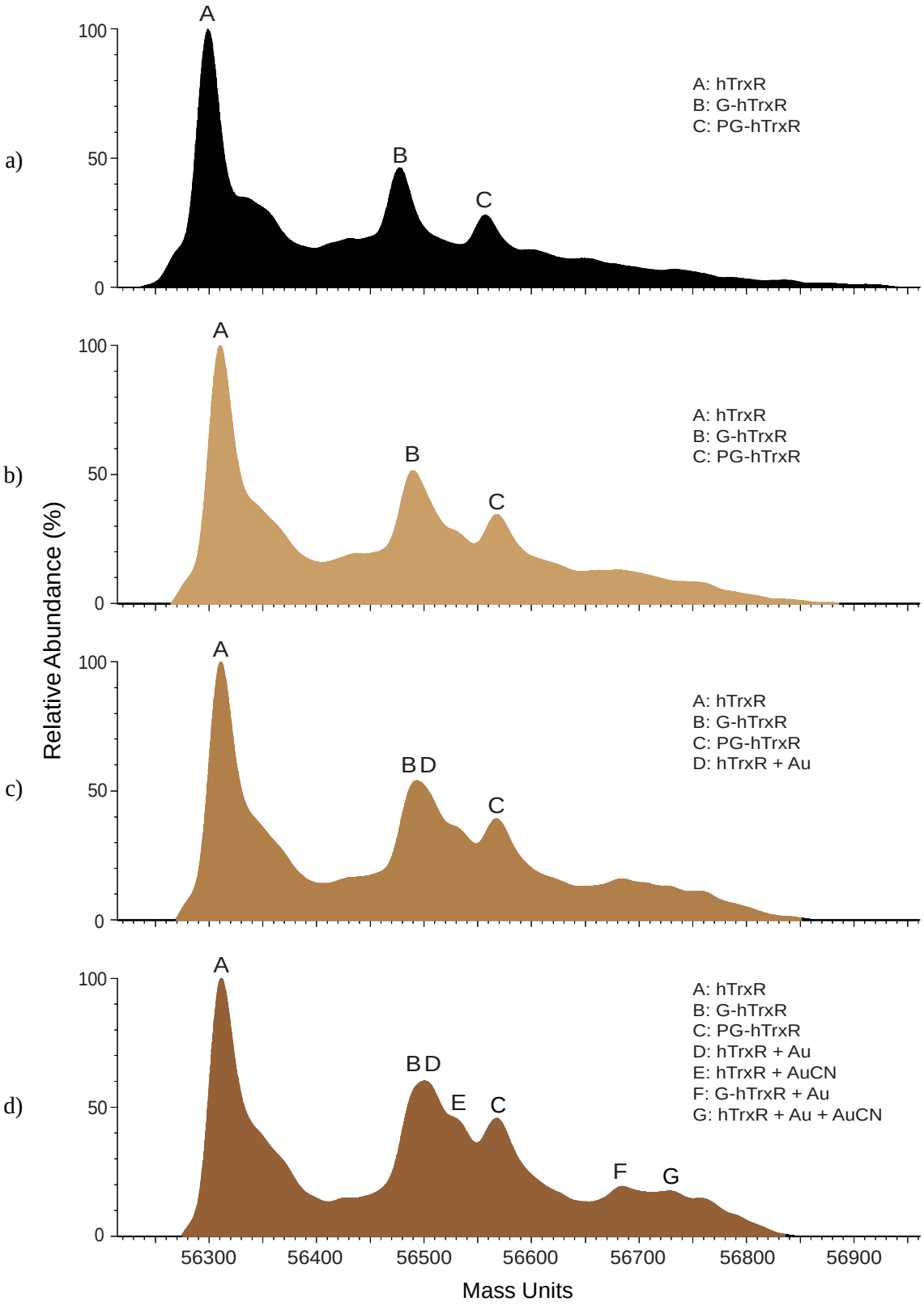

Figure 5.9: Positive ion ESI mass spectra of solutions containing different ratios of $[Au(CN)_2]^-$ and hTrxR, after transformation to a mass scale. **a)** gold : hTrxR = 0:1; **b)** gold : hTrxR = 1:1; **c)** gold : hTrxR = 3:1; and **d)** gold : hTrxR = 5:1. In each case, solutions containing $[Au(CN)_2]^-$ and hTrxR were allowed to react for 4 h on ice before the spectrum was obtained. For ESI-MS, each sample contained 1.1 µM hTrxR in 5% acetic acid and 10 mM ammonium acetate.

Figure 5.10 shows the mass spectra of solutions containing various ratios of auranofin and hTrxR. In the spectrum of the solution containing a 1:1 ratio of auranofin : hTrxR (**Figure 5.10 b**), there is some evidence of broadening of peak B compared to the spectrum shown in **Figure 5.10 a)**. This suggests that some of the protein molecules are now bound to a single Au^+ ion. More convincing evidence of this is provided by the presence of peak E, attributable to ions from hTrxR with one $AuPEt_3$ moiety bound. Increasing the ratio of auranofin to hTrxR to 3:1 gave the spectrum shown in **Figure 5.10 c)**. This shows that the relative abundance of hTrxR + $AuPEt_3$ had increased markedly. In addition, peaks from several other new types of protein adducts were observed, including hTrxR + Au + $AuPEt_3$ and hTrxR + 2 $AuPEt_3$. The spectrum of a solution containing a 5:1 ratio of auranofin to TrxR (**Figure 5.10 d**) showed evidence of further complexation of the protein by Au^+ ions and $AuPEt_3$ moieties, with the peak corresponding to hTrxR + $AuPEt_3$ now the most abundant (peak E). In addition, the peak assigned to hTrxR + Au + 2 $AuPEt_3$ (peak J) was now of substantial abundance. The total number of gold ions or Au-ligand moieties derived from auranofin that became bound to hTrxR was not as great as was previously observed in reactions with aurothiomalate, aurothioglucose or aurothiosulfate. This suggests that there may not be as many binding sites on the protein accessible to auranofin as there are for the other three gold complexes. Despite this, the relative abundance of the peak corresponding to free hTrxR in **Figure 5.10 d**) was lower than in the corresponding spectra of solutions containing a 5:1 ratio of aurothiomalate, aurothioglucose or $[Au(CN)_2]^-$, and hTrxR. This suggests that the smaller number of auranofin binding sites on the protein exhibit a higher affinity towards this gold complex.

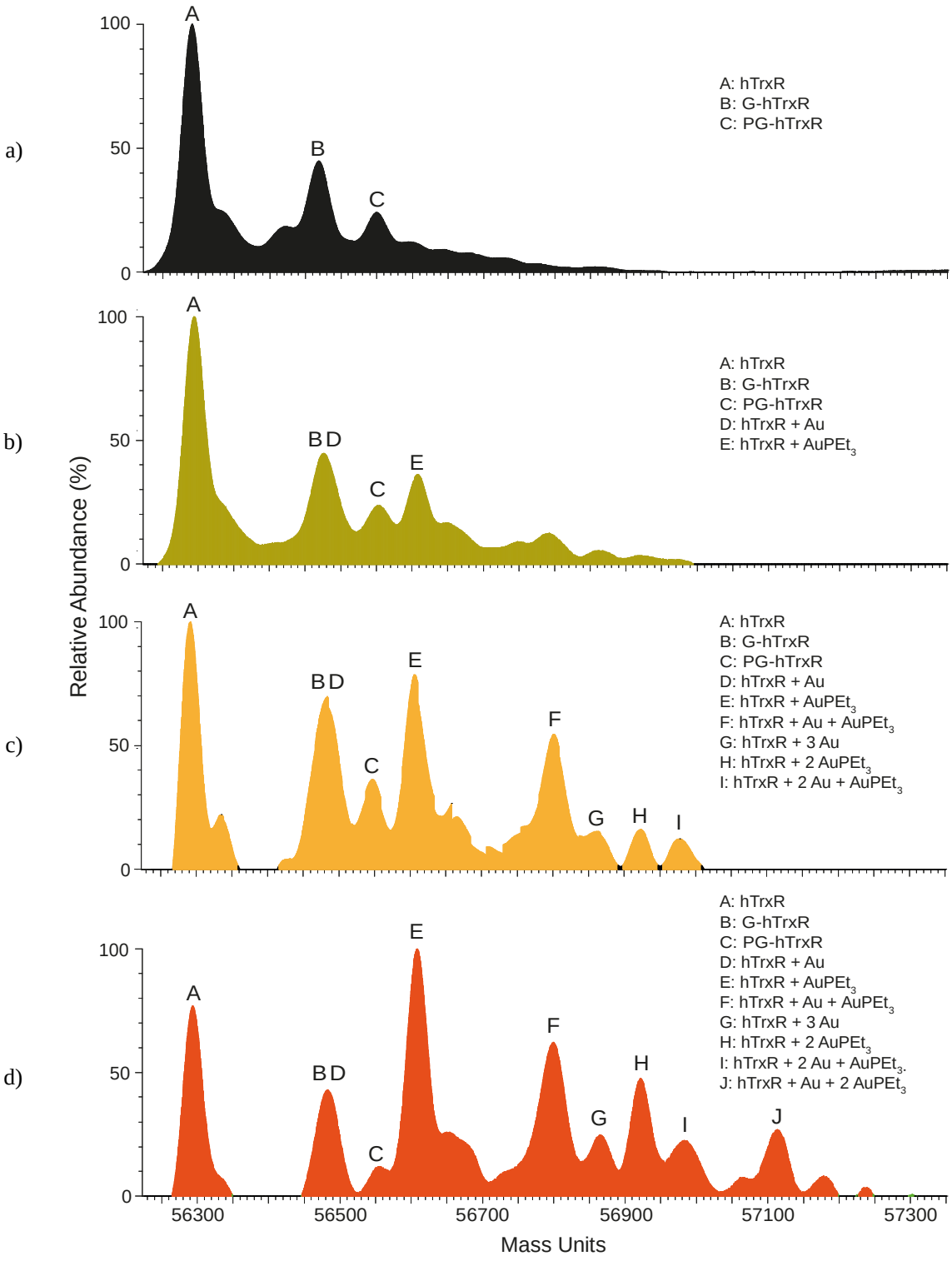

Figure 5.10: Positive ion ESI mass spectra of solutions containing different ratios of auranofin and hTrxR, after transformation to a mass scale. **a)** gold : hTrxR = 0:1; **b)** gold : hTrxR = 1:1; **c)** gold : hTrxR = 3:1; and **d)** gold : hTrxR = 5:1. In each case, solutions containing auranofin and hTrxR were allowed to react for 4 h on ice before the spectrum was obtained. For ESI-MS, each sample contained 1.3 µM hTrxR in 5% acetic acid and 20 mM ammonium acetate.

The results presented in **Figure 5.10** highlight the strength of the Au-P bond in auranofin, an observation that is supported by other studies involving this gold complex.[74,109] For example, previous ESI-MS investigations into the interactions of human serum albumin (HSA) with $AuPEt_3Cl$, a model complex for auranofin, showed that each of the protein adducts observed consisted of HSA molecules bound to one or more $AuPEt_3$ moieties.[88] In the case of reactions between auranofin and hTrxR, the most abundant ions observed in the ESI mass spectra were those attributable to protein molecules with at least one or two $AuPEt_3$ moieties bound. In contrast, ions from protein adducts containing only Au^+ ions were of low abundance. The results obtained here are also consistent with those derived from investigations into the binding of auranofin to serum albumin, performed using ^{1}HNMR spectroscopy,[87] ^{31}P NMR spectroscopy[82] and EXAFS.[82] Each of these studies also provided evidence for the binding of $AuPEt_3$ moieties to the protein.

All of the gold(I) compounds studied showed similar binding behaviour towards hTrxR. Each reacted with the protein to form a mixture of different adducts, with some hTrxR molecules binding to multiple Au^+ ions or gold/ligand fragments, or a mixture of both. There were, however, differences in the extent to which the compounds interacted with the protein that could be related to differences in the lability of the metal-ligand bonds in the initial complex. For example, the dicyanoaurate ion interacted to a limited extent with hTrxR owing to the strength of the Au-CN bonds. In contrast, the polymeric compounds aurothiomalate and aurothioglucose showed more extensive binding than $[Au(CN)_2]^-$ to the protein. However, this was not as extensive as what was observed with the discrete gold(I) compounds aurothiosulfate and auranofin. These latter observations may be attributable to slower rates of bond dissociation in the polymeric molecules limiting the availability of free Au^+ ions or Au-ligand moieties for binding to

the protein. Overall, based on the mass spectrometric results shown in this section, the reactivity of the gold(I) compounds towards hTrxR follows the sequence:

$[Au(CN)_2]^-$ < aurothiomalate ≈ aurothioglucose < auranofin < aurothiosulfate

It has previously been suggested that the strength of a gold-sulfur bond increases as the acidity of the thiol increases.[302,303] Accordingly, the complex containing the most acidic thiol ligand should be expected to be the most stable and therefore exhibit the lowest degree of reactivity towards hTrxR. Comparing the pK_{SH} values reported in literature for the thiol-containing ligands of the aforementioned complexes gives the following order: thiomalic acid (9.9[302]) > thioglucose (7.6[302]) > acetylthioglucose (6.4[303]) > thiosulfuric acid (0.6/1.74[304]). If the above hypothesis is correct, then thiosulfuric acid would be expected to show the least degree of reactivity towards hTrxR, and thiomalic acid the highest level of reactivity. These predictions are the opposite of what was observed, and instead suggest that the most important factor in determining the strength of the Au-S bonds, and therefore their reactivity, may be the basicity of the thiolate anions.

To determine whether the addition of acid prior to ionisation might be causing dissociation of the complexes, experiments were performed where solutions of gold complexes were prepared without protein present, but under similar solution and instrumental conditions. It was not possible to give definitive assignments to the signals observed for all five complexes. However, there were no noteworthy differences between spectra of the gold complexes that had been acidified and spectra of those that had not been acidified. This implies that bond dissociation that leads to hTrxR binding is occurring due to either the ionisation process or the inherent kinetic lability of Au-S bonds. As such, while acidification may be favouring bond dissociation at a non-cellular

pH, the conditions that the reactions were initially performed do approximate normal cellular conditions, and did enable significant binding of gold to the protein to occur.

In order to qualitatively examine the kinetics of the binding interactions between aurothioglucose and TrxR, a 3:1 mixture of the gold complex and hTrxR was prepared and aliquots removed and analysed by mass spectrometry at different time points. The results of this experiment are shown in **Figure 5.11**. After 30 min (**Figure 5.11 a**) peaks attributable to adducts of hTrxR with between two and four Au^+ ions bound were present in relatively low abundance. When the reaction time was increased to 1 h (**Figure 5.11 b**), and 4 h (**Figure 5.11** c), peaks corresponding to adducts of the protein with even larger numbers (up to seven) of Au^+ ions bound were observed, and increased in abundance at the longer reaction time. This trend continued when the reaction mixture was analysed again after 24 h (**Figure 5.11 d**). At this point peak J, corresponding to ions consisting of hTrxR with seven Au^+ bound, was perhaps the most abundant protein adduct in the solution. When a similar experiment was performed using auranofin (**Appendix C.1.4, Figure C.3**), time appeared to have less of an influence on the extent of binding, with the majority of protein adducts containing Au^+ or $AuPEt_3$ forming after just 1 h of reaction. The contrast between the kinetics of these two reactions is most likely attributable to differences in the rates of ligand dissociation in the initial gold complexes, noted earlier. In summary, the rate of dissociation of the bridging thioglucose ligands in aurothioglucose was probably slower than for the acetylthioglucose ligand in auranofin. This would result in free gold ions being made available more slowly in the case of the former compound, resulting in changes to the mass spectra occurring over a much longer period of time.

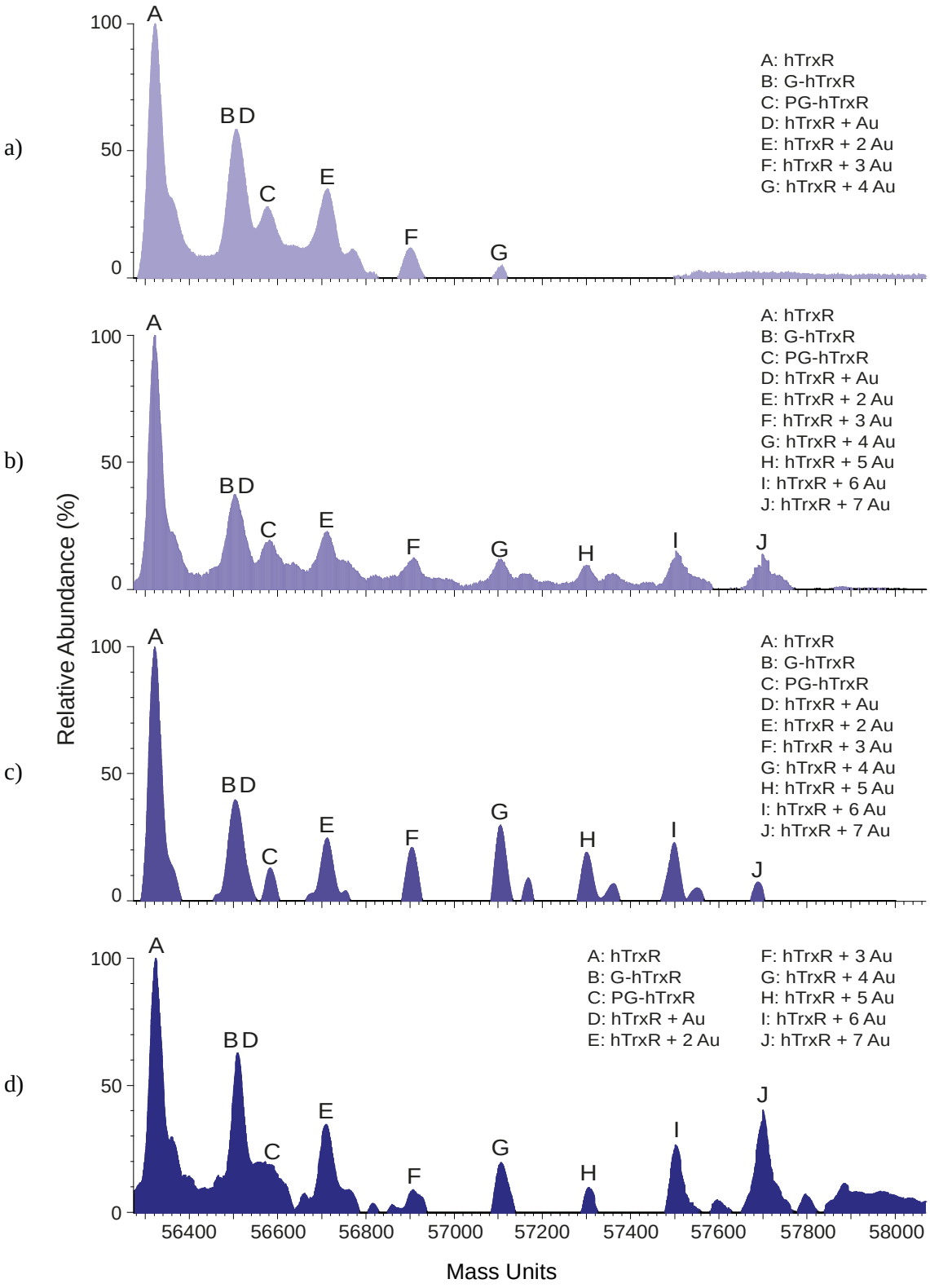

Figure 5.11: Positive ion ESI mass spectra of a solution containing a 3:1 ratio of aurothioglucose to hTrxR obtained after different periods of time, and transformed to a mass scale. Spectra were obtained after the gold complex and protein had reacted for: **a)** 30 min; **b)** 1 h; **c)** 4 h; and **d)** 24 h. For ESI-MS, each sample contained 1.2 µM hTrxR, 20 mM ammonium acetate and 5% acetic acid.

Having established that each of the gold complexes selected for investigation could bind to hTrxR, it was of interest to see whether or not Au NPs might also interact with the protein. However, treatment of TrxR with up to 5 equivalents of Au NPs for as long as 24 h failed to give rise to any new peaks in ESI mass spectra (**Appendix C.1.4, Figure C.4**). There are several possible reasons for this outcome, including that the Au(0) atoms present in Au NPs are unlikely to form bonds with the protein that are sufficiently stable to survive the ESI process. Alternatively, the size of the nanoparticles may be sufficiently large to prevent them from approaching cysteine residues exposed on the surface of hTrxR.

A number of literature studies have also examined the interactions between Au NPs and proteins. One of the earliest such studies used zeta potential measurements and quartz crystal microbalance techniques to examine the binding of Au NPs to bovine serum albumin.[207] It was tentatively concluded that electrostatic forces, possibly involving the carboxylate groups of citrate anions on the surfaces of the Au NPs, and protonated amines of surface lysine residues of the protein, were responsible for the interactions. In a separate study, a combination of techniques including circular dichroism spectroscopy and dynamic light scattering, was used to perform measurements on systems containing citrate-stabilized Au NPs of various sizes, and a range of proteins found in human blood.[208] The results of these investigations led to the development of a model in which the proteins formed an outer layer, or "corona" on the surface of the Au NPs, and a hypothesis that the overall strength of the interactions increased in accordance with nanoparticle size. Binding constants ranging from 10^4 to 10^7 M^{-1} were obtained for these systems, indicating that the overall strength of the binding interactions could vary significantly.

Evidence of interactions between thioredoxin reductase and nanoclusters composed of 25 gold atoms stabilized by a tridecapeptide has also been reported.[209] The positively charged peptide was believed to enhance the solubility of the gold clusters, and also facilitate electrostatic binding interactions with a number of negatively charged amino acid residues near the active site of the enzyme. Molecular docking studies and molecular dynamics simulations were used to further probe the nature of the binding interactions, and improve understanding of the origins of the stability of the resulting assembly. It was also shown that the gold nanoclusters inhibit the activity of TrxR, leading to higher levels of reactive oxygen species and apoptosis in HeLa cells. Silver nanoparticles have also been reported to inhibit selenoprotein synthesis, and the activity of TrxR *in vitro*, resulting in an increase in oxidative stress.[211] However, it should be noted that the mechanism of inhibition was proposed to involve Ag^+ ions leaching from the nanoparticles, as opposed to being a consequence of binding of the nanoparticles themselves to the protein.

The above studies highlight the ability of Au NPs and nanoclusters, as well as nanoparticles composed of other metals, to interact with proteins including TrxR. Each of the techniques used in these literature studies was non-destructive, and therefore well suited for probing weak binding interactions between molecules. In contrast, whilst ESI-MS is known to employ one of the "softer" ionization methods available for obtaining mass spectra, the ability of non-covalent assemblies of molecules to be analysed by this technique does vary depending on the experimental conditions (e.g. desolvation temperature). It is therefore possible that electrostatic interactions were occurring between the Au NPs and TrxR in samples prepared for the mass spectrometry experiments performed as part of this thesis project, but were not sufficiently stable for the resulting complexes to survive the conditions inside the mass spectrometer.

5.4 Experiments Involving Rat Thioredoxin Reductase

All of the results presented earlier in this chapter were obtained from experiments performed using a mutant form of hTrxR in which the active site selenocysteine residue had been replaced by a cysteine. Although both amino acids show a significant degree of affinity towards soft metal ions such as gold(I), it has been reported that the binding interaction exhibited by selenol-containing amino acids and peptides is particularly strong.[162,174,186] Therefore, when it became possible during the later stages of this project to obtain a commercial (Sigma-Aldrich) sample of the native selenol-containing form of TrxR (wild type rat TrxR, rTrxR), a further series of binding experiments was performed using ESI-MS and auranofin. The positive ion ESI mass spectrum of rTrxR after dialysis in ammonium acetate, and subsequent addition of acetic acid and methanol, is shown in **Figure 5.12**. The most abundant peak in the transformed spectrum was at 54514 Da (peak B), with additional peaks of medium abundance at 54330 (peak A) and 54698 Da (peak C), and a number of other peaks of low abundance also present at higher masses. The number of different types of peaks present suggests that a number of different protein species were present in this solution. Calculation of the expected molecular mass of this protein from its sequence (**Appendix C.2.1**) gave a value of 54539.3 Da per monomer, after cleavage of the initiating methionine residue.[228] This value matches closely to that of the most abundant peak (peak B) in the spectrum, confirming that there were significant amounts of rTrxR present. However, the differences in mass between peak B on the one hand, and peaks A and C on the other, could not be rationalised by proposing a specific amino acid had been lost/gained, or by common post-translational modifications or amino acid mutations.

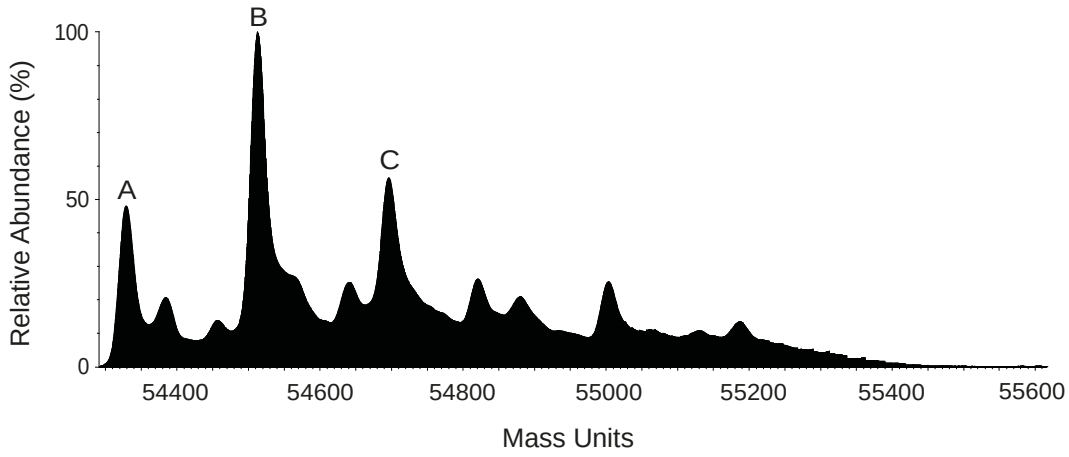

Figure 5.12: Positive ion ESI mass spectrum of 1 µM rTrxR in 18 mM ammonium acetate, 1% acetic acid and 10% methanol. The spectrum has been transformed to a mass scale. Peak B is consistent with the expected mass of rTrxR, whilst peaks A and C are due to as yet unidentified protein species.

In order to elucidate the identity of the protein species giving rise to peaks A and C, a sample of rTrxR was subjected to tryptic digestion and subsequent analysis by LC/MS/MS.[*] The results of this analysis (**Appendix C.2.2, Figure C.5**) showed that there were peptides present that were attributable to two completely different proteins. The first of these was the expected rat thioredoxin reductase 1 (cytoplasmic isoform). Surprisingly, however, rat pyruvate kinase (liver tissue isoform) was also found to be present and in approximately an equal quantity. Pyruvate kinase has a similar mass and isoelectric point to TrxR, which means that it was likely that they were eluted together during purification steps employing size and ion chromatography that would probably have been used by the commercial supplier. Whilst the proteomic analysis identified that rat pyruvate kinase was present in the supplied sample of rTrxR, neither peak A nor peak C in **Figure 5.12** could be assigned to this protein. This indicates that there was likely to be at least three different proteins present in the commercial sample of rTrxR. One potential explanation for peaks A and/or C might be pyruvate kinase (molecular weight 58661.6 Da[228,305]) that was partially proteolysed during the purification procedure. Since it would be difficult to separate all of the proteins present in the

[*] Performed by Dr. Matt Padula (University of Technology, Sydney)

sample of rTrxR in the time remaining at this stage of the PhD project, it was decided to perform a small number of gold binding experiments using the protein as supplied.

Figure 5.13 shows the transformed mass spectra obtained after reaction of various ratios of auranofin with rTrxR. In the spectrum of the solution containing only the protein (**Figure 5.13 a**) peaks A and C have been assigned as contaminants, while peak B is attributed to rat thioredoxin reductase (rTrxR). When the protein was reacted with an equivalent amount of auranofin, the spectrum shown in **Figure 5.13 b)** was obtained. This also contained a peak of medium abundance at 54832 Da (peak D), which is attributable to rTrxR molecules with one $AuPEt_3$ moiety bound. An additional peak of medium abundance was observed at 55014 Da (peak E), which was assigned to the protein contaminant responsible for peak C with one $AuPEt_3$ group bound. This indicates that there was at least one contaminating protein present with an exposed amino acid side chain suitable for binding to this gold drug.

When the ratio of auranofin : rTrxR was increased to 3:1, the resulting spectrum (**Figure 5.13 c**) showed more dramatic changes. In this spectrum, the peak assigned to rTrxR + $AuPEt_3$ was now the most abundant, with an additional peak of medium abundance at 55147 Da (peak F) attributable to protein molecules with two $AuPEt_3$ moieties bound also present. Peak E corresponding to a contaminant protein with one $AuPEt_3$ group bound was now also of high abundance, and an additional peak at 55330 Da (peak G) corresponding to contaminant protein molecules with two $AuPEt_3$ moieties bound was also present. Numerous other new peaks are also present in this spectrum, but were difficult to assign conclusively, although it is likely that some correspond to protein molecules with even larger numbers of $AuPEt_3$ groups, and possibly bare Au^+ ions bound.

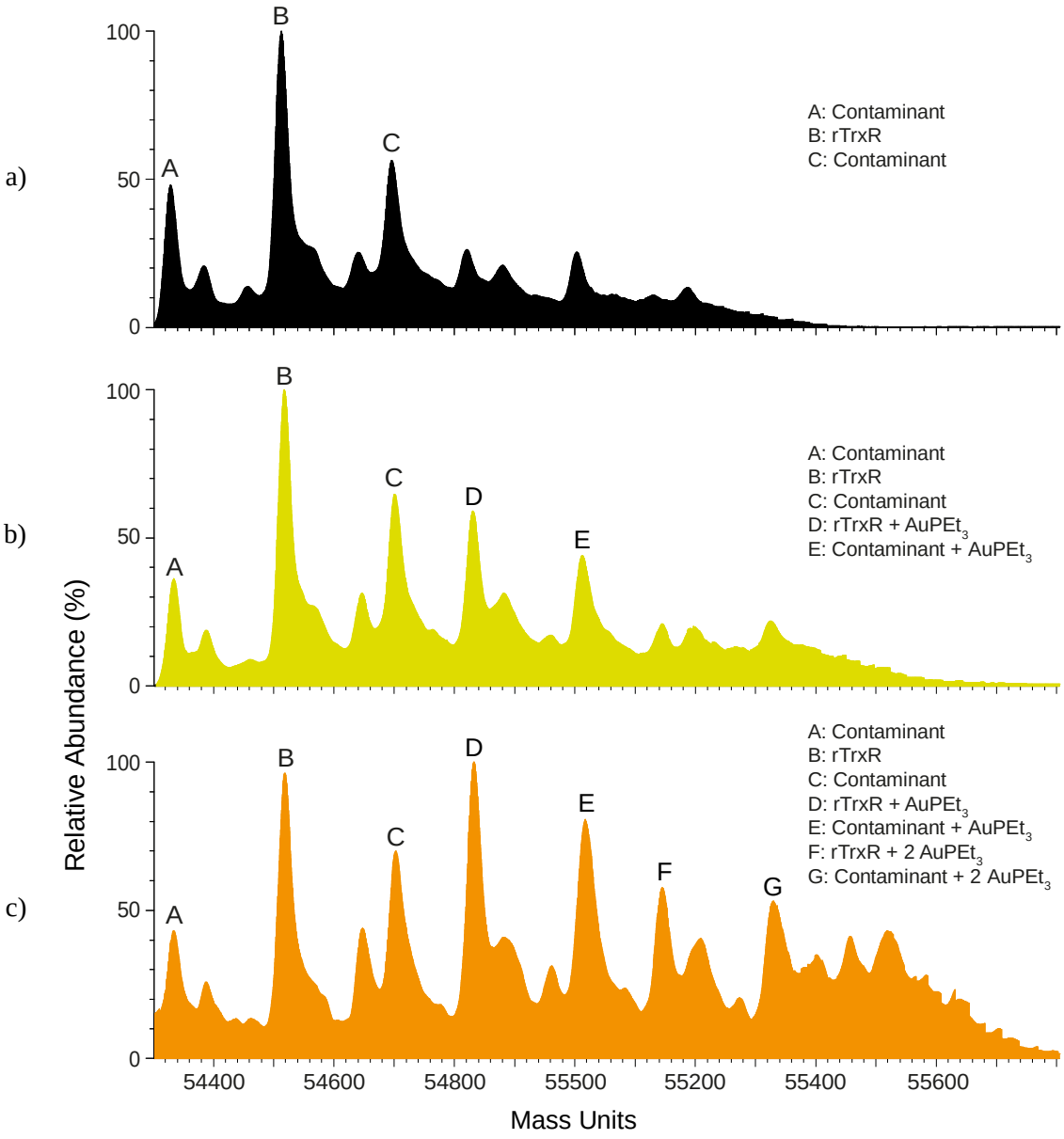

Figure 5.13: Positive ion ESI mass spectra of solutions containing different ratios of auranofin and rTrxR, after transformation to a mass scale. **a)** gold : rTrxR = 0:1; **b)** gold : rTrxR = 1:1; and **c)** gold : rTrxR = 3:1. In each case, solutions containing auranofin and rTrxR were allowed to react for 4 h on ice before the spectrum was obtained. For ESI-MS, each sample contained 1.1 µM rTrxR in 1% acetic acid, 10% methanol and 18 mM ammonium acetate.

When the protein was reacted with five equivalents of auranofin, the resulting spectrum exhibited a very poor signal-to-noise ratio, preventing meaningful assignment of ions. **Figure 5.14** illustrates the origin of the poor signal-to-noise ratio in this spectrum as the amount of auranofin was increased. It shows the raw ESI mass spectra (i.e. not transformed) of solutions containing various ratios of auranofin : rTrxR.

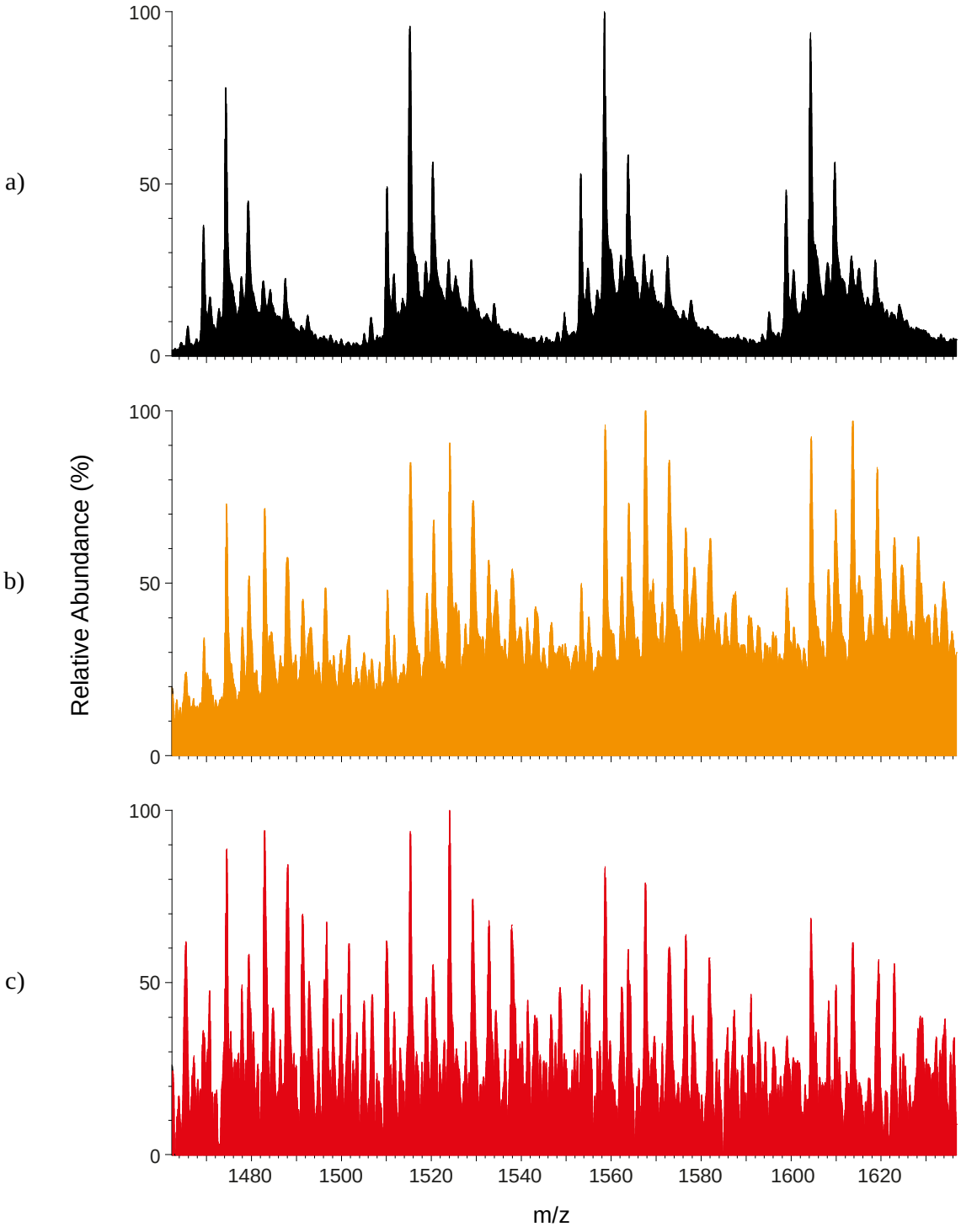

Figure 5.14: Raw positive ion ESI mass spectra of solutions containing different ratios of auranofin and rTrxR: **a)** gold : rTrxR = 0:1; **b)** gold : rTrxR = 3:1; and **c)** gold : rTrxR = 5:1. Solutions containing auranofin and rTrxR were allowed to react for 4 h on ice before a spectrum was obtained. For ESI-MS, each sample contained 1.1 µM rTrxR in 1% acetic acid, 10% methanol and 18 mM ammonium acetate.

For both the spectrum of the solution containing only the protein, and that of the solution containing only the 3:1 ratio of auranofin : rTrxR (**Figure 5.14 a** and **b**, respectively), characteristic envelopes of peaks associated with the various charge states of the protein are clearly visible and separate from each other. However, for the spectrum of the solution containing a 5:1 ratio of auranofin : rTrxR (**Figure 5.14 c**), there is no longer a distinct separation between peak envelopes corresponding to the different charge states of the various proteins and protein adducts. As a consequence, it was not possible to obtain a transformed mass spectrum of sufficient quality. While a similar problem was observed previously for spectra of reaction mixtures containing hTrxR and aurothiosulfate (**Figure 5.8**), it was further exacerbated here due to the presence of one or more contaminating protein species of high relative abundance. Therefore, further studies involving solutions containing higher Au : protein ratios would only be worthwhile after obtaining access to a purer sample of the protein.

One of the most important conclusions to be drawn from this study is that the binding interaction between auranofin and rTrxR is very similar to that observed between this gold drug and hTrxR. In both cases the gold drug largely retained the PEt_3 moiety in its coordination sphere after binding to the protein. In addition, the spectra suggest that a series of dynamic equilibria were established in solution, involving free protein molecules, as well as protein adducts containing different numbers of $AuPEt_3$ moieties. Under the conditions used in these experiments, it did not appear that the presence of the selenol residue significantly affected the extent of binding to the protein by auranofin.

Chapter 6:

Conclusions and Future Directions

6.1 Conclusions

The research presented in this thesis compares a number of aspects of the biological chemistry of gold(I) compounds used for the treatment of rheumatoid arthritis, with those of gold nanoparticles (Au NPs). There have been many studies that focussed solely on the biological activity of one or more anti-arthritic gold(I) compounds, and other studies have examined exclusively the biological effects of various types of Au NPs. However, there have been few, if any, investigations that set out to comprehensively compare the interactions of both classes of gold agents. These comparisons formed the overall aim of this project.

Interest in studying Au NPs stemmed from two studies that reported they elicited powerful *in vivo* anti-inflammatory activity after administration to rats or humans; however, the mechanisms through which these effects occurred were unclear. Conflicting results in the literature concerning the biological activity of Au NPs also provided a focus and impetus for the research presented in this thesis. Most previous studies did not examine the effects of Au NPs prepared using the classical citrate-reduction approach, or on a wide range of inflammation markers, as has been reported here. In addition, prior work did not set out to explore the importance of the shell surrounding and stabilising the nanoparticles on their biological activity. Many of the studies performed in this project focussed on the interactions of the gold compounds and Au NPs with the mouse macrophage cell line, RAW264.7. Macrophages were chosen for these studies due to their integral role in the immune system, and their contribution to rheumatoid arthritis progression.

One specific aim of this project was to compare the cytotoxicity and cellular uptake of Au NPs to that of the gold compounds. The toxicity determined for auranofin

(IC_{50} = 4 µM) was found to be in good agreement with other cytotoxicity values widely reported in the literature. In contrast, the toxicity of aurothiomalate has not been previously studied as extensively, with the lack of toxicity reported here (IC_{50} > 1000 µM) the first measure of cytotoxicity obtained using the MTT assay and macrophage cells. This result is in general agreement with the low toxicity exhibited by this compound in other cytotoxicity assays. The cytotoxicity of aurothiosulfate had been investigated to a lesser degree than aurothiomalate, with the IC_{50} of 650 µM reported here being the first such value determined, and reflecting a low level of toxicity for this compound. Au NPs proved to be essentially non-toxic to the macrophages at concentrations up to 60 µM. The MTT assay could not be performed using higher concentrations of Au NPs as this would have required addition of such large volumes of stock Au NP solution, that substantial dilution of the cellular medium used to culture the macrophages would have occurred. Despite this, it was still possible to conclude that Au NPs were far less toxic than auranofin to the macrophages.

Although treatment of macrophages with Au NPs did not lead to any cytotoxic effects, it still resulted in the incorporation of significant quantities of gold into the cells. Macrophages treated with solutions containing 2.5 µM or 60 µM Au NPs showed higher levels of intracellular gold than cells treated with equivalent amounts of auranofin, aurothiomalate or aurothiosulfate. This was a significant result, as although the cellular uptake of various types of Au NPs had been studied previously, no prior investigation had directly compared the extent of uptake of Au NPs to that of anti-arthritic gold compounds under the same conditions. In addition, the results of this study demonstrated that it was likely sufficient gold was incorporated into cells to elicit a biological response.

Another specific aim of this project was to compare, for the first time, the cellular distribution of Au NPs and gold(I) compounds after uptake by macrophages, using microprobe synchrotron radiation X-ray fluorescence (SR-XRF) imaging. This aim was achieved through experiments performed at two different synchrotrons. Images obtained at the Advanced Photon Source (Argonne National Laboratory, USA) of macrophages treated with aurothiomalate or Au NPs showed that the gold accumulated within the cells in discrete regions. This result was consistent with previous studies that showed that gold(I) compounds used for chrysotherapy become localised in lysosomal bodies, referred to as aurosomes in view of their high gold content. Similarly, Au NPs are taken up by cervical cancer, fibroblast, brain tumour and osteoblast cells through endocytosis, and become localised in lysosomes. SR-XRF images of large numbers of macrophages exposed to Au NPs were also obtained, using the XFM beamline at the Australian Synchrotron (Melbourne). These images showed that the gold was more extensively and evenly distributed between cells than gold incorporated into the cells after exposure to auranofin or aurothiomalate. Furthermore, field emission scanning electron microscopy experiments performed on macrophages treated with Au NPs confirmed that gold localised with the cells was internalised, and not simply surface-bound.

A further aim of this project was to compare the effects of Au NPs and gold(I) compounds on the levels of specific inflammation mediators, in the hope of gaining insights into their mechanisms of action. The effects of auranofin have been documented thoroughly in the literature, with some previous studies having also focussed on the effects of aurothiomalate. Auranofin was shown to have powerful inhibitory effects on production of nitric oxide (NO), reactive oxygen species (ROS), and tumor necrosis factor (TNF), in macrophages activated using lipopolysaccharide

(LPS). In contrast, aurothiomalate had a much weaker inhibitory effect on the production of NO and ROS in macrophages treated with LPS. These results were in concordance with those available in the literature, which indicate that auranofin is in general a stronger inhibitor of the production of inflammation mediators than aurothiomalate. This may be due in part to auranofin being incorporated into cells to a greater extent than aurothiomalate, as demonstrated by the results of the GFAAS experiments presented here. However, it must be remembered that aurothiomalate is generally regarded as a more effective drug than auranofin for the treatment of rheumatoid arthritis. This suggests that the mechanism of anti-arthritic action of aurothiomalate may involve effects on pathways involving other types of inflammation mediators, and/or activity with other classes of cells or biological targets such as enzymes.

Prior to commencement of this thesis, there was already a significant literature on the effects of Au NPs on inflammation markers. The results of these studies were variable, with Au NPs eliciting either a pro- or anti-inflammatory effect. One probable reason for these differences is variations in the identity of the stabilising agent used to prepare the nanoparticles and/or the size of the nanoparticles. As part of the current thesis research program, experiments were carried out in order to try to resolve this unanswered question. The citrate-stabilised Au NPs studied had no significant effect on the LPS-stimulated production of NO, ROS, or the anti-inflammatory cytokine interleukin-10 (IL-10), in macrophages stimulated by LPS. In addition, the Au NPs had only a small inhibitory effect on the production of the pro-inflammatory cytokine TNF. These results were surprising in view of the substantial uptake of gold revealed by GFAAS experiments, and supported by the results of electron microscopy experiments.

In addition, SR-XRF experiments provided evidence that the gold from Au NPs becomes widely distributed throughout individual macrophage cells.

There are several possible explanations for the lack of biological activity exhibited by the Au NPs. First, Au NPs may interact with cells by a mechanism or mechanisms that do not involve the inflammation mediators investigated here. Secondly, the conditions under which the *in vitro* studies presented in this thesis were performed may be a poor approximation for *in vivo* conditions; and some key inflammation processes with which the Au NPs might either interfere or enhance may be absent. Finally, the Au NPs used may not have produced any substantial changes to macrophage function owing to the inertness of the Au(0) atoms. An additional set of studies performed using five different types of commercially available Au NPs, with different sizes and stabilising agents, did not shed any further light on the factors affecting their biological activity. In all cases, the Au NPs were unable to affect the production of the inflammation markers NO and ROS. Further work is therefore required to confirm that Au NPs are efficacious anti-arthritic agents *in vivo*, and if so, how those effects are elicited.

The final specific aim of this thesis was to investigate the binding of gold(I) compounds and Au NPs to the redox enzyme thioredoxin reductase (TrxR). A motivation for investigating this enzyme was the uncommon selenocysteine residue normally present at the C-terminal active site, which has been reported to be a potent target for gold(I) ions, such as those present in most chrysotherapeutic agents and their metabolites. While this enzyme has been studied extensively as a drug target in recent years, few of these investigations attempted to directly probe its interactions with gold(I) compounds. For example, the question of whether any of the initial ligands bound to the metal ion remained after binding to the protein was still unanswered. The

studies presented in this thesis, performed using electrospray ionisation mass spectrometry (ESI-MS) and two forms of TrxR, were able to address this question.

Addition of aurothiomalate, aurothioglucose or aurothiosulfate to solutions containing TrxR resulted in the formation of multiple protein adducts containing between one and seven bare gold ions bound to the enzyme. Little, if any, evidence for retention of any of the initial ligands bound to the metal was found in these experiments. In contrast, when the initial metal complex contained less labile Au-CN and Au-P bonds, protein adducts were formed in which one of the two original ligands was still also bound to the gold ion. Furthermore, the extent of gold binding was lower in these instances. The results obtained with both types of TrxR revealed that there is likely to be a number of suitable binding sites for the gold compounds, in addition to the cysteine and selenocysteine residues at the C-terminus. Further experiments will be required to identify these additional binding sites.

The interactions between Au NPs and TrxR were also investigated for the first time by ESI-MS. The Au NPs showed no sign of binding to the protein. Whether such interactions do occur, and whether ESI-MS is a suitable technique for investigating such interactions, remain open questions. For example, any interactions that might have occurred are unlikely to have been covalent in nature, and therefore may not have survived the ionisation conditions present in the mass spectrometer. Further work using alternative techniques is therefore required to provide a definitive answer to the question of the nature of any interactions between Au NPs and TrxR.

6.2 Future Directions

Despite the number of investigations performed into the biological interactions of Au NPs, there remain a number of areas that need further work. The most important

area concerns the apparent lack of effect Au NPs have upon inflammation mediators. This could be investigated further in a number of ways. One is by expanding the studies to include other inflammation mediators. Such experiments might shed light on whether the biological activity of Au NPs arises from interactions with other classes of inflammation mediators, including pro-inflammatory interleukins, transcription factors, or cell-surface receptors. Additional insight into why the Au NPs had no effect on the production of the inflammation mediators could be obtained from experiments performed using alternative methods of stimulating the macrophages. One such alternative method involves the pro-inflammatory cytokine interferon-γ. This would induce inflammation in the macrophages by a different pathway, which might serve as a better model for inflammation in patients with rheumatoid arthritis. For example, interferon-γ might lead to higher levels of production of the inflammation mediators examined in this thesis, or of other mediators that have not yet been explored. If the latter were subsequently shown to be affected significantly by prior treatment with any of the gold compounds or Au NPs, valuable clues might be obtained about the mechanism of action of the gold agents.

The variability in results obtained from *in vitro* investigations into the biological effects of Au NPs also highlights the need for additional *in vivo* studies to confirm or disprove literature reports indicating they exhibit similar or improved levels of anti-inflammatory activity compared to established chrysotherapeutic agents. These studies should be performed using Au NPs with known and different stabilising agents and/or particle sizes. In addition, they should be performed using different agents to induce symptoms of inflammation in the test animals. Examples of inflammation-inducing agents include *Mycobacterium tuberculosis,* collagen, pristane and LPS. Comparison of

the results of these studies will establish the most promising lead therapeutic agents, and will aid the design of future *in vitro* investigations.

Whilst the effects of a range of Au NPs on production of NO and ROS were studied as part of this research project, in many cases it was not known what the identity of the stabilising molecules were, as this is the proprietary information of the chemical suppliers. This remains a key issue in understanding the biological chemistry and interactions of Au NPs, as variations in the identity of the stabilisers is one of the few possible reasons for different results reported in the literature, and here. It would also be of considerable interest to examine the biological interactions of alloy nanoparticles, such as gold-silver nanoparticles containing known and varying amounts of gold and silver. Studies such as these might provide insight into the importance of the identity of the metal in determining the ability of nanoparticles to impact upon the inflammatory response.

Although a number of useful results were obtained from the inflammation mediator experiments, these required careful interpretation. One reason for this is that the auranofin vehicle (1% DMSO/99% (v/v) incomplete medium) itself resulted in significant inhibition of LPS-induced ROS and TNF formation. If further experiments investigating the effects of auranofin were to be performed, it would be valuable to perform them using a vehicle containing a much lower (e.g. 0.1% (v/v)) concentration of DMSO.

Some issues were also encountered whilst determining the effects of the gold compounds and Au NPs on ROS production. These experiments were performed using a flow cytometry method, which typically resulted in large variations between replicate samples, making meaningful interpretation of the data difficult. It would therefore be

worthwhile to repeat these investigations using an alternative method that involves plate-based fluorescence measurements, instead of flow-cytometric measurements of dichlorofluorescin concentration. Such an approach might provide more concrete evidence of effects being exerted by the gold compounds and Au NPs, which are only being hinted at in the data currently available.

There are now a number of reports, including this thesis, which describe the effects of LPS on the production of cytokines by macrophages, and how this can be affected by pre-treating the cells with gold drugs. However, there still remains a lot to be learnt about the timing of the different cellular responses. In Chapter 4 of this thesis, the production of the anti-inflammatory cytokine IL-10 was described as an auto-regulatory response to increased TNF levels, which resulted from the initial treatment of macrophages with LPS. While it has been shown conclusively in the literature that LPS-stimulated macrophages produce interleukin-1β, which in turn leads to higher levels of IL-10, the same is not true for TNF. Perhaps more importantly, an unanswered question is whether treatment of RAW264.7 cells with LPS leads first of all to elevated levels of TNF or interleukin-1β, or both. In addition, do increases in IL-10 levels correlate more closely to a spike in the levels of just one or both interleukin-1β and TNF? One way to answer this question would be to treat the macrophages with LPS, and then measure the concentrations of all three cytokines at various time points. If, for example, the IL-10 concentration was found to increase rapidly in response to a spike in TNF concentration, and not a change in interleukin-1β levels, this would suggest that the production of IL-10 is being induced as an auto-regulatory response to the sudden increase in TNF levels.

A further question that remains from this work is why the Au NPs used in this thesis did not alter the production of the various inflammation mediators. One possible

explanation is that after entry into the cells, the gold remains in the elemental oxidation state, and is therefore not able to participate readily in reactions with various cellular components. In order to address this possibility, synchrotron radiation X-ray absorption spectroscopic measurements could be performed on macrophages after they have been exposed to gold compounds or Au NPs. This technique enables determination of the oxidation state of a metal atom or ion and also provides information about the ligand donor atoms directly bonded to it. Whilst this technique has previously been used to examine the metabolism of aurothiomalate in rats, it does not appear to have been used to explore the cellular fate of Au NPs and other gold compounds.

Another area of future work involves expansion of the microprobe SR-XRF imaging experiments performed as part of this thesis project. A consequence of the overlap of the gold M line with the sulfur K line in these experiments was that it was not possible to determine whether gold from aurothiomalate or Au NPs was co-localised with sulfur inside the macrophages. This problem was exacerbated by the use of high concentrations of aurothiomalate or Au NPs in experiments involving these gold reagents. Therefore one potential method for overcoming this issue, and determining if Au/S co-localisation does in fact occur, would be to use lower treatment concentrations. It would also be extremely worthwhile to perform additional experiments using thin-sections or three-dimensional tomography of whole cells treated with Au NPs in order to determine whether the internalised gold was located entirely in the cytosol and excluded from the cell nucleus.

Another question that lacks a definitive answer is whether Au NPs can interact with TrxR. Although ESI-MS failed to provide any evidence for such interactions, this may have been a result of the fragile nature of such complexes. It would therefore be worthwhile to explore these systems using other techniques. For example, the

interactions of Au NPs with proteins have previously been probed using circular dichroism spectroscopy and dynamic light scattering.

Although ESI-MS did prove suitable for characterising the binding of the anti-arthritic gold(I) compounds to TrxR, a number of additional experiments involving ESI-MS could be performed to yield further information about these systems. For example, the ESI-MS results presented here did not provide any evidence for the exact location of the gold binding sites. This could potentially be accomplished by first reacting the protein with selective blocking agents such as iodoacetamide, which alkylates free cysteine residues, and then observing by ESI-MS whether gold binding behaviour is altered. This information could also be obtained by using a proteomics approach in which TrxR is reacted with a gold complex, and the resulting mixture of protein adducts subjected to digestion with trypsin, after which the resulting peptide fragments are analysed by mass spectrometry to determine which amino acids the gold has become bound to.

The most important factor that limited the information that could be obtained from the ESI-MS results was the presence of protein molecules containing N-terminal gluconoyl and phosphogluconoyl groups in engineered human TrxR samples. These additional species made unambiguous assignment of some ions to specific gold-TrxR adducts problematic. There are two ways to attempt to rectify this problem. One is to investigate whether a chemical reagent could be used to selectively cleave the amide bond between these additional moieties and the N-terminus of the protein, without hydrolysing any of the other amide bonds in the rest of the protein. Alternatively, it may be possible to take advantage of the observation that the existence of these N-terminal modifications is very dependent on the identity of the amino acids between the hexa-histidyl tag and the initiating methionine residue. Therefore, it may be possible to

engineer plasmids that prevent these modifications from occurring. A final area for improvement concerns the ESI-MS experiments performed using rat TrxR. The spectra of this protein were not as informative as hoped owing to the presence of additional peaks from as yet unidentified protein contaminants, which were present in significant quantities. It will therefore be necessary to purify these protein samples, for example, by chromatographic separation, or to obtain protein with a higher level of purity from another commercial source, before additional information can be obtained from ESI mass spectra concerning the ability of TrxR to bind to different gold complexes or Au NPs.

In conclusion, the work presented in this thesis has contributed to our knowledge of the differences between how gold anti-arthritic compounds and gold nanoparticles interact with biological systems. Despite this, there remains much to be learnt about the origin of these differences in interactions, which is the key to the development of new gold therapeutic agents with improved efficacy. It is hoped that the experiments described in this thesis will guide future research efforts in this area, and thereby pave the way to future discoveries concerning anti-inflammatory gold compounds and nanoparticles.

References

(1) Turesson, C.; O'Fallon, W. M.; Crowson, C. S.; Gabriel, S. E.; Matteson, E. L. *Ann. Rheum. Dis.* **2003**, *62*, 722–727.
(2) Scott, D. L.; Wolfe, F.; Huizinga, T. W. J. *Lancet* **2010**, *376*, 1094–1108.
(3) Symmons, D.; Turner, G.; Webb, R.; Asten, P.; Barrett, E.; Lunt, M.; Scott, D.; Silman, A. *Rheumatology* **2002**, *41*, 793–800.
(4) Alamanos, Y.; Voulgari, P. V; Drosos, A. A. *Semin. Arthritis Rheum.* **2006**, *36*, 182–188.
(5) Alamanos, Y.; Drosos, A. A. *Autoimmun. Rev.* **2005**, *4*, 130–136.
(6) Australian Institute of Health and Welfare. *Arthritis and other musculoskeletal conditions across the life stages*; Australian Government: Canberra, 2014.
(7) Gardner, G. C. *Clin. Appl. Immunol. Rev.* **2005**, *5*, 19–44.
(8) Solomon, D. H.; Karlson, E. W.; Rimm, E. B.; Cannuscio, C. C.; Mandl, L. A.; Manson, J. E.; Stampfer, M. J.; Curhan, G. C. *Circulation* **2003**, *107*, 1303–1307.
(9) Maradit-Kremers, H.; Nicola, P. J.; Crowson, C. S.; Ballman, K. V.; Gabriel, S. E. *Arthritis Rheum.* **2005**, *52*, 722–732.
(10) van der Woude, D.; Houwing-Duistermaat, J. J.; Toes, R. E. M.; Huizinga, T. W. J.; Thomson, W.; Worthington, J.; van der Helm-Van Mil, A. H. M.; De Vries, R. R. P. *Arthritis Rheum.* **2009**, *60*, 916–923.
(11) Jawaheer, D.; Gregersen, P. K. *Rheum. Dis. Clin. North Am.* **2002**, *28*, 1–15.
(12) Carlens, C.; Hergens, M. P.; Grunewald, J.; Ekbom, A.; Eklund, A.; Höglund, C. O.; Askling, J. *Am. J. Respir. Crit. Care Med.* **2010**, *181*, 1217–1222.
(13) Sugiyama, D.; Nishimura, K.; Tamaki, K.; Tsuji, G.; Nakazawa, T.; Morinobu, A.; Kumagai, S. *Ann. Rheum. Dis.* **2010**, *69*, 70–81.
(14) Liao, K. P.; Alfredson, L.; Karlson, E. W. *Curr. Opin. Rheumatol.* **2009**, *21*, 279–283.
(15) Alvarez-Lafuente, R.; Fernández-Gutiérrez, B.; de Miguel, S.; Jover, J. A.; Rollin, R.; Loza, E.; Clemente, D.; Lamas, J. R. *Ann. Rheum. Dis.* **2005**, *64*, 1357–1359.
(16) Ma, Y.; Pope, R. M. *Curr. Pharm. Des.* **2005**, *11*, 569–580.
(17) Rupp, I.; Boshuizen, H. C.; Dinant, H. J.; Jacobi, C. E.; van den Bos, G. A. M. *Scand. J. Rheumatol.* **2009**, *35*, 175–181.
(18) Gao, S.; Wang, L.; Liu, W.; Wu, Y.; Yuan, Z. *J. Inflamm.* **2014**, *11:13*.
(19) Raimund W Kinne; Bräuer, R.; Stuhlmüller, B.; Palombo-Kinne, E.; Burmester, G.-R. *Arthritis Res.* **2000**, *2*, 189–202.
(20) Feldmann, M. *Nat. Rev. Immunol.* **2002**, *2*, 364–371.
(21) Vasanthi, P.; Nalini, G.; Rajasekhar, G. *Asia Pacific Leag. Assoc. Rheumatol. J. Rheumatol.* **2007**, *10*, 270–274.
(22) McInnes, I. B.; Schett, G. *Nat. Rev. Immunol.* **2007**, *7*, 429–442.
(23) Nakao, S.; Ogtata, Y.; Shimizu, E.; Yamazaki, M.; Furuyama, S.; Sugiya, H. *Mol. Cell. Biochem.* **2002**, *238*, 11–18.
(24) Dayer, J. M.; Beutler, B.; Cerami, A. *J. Exp. Med.* **1985**, *162*, 2163–2168.
(25) Thomson, B. M.; Mundy, G. R.; Chambers, T. J. *J. Immunol.* **1987**, *138*, 775–779.
(26) Vane, J. R.; Bakhle, Y. S.; Botting, R. M. *Annu. Rev. Pharmacol. Toxicol.* **1998**, *38*, 97–120.
(27) Kay, J.; Calabrese, L. *Rheumatology* **2004**, *43*, iii2–iii9.
(28) Kahle, P.; Saal, J. G.; Schaudt, K.; Zacher, J.; Fritz, P.; Pawelec, G. *Ann. Rheum. Dis.* **1992**, *51*, 731–734.

(29) Eastgate, J. A.; Wood, N. C.; di Giovine, F. S.; Symons, J. A.; Grinlinton, F. M.; Duff, G. W. *Lancet* **1988**, *2*, 706–709.
(30) Sarsfield, S. J.; Staruch, M. J.; Cranston, W. I.; Hellon, R. F. *J. Exp. Med.* **1985**, *162*, 1208–1222.
(31) Gowen, M.; Wood, D. D.; Ihrie, E. J.; McGuire, M. K.; Russell, R. G. *Nature* **1983**, *306*, 378–380.
(32) Joosten, L. A. B.; Helsen, M. M. A.; Saxne, T.; van de Loo, F. A. J.; Heinegard, D.; van den Berg, W. B. *J. Immunol.* **1999**, *163*, 5049–5055.
(33) Cuzzocrea, S. *Curr. Pharm. Des.* **2006**, *12*, 3551–3570.
(34) Valko, M.; Leibfritz, D.; Moncol, J.; Cronin, M. T. D.; Mazur, M.; Telser, J. *Int. J. Biochem. Cell Biol.* **2007**, *39*, 44–84.
(35) Gelderman, K. A.; Hultqvist, M.; Olsson, L. M.; Bauer, K.; Pizzolla, A.; Olofsson, P.; Holmdahl, R. *Antioxid. Redox Signal.* **2007**, *9*, 1541–1567.
(36) Leo, M. E. De; Tranghese, A.; Passantino, M.; Mordente, A.; Lizzio, M. M.; Galeotti, T.; Zoli, A. *J. Rheumatol.* **2002**, *29*, 2245–2246.
(37) Mirshafiey, A.; Mohsenzadegan, M. *Iran. J. Allergy, Asthma Immunol.* **2008**, *7*, 195–202.
(38) Sharma, J. N.; Al-Omran, A.; Parvathy, S. S. *Inflammopharmacology* **2007**, *15*, 252–259.
(39) Hristov, M.; Erl, W.; Weber, P. C. *Hypertension* **1990**, *16*, 477–483.
(40) MacMicking, J.; Xie, Q. W.; Nathan, C. *Annu. Rev. Immunol.* **1997**, *15*, 323–350.
(41) Moncur, C.; Williams, H. J. *Phys. Ther.* **1995**, *75*, 511–525.
(42) Spangler, R. S. *Semin. Arthritis Rheum.* **1996**, *26*, 435–446.
(43) Hawksworth, E. L.; Andrews, P. C.; Lie, W.; Lai, B.; Dillon, C. T. *J. Inorg. Biochem.* **2014**, *135*, 28–39.
(44) Salmeron, G.; Lipsky, P. E. *Am. J. Med.* **1983**, *75*, 19–24.
(45) Trotter, J. L.; Rodey, G. E.; Gebel, H. M. *N. Engl. J. Med.* **1982**, *306*, 365–366.
(46) Symmons, D. P. M.; Salmon, M.; Farr, M.; Bacon, P. A. *J. Rheumatol.* **1988**, *15*, 575–579.
(47) Russell, R. G.; Graveley, R.; Coxon, F.; Skjodt, H.; Del Pozo, E.; Elford, P.; Mackenzie, A. *Scand. J. Rheumatol. Suppl.* **1992**, *95*, 9–18.
(48) Scott, D. L.; Kinglsey, G. H. *N. Engl. J. Med.* **2006**, *355*, 704–712.
(49) Sokka, T.; Pincus, T. *J. Rheumatol.* **2002**, *29*, 2521–2524.
(50) Pope, J. E.; Hong, P.; Koehler, B. E. *J. Rheumatol.* **2002**, *29*, 255–260.
(51) Jobanputra, P.; Wilson, J.; Douglas, K.; Burls, A. *Rheumatology* **2004**, *43*, 206–210.
(52) Lee, A. T.; Pile, K. *Aust. Prescr.* **2003**, *26*, 36–40.
(53) Kremer, J. M.; Alarcón, G. S.; Lightfoot, R. W.; Willkens, R. F.; Furst, D. E.; Williams, H. J.; Dent, P. B.; Weinblatt, M. E. *Arthritis Rheum.* **1994**, *37*, 316–328.
(54) Sadler, P. J. *Struct. Bond.* **1976**, *29*, 171–214.
(55) Keers, R. Y. *Thorax* **1980**, *35*, 884–889.
(56) Merchant, B. *Biologicals* **1998**, *26*, 49–59.
(57) Eisler, R. *Inflamm. Res.* **2003**, *52*, 487–501.
(58) Forestier, J. *Ann. Med. Interne* **1929**, *53*, 232–237.
(59) Forestier, J. *Ann. Med. Interne* **1930**, *54*, 273–280.
(60) Forestier, J.; Paris, M. D. *Lancet* **1932**, *219*, 441–444.
(61) Forestier, J. *Lancet* **1934**, *224*, 646–648.
(62) Kean, W. F.; Kean, I. R. L. *Inflammopharmacology* **2008**, *16*, 112–125.
(63) Kean, W. F.; Forestier, F.; Kassam, Y.; Buchanan, W. W.; Rooney, P. J. *Semin.*

Arthritis Rheum. **1985**, *14*, 180–186.
(64) Slot, G.; Deville, P. M.; Hill, N. G.; Williams, B.; Fridjohn, M. H. *Lancet* **1934**, *223*, 73–76.
(65) Parr, L. J. A.; Shipton, E. A. *Med. J. Aust.* **1937**, 864–874.
(66) Cecil, R. L.; Kammerer, W. H.; Deprume, F. J. *Ann. Intern. Med.* **1942**, *16*, 811–827.
(67) Felson, D. T.; Anderson, J. J.; Meenan, R. F. *Arthritis Rheum.* **1990**, *33*, 1449–1461.
(68) Simon, T. M.; Kunishima, D. H.; Vibert, G. J.; Lorber, A. *Cancer* **1979**, *44*, 1965–1975.
(69) Simon, T. M.; Kunishima, D. H.; Vibert, G. J.; Lorber, A. *Cancer Res.* **1981**, *41*, 94–97.
(70) Mirabelli, C. K.; Johnson, R. K.; Hill, D. T.; Faucette, L. F.; Girard, G. R.; Kuo, G. Y.; Sung, C. M.; Crooke, S. T. *J. Med. Chem.* **1986**, *29*, 218–223.
(71) Berners-Price, S. J.; Mirabelli, C. K.; Johnson, R. K.; Chloride, I.; Mattern, M. R.; Mccabe, F. L.; Faucette, L. F.; Mong, S.-M.; Sadler, P. J.; Crooke, S. T. *Cancer Res.* **1986**, *46*, 5486–5493.
(72) Hoke, G. D.; Macia, R. A.; Meunier, P. C.; Bugelski, P. J.; Mirabelli, C. K.; Rush, G. F.; Matthews, W. D. *Toxicol. Appl. Pharmacol.* **1989**, *100*, 293–306.
(73) Buckley, R. G.; Elsome, A. M.; Fricker, S. P.; Henderson, G. R.; Theobald, B. R. C.; Parish, R. V.; Howe, B. P.; Kelland, L. R. *J. Med. Chem.* **1996**, *39*, 5208–5214.
(74) Shaw, C. F. *Chem. Rev.* **1999**, *99*, 2589–2600.
(75) Shapiro, D. L.; Masci, J. R. *J. Rheumatol.* **1996**, *23*, 1818–1820.
(76) Tepperman, K.; Zhang, Y.; Roy, P. W.; Floyd, R.; Zhao, Z.; Dorsey, J. G.; Elder, R. C. *Met. Based. Drugs* **1994**, *1*, 433–444.
(77) Okada, T.; Patterson, B. K.; Shui-Qing, Y.; Gurney, M. E. *Virology* **1993**, *192*, 631–642.
(78) White, N. J.; Nosten, F.; Looareesuwan, S.; Watkins, W. M.; Marsh, K.; Snow, R. W.; Kokwaro, G.; Ouma, J.; Hien, T. T.; Molyneux, M. E.; Taylor, T. E.; Newbold, C. I.; Danis, M.; Greenwood, B. M.; Anderson, R. M.; Olliaro, P. *Lancet* **1999**, *353*, 1965–1967.
(79) Greenwood, B.; Mutabingwa, T. *Nature* **2002**, *415*, 670–672.
(80) Navarro, M.; Pérez, H.; Sánchez-Delgado, R. A. *J. Med. Chem.* **1996**, *40*, 1937–1939.
(81) Peters Jr., T. *All About Albumin: Biochemistry, Genetics and Medical Applications*; Academic Press: San Diego, 1995.
(82) Coffer, M. T.; Shaw, C. F.; Eidsness, M. K.; Watkins, J. W.; Elder, R. C. *Inorg. Chem.* **1986**, *25*, 333–339.
(83) Shaw, C. F.; Schaeffer, N. A.; Elder, R. C.; Eidsness, M. K.; Trooster, J. M.; Caliss, G. H. M. *J. Am. Chem. Soc.* **1984**, *106*, 3511–3521.
(84) Kragh-Hansen, U.; Chuang, V. T. G.; Otagiri, M. *Biol. Pharm. Bull.* **2002**, *25*, 695–704.
(85) Pedersen, S. M. *Biochem. Pharmacol.* **1987**, *36*, 2661–2666.
(86) Beck, J. L.; Ambahera, S.; Yong, S. R.; Sheil, M. M.; Jersey, J. De; Ralph, S. F. *Anal. Biochem.* **2004**, *325*, 326–336.
(87) Christodoulou, J.; Sadler, P. J.; Tucker, A. *Eur. J. Biochem.* **1994**, *225*, 363–368.
(88) Talib, J.; Beck, J. L.; Ralph, S. F. *J. Biol. Inorg. Chem.* **2006**, *11*, 559–570.
(89) Graham, G. G.; Kettle, A. J. *Biochem. Pharmacol.* **1998**, *56*, 307–312.
(90) Lewis, G.; Shaw, C. F. *Inorg. Chem.* **1986**, *25*, 58–62.

(91) Marsden, J. O.; House, C. I. *The Chemistry of Gold Extraction*; 2nd ed.; Society for Mining, Metallurgy, and Exploration, Inc.: Littleton, USA, 2006.
(92) Pacheco, E. A.; Tiekink, E. R. T.; Whitehouse, M. W. In *Gold Chemistry: Applications and Future Directions in the Life Sciences*; Mohr, F., Ed.; Wiley-VCH: Weinheim, Germany, 2009; pp. 283–319.
(93) Graham, G. G.; Haavisto, T. M.; Jones, H. M.; Champion, G. D. *Biochem. Pharmacol.* **1984**, *33*, 1257–1262.
(94) James, D. W.; Ludvigsen, N. W.; Cleland, L. G.; Milazzo, S. C. *J. Rheumatol.* **1982**, *9*, 532–535.
(95) Canumalla, A. J.; Al-Zamil, N.; Phillips, M.; Isab, A. A.; Shaw, C. F. *J. Inorg. Biochem.* **2001**, *85*, 67–76.
(96) Schuhmann, D.; Kubicka-Muranyi, M.; Mirtschewa, J.; Günther, J.; Kind, P.; Gleichmann, E. *J. Immunol.* **1990**, *145*, 2132–2139.
(97) Verwilghen, J.; Kingsley, G. H.; Gambling, L.; Panayi, G. S. *Arthritis Rheum.* **1992**, *35*, 1413–1418.
(98) Goebel, C.; Kubicka-Muranyi, M.; Tonn, T.; Gonzalez, J.; Gleichmann, E. *Arch. Toxicol.* **1995**, *69*, 450–459.
(99) Choy, E. H.; Gambling, L.; Best, S. L.; Jenkins, R. E.; Kondeatis, E.; Vaughan, R.; Black, M. M.; Sadler, P. J.; Panayi, G. S. *Br. J. Rheumatol.* **1997**, *36*, 1054–1058.
(100) Shaw, C. F.; Schraa, S.; Gleichmann, E.; Grover, Y. P.; Dunemann, L.; Jagarlamudi, A. *Met. Based. Drugs* **1994**, *1*, 351–362.
(101) Kettle, A. J.; Winterbourn, C. C. *Redox Rep.* **1997**, *3*, 3–15.
(102) Isab, A. A.; Sadler, P. J. *Biochim. Biophys. Acta - Protein Struct.* **1977**, *671*, 109–240.
(103) Shaw, C. F.; Cancro, M. P.; Witkiewicz, P. L. *Inorg. Chem.* **1980**, *19*, 3198–3201.
(104) Zou, J.; Guo, Z.; Parkinson, J. A.; Chen, Y.; Sadler, P. J. *Chem. Commun.* **1999**, 1359–1360.
(105) Oryschak, A. F.; Ghadially, F. N. *J. Pathol.* **1976**, *119*, 183–185.
(106) Ghadially, F. N. *J. Rheumatol.* **1979**, *5*, 45–50.
(107) Elder, R. C.; Eidsness, M. K.; Heeg, M. J.; Tepperman, K. G.; Shaw, C. F.; Schaeffer, N. A. *ACS Symp. Ser.* **1983**, *209*, 385–400.
(108) Elder, R. C.; Eidsness, M. K. *Chem. Rev.* **1987**, *87*, 1027–1046.
(109) Snyder, R. M.; Mirabelli, C. K.; Crooke, S. T. *Biochem. Pharmacol.* **1986**, *35*, 923–932.
(110) Shaw, C. F.; Isab, A. A.; Coffer, M. T.; Mirabelli, C. K. *Biochem. Pharmacol.* **1990**, *40*, 1227–1234.
(111) Wang, Q.; Janzen, N.; Ramachandran, C.; Jirik, F. *Biochem. Pharmacol.* **1997**, *54*, 703–711.
(112) Snowden, N.; Dietch, D. M.; Teh, L. S.; Hilton, R. C.; Haeney, M. R. *Ann. Rheum. Dis.* **1996**, *55*, 616–621.
(113) Hirohata, S. *Clin. Immunol. Immunopathol.* **1996**, *81*, 175–181.
(114) Hirohata, S.; Nakanishi, K.; Yanagida, T.; Kawai, M.; Kikuchi, H.; Isshi, K. *Clin. Immunol.* **1999**, *91*, 226–233.
(115) Hirohata, S.; Yanagida, T.; Hashimoto, H.; Tomita, T.; Ochi, T.; Nakamura, H.; Yoshino, S. *Clin. Immunol. Immunopathol.* **1997**, *84*, 290–295.
(116) Yanni, G.; Nabil, M.; Farahat, M. R.; Poston, R. N.; Panayi, G. S. *Ann. Rheum. Dis.* **1994**, *53*, 315–322.
(117) Yadav, R.; Misra, R.; Naik, S. *Int. J. Immunopharmacol.* **1997**, *19*, 111–114.

(118) Mangalam, A. K.; Aggarwal, A.; Naik, S. *Int. Immunopharmacol.* **2001**, *1*, 1165–1172.
(119) Hall, T. J.; Jeker, H.; Nyugen, H.; Schaeublin, M. *Inflamm. Res.* **1996**, *45*, 230–233.
(120) Newman, P. M.; Shun, S.; To, T.; Robinson, B. G.; Hyland, V. J.; Schrieber, L. *J. Clin. Investig.* **1994**, *94*, 1864–1871.
(121) Heimbürger, M.; Lerner, R.; Palmblad, J. *Biochem. Pharmacol.* **1998**, *56*, 1661–1669.
(122) Handel, M. L.; Defazio, A.; Watts, C. K. W.; Day, R. O.; Sutherland, R. L. *Mol. Pharmacol.* **1991**, *40*, 613–618.
(123) Tanaka, H.; Makino, Y.; Wright, K. D.; Gustafsson, J. A.; Okamoto, K.; Makino, I. *Mol. Pharmacol.* **1995**, *48*, 938–945.
(124) Handel, M. L.; Watts, C. K.; deFazio, a; Day, R. O.; Sutherland, R. L. *Proc. Natl. Acad. Sci. U. S. A.* **1995**, *92*, 4497–4501.
(125) Jeon, K. I.; Jeong, J. Y.; Jue, D. M. *J. Immunol.* **2000**, *164*, 5981–5989.
(126) Mellor, H.; Parker, P. J. *Biochem. J.* **1998**, *332*, 281–292.
(127) Hashimoto, K.; Whitehurst, C. E.; Matsubara, T.; Hirohata, K.; Lipsky, P. E. *J. Clin. Invest.* **1992**, *89*, 1839–1848.
(128) Mustacich, D.; Powis, G. *Biochem. J.* **2000**, *346*, 1–8.
(129) Karplus, P. A.; Schulz, G. E. *J. Mol. Biol.* **1987**, *195*, 701–729.
(130) Zhong, L.; Arnér, E. S. J.; Holmgren, A. *Proc. Natl. Acad. Sci. U. S. A.* **2000**, *97*, 5854–5859.
(131) Fritz-Wolf, K.; Urig, S.; Becker, K. *J. Mol. Biol.* **2007**, *370*, 116–127.
(132) Zhong, L.; Arnér, E. S. J.; Ljung, J.; Aslund, F.; Holmgren, A. *J. Biol. Chem.* **1998**, *273*, 8581–8591.
(133) Powis, G.; Mustacich, D.; Coon, A. *Free Radic. Biol. Med.* **2000**, *29*, 312–322.
(134) Holmgren, A. *Annu. Rev. Biochem.* **1985**, *54*, 237–271.
(135) Fritz-Wolf, K.; Kehr, S.; Stumpf, M.; Rahlfs, S.; Becker, K. *Nat. Commun.* **2011**, *2*, 383.
(136) Cheng, Q.; Sandalova, T.; Lindqvist, Y.; Arnér, E. S. J. *J. Biol. Chem.* **2009**, *284*, 3998–4008.
(137) Jeffery, C. J. *Trends Biochem. Sci.* **1999**, *24*, 8–11.
(138) Thelander, L.; Thelander, L.; Reichard, P.; Reichard, P. *Annu. Rev. Biochem.* **1979**, *48*, 133–158.
(139) Arnér, E. S. J.; Holmgren, A. *Eur. J. Biochem.* **2000**, *267*, 6102–6109.
(140) Powis, G.; Montfort, W. R. *Annu. Rev. Biophys. Biomol. Struct.* **2001**, *30*, 421–455.
(141) Kang, S. W.; Chae, H. Z.; Seo, M. S.; Kim, K.; Baines, I. C.; Rhee, S. G. *J. Biol. Chem.* **1998**, *273*, 6297–6302.
(142) Chae, H. Z.; Chung, S. J.; Rhee, S. G. *J. Biol. Chem.* **1994**, *269*, 27670–27678.
(143) Jin, D. Y.; Chae, H. Z.; Rhee, S. G.; Jeang, K. T. *J. Biol. Chem.* **1997**, *272*, 30952–30961.
(144) Brot, N.; Weissbach, H. *Trends Biochem. Sci.* **1982**, *7*, 137–139.
(145) Schenk, H.; Klein, M.; Erdbrügger, W.; Dröge, W.; Schulze-Osthoff, K. *Proc. Natl. Acad. Sci. U. S. A.* **1994**, *91*, 1672–1676.
(146) Psarra, A.-M. G.; Hermann, S.; Panayotou, G.; Spyrou, G. *Biochem. J.* **2009**, *422*, 521–531.
(147) Silverman, M. N.; Sternberg, E. M. *Ann. N. Y. Acad. Sci.* **2012**, *1261*, 55–63.
(148) Saitoh, M.; Nishitoh, H.; Fujii, M.; Takeda, K.; Tobiume, K.; Sawada, Y.; Kawabata, M.; Miyazono, K.; Ichijo, H. *EMBO J.* **1998**, *17*, 2596–2606.

(149) Ericson, M. L.; Horling, J.; Wendelhansen, V.; Holmgren, A.; Rosen, A. *Lymphokine Cytokine Res.* **1992**, *11*, 201–207.
(150) Rubartelli, A.; Bajetto, A.; Allavena, G.; Wollman, E.; Sitia, R. *J. Biol. Chem.* **1992**, *267*, 24161–24164.
(151) Berggren, M.; Gallegos, A.; Gasdaska, J. R.; Gasdaska, P. Y.; Warneke, J.; Powis, G. *Anticancer Res.* **1996**, *16*, 3459–3466.
(152) Schenk, H.; Vogt, M.; Dröge, W.; Schulze-Osthoff, K. *J. Immunol.* **1996**, *156*, 765–771.
(153) Yoshida, S.; Katoh, T.; Tetsuka, T.; Uno, K.; Matsui, N.; Okamoto, T. *J. Immunol.* **1999**, *163*, 351–358.
(154) Fujii, S.; Nanbu, Y.; Nonogaki, H.; Konishi, I.; Mori, T.; Masutani, H.; Yodoi, J. *Cancer* **1991**, *68*, 1583–1591.
(155) Nakamura, H.; Masutani, H.; Tagaya, Y.; Yamauchi, A.; Inamoto, T.; Nanbu, Y.; Fujii, S.; Ozawa, K.; Yodoi, J. *Cancer* **1992**, *69*, 2091–2097.
(156) Nakamura, H.; Bai, J.; Nishinaka, Y.; Ueda, S.; Sasada, T.; Ohshio, G.; Imamura, M.; Takabayashi, A.; Yamaoka, Y.; Yodoi, J. *Cancer Detect. Prev.* **2000**, *24*, 53–60.
(157) Raffel, J.; Bhattacharyya, A. K.; Gallegos, A.; Cui, H.; Einspahr, J. G.; Alberts, D. S.; Powis, G. *J. Lab. Clin. Med.* **2003**, *142*, 46–51.
(158) Lincoln, D. T.; Ali Emadi, E. M.; Tonissen, K. F.; Clarke, F. M. *Anticancer Res.* **2003**, *23*, 2425–2433.
(159) Gladyshev, V. N.; Factor, V. M.; Housseau, F.; Hatfield, D. L. *Biochem. Biophys. Res. Commun.* **1998**, *251*, 488–493.
(160) Kabuyama, Y.; Kitamura, T.; Yamaki, J.; Homma, M. K.; Kikuchi, S.-I.; Homma, Y. *Biochem. Biophys. Res. Commun.* **2008**, *367*, 491–496.
(161) Maurice, M. M.; Nakamura, H.; Gringhuis, S.; Okamoto, T.; Yoshida, S.; Kullmann, F.; Lechner, S.; van der Voort, E. A. M.; Leow, A.; Versendaal, J.; Muller-ladner, U. L. F.; Yodoi, J.; Tak, P. P.; Breedveld, F. C.; Verweij, C. L. *Arthritis Rheum.* **1999**, *42*, 2430–2439.
(162) Arnér, E. S. J. *Exp. Cell Res.* **2010**, *316*, 1296–1303.
(163) Chen, G. Q.; Zhu, J.; Shi, X. G.; Ni, J. H.; Zhong, H. J.; Si, G. Y.; Jin, X. L.; Tang, W.; Li, X. S.; Xong, S. M.; Shen, Z. X.; Sun, G.; Ma, J.; Zhang, P.; Zhang, T. D.; Gazin, C.; Naoe, T.; Chen, S. J.; Wang, Z. Y.; Chen, Z. *Blood* **1996**, *88*, 1052–1061.
(164) Lu, J.; Chew, E.; Holmgren, A. *Proc. Natl. Acad. Sci. U. S. A.* **2007**, *104*, 12288–12293.
(165) Johansson, L.; Chen, C.; Thorell, J.-O.; Fredriksson, A.; Stone-Elander, S.; Gafvelin, G.; Arnér, E. S. J. *Nat. Methods* **2004**, *1*, 61–66.
(166) Arnér, E. S. J.; Nakamura, H.; Sasada, T.; Yodoi, J.; Holmgren, A.; Spyrou, G. *Free Radic. Biol. Med.* **2001**, *31*, 1170–1178.
(167) Witte, A. B.; Anestål, K.; Jerremalm, E.; Ehrsson, H.; Arnér, E. S. J. *Free Radic. Biol. Med.* **2005**, *39*, 696–703.
(168) Becker, K.; Herold-mende, C.; Park, J. J.; Lowe, G.; Schirmer, R. H. *J. Med. Chem.* **2001**, *44*, 2784–2792.
(169) Lo, Y.; Ko, T.; Su, W.; Su, T.; Wang, A. H. *J. Inorg. Biochem.* **2009**, *103*, 1082–1092.
(170) Gromer, S.; Arscott, L. D.; Williams, C. H. *J. Biol. Chem.* **1998**, *273*, 20096–20101.
(171) Rigobello, M. P.; Messori, L.; Marcon, G.; Cinellu, M. A.; Bragadin, M.; Folda, A.; Scutari, G.; Bindoli, A. *J. Inorg. Biochem.* **2004**, *98*, 1634–1641.

(172) Coronnello, M.; Mini, E.; Caciagli, B.; Cinellu, M. A.; Bindoli, A.; Gabbiani, C.; Messori, L. *J. Med. Chem.* **2005**, *48*, 6761–6765.
(173) Engman, L.; McNaughton, M.; Gajewska, M.; Kumar, S.; Birmingham, A.; Powis, G. *Anticancer. Drugs* **2006**, *17*, 539–544.
(174) Bindoli, A.; Rigobello, M. P.; Scutari, G.; Gabbiani, C.; Casini, A.; Messori, L. *Coord. Chem. Rev.* **2009**, *253*, 1692–1707.
(175) Urig, S.; Fritz-Wolf, K.; Réau, R.; Herold-Mende, C.; Tóth, K.; Davioud-Charvet, E.; Becker, K. *Angew. Chemie Int. Ed.* **2006**, *45*, 1881–1886.
(176) Rackham, O.; Nichols, S. J.; Leedman, P. J.; Berners-Price, S. J.; Filipovska, A. *Biochem. Pharmacol.* **2007**, *74*, 992–1002.
(177) Rubbiani, R.; Can, S.; Kitanovic, I.; Alborzinia, H.; Stefanopoulou, M. *J. Med. Chem.* **2011**, *54*, 8646–8657.
(178) Schuh, E.; Pflüger, C.; Citta, A.; Folda, A.; Rigobello, M. P.; Bindoli, A.; Casini, A.; Mohr, F. *J. Med. Chem.* **2012**, *55*, 5518–5528.
(179) Citta, A.; Schuh, E.; Mohr, F.; Folda, A.; Massimino, M. L.; Bindoli, A.; Casini, A.; Rigobello, M. P. *Metallomics* **2013**, *5*, 1006–1015.
(180) Rubbiani, R.; Schuh, E.; Meyer, A.; Lemke, J.; Wimberg, J.; Metzler-Nolte, N.; Meyer, F.; Mohr, F.; Ott, I. *Medchemcomm* **2013**, *4*, 942–948.
(181) Holenya, P.; Can, S.; Rubbiani, R.; Alborzinia, H.; Jünger, A.; Cheng, X.; Ott, I.; Wölfl, S. *Metallomics* **2014**, *6*, 1591–1601.
(182) Zou, T.; Lum, C. T.; Lok, C. N.; To, W. P.; Low, K. H.; Che, C. M. *Angew. Chemie Int. Ed.* **2014**, *53*, 5810–5814.
(183) Rubbiani, R.; Salassa, L.; De Almeida, A.; Casini, A.; Ott, I. *ChemMedChem* **2014**, *9*, 1205–1210.
(184) Meyer, A.; Oehninger, L.; Geldmacher, Y.; Alborzinia, H.; Wölfl, S.; Sheldrick, W. S.; Ott, I. *ChemMedChem* **2014**, *9*, 1794–1800.
(185) Arcau, J.; Andermark, V.; Rodrigues, M.; Giannicchi, I.; Pérez-Garcia, L.; Ott, I.; Rodríguez, L. *Eur. J. Inorg. Chem.* **2014**, *2014*, 6117–6125.
(186) Hickey, J. L.; Ruhayel, R. A.; Barnard, P. J.; Baker, M. V; Berners-Price, S. J.; Filipovska, A. *J. Am. Chem. Soc.* **2008**, *130*, 12570–12571.
(187) Gabbiani, C.; Mastrobuoni, G.; Sorrentino, F.; Dani, B.; Rigobello, M. P.; Bindoli, A.; Cinellu, M. A.; Pieraccini, G.; Messori, L.; Casini, A. *Med. Chem. Commun.* **2011**, *2*, 50–54.
(188) Giljohann, D. A.; Seferos, D. S.; Daniel, W. L.; Massich, M. D.; Patel, P. C.; Mirkin, C. A. *Angew. Chemie Int. Ed.* **2010**, *49*, 3280–3294.
(189) Brown, C. L.; Whitehouse, M. W.; Tiekink, E. R. T.; Bushell, G. R. *Inflammopharmacology* **2008**, *16*, 133–137.
(190) Turkevich, J.; Stevenson, P. C.; Hillier, J. *Discuss. Faraday Soc.* **1951**, *11*, 55–75.
(191) Frens, G. *Kolloid-Zeitschrift und Zeitschrift für Polym.* **1972**, *250*, 736–741.
(192) Brust, M.; Walker, M.; Bethell, D.; Schriffin, D. J.; Whyman, R. *J. Chem. Soc. Chem. Commun.* **1994**, 801–802.
(193) Perrault, S. D.; Chan, W. C. W. *J. Am. Chem. Soc.* **2009**, *131*, 17042–17043.
(194) Martin, M. N.; Basham, J. I.; Chando, P.; Eah, S. K. *Langmuir* **2010**, *26*, 7410–7417.
(195) Abraham, G. E.; Himmel, P. B. *J. Nutr. Environ. Med.* **1997**, *7*, 295–305.
(196) Brown, C. L.; Bushell, G. R.; Whitehouse, M. W.; Agrawal, D. S.; Tupe, S. G.; Paknikar, K.; Tiekink, E. R. T. *Gold Bull.* **2007**, *40*, 245–250.
(197) Chithrani, B. D.; Ghazani, A. A.; Chan, W. C. W. *Nano Lett.* **2006**, *6*, 662–668.
(198) Chithrani, B. D.; Chan, W. C. W. *Nano Lett.* **2007**, *7*, 1542–1550.

(199) Chithrani, B. D.; Stewart, J.; Allen, C.; Jaffray, D. A. *Nanomedicine Nanotechnology, Biol. Med.* **2009**, *5*, 118–127.
(200) Mustafa, T.; Watanabe, F.; Monroe, W.; Mahmood, M.; Xu, Y.; Saeed, L. M.; Karmakar, A.; Casciano, D.; Ali, S.; Biris, A. S. *J. Nanomed. Nanotechnol.* **2011**, *2*.
(201) Shukla, R.; Bansal, V.; Chaudhary, M.; Basu, A.; Bhonde, R. R.; Sastry, M. *Langmuir* **2005**, *21*, 10644–10654.
(202) Yen, H.-J.; Hsu, S.-H.; Tsai, C.-L. *Small* **2009**, *5*, 1553–1561.
(203) Ma, J. S.; Kim, W. J.; Kim, J. J.; Kim, T. J.; Ye, S. K.; Song, M. D.; Kang, H.; Kim, D. W.; Moon, W. K.; Lee, K. H. *Nitric Oxide* **2010**, *23*, 214–219.
(204) Lim, Y. T.; Kim, J. K.; Shin, Y. B.; Chung, B. H. *Adv. Funct. Mater.* **2006**, *16*, 1015–1021.
(205) Leroy, P.; Sapin-Minet, A.; Pitarch, A.; Boudier, A.; Tournebize, J.; Schneider, R. *Nitric Oxide* **2011**, *25*, 54–56.
(206) Liu, Z.; Li, W.; Wang, F.; Sun, C.; Wang, L.; Wang, J.; Sun, F. *Nanoscale* **2012**, *4*, 7135–7142.
(207) Brewer, S. H.; Glomm, W. R.; Johnson, M. C.; Knag, M. K.; Franzen, S. *Langmuir* **2005**, *21*, 9303–9307.
(208) De Paoli Lacerda, S. H.; Park, J. J.; Meuse, C.; Pristinski, D.; Becker, M. L.; Karim, A.; Douglas, J. F. *ACS Nano* **2010**, *4*, 365–379.
(209) Liu, R.; Wang, Y.; Yuan, Q.; An, D.; Li, J.; Gao, X. *Chem. Commun.* **2014**, *50*, 10687–10690.
(210) Tedesco, S.; Doyle, H.; Blasco, J.; Redmond, G.; Sheehan, D. *Comp. Biochem. Physiol. - C Toxicol. Pharmacol.* **2010**, *151*, 167–174.
(211) Srivastava, M.; Singh, S.; Self, W. T. *Environ. Health Perspect.* **2012**, *120*, 56–61.
(212) Mosmann, T. *J. Immunol. Methods* **1983**, *65*, 55–63.
(213) Hayon, T.; Dvilansky, A.; Shpilberg, O.; Nathan, I. *Leuk. Lymphoma* **2003**, *44*, 1957–1962.
(214) Davis, K. J.; Carrall, J. A.; Lai, B.; Aldrich-Wright, J. R.; Ralph, S. F.; Dillon, C. T. *Dalt. Trans.* **2012**, *41*, 9417–9426.
(215) Paunesku, T.; Vogt, S.; Maser, J.; Lai, B.; Woloschak, G. *J. Cell. Biochem.* **2006**, *99*, 1489–1502.
(216) Paterson, D.; de Jonge, M. D.; Howard, D. L.; Lewis, W.; McKinlay, J.; Starritt, A.; Kusel, M.; Ryan, C. G.; Kirkham, R.; Moorhead, G.; Siddons, D. P.; McNulty, I.; Eyberger, C.; Lai, B. *AIP Conf. Proc.* **2011**, *219*, 219–222.
(217) Munro, K. L.; Mariana, A.; Klavins, A. I.; Foster, A. J.; Lai, B.; Vogt, S.; Cai, Z.; Harris, H. H.; Dillon, C. T. *Chem. Res. Toxicol.* **2008**, *21*, 1760–1769.
(218) Hummer, A. a; Rompel, A. *Metallomics* **2013**, *5*, 597–614.
(219) Dillon, C. T. *Aust. J. Chem.* **2012**, *65*, 204–217.
(220) Dillon, C. T.; Lay, P. A.; Kennedy, B. J.; Stampfl, A. P. J.; Cai, Z.; Ilinski, P.; Rodrigues, W.; Legnini, D. G.; Lai, B.; Maser, J. *J. Biol. Inorg. Chem.* **2002**, *7*, 640–645.
(221) Waern, J. B.; Harris, H. H.; Lai, B.; Cai, Z.; Harding, M. M.; Dillon, C. T. *J. Biol. Inorg. Chem.* **2005**, *10*, 443–452.
(222) Carter, E. A.; Rayner, B. S.; McLeod, A. I.; Wu, L. E.; Marshall, C. P.; Levina, A.; Aitken, J. B.; Witting, P. K.; Lai, B.; Cai, Z.; Vogt, S.; Lee, Y.-C.; Chen, C.-I.; Tobin, M. J.; Harris, H. H.; Lay, P. A. *Mol. Biosyst.* **2010**, *6*, 1316–1322.
(223) Weekley, C. M.; Aitken, J. B.; Vogt, S.; Finney, L. A.; Paterson, D. J.; De Jonge, M. D.; Howard, D. L.; Musgrave, I. F.; Harris, H. H. *Biochemistry* **2011**, *50*,

1641–1650.
(224) Sun, J.; Zhang, X.; Broderick, M.; Fein, H. *Sensors* **2003**, *3*, 276–284.
(225) Chen, X.; Zhong, Z.; Xu, Z.; Chen, L.; Wang, Y. *Free Radic. Res.* **2010**, *44*, 587–604.
(226) Bartlett, R.; Yerbury, J. J.; Sluyter, R. *Mediators Inflamm.* **2013**, *2013*.
(227) Talib, J. Analysis of the Reactivty of Human Serum Albumin with Gold(I)-based Anti-Arthritic Drugs Using Electrospray Ionisation Mass Spectrometry, University of Wollongong, 2004.
(228) SIB Swiss Institute of Bioinformatics. ExPASy - ProtParam Tool http://web.expasy.org/protparam/.
(229) Gasteiger, E.; Hoogland, C.; Gattiker, A.; Duvaud, S.; Wilkins, M. R.; Appel, R. D.; Bairoch, A. In *The Proteomics Protocols Handbook*; Walker, J. M., Ed.; Humana Press, 2005; pp. 571–607.
(230) Perkins, D. N.; Pappin, D. J. C.; Creasy, D. M.; Cottrell, J. S. *Electrophoresis* **1999**, *20*, 3551–3567.
(231) Link, S.; Wang, Z. L.; El-Sayed, M. A. *J. Phys. Chem. B* **1999**, *103*, 3529–3533.
(232) Shalkevich, N.; Shalkevich, A.; Si-Ahmed, L.; Bürgi, T. *Phys. Chem. Chem. Phys.* **2009**, *11*, 10175–10179.
(233) Doyen, M.; Bartik, K.; Bruylants, G. *J. Colloid Interface Sci.* **2013**, *399*, 1–5.
(234) Berne, B. J.; Pecora, R. *Dynamic Light Scattering: With Applications to Chemistry, Biology, and Physics*; Courier Corporation: Toronto, 2000.
(235) Lee, S.; Kim, E.; Hyun, S.-H. *Int. J. Mol. Med.* **2014**, *34*, 1372–1380.
(236) Yu, Z.-W.; Quinn, P. J. *Biosci. Rep.* **1994**, *14*, 259–281.
(237) Marzano, C.; Gandin, V.; Folda, A.; Scutari, G.; Bindoli, A.; Rigobello, M. P. *Free Radic. Biol. Med.* **2007**, *42*, 872–881.
(238) Snyder, R. M.; Mirabelli, C. K.; Crooke, S. T. *Biochem. Pharmacol.* **1987**, *36*, 647–654.
(239) Graham, G. G.; Whitehouse, M. W.; Bushell, G. R. *Inflammopharmacology* **2008**, *16*, 126–132.
(240) Wu, M. L.; Tsai, W. J.; Ger, J.; Deng, J. F.; Tsay, S. H.; Yang, M. H. *J. Toxicol. Clin. Toxicol.* **2001**, *39*, 739–743.
(241) Karadağ, A.; Aydın, A.; Dede, S.; Tekin, Ş.; Yanar, Y.; Çadırcı, B. H.; Soylu, M. S.; Andaç, Ö. *New J. Chem.* **2015**, *39*, 8136–8152.
(242) Gabriel, J. M. *J. Hist. Med. Allied Sci.* **2013**, *69*, 604–632.
(243) Omata, Y.; Folan, M.; Shaw, M.; Messer, R. L.; Lockwood, P. E.; Hobbs, D.; Bouillaguet, S.; Sano, H.; Lewis, J. B.; Wataha, J. C. *Toxicol. Vitr.* **2006**, *20*, 882–890.
(244) Calamai, P.; Carotti, S.; Guerri, A.; Mazzei, T.; Messori, L.; Mini, E.; Orioli, P.; Speroni, G. P. *Anticancer. Drug Des.* **1998**, *13*, 67–80.
(245) Vijayakumar, S.; Ganesan, S. *J. Nanomater.* **2012**, *2012*.
(246) Gerber, R. C.; Paulus, H. E.; Bluestone, R.; Pearson, C. M. *Ann. Rheum. Dis.* **1972**, *31*, 308–310.
(247) Heath, M. J.; Gillett, G. T.; Swannell, A. J.; Williams, C. R.; Palmer, T. *Ann. Rheum. Dis.* **1987**, *46*, 827–829.
(248) Heath, M. J. *Ann. Rheum. Dis.* **1988**, *47*, 18–21.
(249) Varghese, E.; Büsselberg, D. *Cancers* **2014**, *6*, 2243–2258.
(250) Grootveld, M.; Blake, D. R.; Sahinoglu, T.; Claxson, A. W.; Mapp, P.; Stevens, C.; Allen, R. E.; Furst, A. *Free Radic. Res. Commun.* **1990**, *10*, 199–220.
(251) Burdette, D. L.; Yarbrough, M. L.; Orvedahl, A.; Gilpin, C. J.; Orth, K. *Proc. Natl. Acad. Sci. U. S. A.* **2008**, *105*, 12497–12502.

(252) Aderem, A.; Underhill, D. M. *Annu. Rev. Immmunology* **1999**, *17*, 593–623.
(253) Bozzola, J. J.; Russell, L. D. *Electron Microscopy: Principles and Techniques for Biologists*; Second.; Jones and Bartlett Publishers: Sudbury, USA, 1999.
(254) Goldstein, A.; Soroka, Y.; Frušić-Zlotkin, M.; Popov, I.; Kohen, R. *J. Microsc.* **2014**, *256*, 237–247.
(255) Bondeson, J.; Sundler, R. *Biochem. Pharmacol.* **1995**, *50*, 1753–1759.
(256) Trávníček, Z.; Starha, P.; Vančo, J.; Silha, T.; Hošek, J.; Suchý, P.; Pražanová, G. *J. Med. Chem.* **2012**, *55*, 4568–4579.
(257) Yamashita, M.; Niki, H.; Yamada, M.; Mue, S.; Ohuchi, K. *Eur. J. Pharmacol.* **1997**, *338*, 151–158.
(258) Youn, H. S.; Lee, J. Y.; Saitoh, S. I.; Miyake, K.; Hwang, D. H. *Biochem. Biophys. Res. Commun.* **2006**, *350*, 866–871.
(259) Han, S.; Kim, K.; Kim, H.; Kwon, J.; Lee, Y.-H.; Lee, C.-K.; Song, Y.; Lee, S.-J.; Ha, N.; Kim, K. *Arch. Pharm. Res.* **2008**, *31*, 67–74.
(260) Danis, V. A.; Kulesz, A. J.; Nelson, D. S.; Brooks, P. M. *Clin. Exp. Immunol.* **1990**, *79*, 335–340.
(261) Yamamato, Y.; He, P.; Klein, T. W.; Friedman, H. *J. Endotoxin Res.* **1994**, *1*, 181–187.
(262) Zetterstrom, C. K.; Jiang, W.; Wahamaa, H.; Ostberg, T.; Aveberger, A.-C.; Schierbeck, H.; Lotze, M. T.; Andersson, U.; Pisetsky, D. S.; Harris, H. E. *J. Leukoc. Biol.* **2008**, *83*, 31–38.
(263) Vuolteenaho, K.; Kujala, P.; Moilanen, T.; Moilanen, E. *Scand. J. Rheumatol.* **2005**, *34*, 475–479.
(264) Belsky, Y. P.; Ivanova, A. N.; Danilets, M. G.; Belska, N. V; Ligatcheva, A. A.; Uchasova, E. G.; Reikhart, D. V. *Bull. Exp. Biol. Med.* **2011**, *151*, 190–193.
(265) Philpott, N. J.; Turner, A. J.; Scopes, J.; Westby, M.; Marsh, J. C.; Gordon-Smith, E. C.; Dalgleish, A. G.; Gibson, F. M. *Blood* **1996**, *87*, 2244–2251.
(266) Daigneault, M.; Preston, J. A.; Marriott, H. M.; Whyte, M. K. B.; Dockrell, D. H. *PLoS One* **2010**, *5*, e8668.
(267) Cardaci, S.; Filomeni, G.; Rotilio, G.; Ciriolo, M. R. *Mol. Pharmacol.* **2008**, *74*, 1234–1245.
(268) Walz, D. T.; DiMartino, M. J.; Griswold, D. E.; Intoccia, A. P.; Flanagan, T. L. *Am. J. Med.* **1983**, *75*, 90–108.
(269) Davis, P.; Johnston, C.; Miller, C. L.; Wong, K. *Arthritis Rheum.* **1983**, *26*, 82–86.
(270) Miyachi, Y.; Yoshioka, A.; Imamura, S.; Niwa, Y. *Br. J. Rheumatol.* **1987**, *116*, 39–46.
(271) Roisman, F. R.; Walz, D. T.; Finkelstein, A. E. *Inflammation* **1983**, *7*, 355–362.
(272) Hurst, N. P.; Gorjatschko, L.; Betts, W. H.; Zalewski, P. D.; Forbes, I. J. *Rheumatol. Int.* **1989**, *8*, 245–250.
(273) Corey, E. J.; Mehrotra, M. M.; Khan, A. U. *Science* **1987**, *236*, 68–69.
(274) Kataoka, K.; Handa, H.; Nishizawa, M. *J. Biol. Chem.* **2001**, *276*, 34074–34081.
(275) Piryazev, A. P.; Azizova, O. A.; Aseichev, A. V; Dudnik, L. B.; Sergienko, V. I. *Bull. Exp. Biol. Med.* **2013**, *156*, 101–103.
(276) Barathmanikanth, S.; Kalishwaralal, K.; Sriram, M.; Pandian, S. R. K.; Youn, H.-S.; Eom, S.; Gurunathan, S. *J. Nanobiotechnology* **2010**, *8*.
(277) Mateo, D.; Morales, P.; Ávalos, A.; Haza, A. I. *Toxicol. Mech. Methods* **2014**, *24*, 161–172.
(278) Pan, Y.; Leifert, A.; Ruau, D.; Neuss, S.; Bornemann, J.; Schmid, G.; Brandau, W.; Simon, U.; Jahnen-Dechent, W. *Small* **2009**, *5*, 2067–2076.

(279) Chompoosor, A.; Saha, K.; Ghosh, P. S.; Macarthy, D. J.; Miranda, O. R.; Zhu, Z.-J.; Arcaro, K. F.; Rotello, V. M. *Small* **2010**, *6*, 2246–2249.
(280) Van Der Bruggen, T.; Nijenhuis, S.; Van Raaij, E.; Verhoef, J.; Van Asbeck, B. S. *Infect. Immun.* **1999**, *67*, 3824–3829.
(281) Rouzer, C. A.; Jacobs, A. T.; Nirodi, C. S.; Kingsley, P. J.; Morrow, J. D.; Marnett, L. J. *J. Lipid Res.* **2005**, *46*, 1027–1037.
(282) Xue, B.; Wu, Y.; Yin, Z.; Zhang, H.; Sun, S.; Yi, T.; Luo, L. *FEBS Lett.* **2005**, *579*, 4081–4087.
(283) Bastús, N. G.; Sánchez-Tilló, E.; Pujals, S.; Farrera, C.; Kogan, M. J.; Giralt, E.; Celada, A.; Lloberas, J.; Puntes, V. *Mol. Immunol.* **2009**, *46*, 743–748.
(284) Evans, G. F.; Zuckerman, S. H. *Agents Actions* **1989**, *26*, 329–334.
(285) Mangalam, A. K.; Aggarwal, A.; Naik, S. *Cell. Immunol.* **2002**, *219*, 1–10.
(286) Eberlein, M.; Scheibner, K. a; Black, K. E.; Collins, S. L.; Chan-Li, Y.; Powell, J. D.; Horton, M. R. *J. Inflamm.* **2008**, *5*.
(287) Kingston, M.; Pfau, J. C.; Gilmer, J.; Brey, R. *J. Immunotoxicol.* **2016**, *13*, 198–208.
(288) Howard, M.; O'Garra, A. *Immunol. Today* **1992**, *13*, 198–200.
(289) Bogdan, C.; Vodovotz, Y.; Nathan, C. *J. Exp. Med.* **1991**, *174*, 1549–1555.
(290) Lampa, J.; Klareskog, L.; Ronnelid, J. *J. Rheumatol.* **2002**, *29*, 21–28.
(291) Liptrott, N. J.; Kendall, E.; Nieves, D. J.; Farrell, J.; Rannard, S.; Fernig, D. G.; Owen, A. *Nanomedicine* **2014**, *9*, 1–13.
(292) Gurung, P.; Li, B.; Subbarao Malireddi, R. K.; Lamkanfi, M.; Geiger, T. L.; Kanneganti, T.-D. *Sci. Rep.* **2015**, *5*.
(293) Becker, K.; Gromer, S.; Schirmer, R. H.; Müller, S. *Eur. J. Biochem.* **2000**, *267*, 6118–6125.
(294) Fujii, T.; Hamaoka, R.; Fujii, J.; Taniguchi, N. *Arch. Biochem. Biophys.* **2000**, *378*, 123–130.
(295) Heiss, E.; Gerhäuser, C. *Antioxid. Redox Signal.* **2005**, *7*, 1601–1611.
(296) Zhang, G.; Nitteranon, V.; Guo, S.; Qiu, P.; Wu, X.; Li, F.; Xiao, H.; Hu, Q.; Parkin, K. L. *Chem. Res. Toxicol.* **2013**, *26*, 456–464.
(297) Gasdaska, J. R.; Harney, J. W.; Gasdaska, P. Y.; Powis, G.; Berry, M. J. *J. Biol. Chem.* **1999**, *274*, 25379–25385.
(298) Lössl, P.; Snijder, J.; Heck, A. J. R. *J. Am. Soc. Mass Spectrom.* **2014**, *25*, 906–917.
(299) Geoghegan, K. F.; Dixon, H. B. F.; Rosner, P. J.; Hoth, L. R.; Lanzetti, A. J.; Borzilleri, K. A.; Marr, E. S.; Pezzullo, L. H.; Martin, L. B.; LeMotte, P. K.; McColl, A. S.; Kamath, A. V; Stroh, J. G. *Anal. Biochem.* **1999**, *267*, 169–184.
(300) Nilsson, J.; Stahl, S.; Lundeberg, J.; Uhle, M.; Nygren, P.-A. *Protein Expr. Purif.* **1997**, *11*, 1–16.
(301) Trauger, S. a.; Webb, W.; Siuzdak, G. *Spectroscopy* **2002**, *16*, 15–28.
(302) Isab, A. A.; Sadler. *J. Chem. Soc. Dalt. Trans.* **1982**, 135–141.
(303) Shaw, C. F.; Coffer, M. T.; Klingbeil, J.; Mirabelli, C. K. *J. Am. Chem. Soc.* **1988**, *110*, 729–734.
(304) Page, F. M. *J. Chem. Soc.* **1953**, 1719–1724.
(305) UniProtKB - P12928 http://www.uniprot.org/uniprot/P12928 (accessed Jan 20, 2015).

Appendix A:

Preparation of Solutions used in Cell Assays and Graphite Furnace Operating Conditions

A.1 PBS

PBS solution was prepared by dissolving one Oxoid (Thermo Fisher) PBS tablet in Milli-Q H_2O and diluting to a final volume of 100 mL. This solution was then sterilized by autoclaving and stored at 4 °C.

A.2 Saline Solution

Trace metals pure saline solution was prepared by dissolving 0.90 g of trace metals pure NaCl in Milli-Q H_2O, which was diluted to a final volume of 100 mL and stored at 4 °C.

A.3 D-PBS

D-PBS was prepared by dissolving 0.20 g KCl, 0.20 g KH_2PO_4, 8.00 g NaCl and 1.14 g of Na_2HPO_4 in Milli-Q H_2O, which was diluted to a final volume of 1.00 L and stored at 4 °C.

A.4 10×D-PBS

10×D-PBS was prepared by dissolving 0.20 g KCl, 0.20 g KH_2PO_4, 8.00 g NaCl and 1.14 g of Na_2HPO_4 in ~90 mL of Milli-Q H_2O, and adjusting the pH to 7.4 if necessary, before being diluted to 100 mL and stored at 4 °C.

A.5 ELISA Wash Buffer

ELISA wash buffer was prepared similarly, by adding 500 µL of TWEEN to D-PBS solution prior to the final dilution to a volume of 1.00 L. This resulted in a solution with a final concentration of 0.5% v/v TWEEN/D-PBS, which was passed through a 20 µm filter before use.

A.6 Incomplete NaCl Medium

Incomplete NaCl medium was prepared by first dissolving 0.20 g NaOH, 0.38 g KCl, 2.39 g HEPES and 8.18 g NaCl in ~900 mL of Milli-Q H_2O, and adjusting the pH to 7.5 with 1 M NaOH solution. The solution was then diluted to a final volume of 1.00 L using Milli-Q H_2O and stored at 4 °C.

A.7 Complete NaCl Medium

Complete NaCl medium was prepared by addition of 0.09 g of glucose to 100 mL of incomplete NaCl medium, then re-adjusting the pH to 7.5 if required. The solution was stored at -20 °C.

A.8 TrxR Dialysis Buffers

TrxR dialysis buffers were prepared by first dissolving 3.85 g (100 mM) or 19.27 g (500 mM) ammonium acetate in ~450 mL of Milli-Q H_2O. The pH of the solution was then adjusted to 7.2 with 1 M ammonia and acetic acid solution as required and diluted to a final volume of 500 mL using Milli-Q H_2O before being stored at 4 °C. For buffers containing DTT, 77.1 mg of DTT was added to the final solution immediately prior to dialysis.

A.9 Graphite Furnace AAS Operating Conditions

Table A.1: Operating conditions for analysis of gold in digested cell samples using GFAAS.

Stage	Temperature (°C)	Ramp Time (s)	Hold Time (s)	Gas Flow (mL/min)
Dry 1	110	1	30	250
Dry 2	130	15	30	250
Ash	800	10	20	250
Atomization	1800	0	5	0
Clean Out	2450	1	3	250

Appendix B:

SR-XRF Images & Spectra

B.1 Microprobe SR-XRF Images

B.1.1 Advanced Photon Source

All samples were prepared by incubating the cells with the treatment solution at 37 °C under an atmosphere of 5% CO_2 for 24 h. All maps were collected with the following operating conditions: beam energy = 13.450 keV; beam size = 0.5 µm; step size = 0.5 µm; and dwell time = 0.5 s/pt. All elemental concentrations below each map have the units µg/cm^2.

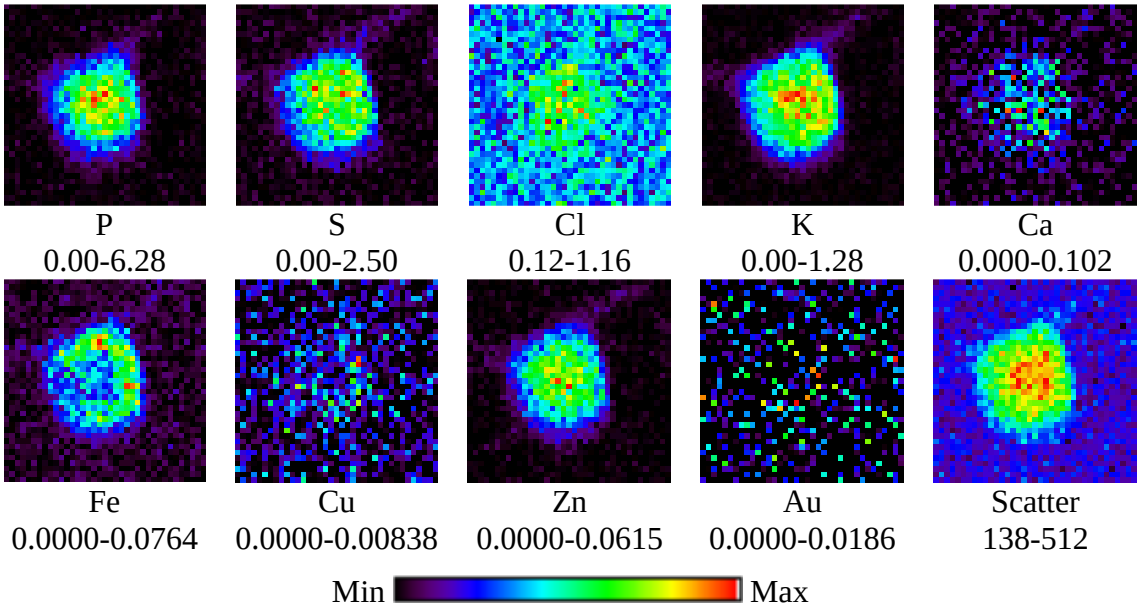

Figure B.1: Microprobe SR-XRF elemental maps obtained from RAW264.7 cells treated with treatment medium only. Scan dimensions (H x V) were 18.5 µm × 18.5 µm.

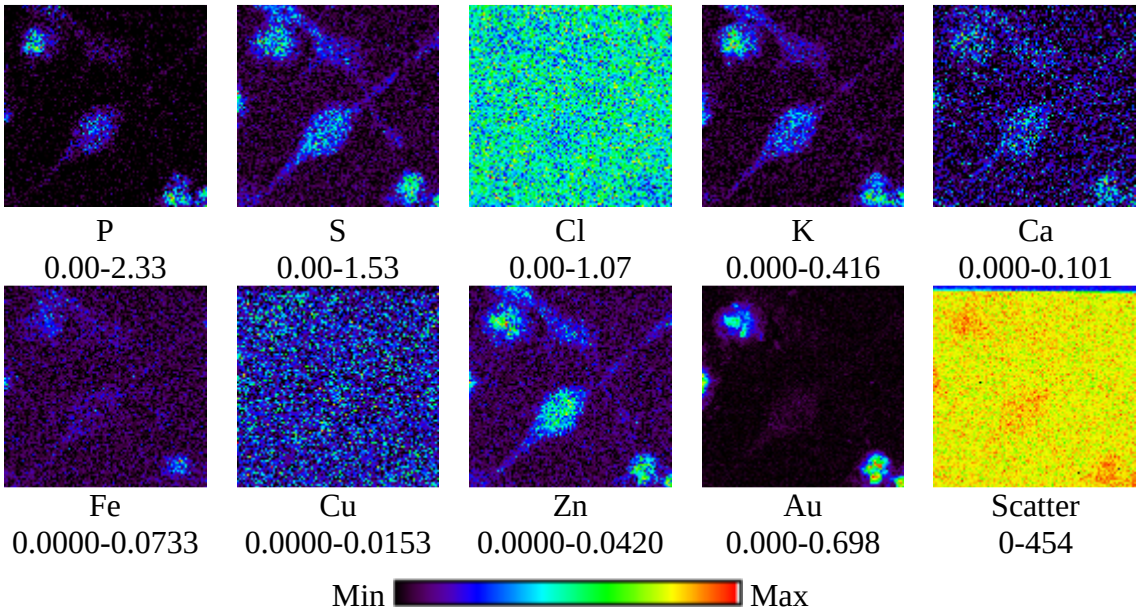

Figure B.2: Microprobe SR-XRF elemental maps obtained from RAW264.7 cells treated with 2.5 µM auranofin. Scan dimensions (H x V) were 50.5 µm × 50.5 µm.

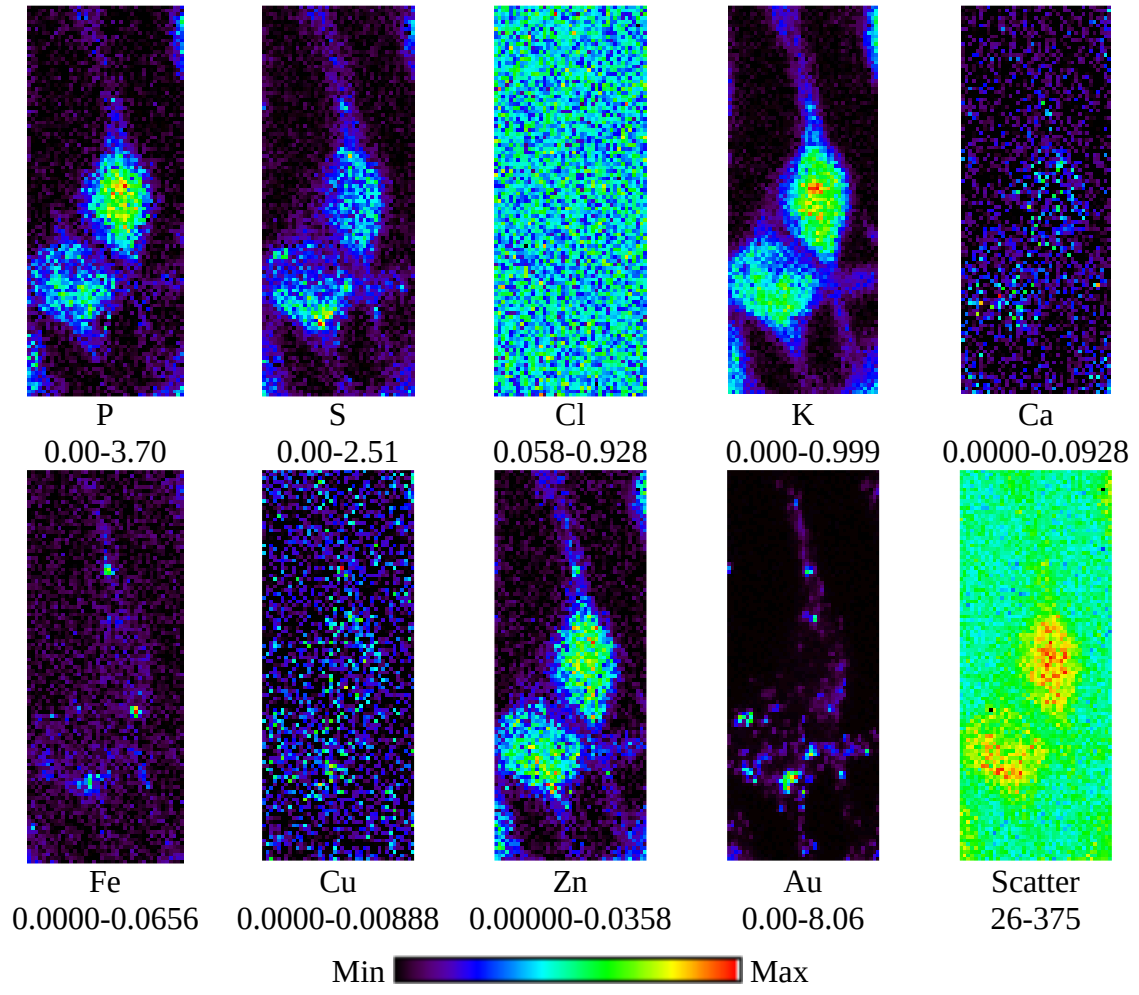

Figure B.3: Microprobe SR-XRF elemental maps obtained from RAW264.7 cells treated with 1000 µM aurothiomalate. Scan dimensions (H x V) were 20.5 µm × 52.5 µm.

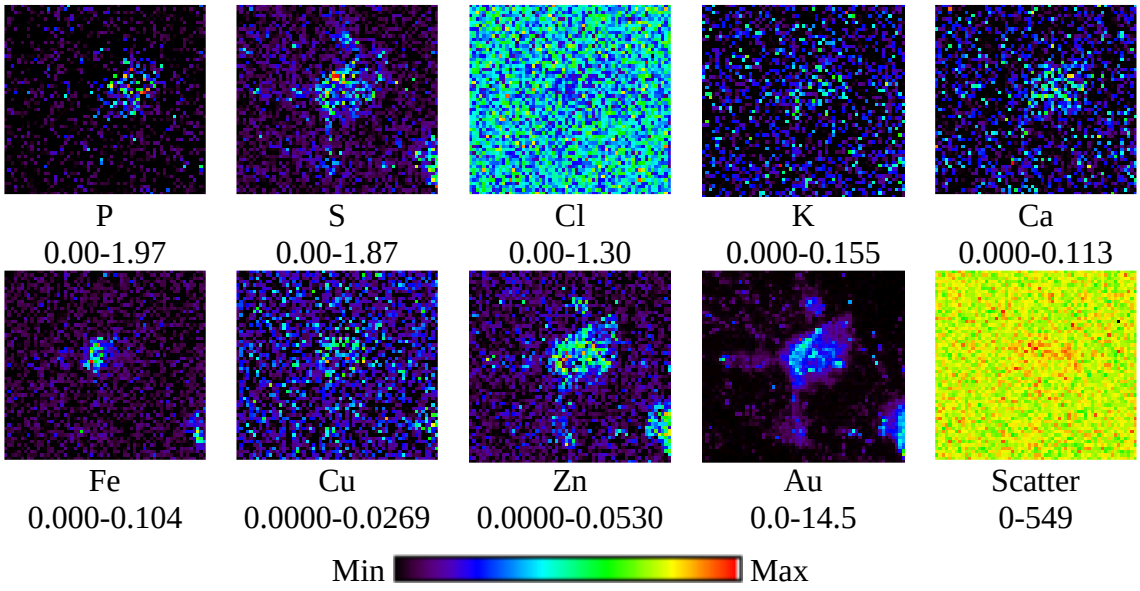

Figure B.4: Microprobe SR-XRF elemental maps obtained from RAW264.7 cells treated with 100 µM $HAuCl_4$. Scan dimensions (H x V) were 30.5 µm × 28.5 µm.

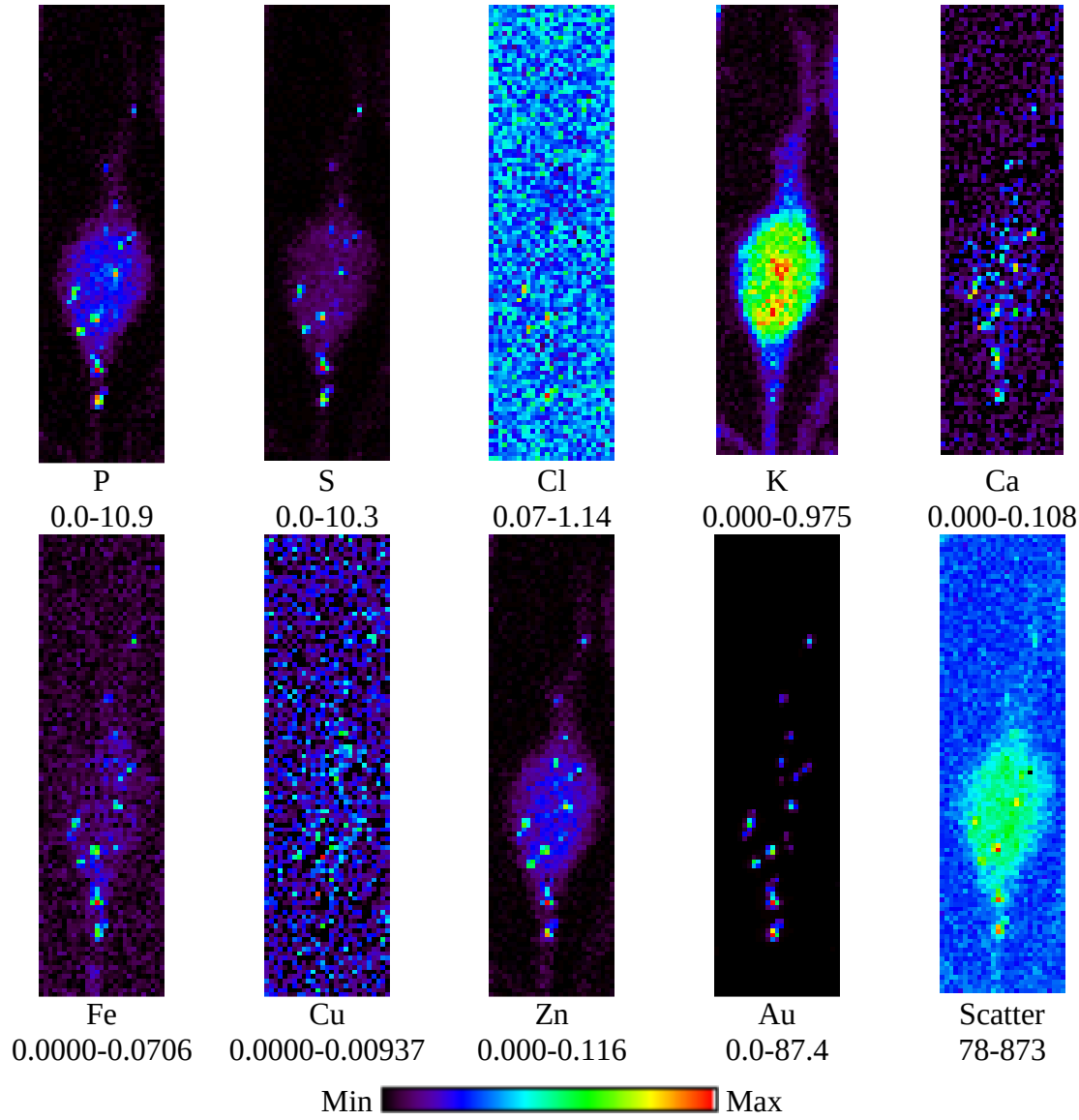

Figure B.5: Microprobe SR-XRF elemental maps obtained from RAW264.7 cells treated with 60 µM Au NPs. Scan dimensions (H x V) were 13.5 µm × 50.5 µm.

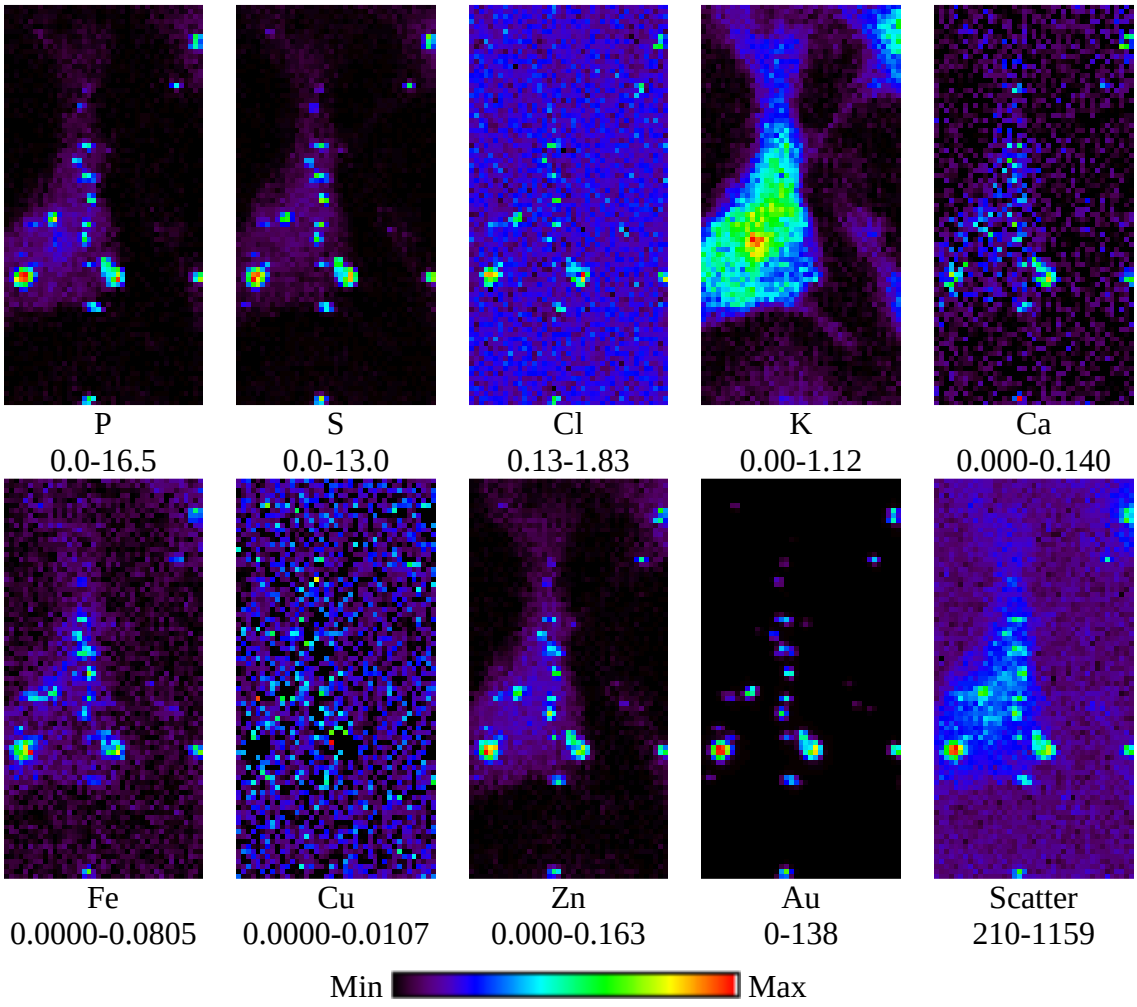

Figure B.6: Microprobe SR-XRF elemental maps obtained from a second set of RAW264.7 cells treated with 60 µM Au NPs. Scan dimensions (H x V) were 20.5 µm × 40.5 µm.

B.1.2 Australian Synchrotron

All samples were prepared by incubating the cells with the treatment solution at 37 °C under an atmosphere of 5% CO_2 for 24 h. All maps were collected with the following operating conditions: beam energy = 12.055 keV; beam size = 2 µm; step size = 2 µm; dwell time = 1 s/pt; and scan dimensions (H × V) 120 µm × 120 µm. All values below each map represent relative quantifications of the elements and are unitless.

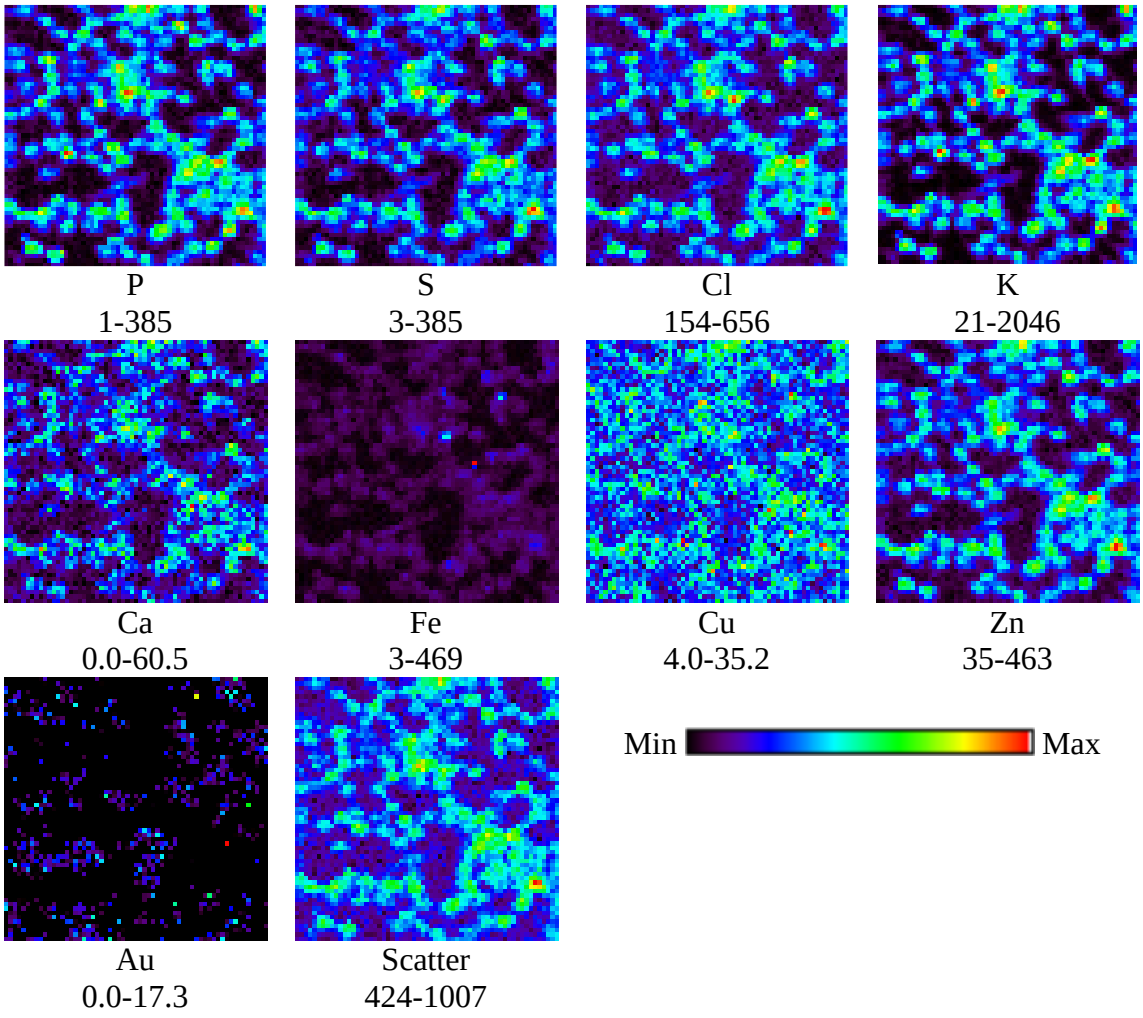

Figure B.7: Microprobe SR-XRF elemental maps for RAW264.7 cells treated with treatment medium only.

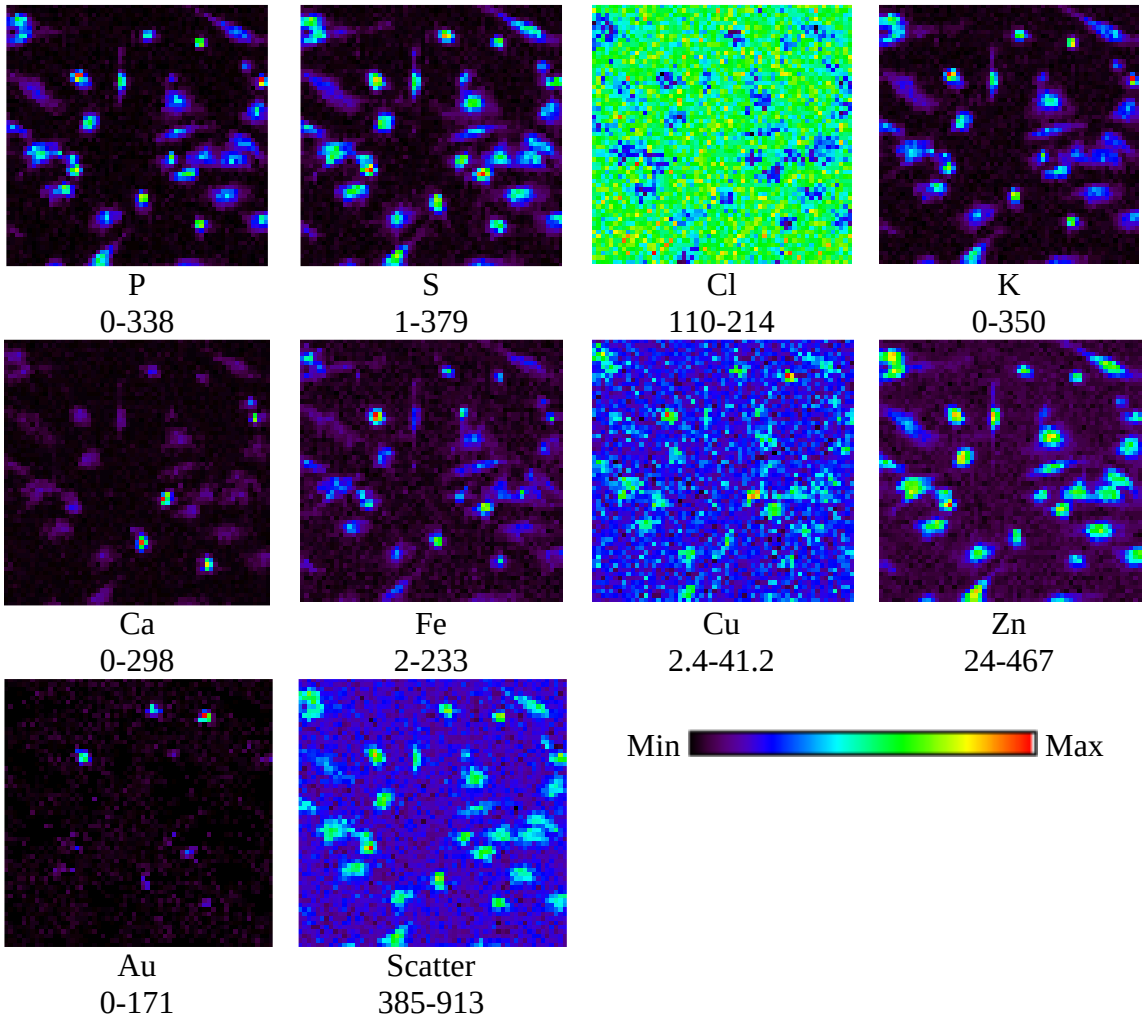

Figure B.8: Microprobe SR-XRF elemental maps for RAW264.7 cells treated with 2.5 µM auranofin.

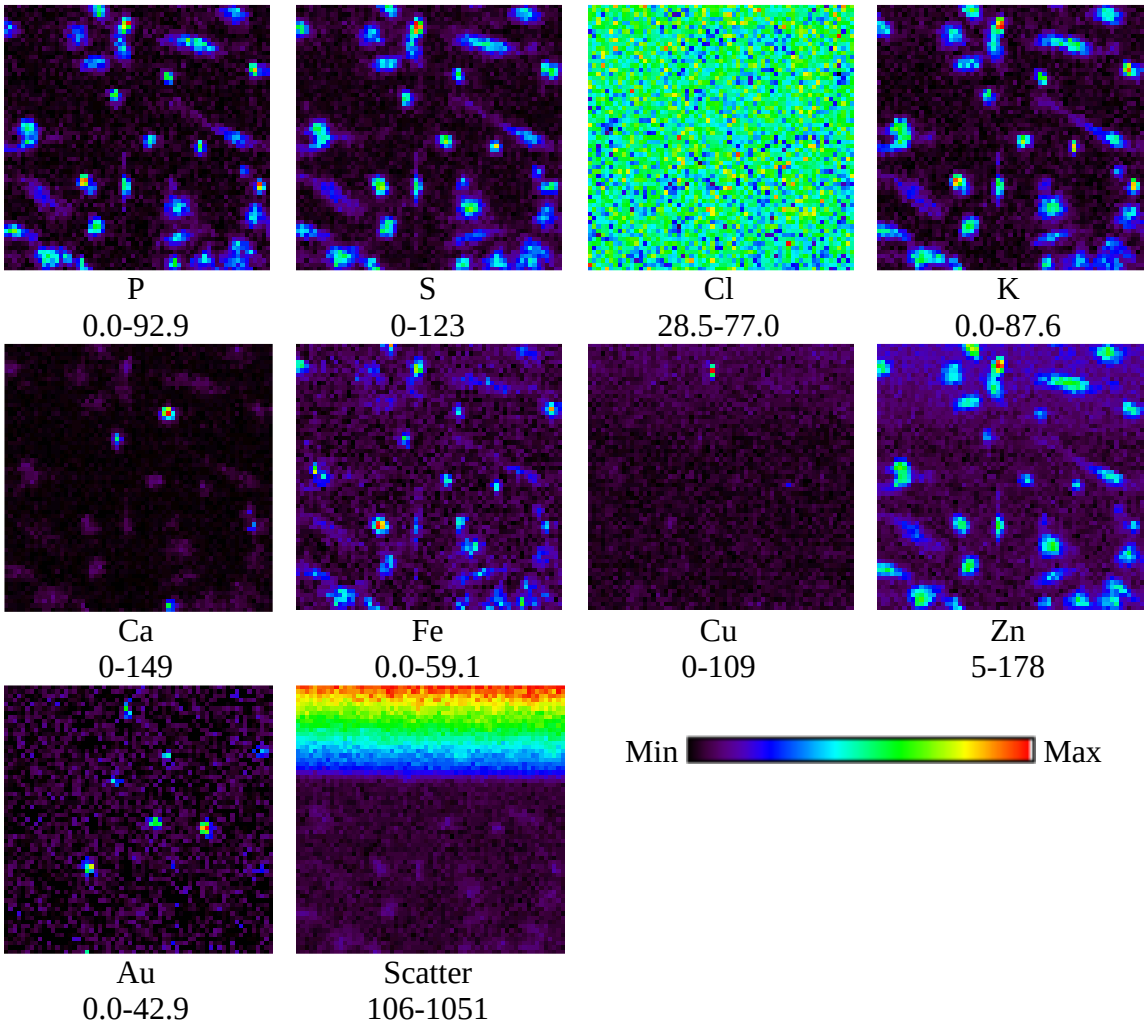

Figure B.9: Microprobe SR-XRF elemental maps for a second set of RAW264.7 cells treated with 2.5 µM auranofin.

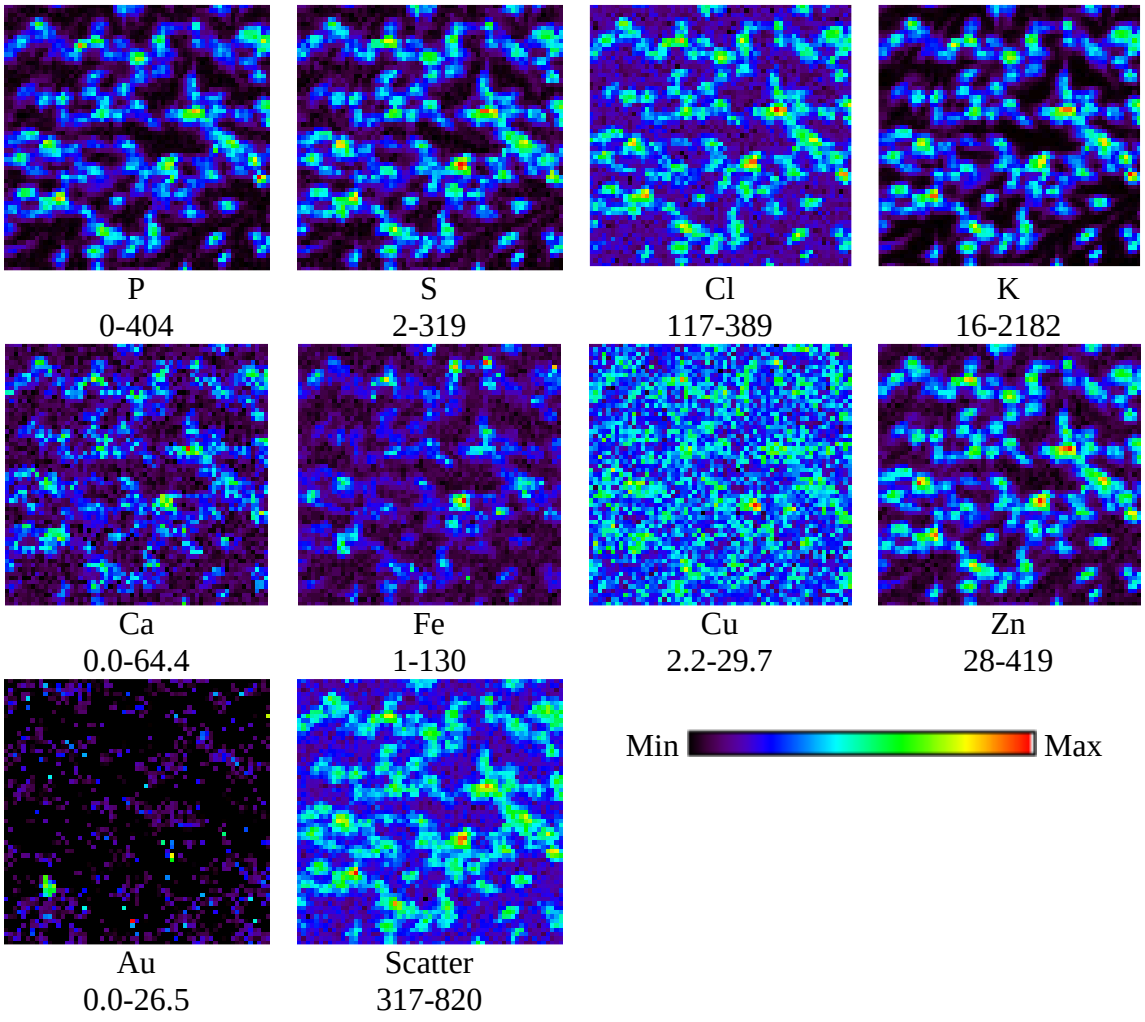

Figure B.10: Microprobe SR-XRF elemental maps for RAW264.7 cells treated with 2.5 µM aurothiosulfate.

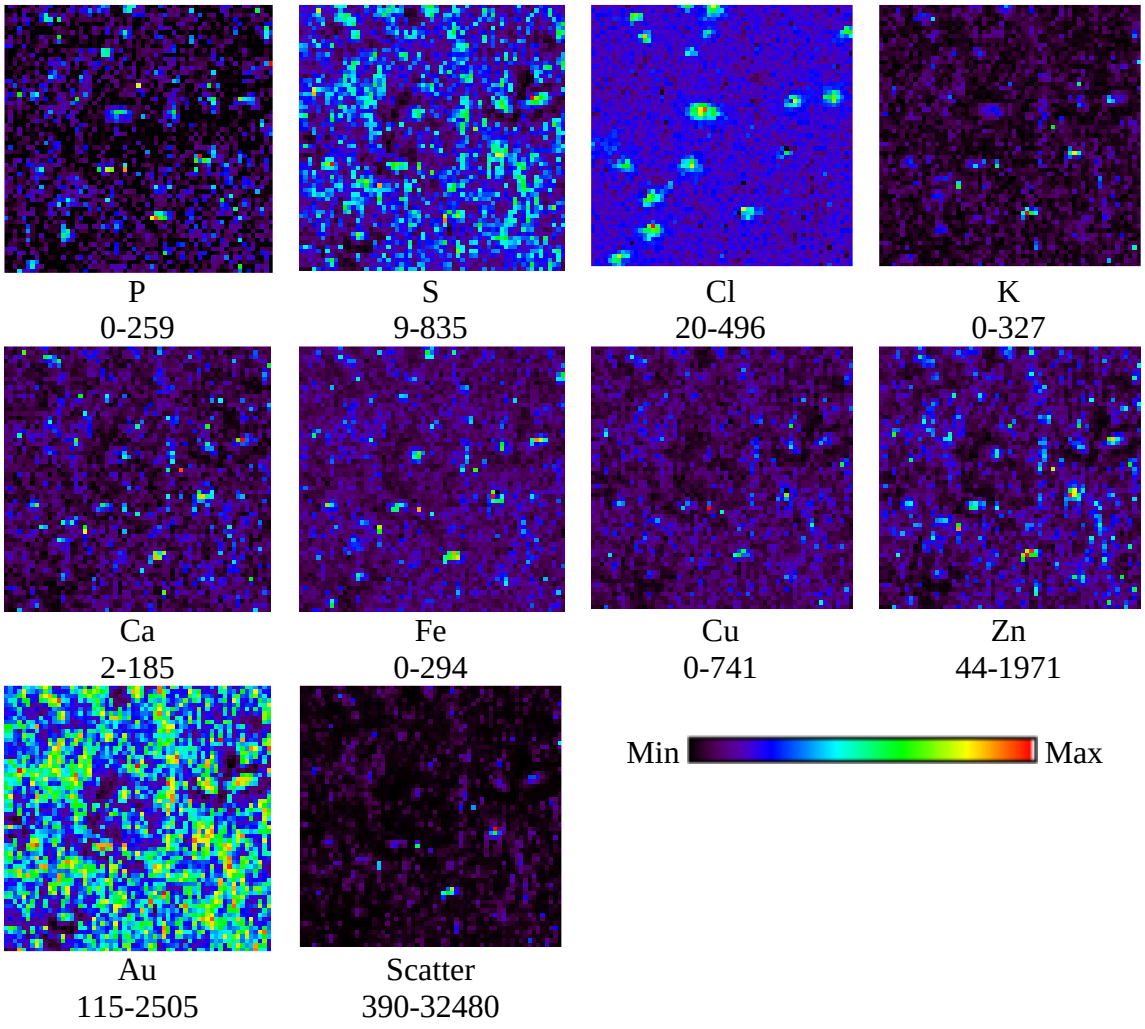

Figure B.11: Microprobe SR-XRF elemental maps for RAW264.7 cells treated with 500 µM aurothiosulfate.

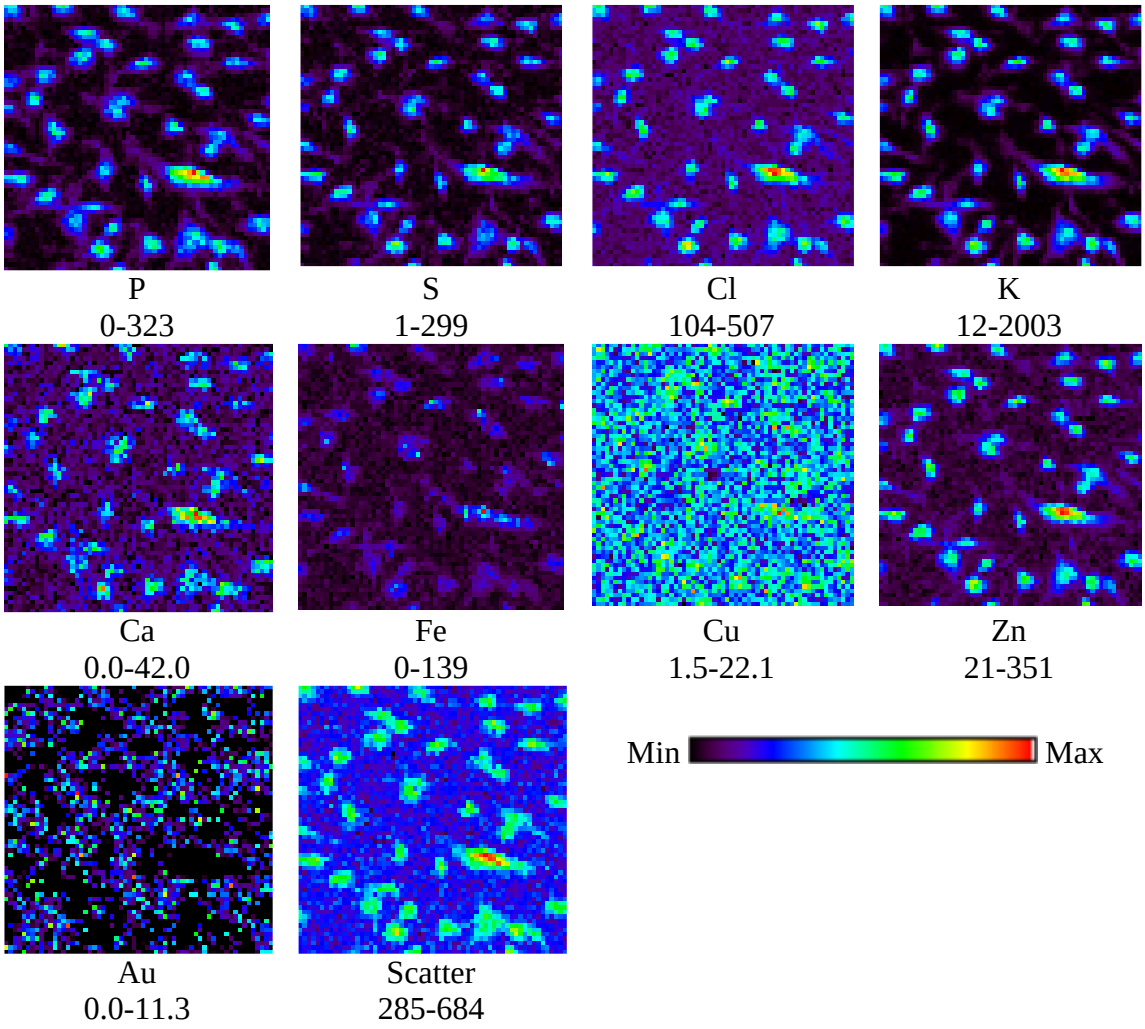

Figure B.12: Microprobe SR-XRF elemental maps for RAW264.7 cells treated with 2.5 µM aurothiomalate.

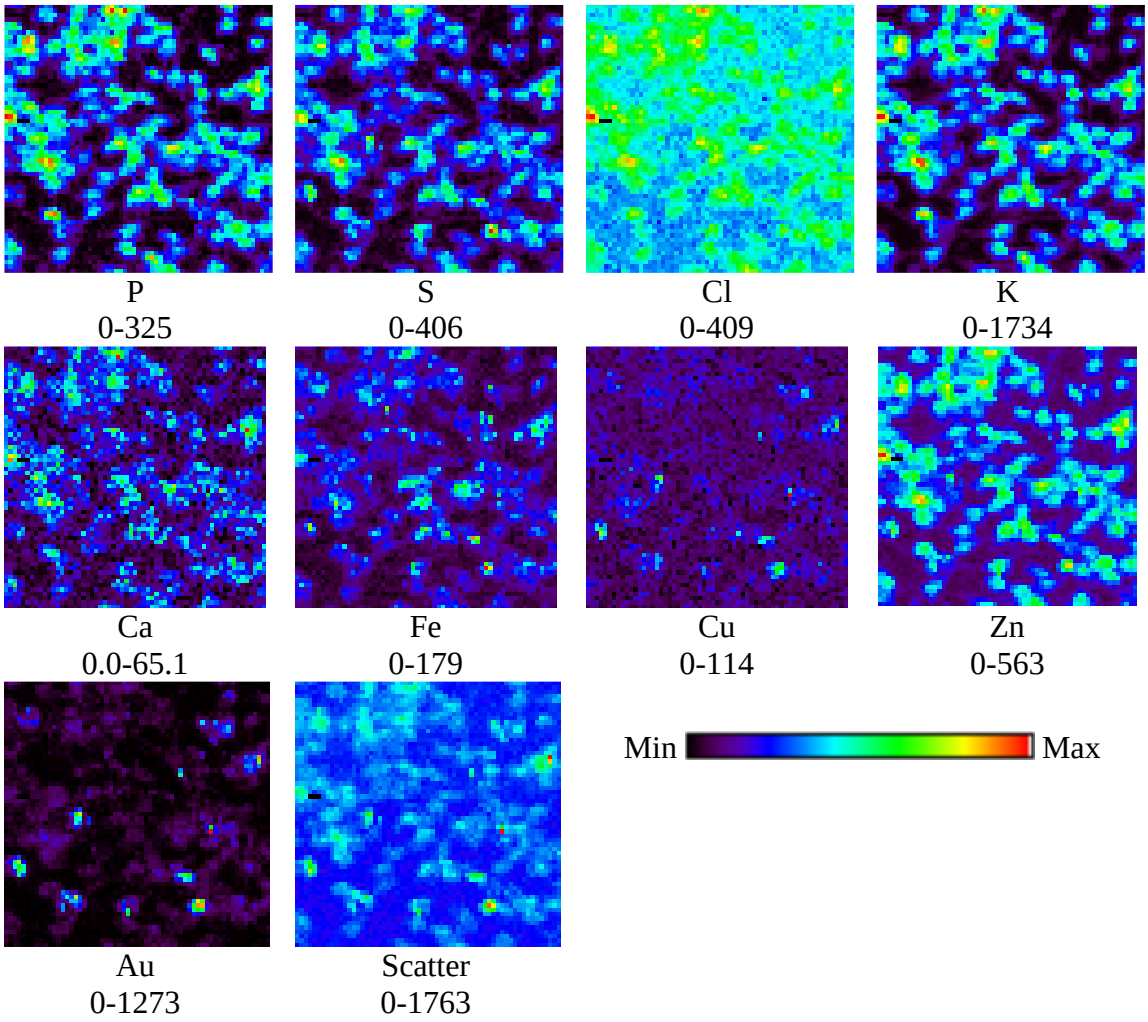

Figure B.13: Microprobe SR-XRF elemental maps for RAW264.7 cells treated with 1000 µM aurothiomalate.

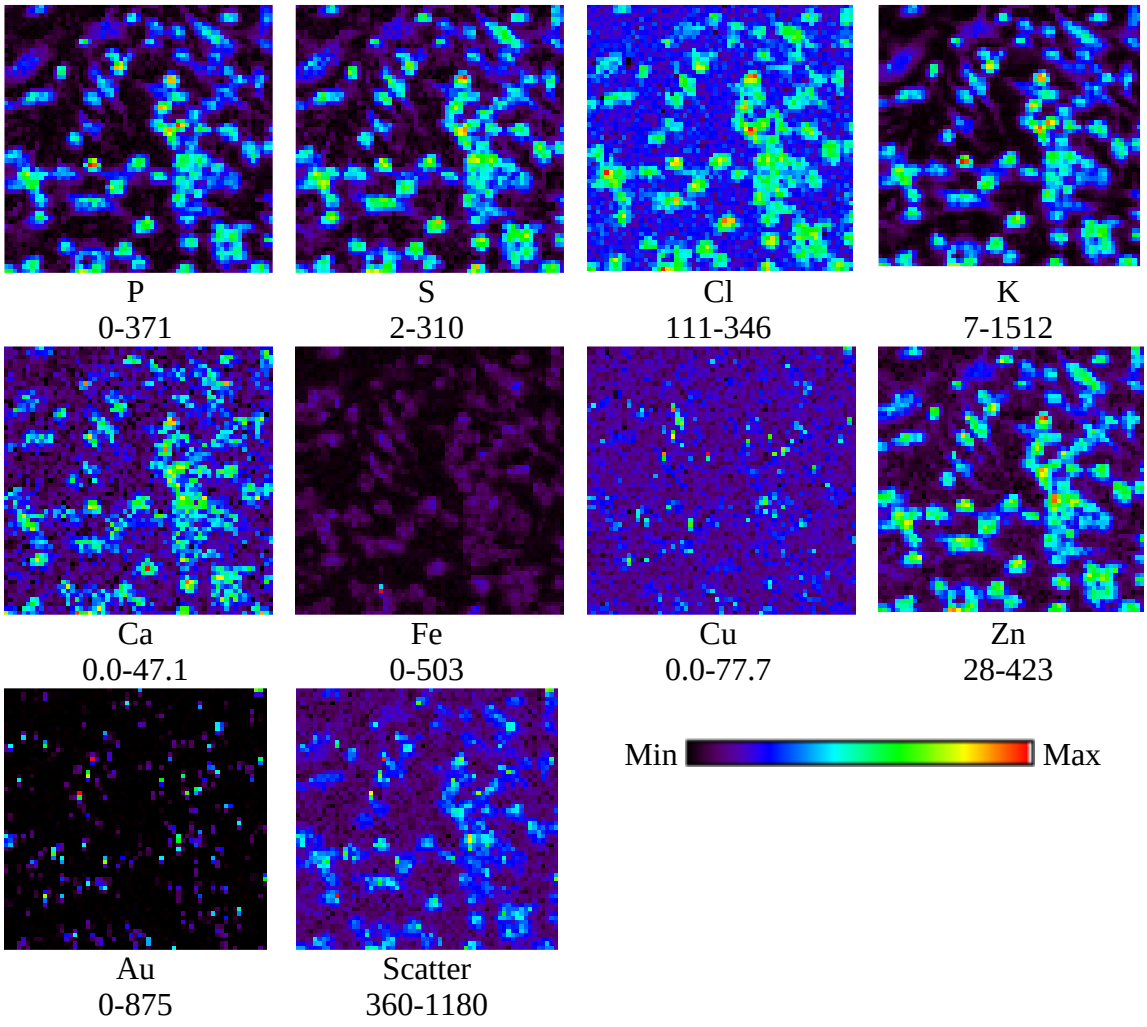

Figure B.14: Microprobe SR-XRF elemental maps for RAW264.7 cells treated with 2.5 µM Au NPs.

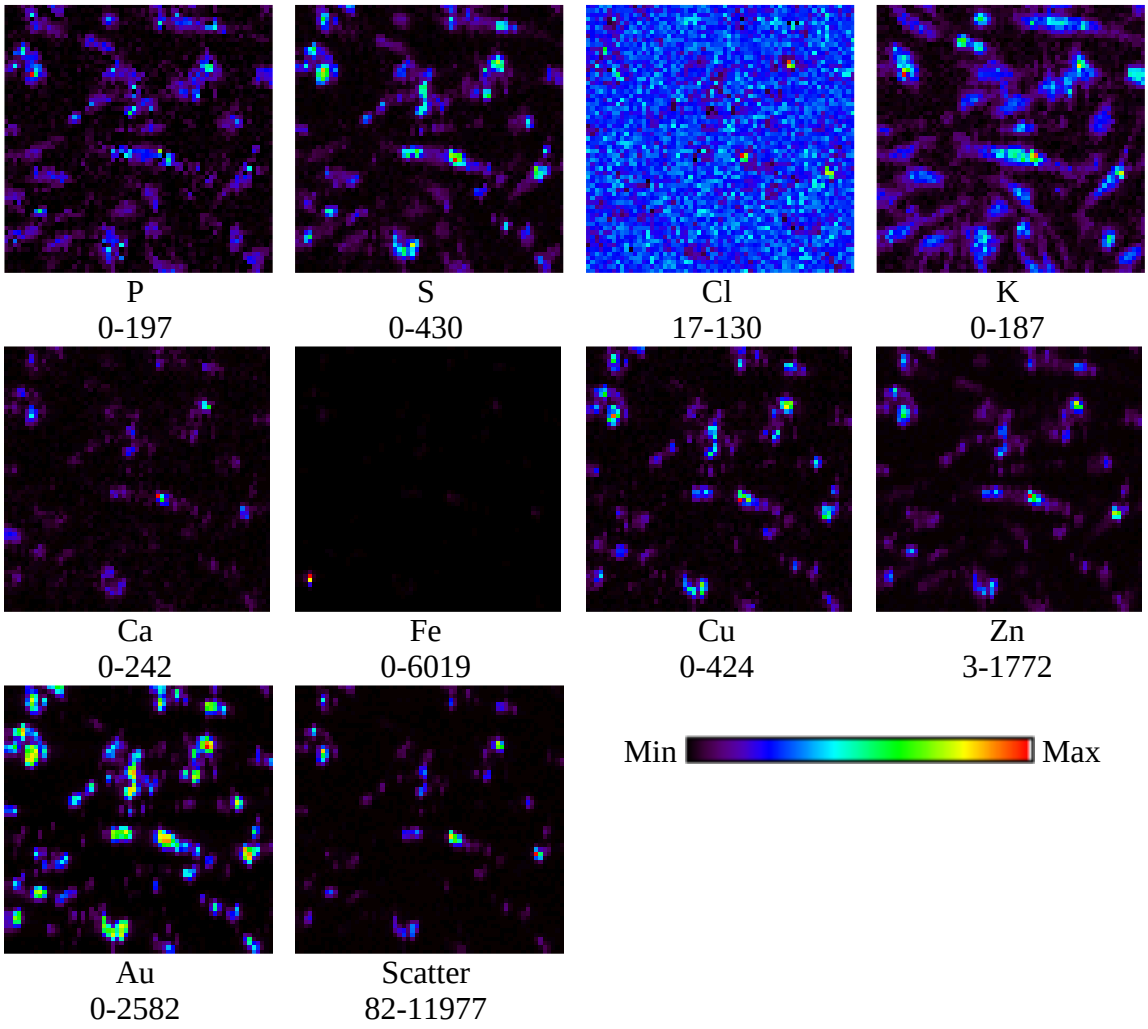

Figure B.15: Microprobe SR-XRF elemental maps for RAW264.7 cells treated with 60 µM Au NPs.

B.2 SR-XRF Spectra

Below are the integrated SR-XRF spectra for the corresponding SR-XRF images presented in **Sections B.1.1** and **B.1.2**. In each image, the black spectrum is the integrated spectrum, the green spectrum is the fitted spectrum, and the red spectrum is the assigned Kα lines. Vertical lines indicate the expected energy positions of gold L or M lines.

B.2.1 Advanced Photon Source

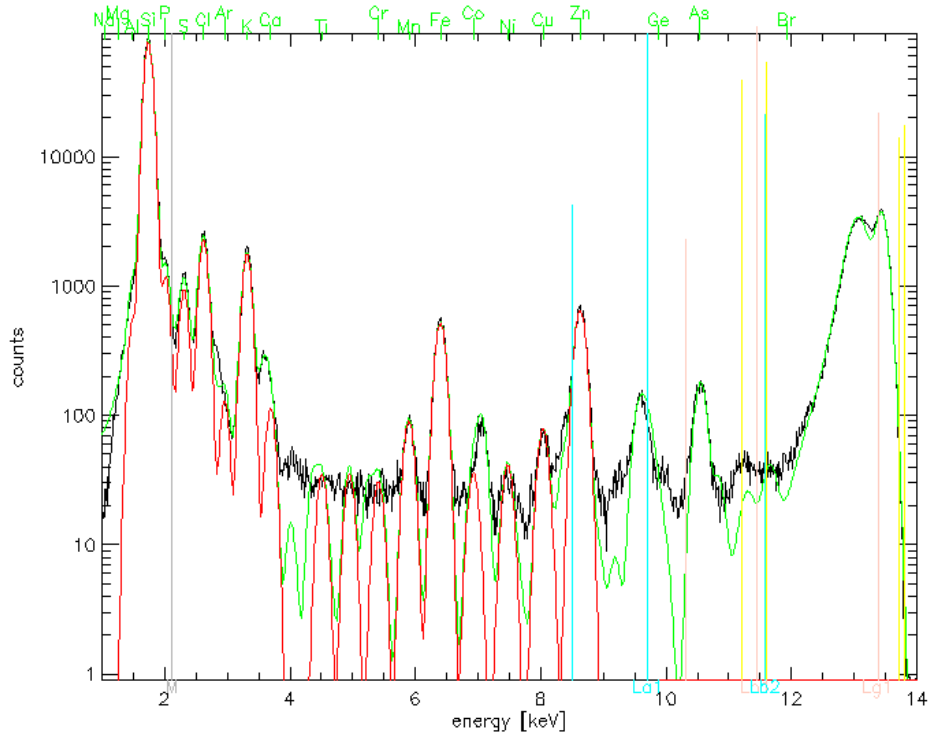

Figure B.16: Integrated (black), fitted (green) and assigned Kα lines (red) of microprobe SR-XRF spectra of RAW264.7 cells treated for 24 h with treatment medium. Vertical lines indicate the expected positions of Au L and M lines.

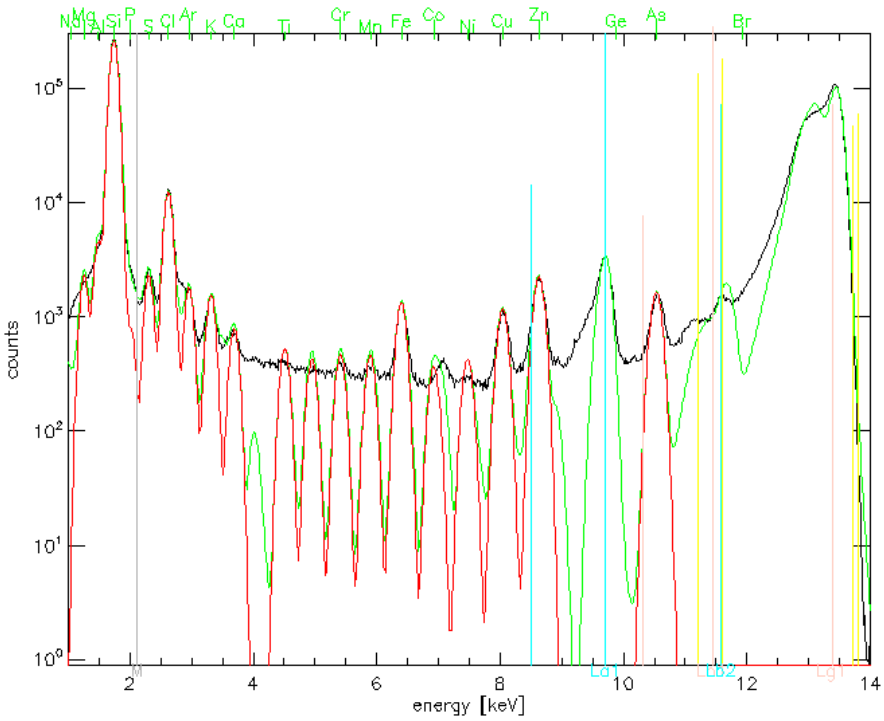

Figure B.17: Integrated (black), fitted (green) and assigned Kα lines (red) of microprobe SR-XRF spectra of RAW264.7 cells treated for 24 h with 2.5 µM auranofin. Vertical lines indicate the expected positions of Au L and M lines.

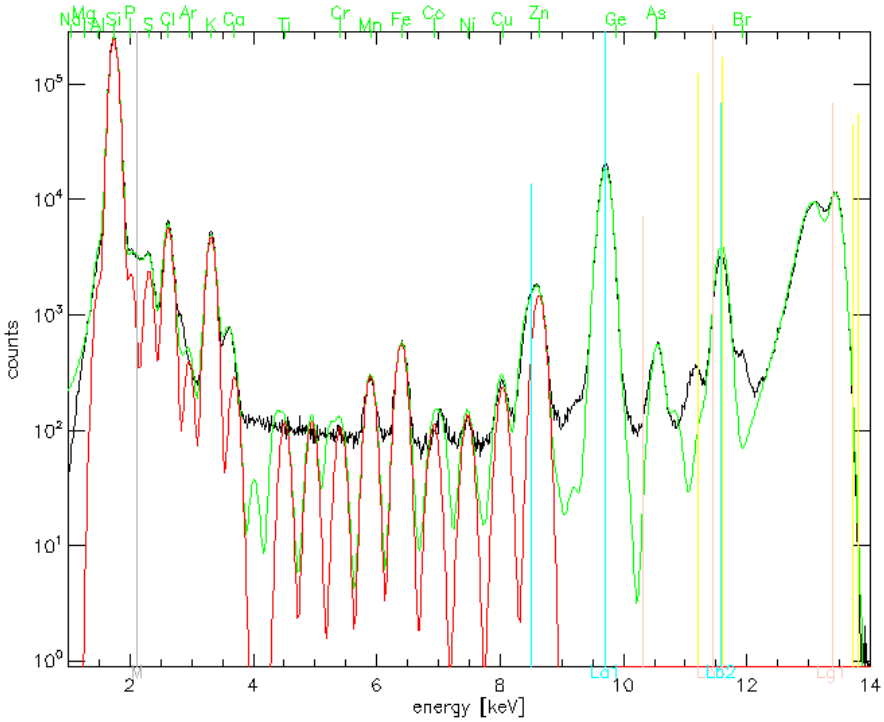

Figure B.18: Integrated (black), fitted (green) and assigned Kα lines (red) of microprobe SR-XRF spectra of RAW264.7 cells treated for 24 h with 1000 µM aurothiomalate. Vertical lines indicate the expected positions of Au L and M lines.

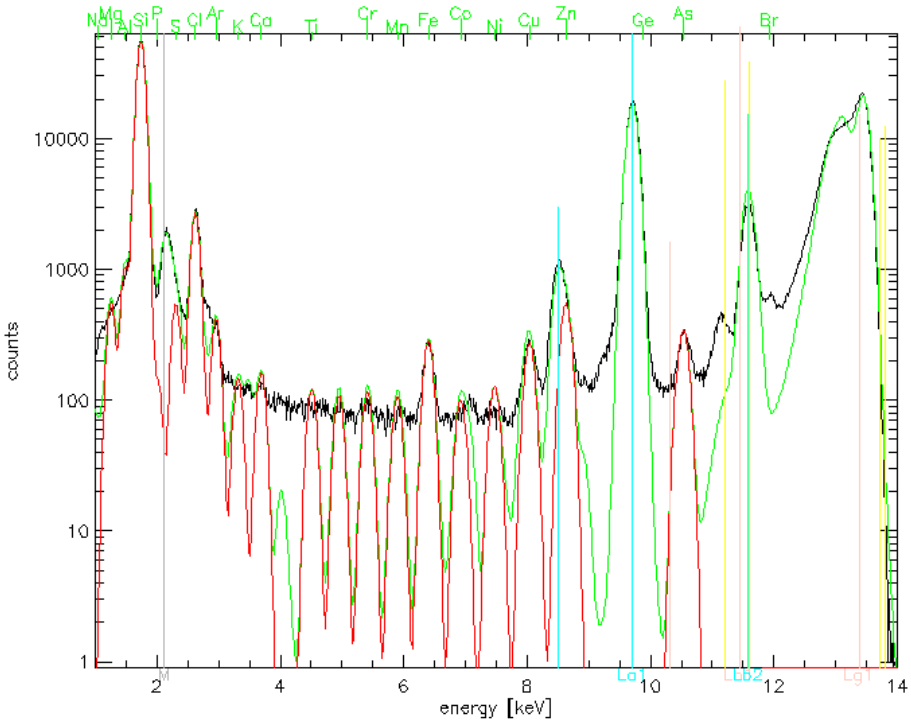

Figure B.19: Integrated (black), fitted (green) and assigned Kα lines (red) of microprobe SR-XRF spectra of RAW264.7 cells treated for 24 h with 100 µM $HAuCl_4$. Vertical lines indicate the expected positions of Au L and M lines.

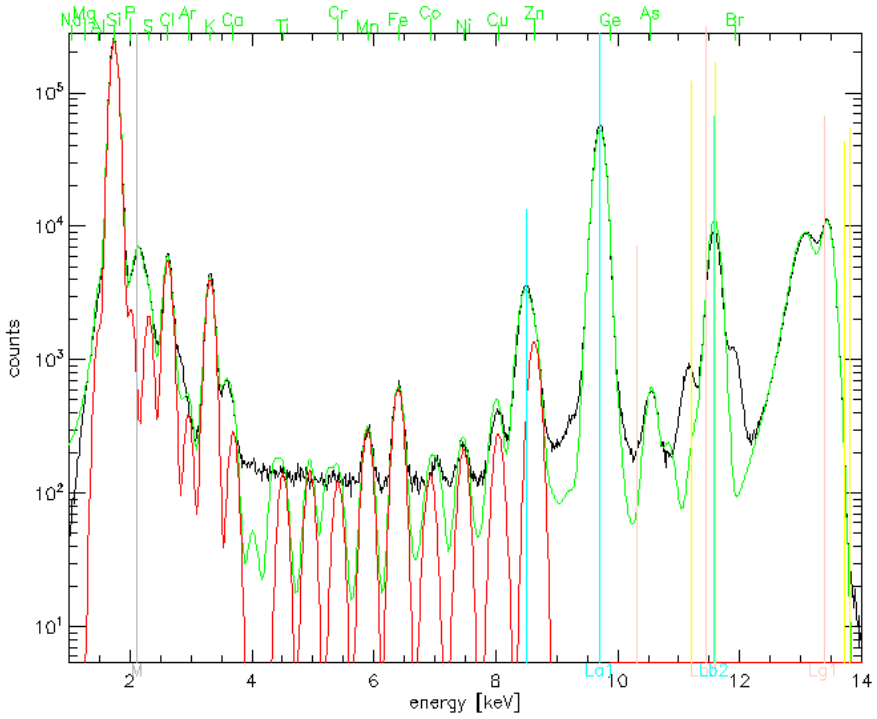

Figure B.20: Integrated (black), fitted (green) and assigned Kα lines (red) of microprobe SR-XRF spectra of RAW264.7 cells treated for 24 h with 60 µM Au NPs. Vertical lines indicate the expected positions of Au L and M lines.

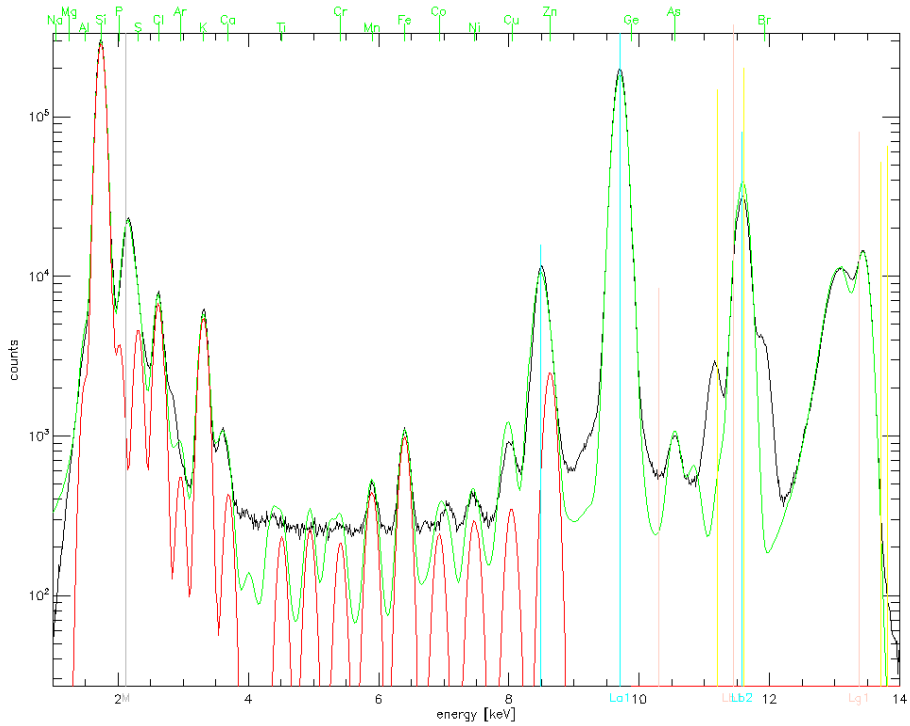

Figure B.21: Integrated (black), fitted (green) and assigned Kα lines (red) of microprobe SR-XRF spectra of RAW264.7 cells treated for 24 h with 60 µM Au NPs. Vertical lines indicate the expected positions of Au L and M lines.

B.2.2 Australian Synchrotron

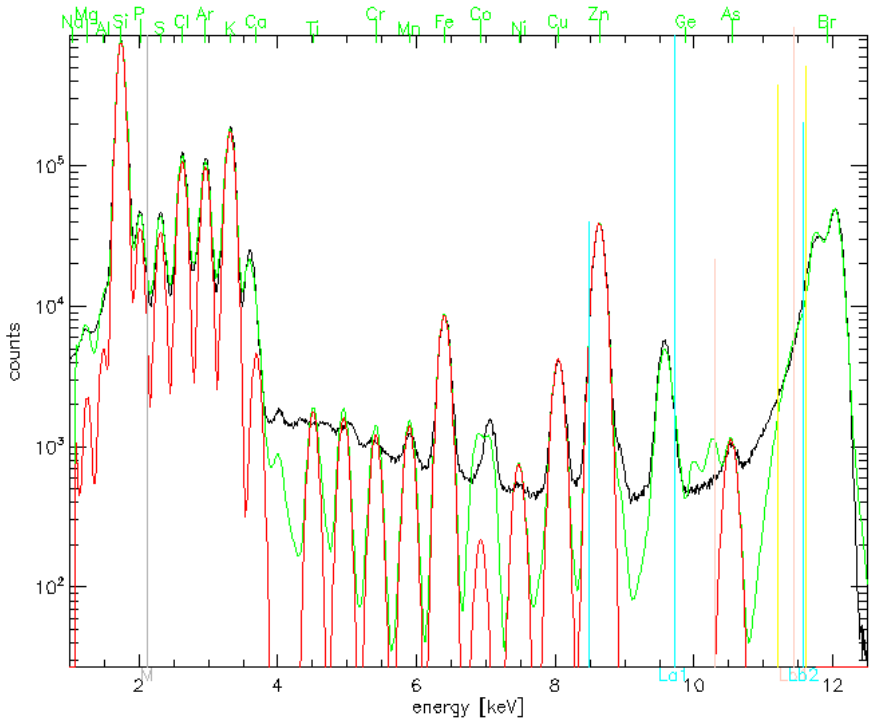

Figure B.22: Integrated (black), fitted (green) and assigned Kα lines (red) of microprobe SR-XRF spectra of RAW264.7 cells treated for 24 h with treatment medium. Vertical lines indicate the expected positions of Au L and M lines.

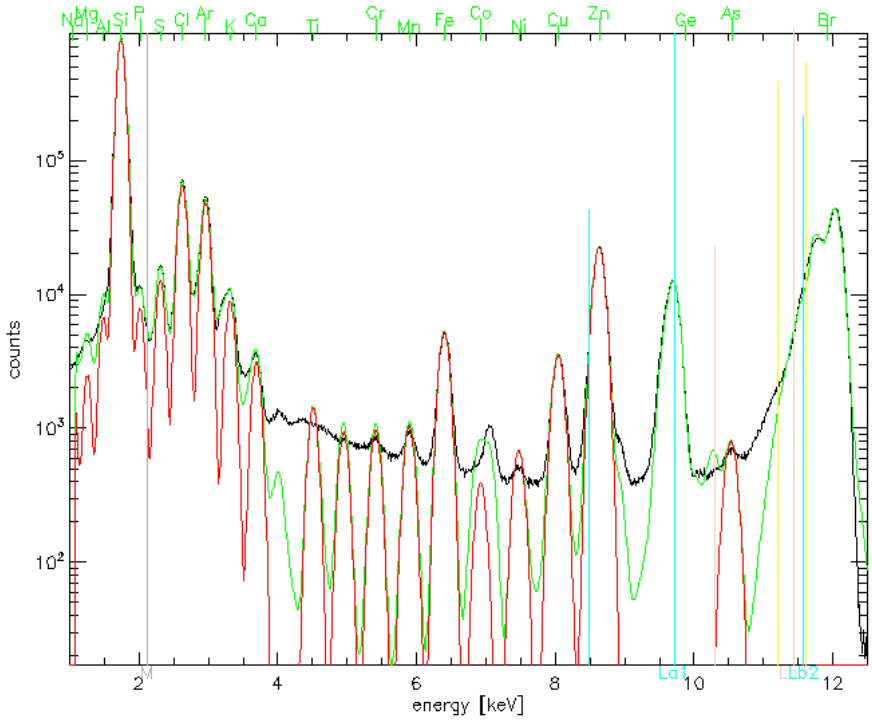

Figure B.23: Integrated (black), fitted (green) and assigned Kα lines (red) of microprobe SR-XRF spectra of RAW264.7 cells treated for 24 h with 2.5 µM auranofin. Vertical lines indicate the expected positions of Au L and M lines.

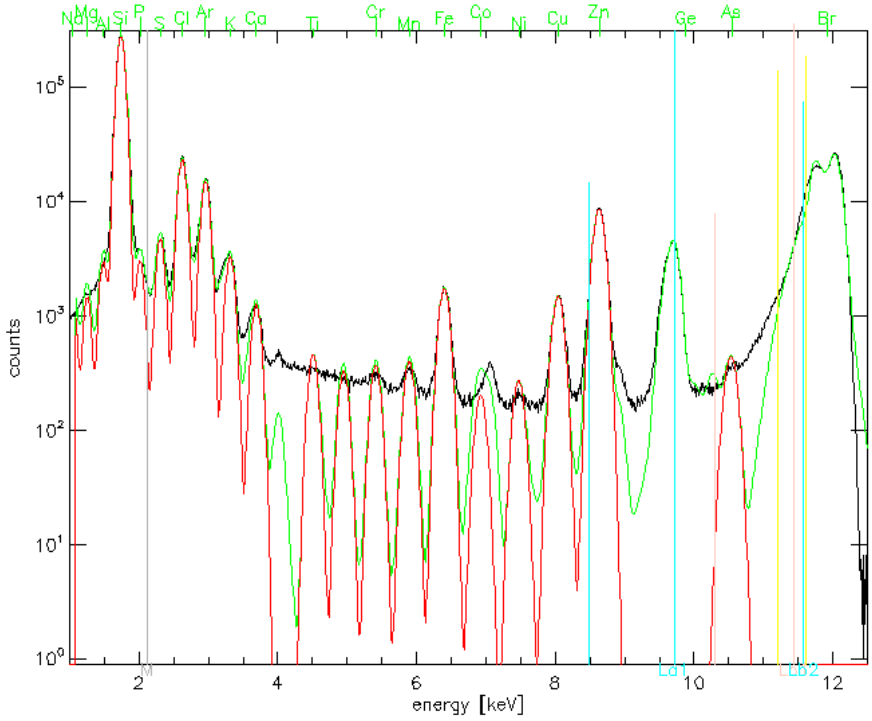

Figure B.24: Integrated (black), fitted (green) and assigned Kα lines (red) of microprobe SR-XRF spectra of a second set of RAW264.7 cells treated for 24 h with 2.5 µM auranofin. Vertical lines indicate the expected positions of Au L and M lines.

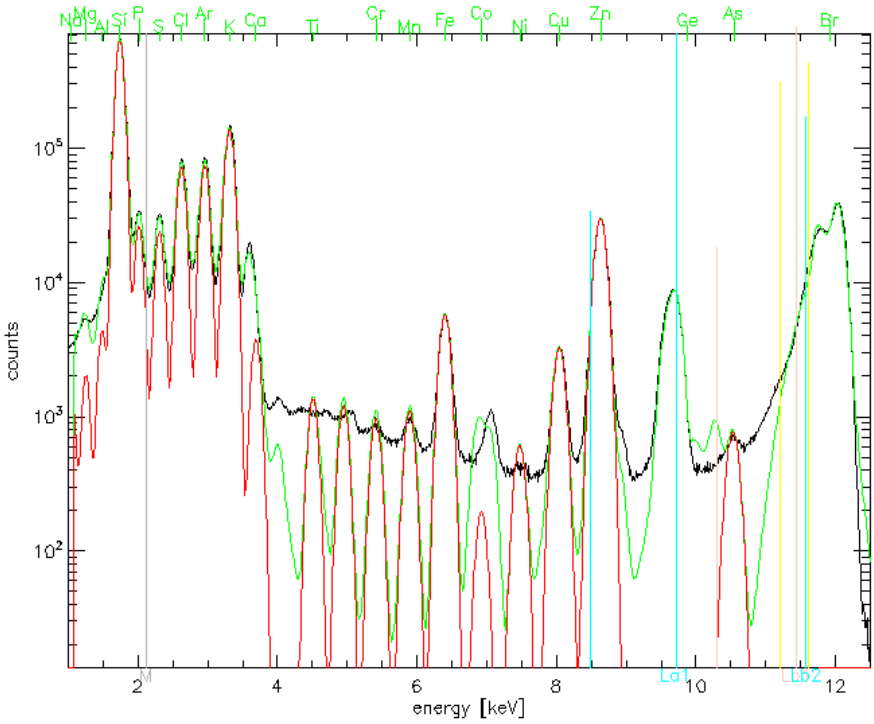

Figure B.25: Integrated (black), fitted (green) and assigned Kα lines (red) of microprobe SR-XRF spectra of RAW264.7 cells treated for 24 h with 2.5 µM aurothiosulfate. Vertical lines indicate the expected positions of Au L and M lines.

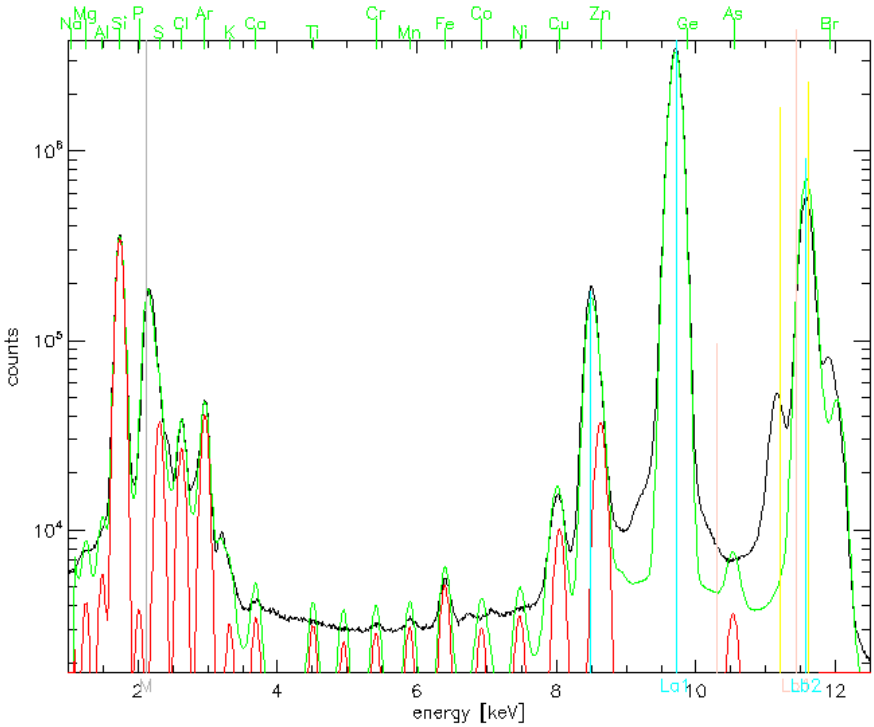

Figure B.26: Integrated (black), fitted (green) and assigned Kα lines (red) of microprobe SR-XRF spectra of RAW264.7 cells treated for 24 h with 500 µM aurothiosulfate. Vertical lines indicate the expected positions of Au L and M lines.

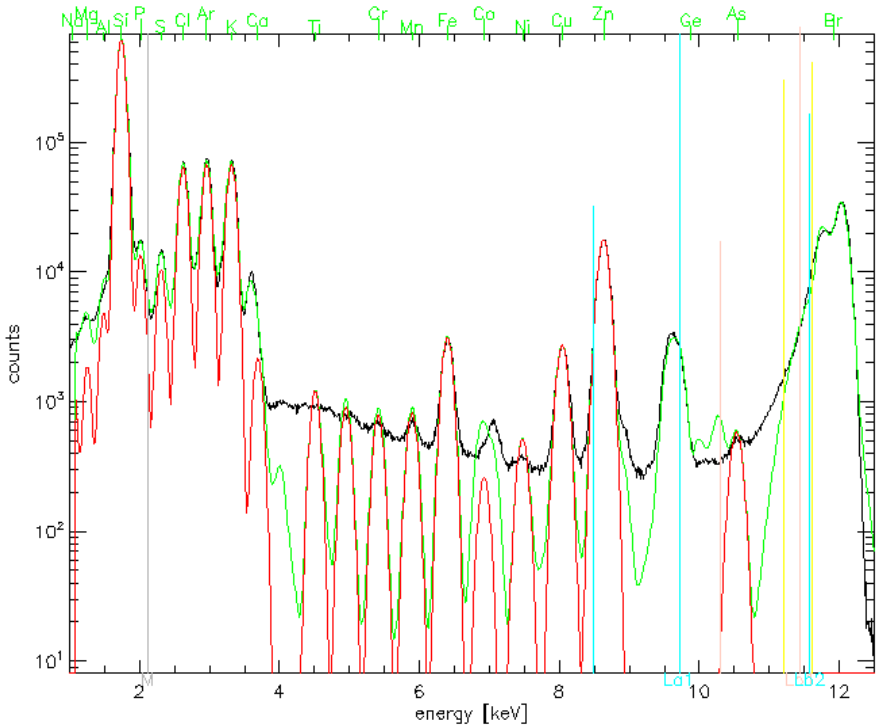

Figure B.27: Integrated (black), fitted (green) and assigned Kα lines (red) of microprobe SR-XRF spectra of RAW264.7 cells treated for 24 h with 2.5 µM aurothiomalate. Vertical lines indicate the expected positions of Au L and M lines.

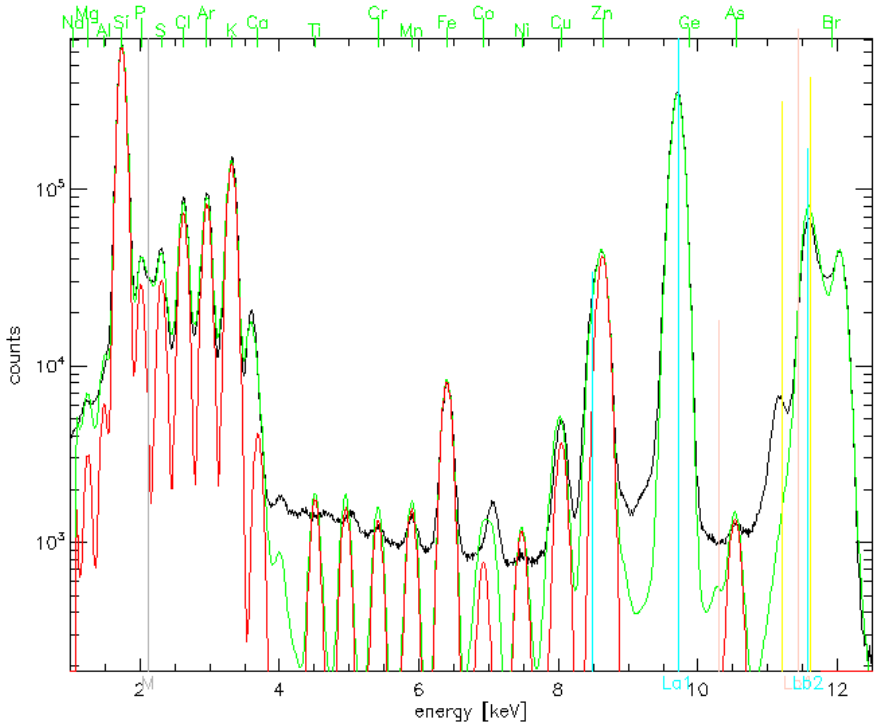

Figure B.28: Integrated (black), fitted (green) and assigned Kα lines (red) of microprobe SR-XRF spectra of RAW264.7 cells treated for 24 h with 1000 µM aurothiomalate. Vertical lines indicate the expected positions of Au L and M lines.

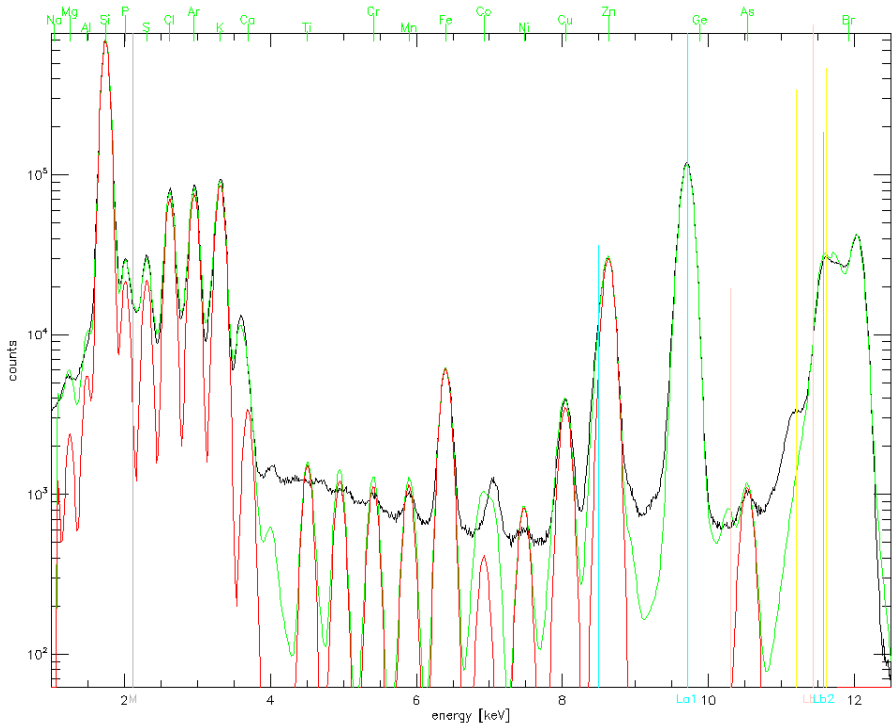

Figure B.29: Integrated (black), fitted (green) and assigned Kα lines (red) of microprobe SR-XRF spectra of RAW264.7 cells treated for 24 h with 2.5 µM Au NPs. Vertical lines indicate the expected positions of Au L and M lines.

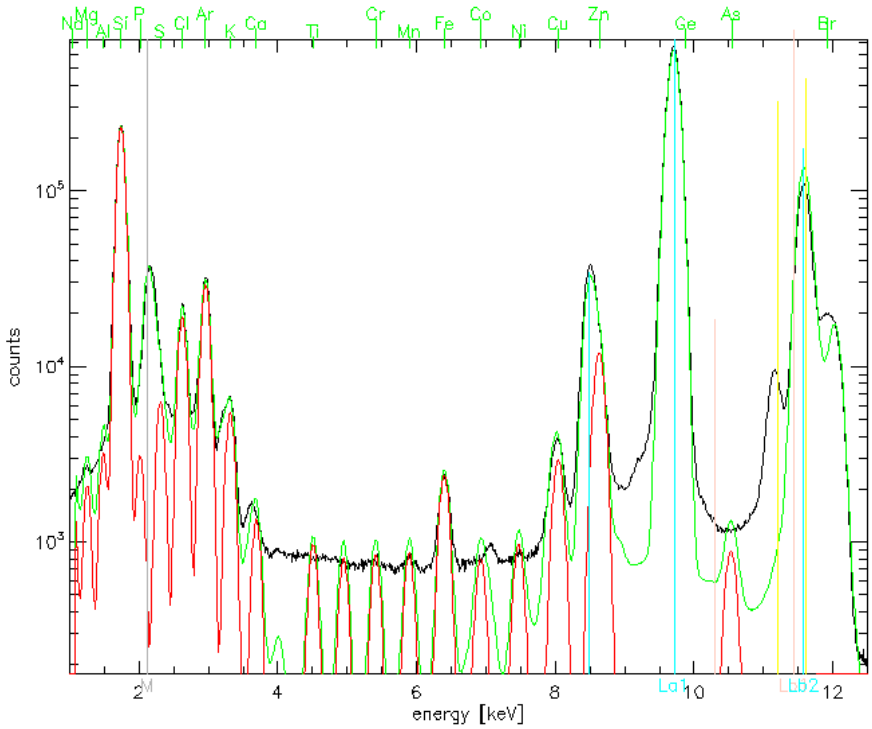

Figure B.30: Integrated (black), fitted (green) and assigned Kα lines (red) of microprobe SR-XRF spectra of RAW264.7 cells treated for 24 h with 60 µM Au NPs. Vertical lines indicate the expected positions of Au L and M lines.

Appendix C:

Thioredoxin Reductase Sequences, Spectra and Proteomics

C.1 Human Thioredoxin Reductase

C.1.1 Amino Acid Sequence

Below is the full sequence of the mutant human TrxR plasmid as provided by Yan-Chung Lo and Andrew Wang (Academia Sinica, Taiwan). It is presented in a monospace font.

```
MAHHHHHHVDDDDKMNGPEDLPKSYDYDLIIIGGGSGGLAAAKEAAQYGKKVMVLDFVT
PTPLGTRWGLGGTCVNVGCIPKKLMHQAALLGQALQDSRNYGWKVEETVKHDWDRMIEA
VQNHIGSLNWGYRVALREKKVVYENAYGQFIGPHRIKATNNKGKEKIYSAERFLIATGE
RPRYLGIPGDKEYCISSDDLFSLPYCPGKTLVVGASYVALECAGFLAGIGLDVTVMVRS
ILLRGFDQDMANKIGEHMEEHGIKFIRQFVPIKVEQIEAGTPGRLRVVAQSTNSEEIIE
GEYNTVMLAIGRDACTRKIGLETVGVKINEKTGKIPVTDEEQTNVPYIYAIGDILEDKV
ELTPVAIQAGRLLAQRLYAGSTVKCDYENVPTTVFTPLEYGACGLSEEKAVEKFGEENI
EVYHSYFWPLEWTIPSRDNNKCYAKIICNTKDNERVVGFHVLGPNAGEVTQGFAAALKC
GLTKKQLDSTIGIHPVCAEVFTTLSVTKRSGASILQAGCCG
```

C.1.2 ESI Mass Spectrum of hTrxR in Formic Acid

Figure C.1 below shows the positive ion ESI mass spectrum of hTrxR after it had been transformed to a mass scale. The solution of the protein was dialysed three times for 3 hours each against 0.1% formic acid prior to mass spectral analysis.

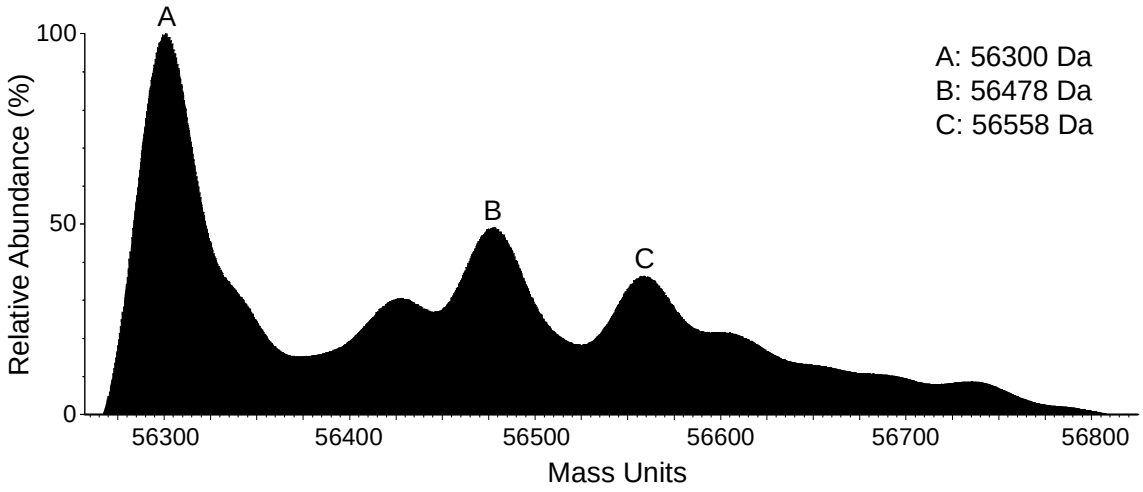

Figure C.1: Positive ion ESI mass spectrum of 1.1 µM hTrxR in 0.1% formic acid.

C.1.3 Proteomics Results

Figure C.2 shows the list of highest abundance fragments obtained from a trypsin digest of recombinant hTrxR. The digestion was analysed by LC/MS/MS, and after identification of the peptide fragments, was compared to a protein database using the search engine Mascot.[230] This work was performed by Dr. Matt Padula of the University of Technology, Sydney.

1. 2::E9PIR7 Mass: 53133 Score: 1123 Matches: 20(20) Sequences: 14(14) emPAI: 2.12
tr|E9PIR7|TXNRD1 Thioredoxin reductase 1, cytoplasmic n=2 Tax_Id=9606 [Homo sapiens]
Check to include this hit in error tolerant search or archive report

Query	Observed	Mr(expt)	Mr(calc)	ppm	Miss	Score	Expect	Rank	Unique	Peptide
143	522.3277	1042.6408	1042.6386	2.11	0	71	0.019	1	U	R.KIGLETVGVK.I
159	550.8064	1099.5983	1099.5986	-0.20	0	71	0.043	1		A.LLGQALQDSR.N
175	578.7953	1155.5760	1155.5884	-10.73	0	71	0.044	1		K.VEQIEAGTPGR.L
212	621.8431	1241.6716	1241.6728	-0.98	0	71	0.043	1		Q.AALLGQALQDSR.N
222	640.3015	1278.5885	1278.6026	-11.04	0	72	0.044	1		K.IGEHMEEHGIK.F
268	721.3565	1440.6985	1440.7031	-3.19	0	72	0.046	1	U	R.MIEAVQNHIGSLN.W + Oxidation (M)
301	823.4509	1644.8872	1644.8909	-2.26	0	72	0.048	1		K.VMVLDFVTPTPLGTR.W
317	876.4624	1750.9101	1750.9148	-2.66	0	(77)	0.017	1		K.LMHQAALLGQALQDSR.N
320	884.4498	1766.8850	1766.9097	-14.02	0	98	0.00015	1		K.LMHQAALLGQALQDSR.N + Oxidation (M)
323	895.4891	1788.9637	1788.9808	-9.57	0	88	0.0013	1		K.KVMVLDFVTPTPLGTR.W + Oxidation (M)
341	632.6677	1894.9814	1895.0047	-12.30	0	(80)	0.011	1		K.KLMHQAALLGQALQDSR.N + Oxidation (M)
342	948.5078	1895.0010	1895.0047	-1.96	0	105	2.8e-05	1		K.KLMHQAALLGQALQDSR.N + Oxidation (M)
344	970.9869	1939.9593	1939.9891	-15.33	0	99	0.00014	1	U	K.SYDYDLIIIGGGSGGLAAAK.E
348	1012.5006	2022.9867	2022.9932	-3.18	0	89	0.0015	1	U	N.SEEIIEGEYNTVMLAIGR.D
370	908.4525	2722.3358	2722.3483	-4.60	0	(78)	0.027	1	U	R.VVAQSTNSEEIIEGEYNTVMLAIGR.D
371	908.4611	2722.3615	2722.3483	4.82	0	112	9.9e-06	1	U	R.VVAQSTNSEEIIEGEYNTVMLAIGR.D
372	908.7805	2723.3198	2723.3323	-4.62	0	(82)	0.01	1	U	R.VVAQSTNSEEIIEGEYNTVMLAIGR.D + Deamidated (NQ)
374	1362.6689	2723.3232	2723.3323	-3.37	0	(90)	0.0019	1	U	R.VVAQSTNSEEIIEGEYNTVMLAIGR.D + Deamidated (NQ)
375	1368.1825	2734.3504	2734.3589	-3.11	0	79	0.021	1	U	K.IPVTDEEQTNVPYIYAIGDILEDK.V
377	913.7847	2738.3322	2738.3432	-4.02	0	(92)	0.0012	1	U	R.VVAQSTNSEEIIEGEYNTVMLAIGR.D + Oxidation (M)

Proteins matching the same set of peptides:
2::B2R5P6 Mass: 54512 Score: 1123 Matches: 20(20) Sequences: 14(14)
tr|B2R5P6|TXNRD1 Thioredoxin reductase 1, cytoplasmic n=2 Tax_Id=9606 [Homo sapiens]
2::Q16881-5 Mass: 54720 Score: 1123 Matches: 20(20) Sequences: 14(14)
sp|Q16881-5|TXNRD1 Isoform 5 of Thioredoxin reductase 1, cytoplasmic n=3 Tax_Id=9606 [Homo sapiens]
2::E2QRB9 Mass: 59542 Score: 1122 Matches: 20(20) Sequences: 14(14)
tr|E2QRB9|TXNRD1 Thioredoxin reductase 1, cytoplasmic n=2 Tax_Id=9606 [Homo sapiens]
2::Q16881-2 Mass: 59750 Score: 1122 Matches: 20(20) Sequences: 14(14)
sp|Q16881-2|TXNRD1 Isoform 2 of Thioredoxin reductase 1, cytoplasmic n=2 Tax_Id=9606 [Homo sapiens]
2::ENSP00000373506 Mass: 60174 Score: 1121 Matches: 20(20) Sequences: 14(14)
ens|ENSP00000373506|ENSG00000198431 transcript:ENST00000388854 gene_biotype:protein_coding transcript_biotype:protein_coding n=
2::B7Z2S5 Mass: 59984 Score: 1121 Matches: 20(20) Sequences: 14(14)
tr|B7Z2S5|TXNRD1 Thioredoxin reductase 1, cytoplasmic n=2 Tax_Id=9606 [Homo sapiens]
2::Q16881-4 Mass: 60382 Score: 1121 Matches: 20(20) Sequences: 14(14)
sp|Q16881-4|TXNRD1 Isoform 4 of Thioredoxin reductase 1, cytoplasmic n=2 Tax_Id=9606 [Homo sapiens]
2::ENSP00000432812 Mass: 62044 Score: 1121 Matches: 20(20) Sequences: 14(14)
ens|ENSP00000432812|ENSG00000198431 transcript:ENST00000526950 gene_biotype:protein_coding transcript_biotype:protein_coding n=
2::E9PNQ6 Mass: 61996 Score: 1121 Matches: 20(20) Sequences: 14(14)
tr|E9PNQ6|TXNRD1 Thioredoxin reductase 1, cytoplasmic n=1 Tax_Id=9606 [Homo sapiens]
2::E7ESI6 Mass: 63940 Score: 1120 Matches: 20(20) Sequences: 14(14)

Figure C.2: Protein identification results for hTrxR obtained using the search engine Mascot. Obtained by personal communication from Dr. Matt Padula, University of Technology, Sydney on 12/03/2015.

C.1.4 Gold Binding Results

Figure C.3 shows the positive ion ESI mass spectra obtained using a solution containing a 3:1 ratio of auranofin : hTrxR that had been allowed to react for different periods of time. **Figure C.4** shows the positive ion ESI mass spectra obtained of a solution containing a 5:1 ratio of Au NPs : hTrxR after it had been allowed to react for 1 h, 4 h and 24 h. The spectrum of a solution containing hTrxR only is included for comparison.

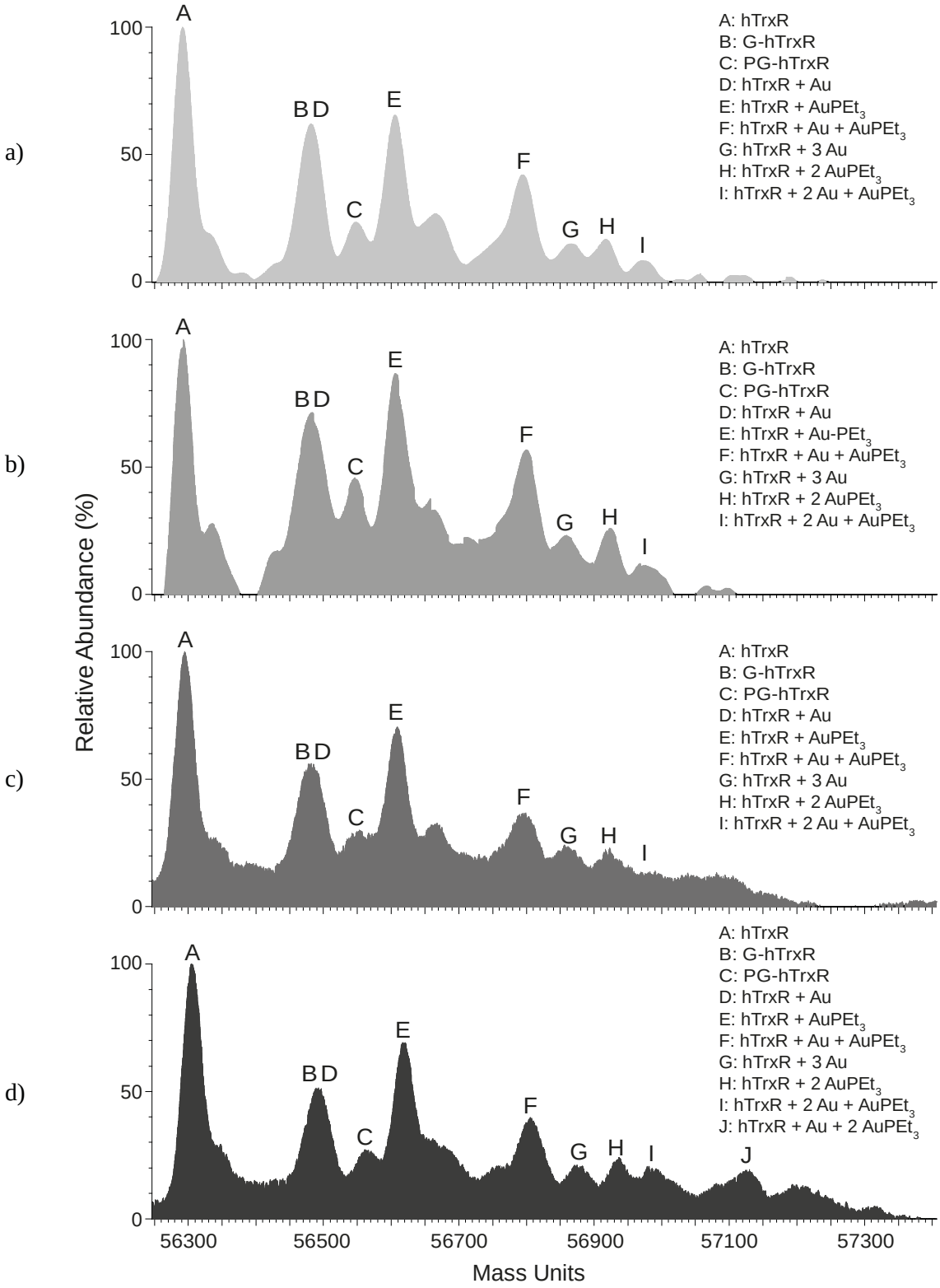

Figure C.3: Positive ion ESI mass spectra of a solution containing a 3:1 ratio of auranofin : hTrxR, transformed to a mass scale. The solution was analysed after being allowed to react for: **a)** 30 min; **b)** 1 h; **c)** 4 h; and **d)** 24 h. For ESI-MS, each sample contained 1.2 µM hTrxR, 20 mM ammonium acetate and 5% acetic acid.

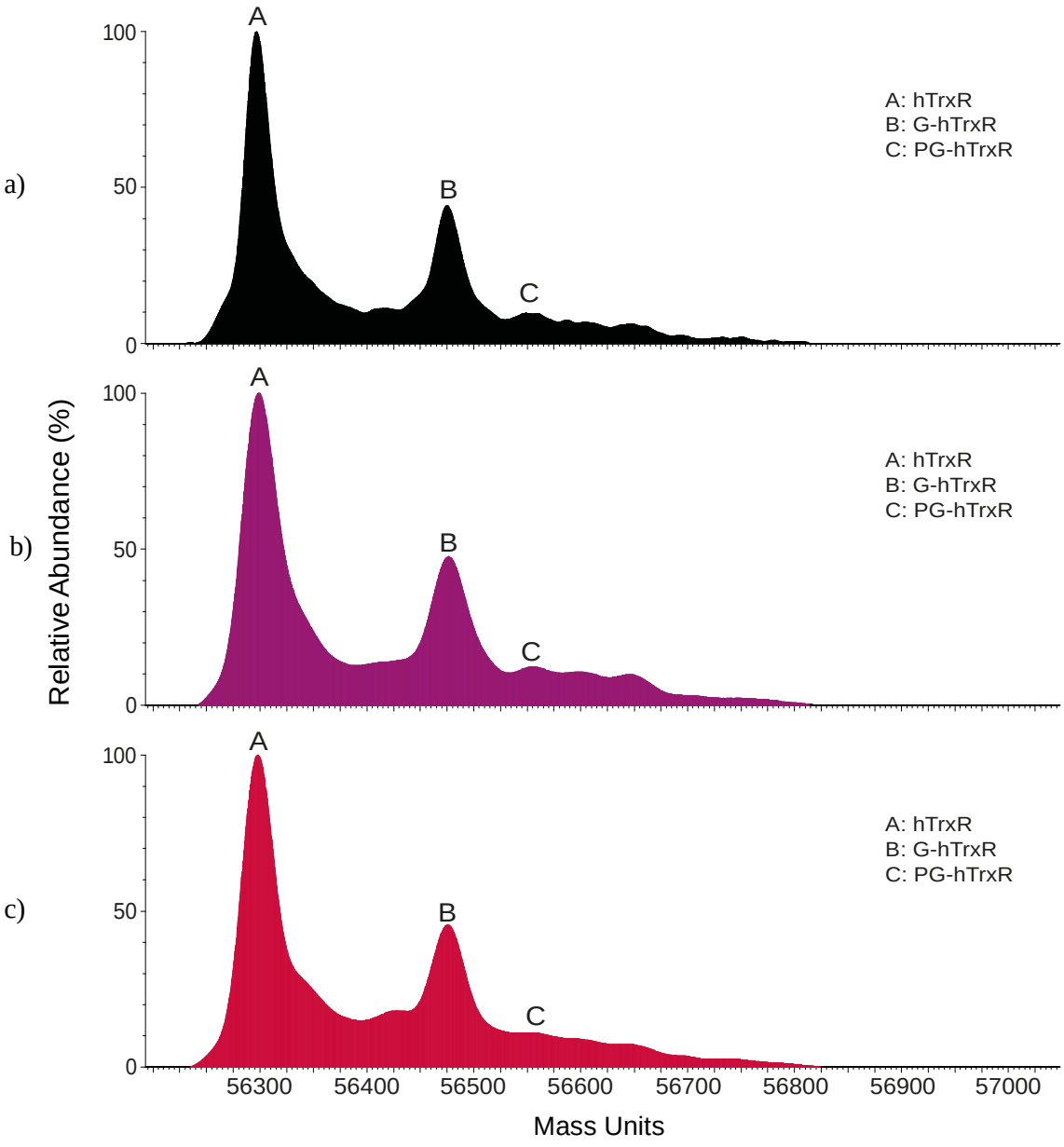

Figure C.4: Positive ion ESI mass spectra of a solution containing a 5:1 ratio of Au NPs : hTrxR, after transformation to a mass scale: **a)** is a spectrum of a solution containing hTrxR only, included for comparison. The solution reaction mixture was analysed after being allowed to react for: **b)** 1 h and **c)** 24 h. For ESI-MS, each sample contained 1.2 µM hTrxR, 20 mM ammonium acetate and 5% acetic acid.

C.2 Rat Thioredoxin Reductase

C.2.1 Amino Acid Sequence

Below is the full sequence of rat TrxR obtained by searching the UniProt database for rat thioredoxin reductase (http://www.uniprot.org/ accessed 14/10/2014). It is presented in a monospace font.

```
MNDSKDAPKSYDFDLIIIGGGSGGLAAAKEAAKFDKKVMVLDFVTPTPLGTRWGLGGTC
VNVGCIPKKLMHQAALLGQALKDSRNYGWKLEDTVKHDWEKMTESVQNHIGSLNWGYRV
ALREKKVVYENAYGKFIGPHKIMATNNKGKEKVYSAERFLIATGERPRYLGIPGDKEYC
ISSDDLFSLPYCPGKTLVVGASYVALECAGFLAGIGLDVTVMVRSILLRGFDQDMANKI
GEHMEEHGIKFIRQFVPTKIEQIEAGTPGRLKVTAKSTNSEETIEDEFNTVLLAVGRDS
CTRTIGLETVGVKINEKTGKIPVTDEEQTNVPYIYAIGDILEGKLELTPVAIQAGRLLA
QRLYGGSTVKCDYDNVPTTVFTPLEYGCCGLSEEKAVEKFGEENIEVYHSFFWPLEWTV
PSRDNNKCYAKVICNLKDNERVVGFHVLGPNAGEVTQGFAAALKCGLTKQQLDSTIGIH
PVCAEIFTTLSVTKRSGGDILQSGCUG
```

C.2.2 Proteomics Results

Figure C.5 shows the list of highest abundance fragments obtained from a trypsin digest of commercially obtained rTrxR. The digestion was analysed by LC/MS/MS, and after identification of the peptide fragments, was compared to a protein database using Mascot.[230] This work was performed by Dr. Matt Padula of the University of Technology, Sydney.

1. 2::O89049 Mass: 54637 Score: 759 Matches: 12(12) Sequences: 9(9) emPAI: 0.90
sp|O89049|Txnrd1 Thioredoxin reductase 1, cytoplasmic n=1 Tax_Id=10116 [Rattus norvegicus]
Check to include this hit in error tolerant search or archive report

Query	Observed	Mr(expt)	Mr(calc)	ppm	Miss	Score	Expect	Rank	Unique	Peptide
112	585.8115	1169.6085	1169.6080	0.41	0	91	0.0005	1	U	K.KVVYENAYGK.F
148	640.3135	1278.6125	1278.6026	7.69	0	73	0.034	1		K.IGEHMEEHGIK.F
167	697.4017	1392.7889	1392.7911	-1.57	0	80	0.0055	1	U	K.LMHQAALLGQALK.D
170	705.4029	1408.7912	1408.7860	3.66	0	(75)	0.017	1	U	K.LMHQAALLGQALK.D + Oxidation (M)
185	761.4505	1520.8865	1520.8861	0.32	0	(81)	0.0035	1	U	K.KLMHQAALLGQALK.D
192	769.4556	1536.8967	1536.8810	10.2	0	88	0.00062	1	U	K.KLMHQAALLGQALK.D + Oxidation (M)
207	831.4554	1660.8963	1660.8859	6.29	0	73	0.044	1		K.VMVLDFVTPTPLGTR.W + Oxidation (M)
234	963.0046	1923.9946	1923.9942	0.22	0	79	0.013	1	U	K.SYDFDLIIIGGGSGGLAAAK.E
241	1011.5134	2021.0122	2020.9953	8.36	0	84	0.0049	1	U	N.SEETIEDEFNTVLLAVGR.D
252	1163.0616	2324.1087	2324.1019	2.89	0	(95)	0.00042	1	U	K.STNSEETIEDEFNTVLLAVGR.D + Deamidated (NQ)
253	1163.0713	2324.1280	2324.1019	11.2	0	140	1.3e-08	1	U	K.STNSEETIEDEFNTVLLAVGR.D + Deamidated (NQ)
261	1339.1949	2676.3751	2676.3534	8.12	0	83	0.0088	1		K.IPVTDEEQTNVPYIYAIGDILEGK.L

Proteins matching the same set of peptides:
2::R9PXU4 Mass: 54415 Score: 758 Matches: 12(12) Sequences: 9(9)
tr|R9PXU4|Txnrd1 Thioredoxin reductase 1, cytoplasmic n=2 Tax_Id=10116 [Rattus norvegicus]

2. 2::P12928-2 Mass: 58757 Score: 533 Matches: 9(9) Sequences: 7(7) emPAI: 0.63
sp|P12928-2|Pklr Isoform L-type of Pyruvate kinase PKLR n=3 Tax_Id=10116 [Rattus norvegicus]
Check to include this hit in error tolerant search or archive report

Query	Observed	Mr(expt)	Mr(calc)	ppm	Miss	Score	Expect	Rank	Unique	Peptide
33	415.7421	829.4697	829.4658	4.70	0	75	0.013	1	U	K.ASDVLAVR.D
56	479.7919	957.5693	957.5607	8.95	0	82	0.0021	1	U	R.KASDVLAVR.D
197	788.4581	1574.9017	1574.8920	6.19	0	75	0.02	1	U	R.IYIDDGLISLVVQK.I
204	817.9132	1633.8119	1633.8199	-4.90	0	74	0.035	1	U	R.DPTEVTAIGAVEASFK.C
213	872.4445	1742.8745	1742.8596	8.51	0	(75)	0.029	1	U	K.GSFPVEAVMMQHAIAR.E
220	888.4359	1774.8572	1774.8495	4.39	0	76	0.024	1	U	K.GSFPVEAVMMQHAIAR.E + 2 Oxidation (M)
225	911.4780	1820.9414	1820.9342	3.95	0	96	0.00027	1		K.KFDEILEVSDGIMVAR.G
228	919.4681	1836.9216	1836.9291	-4.09	0	(78)	0.018	1		K.KFDEILEVSDGIMVAR.G + Oxidation (M)
259	879.1423	2634.4051	2634.3864	7.07	0	81	0.012	1	U	R.KGVNLPNTEVDLPGLSEQDLLDLR.F

Proteins matching the same set of peptides:
2::P12928 Mass: 62162 Score: 533 Matches: 9(9) Sequences: 7(7)
sp|P12928|Pklr Pyruvate kinase PKLR n=2 Tax_Id=10116 [Rattus norvegicus]

Figure C.5: Protein identification results for rTrxR obtained using the search engine Mascot. Obtained by personal communication from Dr. Matt Padula, University of Technology, Sydney on 12/03/2015.